STRAINED AROMATIC MACROCYCLES AS THE BUILDING BLOCKS FOR

FUNCTIONAL MATERIALS

by

PENGHAO LI

A DISSERTATION

Presented to the Department of Chemistry and Biochemistry
and the Graduate School of the University of Oregon
in partial fulfillment of the requirements
for the degree of
Doctor of Philosophy

June 2017

DISSERTATION APPROVAL PAGE

Student: Penghao Li

Title: Strained Aromatic Macrocycles as the Building Blocks for Functional Materials

This dissertation has been accepted and approved in partial fulfillment of the requirements for the Doctor of Philosophy degree in the Department of Chemistry and Biochemistry by:

Michael Haley	Chairperson
Ramesh Jasti	Advisor
Darren Johnson	Core Member
James Imamura	Institutional Representative

and

Scott L. Pratt	Dean of the Graduate School

Original approval signatures are on file with the University of Oregon Graduate School.

Degree awarded June 2017

DISSERTATION ABSTRACT

Penghao Li

Doctor of Philosophy

Department of Chemistry and Biochemistry

June 2017

Title: Strained Aromatic Macrocycles as the Building Blocks for Functional Materials

Commonly viewed as the shortest cross sections of armchair carbon nanotubes (CNTs), cycloparaphenylenes (CPPs) represent a unique class of conjugated macrocycles with rigid backbones. In addition to their utility in seeding the growth of uniform CNTs, these strained nanohoops and their derivatives have unique optoelectronic and supramolecular properties for potential applications in materials science. Herein we present our efforts in designing novel nanohoop architectures and new types of strained macrocycles that serve as building blocks for functional materials.

Chapter I briefly reviewed the under-represented reactivity studies of strained aromatic macrocycles. Chapter II describes our early efforts in probing the structure-property relationships of oligophenylene macrocycles focusing on the understanding of the influence of structural bending and cyclic conjugation on the optoelectronic properties. Chapter III reports the reactivity study of 1,4-anthracene-incorporated [12]CPP, a model substrate to examine the feasibility of using anthracene as the functional handle to crosslink nanohoops. Chapter IV presents the synthesis of a molecular propeller with three nanohoop blades and examines its unique hexagonal layered packing structure. In Chapter V, we disclose the synthesis of strained stilbene macrocycles suitable for ring-opening metathesis polymerization (ROMP) as well as the

initial ROMP studies of this monomeric system.

This dissertation includes previously published and unpublished co-authored material.

CURRICULUM VITAE

NAME OF AUTHOR: Penghao Li

GRADUATE AND UNDERGRADUATE SCHOOLS ATTENDED:

> University of Oregon, Eugene, Oregon
> Boston University, Boston, Massachusetts
> Nankai University, Tianjin, P. R. China

DEGREES AWARDED:

> Doctor of Philosophy, Chemistry, 2017, University of Oregon
> Master of Arts, Chemistry, 2014, Boston University
> Bachelor of Science, Chemistry, 2011, Nankai University

AREAS OF SPECIAL INTEREST:

> Physical Organic Chemistry
> Synthetic Organic Chemistry
> Polymer Chemistry
> Organic Materials

PROFESSIONAL EXPERIENCE:

> Teaching Fellow, University of Oregon, 2014-2017
>
> Teaching Fellow, Boston University, 2011-2014

GRANTS, AWARDS, AND HONORS:

> Fundamental Science Scholarship, Nankai University, 2008-2011
>
> Third-Grade Scholarship for Excellent Undergraduate Student, Nankai
>   University, 2007-2008
>
> Physical Organic Gordon Research Seminar Speaker, Gordon Conference, 2015

PUBLICATIONS:

Li, P.; Sisto, T. J.; Darzi, E. R.; Jasti, R. The Effects of Cyclic Conjugation and Bending on the Optoelectronic Properties of Paraphenylenes. *Org. Lett.* **2014**, *16* (1), 182-185.

Li, P.; Wong, B. M.; Zakharov, L. N.; Jasti, R. Investigating the Reactivity of 1,4-Anthracene-Incorporated Cycloparaphenylene. *Org. Lett.* **2016**, *18* (7), 1575-1577.

Li, P.; Zakharov, L. N.; Jasti, R. A Molecular Propeller with Three Nanohoop Blades: Synthesis, Characterization and Solid State Packing. *Angew. Chem. Int. Ed.* **2017**, *56* (19), 5237-5241; *Angew. Chem.* **2017**, *129* (19), 5321-5325.

ACKNOWLEDGMENTS

I wish to express sincere gratitude to Prof. Ramesh Jasti, for his guidance and support through graduate school. I would also like to thank my former mentors, Prof. Huiqi Zhang and Prof. Guoqing Pan, for early training and support for applying graduate school. I would like to thank Dr. Jialong Xia, Dr. Matt Golder and Dr. Evan Darzi for teaching me basic skills in organic chemistry when I first joined the lab and for been role models as diligent scientists with a strong work ethic. I want to say thank you to all Jasti lab members, Dr. Elizabeth Hirst, Dr. Paul Evans, Dr. Tom Sisto, Brittany White, Han Xiao, Eric Boon, Jeff Van Raden, Curtis Colwell, Erik Leonardt, Terri Lovel for making the lab a welcoming place full of joys.

I would like to thank my thesis committee of Prof. Mike Haley, Prof. Darren Johnson and Prof. James Imamura.

Special thanks give to Dr. Jonathan Boyce, Dr. Gabe Rudebush, Bin Cai, Yuntao Shi, Zhe Li, Chenmin Cao, Xirui Hu for their friendship.

Finally, I would like to thank my parents, Guoping and Jinmei, and my sister Minrui for their unconditional love and enduring support through my entire life.

For my father, mother and sister.

TABLE OF CONTENTS

LIST OF FIGURES

Figure

Page

LIST OF TABLES

LIST OF SCHEMES

CHAPTER I

THE REACTIVITY OF STRAINED AROMATIC MACROCYCLES

This chapter was written by myself and edited by Prof. Ramesh Jasti.

Chapter II is based on co-authored work published in *Organic Letters* in 2014. Dr. Thomas Sisto performed electrochemical characterizations and was involved in the preparation of the main manuscript. Dr. Evan Darzi was involved in the development of the synthesis and assisted with the preparation of the supporting information. Prof. Ramesh Jasti edited this chapter and the original manuscript.

Chapter III is based on published work in *Organic Letters* in 2016. Prof. Bryan Wong (UC Riverside) conducted the computational studies and wrote the corresponding section in the main manusript. Dr. Lev Zakharov performed the X-ray crystallographic analysis. The manuscript was edited by Prof. Ramesh Jasti.

Chapter IV is based on published work in *Angewandte Chemie* in 2017. Dr. Lev Zakharov performed the crystollographic analysis and assisted with the preparation of supporting information. Editing was provided by Prof. Ramesh Jasti.

Chapter V is based on unpublished work. Dr. Yosuke Ashikari and Prof. Andrew J. Boydston from University of Washington provided assistance with the polymerization studies as well as the initial characterization of the polymers. Dr. Lev N. Zakharov conducted the X-ray crystallographic studies. Editing was provided by Prof. Ramesh Jasti.

1.1. Introduction

Strained organic molecules provide a unique platform on which the reactivity associated with the inherent strain can be exploited to fulfill chemical transformations that are otherwise difficult or impossible.[1-7] Representative examples are copper-free Huisgen 1,3-dipolar cycloaddition of cyclooctynes[2-4] and cycloheptynes[8] that has been widely employed in biological systems, and the ring opening metathesis polymerization

(ROMP) of norbornenes and oxonorbornes that gives access to functional polymeric materials with unique topologies.[9-10]

Over the last two decades, conformationally distorted aromatic macrocycles have been gaining increasing attention due to their aesthetic molecular architectures, unique solid state packing motifs as well as useful physical properties for potential material applications.[11-12] Similar to the case of strained small molecules, the imposed ring strain in macrocycles influences their chemical behaviors.[6-7, 13] On one hand, this can lead to enhanced chemical reactivity compared to the acyclic (non-strained) analogues. On the other hand, it can cause instability and result in unwanted reaction pathways that complicate the synthetic design. Thus, understanding the mechanism of the strain-related reactivity in macrocycles is beneficial for the design and synthesis of novel macrocyclic architectures, and will offer guidance for the construction of complex functional materials using the strained macocycles as building blocks.

This chapter focuses on the survey of the studies on the reactivity of strained macrocycles. Discussions are divided into three major aspects: (1) anomalous chemical transformations, (2) strain-promoted cycloadditions and (3) enthalpy-driven ring opening polymerization/oligomerization.

1.2. Anomalous Chemical Transformations

The abnormal chemical behaviors of strained cyclophanes have been well documented.[6-7] As early as in 1978, Bickelhaupt and coworkers discovered that the photo irradiation induced the valence isomerization of strained [6]paracyclophane **I.1** to form the Dewar-type isomer **I.2**.[14] Later in 1990, Tobe and coworker observed a similar transformation wherein [6](1,4)naphthalenophane **I.3** isomerized to **I.4** upon photo irradiation (**Figure 1.1**).[15] Such transformation was not possible for non-strained benzene and naphthalene derivatives under similar conditions. Tobe and coworkers attributed this unique valence isomerization to the extreme level of strain that forces the bridged ring to adopt a boat-like conformation thus lowering the activation energy of the transformation. The reverse isomerization to regain aromaticity was also observed upon thermal activation.
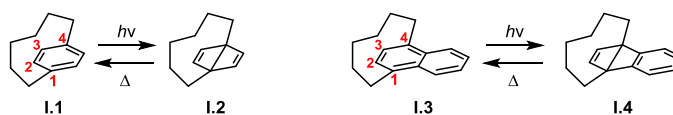
Figure 1.1. Reversible photochemical valence isomerization of [6]paracyclophane (**I.1**) and [6](1,4)-naphthalenophane (**I.3**).[14-15]

Anthracene is well known to undergo photo-induced [4+4]-cycloaddition to give dimeric product joined at the C9 and C10 positions.[16] However, irradiation of [6](1,4)anthracenophane **I.5** afforded a series of [2+2]-dimers (e.g. **I.6a-b**) of which two anthracene moieties are connected at C1 and C2 (**Figure 1.2**).[17] Neither the [4+4]-photodimer **I.7** nor the Dewar-type isomer **I.8** were formed. The lack of stereoselectivity of the observed [2+2]-cycloaddition indicated that the process proceeds via the excited triplet state, which is different from the case of [4+4]-cycloaddition and valence isomerization that proceed via the excited singlet state. Thus, it was suggested that the distorted anthracene undergoes facile intersystem crossing upon photoexcitation, leading to the population of triplet state that favors the [2+2]-cycloaddition. Additionally, computational studies indicated that the C1-C2 bond has an enhanced double bond character which might also influence the photochemical process.
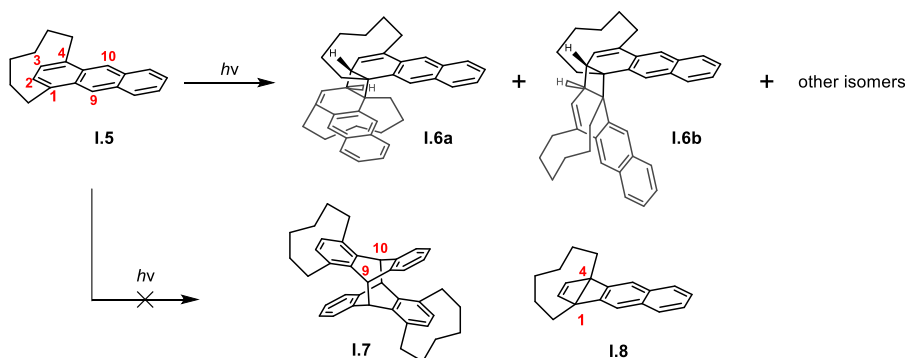
Figure 1.2. Anomalous photo-induced [2+2]-dimerization of [6](1,4)-anthracenophane (**I.5**).[17]

Furthermore, **I.5** reacted rapidly with tetracyanoethylene (TCNE) in a polar solvent (dichloromethane), giving exclusively [2+2]-adduct **I.9** instead of [4+2]-adduct

3

I.10 (**Figure 1.3**).[18] This was also explained by the enhanced double bond character of C1-C2 bond. It was proposed that the reaction is likely to take place via a zwitterion intermediate **I.11** that releases strain energy in the bridged ring.
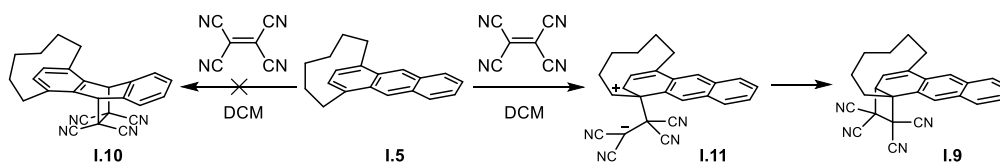
Figure 1.3. [2+2] Cycloaddition of **I.5** with TCNE to form **I.9** via possible zwitterion intermediate **I.11**.[18]

In 2016, Jasti and coworkers reported the ring strain-releasing cationic rearrangement of a [8]cycloparaphenylene derivative **I.12** (**Figure 1.4**).[19] Subjecting **I.12** to cationic Scholl reaction conditions resulted in a complex mixture of isomeric products (e.g. **I.13**) rather than the target triphenylene cycle **I.14**. Computational investigations implied that the rearrangement via 1,2-aryl shift with a presumable cationic intermediate **I.13a** is thermodynamically and kinetically favored over the formation of **I.14** via a possible intermediate **I.14a**. This study provides a valuable insight that chemical transformations involving cationic intermediates should be avoided when designing synthetic sequence using strained macrocycles as starting materials.
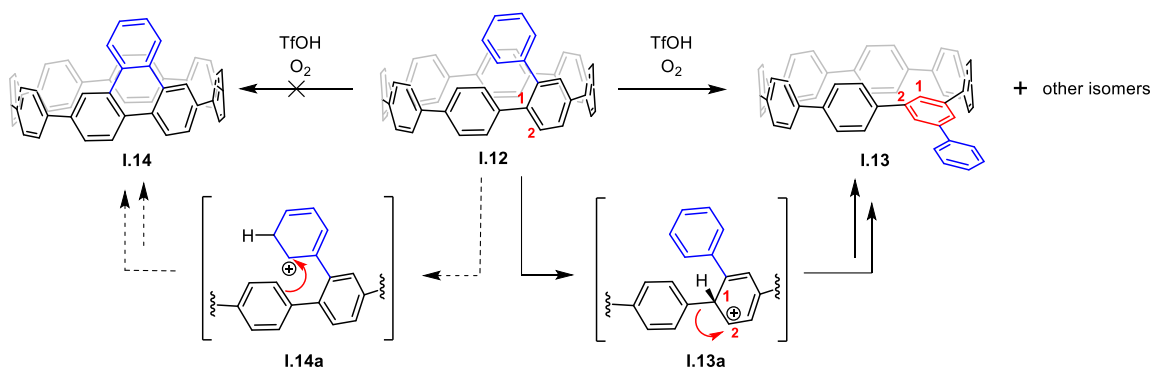
Figure 1.4. Cationic rearrangement of nanohoop **I.12** under Scholl reaction conditions.[19]

4

1.3. Strain Promoted Cycloaddtions

Angle-strained cycloalkynes experience copper-free Huisgen 1,3-dipolar cycloaddition with azides.[2-3] This facile transformation is well-tolerated in cellular system, and has been recognized as a powerful tool in bioorthogonal chemistry.[3] There are so far only two examples that study the reactivity of strained macrocyclic alkynes.

In 2016, Stoddart and coworkers reported a tetracationic bisalkyne cyclophane **I.15** that undergoes tandem cascading cycloadditions with dienes and azides (**Figure 1.5**).[20] The enhanced reactivity of **I.15** towards azides and dienes is attributed to the electron-deficient pyridinium units and the ring strain in the cyclophane backbone. Reactions of **I.15** with cyclopentadiene and 1-azidoadamantane afforded bis-adducts **I.16** and **I.17** respectively in high efficiency. It is noteworthy that the mono-adducts **I.16a** and **I.17a** were not observed during the reactions by NMR. Computational modeling indicated that the alkyne in the mono-adducts (**I.16a** and **I.17a**) is more strained than the alkynes in the starting material **I.15**. This resulted in a much more reactive alkyne for the consecutive cycloaddition. Such cooperative reactivity wherein the first reaction activates the second is expected to be of use to prepare complex molecular structures.
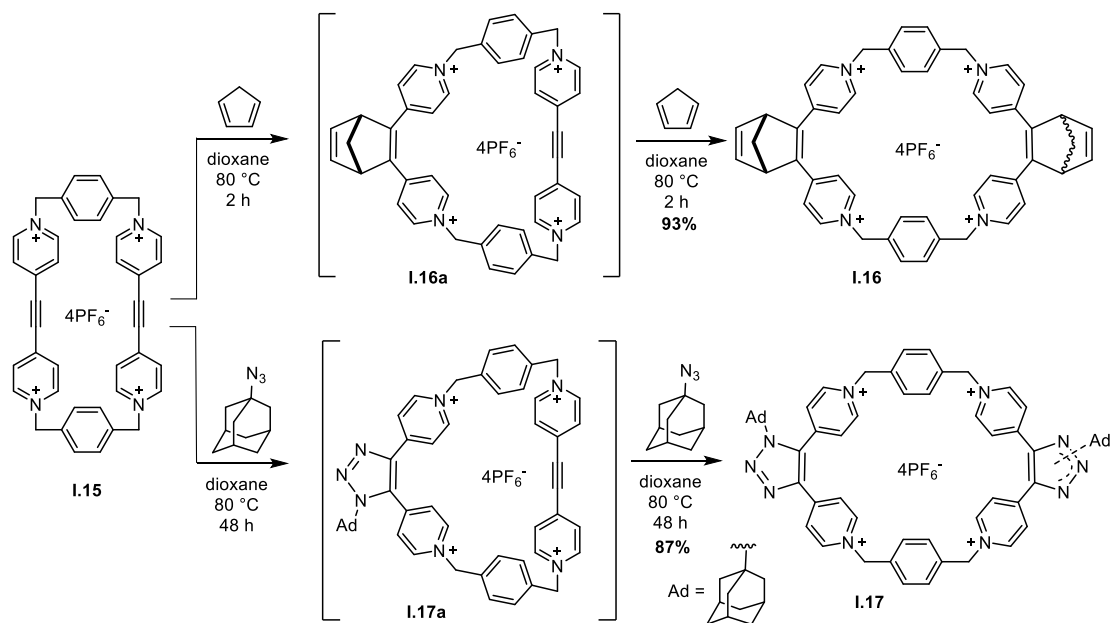
Figure 1.5. Tandem cascading cycloadditions of tetracationic cyclophane **I.15** via highly reactive mono-adducts **I.16a** and **I.17a**.[20]

5

A concurrent report from the Moore group disclosed the synthesis of a strained alkyne-embedded macrocycle **I.21** that is capable of undergoing three-fold 1,3-dipolar cycloaddition with azides (**Figure 1.6**).[21] Utilizing alkyne metathesis with catalyst **I.19**, V-shaped building unit **I.18** was efficiently assembled into macrocycle **I.20** in a quantitative yield. The subsequent reductive aromatization using sodium naphthalenide (NaNaph) afforded strained macrcocyle **I.21** with a strain energy of 47.8 kcal/mol. The alkyne angle of **I.21** was calculated to be 166°, which is comparable to the values of cycloalkynes reported by Bertozzi.[3] When heated at 50 °C, **I.21** reacted with three equivalent of azide **I.22** to form tris-triazo compound **I.23** as a mixture of two isomers. The thermodynamics of the multi-fold cycloaddition was theoretically investigated, suggesting that the enthalpy gain via release of strain in each cycloaddition increases as the reaction proceeds. This macrocycle represents a useful building block for complex carbon-rich architectures.
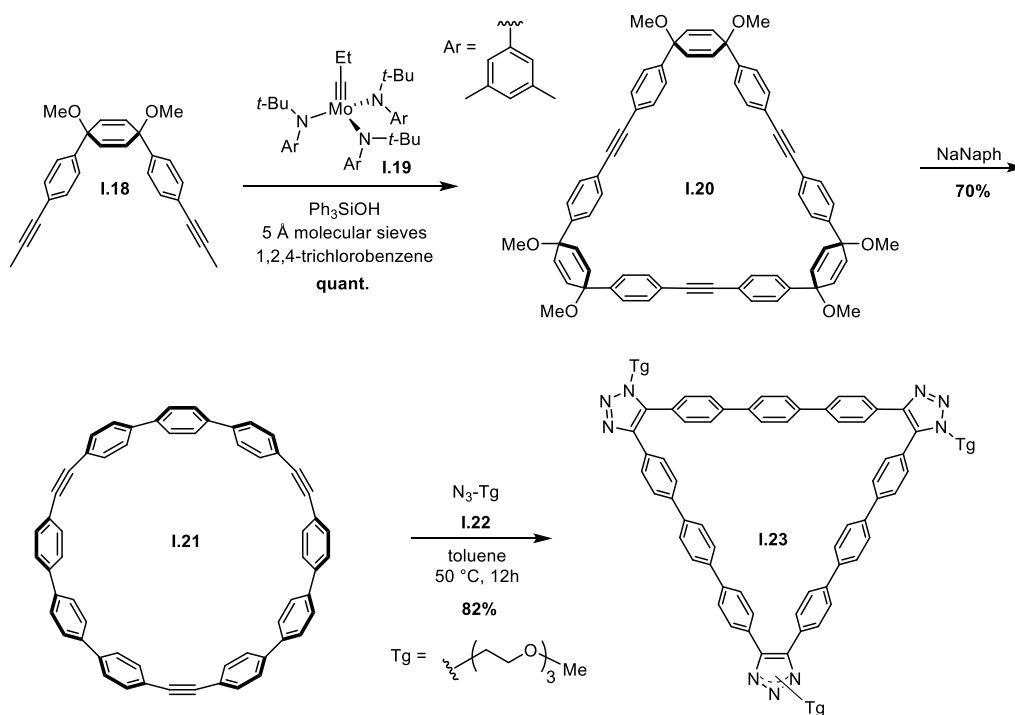
Figure 1.6. Alkyne metathesis as an efficient strategy to synthesize macrocyclic alkyne (**I.21**) and the strain-promoted cycloaddition of **I.21** with azide **I.22**.[21]

1.4. Enthalpy-Driven Ring Opening Polymerization/Oligomerization

Ring-opening polymerization (ROP) is a well-established strategy in polymer chemistry to access structurally and chemically unique polymeric materials.[22-23] With the development of stable and functionality-tolerant ruthenium-based metathesis catalysts, ring opening metathesis polymerization (ROMP) has emerged as one of the most popular methods of ROP.[24] The most widely used ROMP monomers are strained bicyclic olefins including norbornenes and oxonorbornenes.[9-10] The ring strain stored in the cyclic system provides the enthalpic driving force for chain growth and compensates for the entropy loss in the ROMP process. However, the enthalpy-driven ROMP of strained macrocyclic monomers is under explored with only a few examples.

Bazan and coworkers pioneered the ROMP of strained paracyclophanes in 1994.[25] Schrock-type molybdenum carbene complex **I.25** was discovered to initiate the polymerization of **I.24** to produce polymer **I.26** with high regio-regularity (98% *cis*-double bond) and a narrow polydispersity of 1.1 (**Figure 1.7a**), indicating a living polymerization process. The ROMP of paracyclophanes was later applied to synthesize well-defined poly(*para*-phenylvinylene) (PPV), which was not achievable using the Gilch polymerization method. To circumvent the synthetic challenge posed by the insolubilty of unsubstituted PPV units, paracyclophane **I.27** with a solubilizing silyloxy group was designed as the masked precursor for unsubstituted PPV polymers (**Figure 1.7b**).[26] Indeed, ROMP of **I.27** with **I.25** formed a soluble and monodispered polymer **I.28**, which was successfully converted to the target PPV **I.29**.
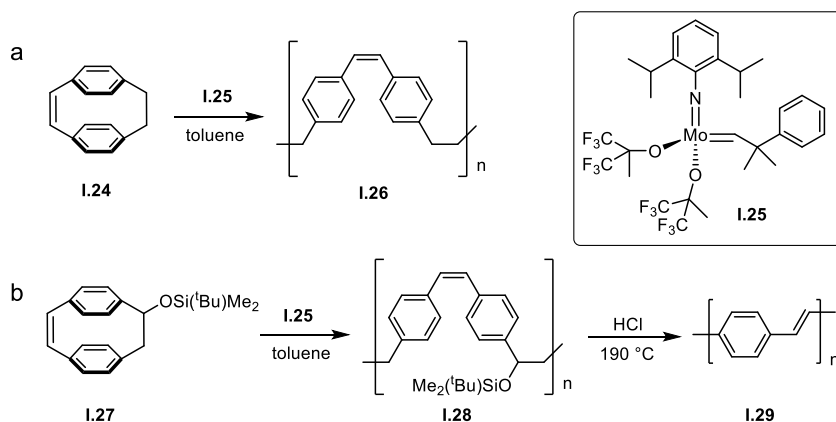
Figure 1.7. a) ROMP of paracyclophane **I.24** with Schrock initiator **I.25**. b) ROMP of paracyclophane **I.27** toward the synthesis of PPV polymer **I.29**.[26]

In order to produce soluble PPV polymers with improved processibility, a series of substituted cyclophane precursors such as **I.30**-**32** were designed by the groups of Turner[27-28] and Bunz[29] (**Figure 1.8**). Bench stable Ruthenium complexes **I.33** or **I.34** were utilized as the initiator for the synthesis of highly functionalized polymer **I.35-37**. Satisfyingly, moderate to good polydispersities were achieved. Additionally, the molecular weight of these polymer could be controlled by varying the monomer to initiator ratio, demonstrating that the polymerizations are living and controlled. These synthetic developments have further allowed access to a variety of PPV polymers with different optical and electronic properties.
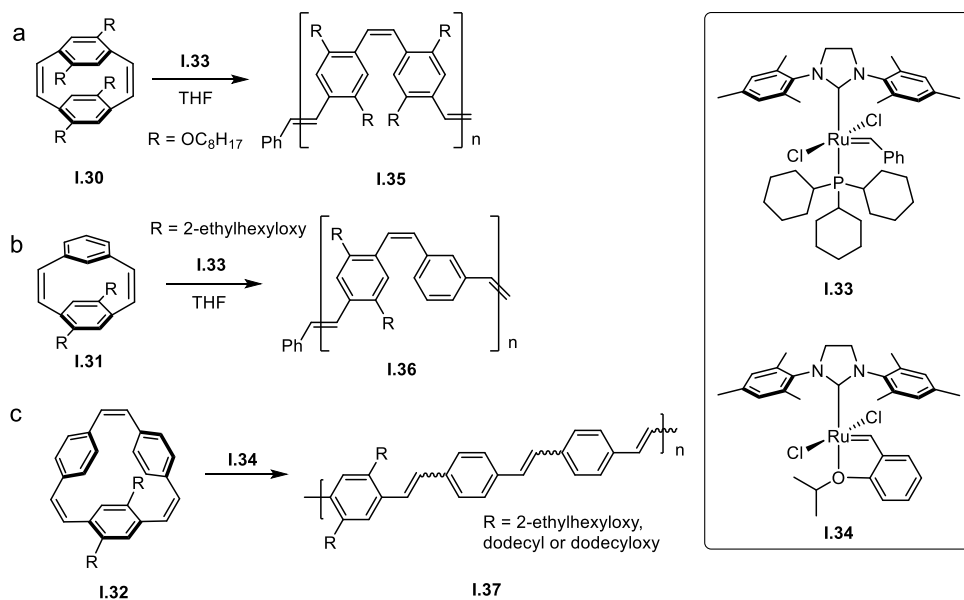
Figure 1.8. a-c) ROMPable functionalized cyclophanes (**I.30-32**) as the precursors for PPV related polymers.[27-29]

In 2008, Nuckolls and workers reported the living ROMP of dibenzo[a,e]-[8]annulene **I.38** which is composed of a "kinked" *trans* alkene that is distorted out of planarity and an expanded *cis* double with an angle of 142° (**Figure 1.9**).[30] Polymer **I.40** with polydispersity below 1.1 was achieved using initiator **I.39** and ancillary tricyclophenylphosphane and the molecular weight was controllable via the variation of

monomer to initiator ratio. Additionally, equal amount of *cis* and *trans* double bonds in the polymer backbone was observed in ^{1}H NMR. This high regio-regularity was ascribed to the selective metathesis of the *cis* double bond which is more strained and possesses the majority of the HOMO (highest occupied molecular orbital) density.
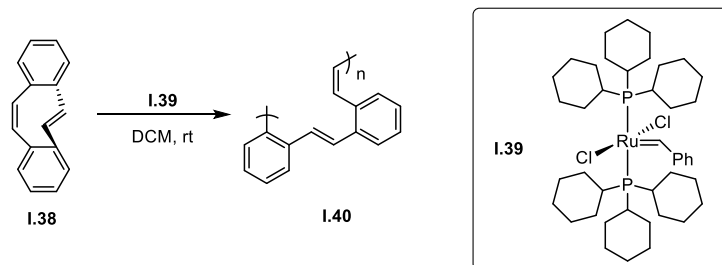
Figure 1.9. ROMP of kinked dibenzo[a,e]-[8]annulene **I.38**.[30]

Strained ene-yne annulene **I.41** was first synthesized by Sondheimer and coworkers in 1974.[31] Due to the severe ring string introduced by the triple bond, **I.41** is unstable and decomposes rapidly at ambient conditions. New reactivity of **I.41** with alkene and alkyne metathesis catalysts was disclosed also by the Nuckolls group in 2008 (**Figure 1.10a**).[32] Interestingly, the metathesis reaction of **I.41** with Ruthenium complex **I.33** yielded structurally unique trimeric products **I.42a-b**, presumably via an alkyne-trimerization mechanism. ROMP of **I.41** was initiated by Schrock alkyne metathesis catalyst **I.43** to form polymer **I.42c** with a polydispersity of 2.4. The relatively broad polydispersity was caused by the inefficient chain initiation as well as the low solubility of the monomer. Later in 2010, the same group designed a stable and functionalized [8]annulene **I.44** with improved stability.[33] Living ROMP of **I.44** was achieved utilizing tungsten complex **I.43** and 2-nitrophenol as activating ligand (**Figure 1.10b**). The resulted monodispersed (PDI < 1.1) polymer **I.45** possess a unique chemical sequence that can be exploited to create novel properties.

9
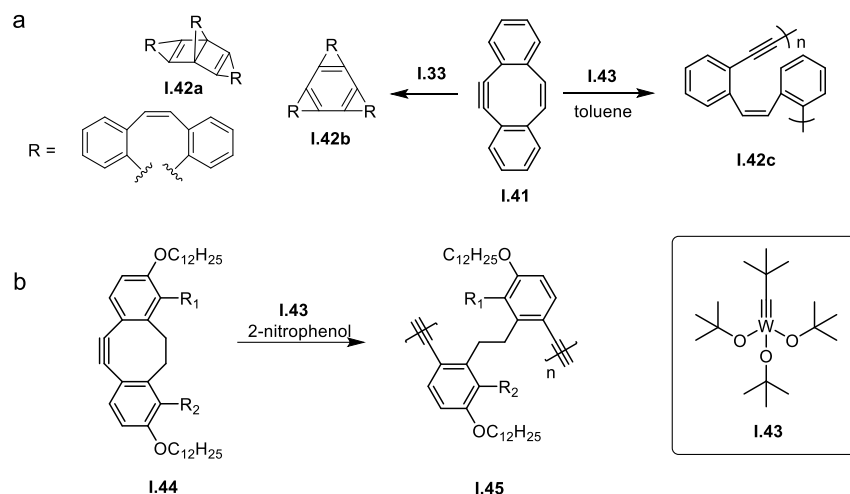
Figure 1.10. a) Reactivity of a strained ene-yne annulene (**I.41**) with alkene metathesis catalyst **I.33** and alkyne metathesis catalyst **I.42**.[32] b) ROMP of strained alkyne **I.44**.[33]

In 2001, reports from Colquhorn and coworkers described the ring-expanding oligomerization of a strained ether-sulfone macrocycle **I.47**, which was synthesized via nickel-mediated intramolecular homocoupling of **I.46** (**Figure 1.11**).[34] The high ring strain is evident as crystallographic analysis showed that the biphenylene unit is severely distorted from collinearity. In dilute solution at 150 °C, the ring expansion of **I.47** was triggered by catalytic amount of nucleophilic fluoride ion, forming less strained larger cyclic oligomers **I.48**.
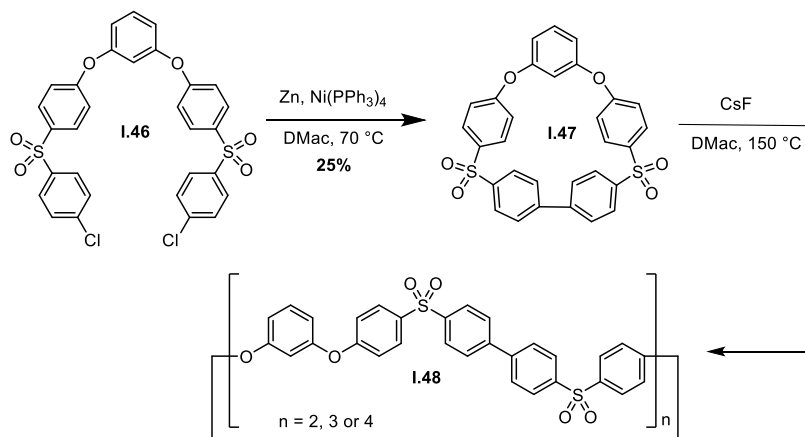
Figure 1.11. Ring-expanding oligomerization of strained macrocycle **I.47** synthesized from intramolecular homocoupling of **I.46**.[34]

10

Four years later in 2005, the same group reported the first example of enthalpy-driven nucleophilic ring opening polymerization (ROP) of macrocyclic monomers (**Figure 1.12a**).[35] Similar to the synthesis of **I.47**, nickel-catalyzed intramolecular coupling was applied to access the strained biaryl macrocycle **I.50** from the precursor **I.49**. ROP of **I.50** was best initiated with potassium 4,4'-biphenoxide, producing soluble and high molecular weight polymer **I.51** with high conversion. A random distribution of monomer sequence was observed for **I.51**, which is due to the existence of two ring-opening sites on the macrocycle. In comparison, the analogous polymer **I.52** prepared form the polycondensation method exhibited simple alternating monomer consequence (**Figure 1.12b**). Compared to **I.52,** polymer **I.51** exhibited higher viscosity, a key parameter for thermoplastic processing, demonstrating that ROP of strained macrocyclic monomers is a useful strategy to synthesize high performance polymeric materials.
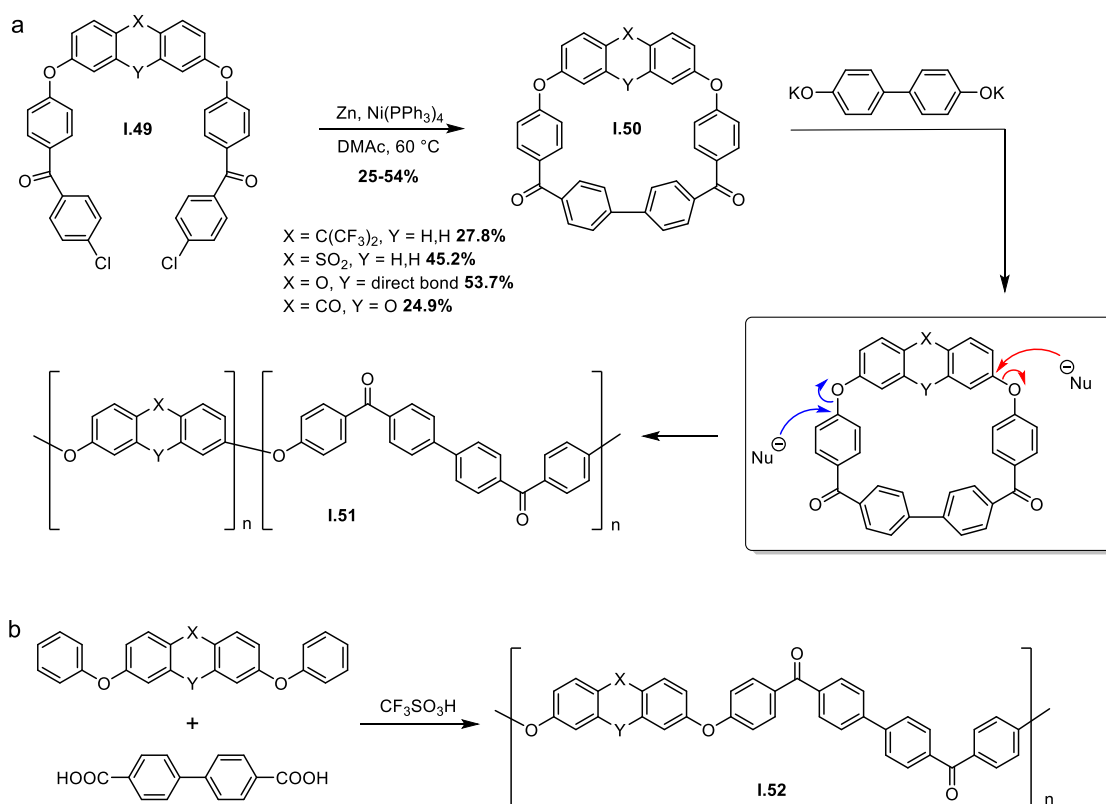
Figure 1.12. a) Ring opening polymerization of strained biaryl macrocycle **I.50** to form random polymer **I.51**. b) Polycondensation to synthesize polymer **I.52**.[35]

11

1.5. Bridge to Chapter II

Central to the theme of this dissertation is the design of strained aromatic macrocycles as building blocks for the construction of function materials. This chapter serves to provide a background for strain-promoted transformations in macrocyclic systems, an aspect that is crucial to the whole dissertation. In Chapter II, we describe our early efforts in systematically probing the structure-property relationships of strained oligophenylene macrocycles.

CHAPTER II

THE EFFECTS OF CYCLIC CONJUGATION AND BENDING ON THE
OPTOELECTRONIC PROPERTIES OF PARAPHENYLENES

From Li, P.; Sisto, T. J.; Darzi E. R.; Jasti, R., The Effects of Cyclic Conjugation and Bending on the Optoelectronic Properties of Paraphenylenes. *Org*. *Lett*. **2014,** *16* (1), 182-185.

Cycloparaphenylenes (CPPs) have optoelectronic properties that are unique when compared to their acyclic oligoparaphenylene counterparts. The synthesis and characterization of two bent heptaphenyl-containing macrocycles has been achieved in order to probe the effects of bending and cyclic conjugation on the properties of the CPPs. The study suggests that both bending and cyclic conjugation play a role in the novel properties of the CPPs.

2.1. Introduction

The [n]cycloparaphenylenes (CPPs) are structurally unique macrocycles consisting of *n* para-linked benzene units (**Figure 2.1**). Since first synthesized and characterized in 2008, numerous routes to a variety of [n]CPPs have been reported by the Jasti,[1-6] Itami,[7-10] and Yamago[11-14] laboratories. Although often cited for their potential application in the bottom-up growth of uniform carbon nanotubes,[15-18] the CPPs have unique optoelectronic properties in their own right. As new conjugated organic materials, the CPPs are attractive due to their size-dependent optoelectronic properties,[1,2,12] as well as their guest-host properties[4,19-21] and highly porous solid state structures.[5,8,9,13] The CPPs have increasing HOMO energies and decreasing LUMO energies (narrowing band gap) with decreasing molecular size.[12] This behavior is exactly opposite to that observed in the case of acyclic paraphenylenes.[21-22] In addition, solubility of the CPPs is vastly improved as compared to the linear oligoparaphenylenes, presumably due to differences in the number of intermolecular π-π contacts accessible when comparing nonplanar compounds to flat linear compounds (*vide infra*). All known CPPs (sizes [6]-[18]CPP)

13

are soluble, while unsubstitued paraphenylenes larger than sexiphenyl are completely insoluble.[23]

When rationalizing the origin of the unique optoelectronic properties of the CPPs versus acyclic oligoparaphenylenes, the most obvious structural differences are the bent phenylene units, the cyclic conjugation, and the smaller torsional angles of the CPPs.[24] A fundamental understanding of the effects that structure has on optoelectronic properties is paramount when designing better-performing conjugated organic materials.[24-28] To probe the effects these structural characteristics have on the properties of the CPPs, we have synthesized alkyl-tethered heptaphenyl-containing macrocycles **II.1** and **II.2** (**Figure 2.1**). Drawing inspiration from the related studies by Bodwell and coworkers,[29-32] we recognized that we can systematically vary the degree of bending of the heptaphenyl moiety through the insertion of various length alkyl chains into the backbone of a macrocycle. This alkyl tether also serves to break the conjugation of the macrocycle. Comparison of [7]CPP to macrocycle **II.1** by cyclic voltammetry, absorption, and fluorescence experiments allows for an approximation of the effect of cyclic conjugation due to their similar degrees of bending and torsional angles (*vide infra*). Comparison of **II.1**, **II.2**, and linear heptaphenyl **II.3** allows for insight into the effects of bending. Herein, we report the syntheses and characterization of **II.1** and **II.2** in order to gain insight into these phenomena.
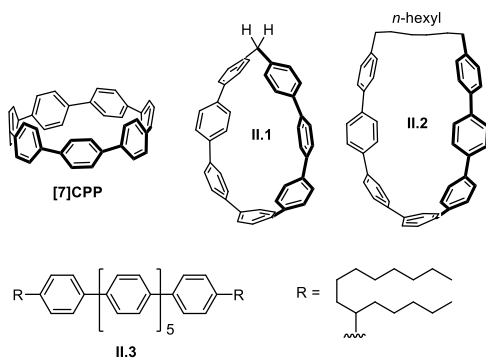
Figure 2.1. DFT optimised geometries of [7]CPP, **II.1** and **II.2**, along with previously reported linear heptaphenyl **II.3**.[22]

2.2. Results and Discussion

2.2.1. Synthesis

Our strategy for the synthesis of **II.1** and **II.2** relies upon the 3,6-*syn*-dimethoxycyclohexa-1,4-diene moieties of fragment **II.6** as masked arene units to provide the curvature necessary for a macrocyclization reaction with tethers **II.9** and **II.10** (**Schemes 2.1** and **2.2**). Subsequent aromatization of the resultant macrocycles would lead to **II.1** and **II.2**. To synthesize **II.6**, we began with lithium halogen exchange of **II.4**[2] followed by addition of monoketal protected benzoquinone (**Scheme 2.1**). Subsequent deprotection of the crude reaction mixture at room temperature with 10% aqueous acetic acid yields hydroxy ketone **II.5** in 90% yield over 2 steps. Deprotonation of **II.5** with NaH at −78 °C leads to a charged sodium alkoxide that directs addition of lithiated 1,4-bromochlorobenzene in a diastereoselective manner.[2] This addition is followed by a simple iodomethane quench to lead directly to dichloride **II.6** in 90% yield. Noteably, this synthesis can readily produce tens of grams of **II.6** from commercially available quionone monoketal using standard two-liter glassware. Synthesis of alkyl tethered coupling partners **II.9** and **II.10** began with dibromides **II.7**[33] and **II.8**,[34] and is achieved in 90% and 99% yield respectively through simple lithium halogen exchange and subsequent quench with isopropoxyboronic acid pinacol ester (**Scheme 2.1**).

With the necessary fragments in hand, we turned our attention to preparing the macrocyclic precursors to structures **II.1** and **II.2**. A Suzuki coupling[34] of dichloride **II.6** and either bisboronate **II.9** or **II.10** formed macrocycles **II.11** and **II.12** in 14% and 21% yield respectively. The yields are predictably low due to the high strain of the macrocycles and the indiscriminate nature of the coupling reaction, which leads to high amounts of oligomerization. Subjecting macrocycles **II.11** and **II.12** to single electron reductant sodium napthalenide at −78 °C gives bent heptaphenyls **II.1** and **II.2** in 39% and 47% yield respectively. Characterization by NMR (^{1}H and ^{13}C), IR, and MALDI-TOF confirmed the structural assignment.
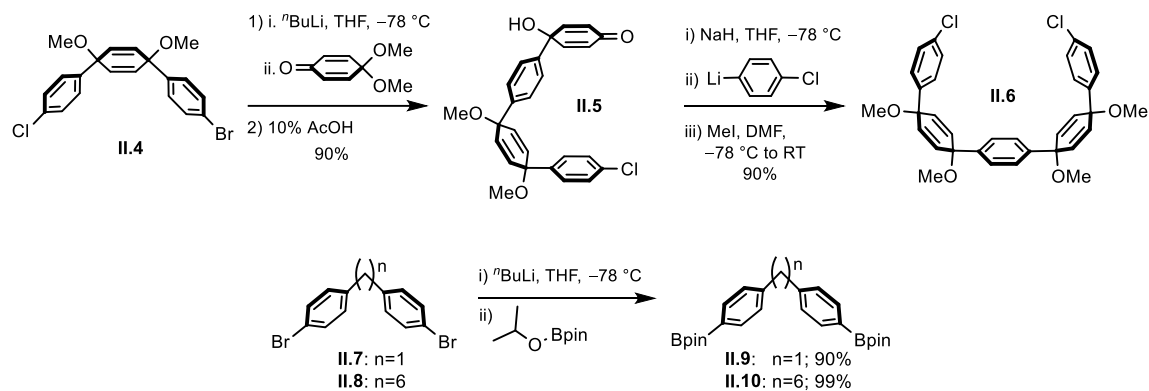
Scheme 2.1. Synthetic route to coupling partners **II.6**, **II.9** and **II.10**.
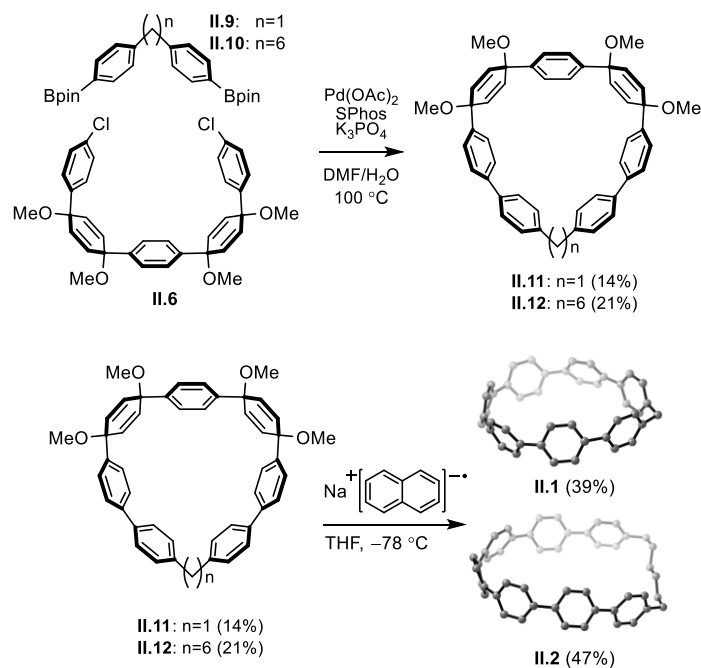
Scheme 2.2. Macrocyclization and aromatization reactions to prepare bent *p*-heptaphenyls **II.1**, and **II.2**.

2.2.2. Photophysical and Electrochemical Properties

With the syntheses complete, we next probed the electronic differences between each molecule utilizing cyclic voltammetry (**Table 2.1**). Similar to all CPPs, [7]CPP shows a reversible peak in the negative potential range corresponding to a reduction wave with a half-wave potential of -2.57 V (vs. Fc/Fc$^+$), along with a reversible peak in the

possitive potential range, corresponding to an oxidation wave with a half-wave potential of 0.53 V (vs. Fc/Fc$^+$). Compound **II.1** exhibits a quasi-reversible peak corresponding to a reduction wave, however the half-wave potential is significantly higher at -2.74 V (vs. Fc/Fc$^+$). Additionally, the oxidation of **II.1** is irreversible with an on-set potential at 0.63 V (vs. Fc/Fc$^+$). Since macrocycle **II.1** contains phenylene units close to as bent as [7]CPP and the torsional angles between phenyl units are also similar (*vide infra*), one can conclude that cyclic conjugation plays a substantial role in raising the HOMO and lowering of the LUMO in the CPPs. Similar to macrocycle **II.1**, structure **II.2** has a quasi-reversible peak corresponding to a reduction wave with a half-wave potential at -2.75 V (vs. Fc/Fc$^+$) and an irreversible peak corresponding to an oxidation wave with an onset potential of 0.71 V (vs. Fc/Fc$^+$). Macrocycles **II.1** and **II.2** are very similar with only a slight increase in potentials as compared to the difference between [7]CPP and **II.1**. The oxidation potential of **II.3**, as reported by Rathore,[21] shows a first half-wave of 1.4 V versus SCE, which correlates to a half-wave potential of 1 V versus Fc/Fc$^+$. This large difference in oxidation potentials between **II.2** and **II.3** provides experimental evidence for bending in oligophenylenes also leading to narrowing of bandgaps (i.e. raising of the HOMO and lowering of the LUMO).

Table 2.1. Cyclic voltammetry data for [7]CPP, **II.1**, **II.2** and **II.3**. (V versus ferrocene/ferrocenium couple)

entry	E_{red} (V) (half-wave)	E_{ox} (V) (onset)
[7]CPP	−2.57	0.47
II.1	−2.74	0.63
II.2	−2.75	0.71
II.3[22]	N/A	1.0

Next we investigated the UV-Vis and fluorescence spectra of the new bent heptaphenyl-containing macrocycles in order to compare with [7]CPP. Macrocycle **II.1** displayed an absorption maximum of 321 nm along with a small shoulder peak at 390 nm (**Figure 2.2** and **Table 2.2**). The extinction coeffecients for these features are 5.15×10^4 M^{-1}cm^{-1} and 0.814×10^4 M^{-1}cm^{-1} respectively. Macrocycle **II.2** has a similar absorption

pattern, displaying one large absorption maximum and one smaller shoulder peak (λ_{abs1} = 319 nm, $\varepsilon_1 = 4.45 \times 10^4$ M^{-1}cm^{-1}; λ_{abs2} = 375 nm, $\varepsilon_2 = 1.43 \times 10^4$ M^{-1}cm^{-1}). For comparison, [7]CPP displays an absorption maximum at 340 nm ($\varepsilon = 6.58 \times 10^4$ M^{-1}cm^{-1}) along with a very weak shoulder peak at 408 nm ($\varepsilon = 0.316 \times 10^4$ M^{-1}cm^{-1}). Linear heptaphenyl **II.3** displays a single absorption at 326 nm with an extinction coefficient of 9.16×10^4 M^{-1}cm^{-1}.[22] Noteably, the HOMO-LUMO transition that is forbidden in the CPPs (the minor red-red-shifted absorption) becomes more prominent as symmetry is broken by the alkyl tether.[24,36,37] A large difference also exists between the wavelength of the HOMO-LUMO transitions of the bent molecules when compared to the linear paraphenylene, consistent with cyclic voltammetry data. TD-DFT calculations confirm this trend by showing that the $\lambda_{HOMO-LUMO}$ blue shifts while the oscillator strength increases moving from [7]CPP through the methylene spaced heptaphenyl macrocycles (1-20 methylenes, see **Figure 2.12**). Fluorescence data was also collected for each of the final compounds (**Figure 2.2** and **Table 2.2**). [7]CPP displays a weak fluorescence emission at 588 nm ($\phi_f = 0.006$), while **II.1** and **II.2** emit strongly at blue-shifted values of 502 nm ($\phi_f = 0.23$) and 469 nm ($\phi_f = 0.25$). Acyclic analogue **II.3** is reported to emit at 408 nm, interestingly with a much higher quantum yield of 1.0.[22]
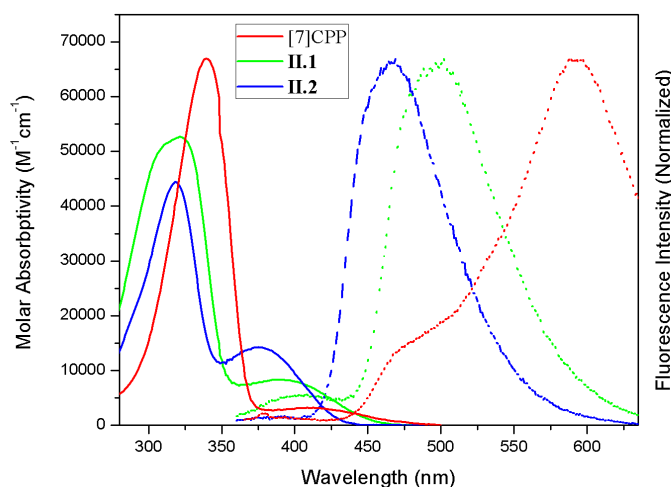
Figure 2.2. UV-vis absorption and fluorescence for [7]CPP, **II.1**, and **II.2**.

Table 2.2. Summary of the experimental and calculated optoelectronic data of [7]CPP, **II.1**, **II.2** and **II.3**.

entry	λ_{abs1} (nm)	$\varepsilon_1 \times 10^4$ (M^{-1}cm^{-1})	λ_{abs2} (nm)	$\varepsilon_2 \times 10^4$ (M^{-1}cm^{-1})	λ_{em} (nm)	φ_F	λ'_{abs1} (nm)	λ'_{abs2} (nm)
[7]CPP	340	6.58	408	0.316	588	0.006	340	475
II.1	321	5.15	390	0.814	502	0.23	321	412
II.2	319	4.45	375	1.43	469	0.25	325	395
II.3[9]	326	9.16	NA	NA	408	1.0	343	NA

2.2.3. Theoretical Investigation

In order to further understand the molecular geometry and electronic structures of this class of molecules, we performed theoretical calculations for bent heptaphenyls with methylene tether lengths from one to twenty carbons (**Figure 2.3**). [7]CPP and linear *p*-heptaphenyl were also calculated for comparison. Predictably, as the tether is increased in size the heptaphenyl becomes less bent. As this occurs, the HOMO energies decrease while the LUMO energies increase, though structural anomalies provide small fluctuations within the larger overall trend. In addition, we observe a trend of slightly increasing average torsional angles when moving from [7]CPP to macrocycle **II.1** to macrocycle **II.2** to acyclic analogue heptaphenyl (25.5°, 29.9°, 30.3°, and 36.3° respectively). When evaluating the data, the most important finding was the significant difference between the bandgap of [7]CPP and any tethered macrocycle, presumably due to cyclic conjugation. Furthermore, another large difference exists between the HOMO energy level of the largest tethered macrocycle and linear heptaphenyl.

2.3. Outlook and Conclusion

In the last eight years, the cycloparaphenylenes have become synthetically accessible in various sizes and on gram-scale. Throughout the development of these syntheses, characterization of the optoelectronic properties of the cycloparaphenylenes has revealed striking differences when compared to acyclic paraphenylenes. We have demonstrated experimentally that there are two structural features, bending and cyclic conjugation, that play a prominent role in the optoelectronic differences between the CPPs and OPPs. By breaking the cyclic conjugation of [7]CPP with one methylene, we

have shown that this similarly bent heptaphenyl **II.1** is significantly harder to oxidize and reduce. Decreasing the bending of the heptaphenyl unit by increasing the macrocycle tether length results in a minor increase in the oxidation and reduction potentials. Similarly, we have shown that bent heptaphenyl has substantially different optical properties compared to acyclic heptaphenyl, while being much easier to oxidize and reduce. This series of compounds has allowed for the experimental demonstration that the bending and cyclic conjugation of the CPPs provides optoelectronic characteristics and solubility rendering them novel building blocks to new conjugated organic materials.
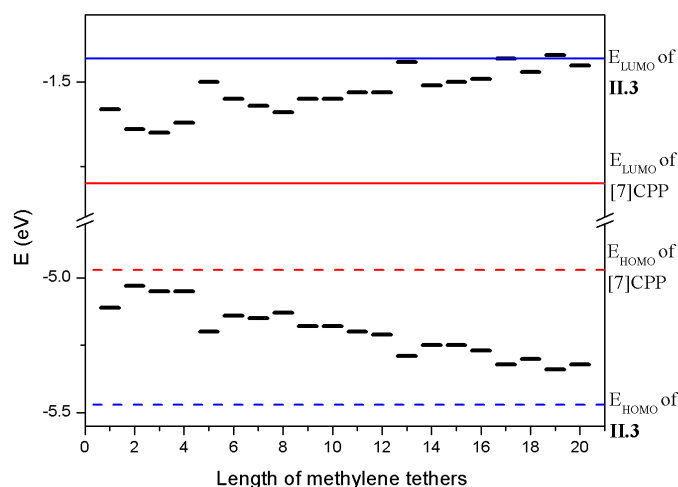
Figure 2.3. DFT calculated HOMO and LUMO energies for [7]CPP, liear *p*-heptaphenyl, *p*-heptaphenyl macrocycles with tether length from 1 to 20 methylenes.

2.4. Experimental Sections

2.4.1. General Experimental Details

Moisture and oxygen sensitive reactions were carried out under nitrogen atmosphere using standard syringe/septa technique. All the glassware was thoroughly washed, dried in oven at 140°C overnight and cooled under nitrogen atmosphere before use. All reagents were obtained commercially. Bis(4-bromophenyl)methane and 1,6-Bis(4-bromophenyl)-*n*-hexane were prepared following known literature procedure.[33-34] Tetrahydrofuran, dichloromethane and dimethylformamide were dried by filtration through alumina according to the method descried by Grubbs.[38] Silica column

20

chromatography was conducted with Zeochem Zeoprep n60 Eco 40-63 µm silica gel. Thin Layer Chromatography (TLC) was performed using Sorbent Technologies Silica Gel XHT TLC plates. Developed plates were visualized using UV light at wavelength of 254 and 365 nm.

^{1}H NMR spectra and ^{13}C NMR spectra were recorded respectively at 500 MHz and 125 MHz on a Varian VNRS. Deuterated chloroform was used as NMR solvent for all the compounds and all spectra were referenced to TMS. The matrix used for MALDI was a solution of 7,7,8,8-tetracyanquinodimethane in THF with 1% silver trifluoroacetate as a promoter.[38]

2.4.2. Synthetic Details
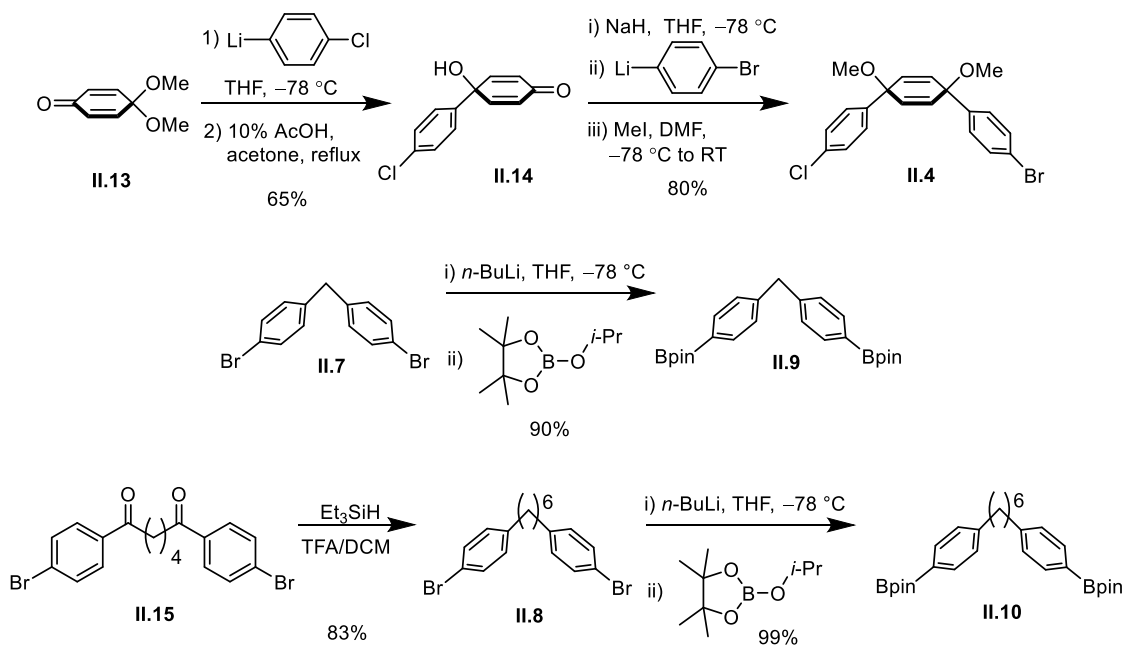
Scheme 2.3. Synthesis of key intermediates **II.4**, **II.9** and **II.10**.

4'-Chloro-1-hydroxy-[1,1'-biphenyl]-4(1H)-one **II.14**
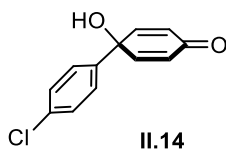
The procedure for **II.14** was adapted from prior literature procedures.[39]

21

4-Chloro-1-bromobenzene (74.3 g, 0.388 mol, 1.5 eq) was dissolved in THF (300 mL) and cooled to −78°C. *n*-BuLi (2.5 M in hexanes, 120 mL, 0.427 mol, 1.1 eq) was added dropwise via addition funnel. The reaction was stirred for 30 minutes at −78°C to give the lithiated species as a milky white solution.

After 30 minutes, **II.13** (15 g, 97.4 mmol, 1 eq) was injected neat. The reaction was stirred for 1.5 hours at −78°C. The reaction was quenched with H_2O and allowed to warm to room temperature. The mixture was extracted with DCM. After separation of the phases, the aqueous layer was washed with DCM (3×50 mL). The combined organic layers were washed with brine and dried over sodium sulfate before being filtered and concentrated down to a solid. The solid was carried on crude.

The solid from above was dissolved in acetone (150 mL). An equal volume of 10% AcOH (150 mL) was added. The solution was refluxed for 1 hour. Following completion of the reaction, the mixture was cooled to room temperature and quenched with saturated bicarbonate. The acetone was removed by rotary evaporation. The remaining aqueous layer was extracted with DCM (3×100 mL). The combined organic layers were washed with brine and dried over sodium sulfate before being concentrated down to a yellow solid. The solid was then purified by washing with hexanes to yield a white solid (32 g, 65% yield). m.p. 172-173°C. IR (neat): 3381, 3104, 3070, 1662, 1617, 1485, 1397, 1282, 1171, 1093, 1059, 1010, 946, 867, 829, 725 cm^{-1}; ^{1}H NMR (500 MHz, CDCL$_3$): δ(ppm) 7.42 (d, *J* = 10.8 Hz, 2H, Ar-H), 7.35 (d, *J* = 10.8 Hz, 2H, Ar-H), 6.86 (d, *J* = 12.5 Hz, 2H, CH=CH), 6.24 (d, *J* = 12.5 Hz, 2H, CH-CH), 2.6 (s, 1H, OH); ^{13}C NMR(125 MHz, CDCl$_3$): δ(ppm) 185.69, 150.55, 137.35, 134.61, 129.29, 127.31, 127.01, 70.86; HRMS (Q-TOF, ES+) m/z calcd for $C_{12}H_{10}ClO_2$ (M+H)$^+$ 221.0369, found 221.063.

(1's,4's)-4-bromo-4''-chloro-1',4'-dimethoxy-1',4'-dihydro-1,1':4',1''-terphenyl **II.4**
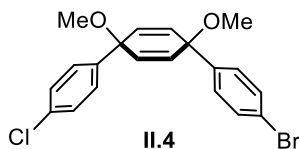
II.14 (30 g, 0.14 mol, 1 eq) was dissolved in dry THF (250mL) in a flame dried 500mL flask equipped with a stir bar and was cooled to −78°C for 1 hour. In a separate

flame dried 1 L flask equipped with as stir bar was added 1,4-dibromobenzene (70.5 g, 0.30 mol, 2.2eq) and dry THF (300 mL). This was cooled to −78°C for 1 hour. NaH (7.1 g, 0.18 mol, 1.3) was added to the cooled ketone as a solid and was allowed to stir for 2 hours. Meanwhile, *n*-BuLi (130.3 mL, 0.13 mol, 2.3 eq) was added drop wise over 1 hour to the 1,4-dibromobezene solution. The deprotonated quinol was then transferred to the 1-bromo-4-lithiobenzene via cannulation. The resulting slurry was allowed to stir at −78°C for 2 hours at which point iodomethane (84.6 mL, 1.36 mol. 10 eq) was added to the slurry followed by dry DMF (200mL). The reaction was allowed to warm to room temperature overnight while stirring. The reaction was quenched with H_2O and extracted Et_2O (3 × 200 mL). The combined organic layers were washed H_2O (3 × 300 mL), brine (1 × 300 mL), dried over Na_2SO_4. The organic layer was concentrated under reduced pressure to give a yellow oil. This was diluted with hexane (200 mL) which was then reduced down under reduced pressure to give an off yellow solid. The solid was recrystallized in hot hexanes to give the product as a white crystalline solid (44.1 g, 80%). Characterization was consistent with what was previously reported. [2]

(1''s,4''s)-4'''-chloro-1,1'',4''-trimethoxy-1'',4''-dihydro-[1,1':4',1'':4'',1'''-quaterphenyl]-4(1H)-one **II.5**
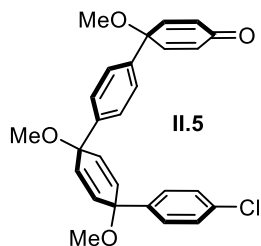
        II.4 (12.4 g, 30.5 mmol, 1 eq) was added to a dry flask and dissolved in dry THF (200 mL). The solution was cooled to −78°C. *n*-BuLi (2.5 M in hexanes, 13.5 mL, 33.6 mmol, 1.1 eq) was added dropwise over 5 minutes. After stirring at −78°C for 10 minutes, **II.13** (6.12 g, 39.7 mmol, 1.3 eq) was added neat. The reaction was stirred for 1 hour before being quenched with H_2O. The aqueous layer was then washed with diethyl ether (3 × 100 mL). The combined organic layers were washed with brine and dried over Na_2SO_4, and concentrated down to a yellow oil. Upon trituration and washing with cold hexanes, the oil became solid. This solid was dissolved in acetone (50 mL) and 5%

AcOH/H$_2$O was added (50 mL). The solution was stirred at room temperature for 1 hour. The solution was neutralized with sodium bicarbonate and extracted with diethyl ether (3 × 100 mL). The combined organic layers were washed with brine and dried over Na$_2$SO$_4$. The solution was concentrated under reduced pressure to yield a solid. The solid was washed with cold hexanes to give white crystals (4.5 g, 85%). m.p. 168-170° C. IR (neat) 3419, 2936, 2106, 1661, 1621, 1486, 1401, 1031, 1014, 946, 855, 833, 729 cm^{-1}; ^{1}H NMR (500 MHz, CDCl$_3$): δ(ppm) 7.41 (d, J = 8.6 Hz, 2H, Ar-H), 7.38 (d, J = 8.6 Hz, 2H, Ar-H), 7.32 (d, J = 8.6 Hz, 2H, Ar-H), 7.27 (d, J = 8.6 Hz, 2H, Ar-H), 6.86 (d, J = 10 Hz, 2H, CH=CH), 6.20 (d, J = 10 Hz, 2H, CH=CH), 6.08 (s, 4H, CH=CH), 3.42 (s, 6H, OCH$_3$); ^{13}C NMR (100 MHz, CDCl$_3$): δ(ppm) 185.90, 150.88, 143.79, 142.05, 138.33, 133.68, 133.65, 133.49, 128.75, 127.60, 127.09, 126.73, 125.64, 74.72, 74.58, 71.05, 52.25; HRMS (Q-TOF, ES+) m/z calcd for C$_{26}$H$_{24}$ClO$_4$ (M+H)$^+$: 435.1363, Found: 435.1341.

(1's,4's)-4,4''''-dichloro-1',1''',4',4'''-tetramethoxy-1',1''',4',4'''-tetrahydro-1,1':4',1'':4'',1''':4''',1''''-quinquephenyl **II.6**
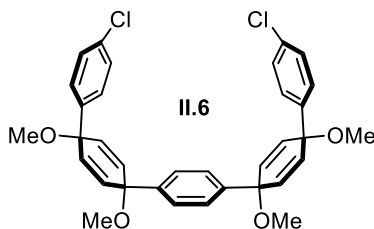
Ketone **II.5** (10 g, 23 mmol, 1 eq) and 1-bromo-4-chlorobenzene (9.68 g, 51 mmol, 2.2 eq) were added to a dry round bottom flask and dissolved in dry THF (200 mL). The solution was cooled to −78°C for 1 hour. To this solution was added NaH (1.1 g, 27.6 mmol, 1.2 eq) as a solid. The reaction was stirred for 2 hours. After 2 hours, *n*-BuLi (22.3 mL, 55.6 mmol, 2.4 eq) was added drop-wise. The reaction was stirred for 2 hours at which time MeI (14.3 mL, 230 mmol, 10 eq) and dry DMF (100 mL) were added. The reaction was allowed to warm to room temperature overnight while stirring. The reaction was quenched with H$_2$O and extracted with diethyl ether (3 × 200 mL). The combined organic layers were washed with brine, dried with Na$_2$SO$_4$ and concentrated under reduced pressure to give a solid. The solid was washed with cold hexanes to give the product as a white powder (10 g, 76%). m.p. 150-153° C. IR (neat): 2985, 2940,

2897, 2824, 1489, 1402, 1174, 1083, 949, 824, 770 cm^{-1}; ^{1}H NMR (500 MHz, CDCl$_3$): δ(ppm) 7.29 (overlap, 8H, Ar-H), 6.10 (d, J = 10.4 Hz, 4H, CH=CH), 6.05 (d, J= 10.4 Hz, 4H, CH=CH), 3.42 (s, 6H, OCH$_3$); ^{13}C NMR(100 MHz, CDCl$_3$): δ(ppm) 142.65, 141.96, 133.62, 133.37, 133.06, 128.46, 127.42, 126.02, 74.55, 74.43, 52.02; HRMS (Q-TOF, ES+) m/z calcd for C$_{34}$H$_{33}$Cl$_2$O$_4$ (M+H)$^+$: 575.1756, found 575.1756.

Bis(4-(4,4,5,5-tetramethyl-1,3,2-dioxaborolan-2-yl)phenyl)methane **II.9**
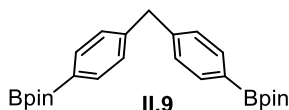
Bis(4-bromophenyl)methane (Compound **II.7**) was synthesized following literature procedure.[33]

II.7 (4.325 g, 13.27 mmol, 1 eq) was dissolved in 200 mL THF and cooled to −78°C. Then *n*-BuLi (10.6 mL, 26.53 mmol, 2 eq) was syringed into the cooled solution over the course of 3 min. Immediately, neat isopropyl pinacol borate (10.8 mL, 53.06 mmol, 4 eq) was quickly added in stream. The mixture was stirred at −78°C for 5 min and allowed to warm to room temperature slowly. After two hours, the reaction was carefully quenched with water (100 mL).

The mixture was extracted with dichloromethane (3 × 100 mL) and combined the organic layers were washed with brine and dried over sodium sulfate. After concentrating under reduced pressure, the crude product was put on high vacuum to remove volatile which yielded 1 as white powder (5.02 g, 90%). m.p. 229-230 °C. IR (neat) 2975, 2939, 2861, 1609, 1399, 1358, 1319, 1164, 1106, 1088, 1019, 962, 858, 782, 677 cm^{-1}; ^{1}H NMR (500 MHz, CDCl$_3$): δ(ppm) 7.73 (d, J = 10 Hz, 4H, Ar-H), 7.18 (d, J = 10 Hz, 4H, Ar-H), 4.00 (s, 2H, CH$_2$), 1.32 (s, 24H, CH$_3$); ^{13}C NMR (125MHz, CDCl$_3$): δ(ppm) 144.10, 135.01, 128.42, 83.66, 42.31, 24.86, C-B signal not observed. HRMS (TOF MS ES+) m/z calcd for C$_{25}$H$_{35}$B$_2$O$_4$ (M+H)$^+$: 421.2721, Found: 421.2730.

1,6-Bis(4-bromophenyl)hexane **II.8**

II.8
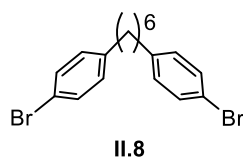
  II.15 was prepared following literature procedure.[34]

  II.15 (3.125 g, 7.368 mmol, 1 eq) was dissolved in a mixture of 50 mL DCM and TFA. Then triethylsilane (11.8 mL, 73.68 mmol, 10 eq) was slowly added and solution was stirred at room temperature overnight. After cooled the reaction with salt-ice-bath for 30 minuesi, the reaction was quenched with concentrated sodium hydroxide solution until TFA was fully neutralized (monitored by pH paper). Afterwards, the mixture was extracted with DCM (3 × 70 mL). The combined organic phase was sequentially washed with water (2 × 100 mL) and brine solution (100 mL). After dried over sodium sulfate, the solution was concentrated and resulting colorless oil was purified by column chromatography (silica, hexanes) to yield **II.15** as white solid (2.43 g, 83%, m.p. 63-64 °C). IR (neat) 2927, 2852, 1484, 1466, 1300, 1068, 1006, 798; ^{1}H NMR (500 MHz, CDCl$_3$): δ(ppm) 7.39 (d, J = 8.2 Hz, 4H, Ar-H), 7.04 (d, J = 8.2 Hz, 4H, Ar-H),, 2.55 (t, J = 7.7 Hz, 4H, CH$_2$), 1.59 (m, 4H, CH$_2$), 1.34 (m, 4H, CH$_2$); ^{13}C NMR (125 MHz, CDCl$_3$): δ(ppm) 141.63, 161.26, 130.15, 119.30, 35.28, 31.17, 28.94. Characterization was consistent with what was previously reported.[34]

1,6-bis(4-(4,4,5,5-tetramethyl-1,3,2-dioxaborolan-2-yl)phenyl)hexane **II.10**

II.10
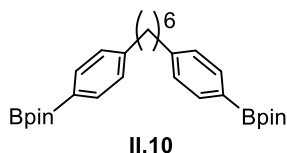
  The procedure is same as making **II.9**. **II.8** (2.259 g, 5.702 mmol, 1 eq), THF (100 mL), *n*-BuLi (4.75 mL, 11.40 mmol, 2 eq), neat isopropyl pinacol borate (4.65 mL, 22.81 mmol, 4 eq), product as white solid (2.764 g, 98.8%, m.p. 124-125 °C). IR (neat) 2978, 2924, 2853, 1609, 1515, 1271, 1140, 1019, 961, 859, 822, 739, 656; ^{1}H NMR (500 MHz, CDCl$_3$): δ(ppm) 7.74 (d, J = 8.2 Hz, 4H, Ar-H), 7.19 (d, J = 8.2 Hz, 4H, Ar-H), 2.61 (t, J = 7.7 Hz, 4H, CH$_2$), 1.62 (m, 4H, CH$_2$), 1.35 (m, 28H, CH$_3$ and CH$_2$); ^{13}C NMR (125 MHz, CDCl$_3$): δ(ppm) 146.27, 134.82, 127.88, 83.58, 36.13, 31.21, 29.09, 24.87, C-

B signal not observed. HRMS (TOF MS ES+) m/z calcd for $C_{30}H_{44}B_2O_4Na$ (M+Na)$^+$: 513.3323, found 513.3333.

(31s,34s)-31,34,51,54-tetramethoxy-1,2,4,6,7(1,4)-pentabenzena-3,5(1,4)-dicyclohexanacyclooctaphane-32,35,52,55-tetraene **II.11**
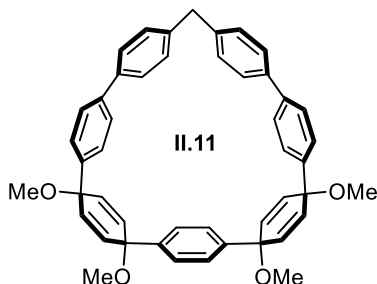
II.6 (500 mg, 0.869 mmol, 1 eq), **II.9** (401 mg, 0.955 mmol, 1.1 eq), Pd(OAc)$_2$ (32 mg, 0.139 mmol, 0.16 eq), K$_3$PO$_4$ (369 mg, 1.738 mmol, 2 eq) and S-Phos (143 mg, 0.348 mmol, 0.4 eq) were charged in 1 L round bottom flask equipped with a condenser and a stir bar. The flask was evacuated and backfilled with nitrogen for 10 times, after which 300 mL degassed DMF/H$_2$O (9:1) was added under nitrogen atmosphere. The mixture was heated at 100 °C and stirred for 18 hours.

Upon cooling to room temperature, the reaction mixture was passed through a celite plug. The filtrate was added H$_2$O (100 mL) and extracted with DCM (3 × 100 mL). The combined organic layer was washed with 5 wt% LiCl aqueous solution (10 × 250 mL) and brine (250 mL), then dried over anhydrous Na$_2$SO$_4$. The solution was concentrated and crude was purified by column chromatography (silica, 0% to 15% ethyl acetate in DCM) to yield product as white solid (79 mg, 13.6%). d.p. > 310 °C. IR (neat) 3023, 2945, 2925, 2820, 1493, 1433, 1187, 1115,850, 816, 716; ^{1}H NMR (500 MHz, CDCl$_3$): δ(ppm) 7.39 (d, *J* = 8.5 Hz, 4H, Ar-H), 7.30 (s, 4H, Ar-H), 7.24 (d, *J* = 8.5 Hz, 4H, Ar-H), 7.20 (d, *J* = 8.3 Hz, 4H, Ar-H), 7.12 (d, *J* = 8.3 Hz, 4H, Ar-H), 6.11 (d, *J* = 10.3 Hz, 4H, CH=CH), 5.98 (d, *J* = 10.3 Hz, 4H, CH=CH), 3.92 (s, 2H, CH$_2$), 3.43 (s, 6H, CH$_3$), 3.37 (s, 6H, CH$_3$); ^{13}C NMR (125 MHz, CDCl$_3$): δ(ppm) 143.23, 142.94, 142.02, 140.78, 138.54, 133.26, 132.84, 128.01, 127.70, 127.51, 126.02, 125.94, 74.26, 73.94, 52.20, 51.63, CH$_2$ peak was not detected due to the poor solubility in available deuterated solvent; MALDI-TOF m/z calcd for $C_{47}H_{42}O_4$ (M)$^+$: 670.31, found: 670.61.

(31s,34s)-31,34,51,54-tetramethoxy-1,2,4,6,7(1,4)-pentabenzena-3,5(1,4)-dicyclohexanacyclotridecaphane-32,35,52,55-tetraene **II.12**
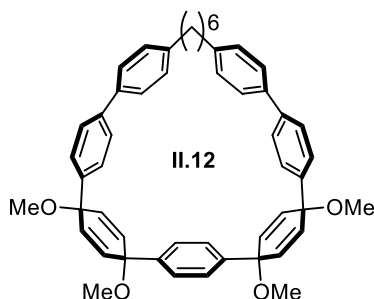
The procedure is same as **II.11**. **II.6** (500 mg, 0.869 mmol, 1 eq), **II.12** (426 mg, 0.869 mmol, 1 eq), Pd(OAc)$_2$ (32 mg, 0.139 mmol, 0.16 eq), K$_3$PO$_4$ (369 mg, 1.738 mmol, 2 eq) and S-Phos (143 mg, 0.348 mmol, 0.4 eq), column chromatography (silica, 0% to 20% ethyl acetate in DCM), product as colorless oil (133mg, 20.6%). m.p. 213-214 °C. IR (neat) 3022, 2990, 2852, 2820, 1493, 1450, 1085, 1005, 946, 799, 719; ^{1}H NMR (500 MHz, CDCl$_3$): δ(ppm) 7.62 (d, *J* = 8.4 Hz, 4H, Ar-H), 7.54 (d, *J* = 8.4 Hz, 4H, Ar-H), 7.44-7.48 (overlap, 8H, Ar-H), 6.96 (d, *J* = 8.1 Hz, 4H, Ar-H), 6.12 (s, 8H, CH=CH), 3.48 (s, 6H, CH$_3$), 3.45 (s, 6H, CH$_3$), 2.50-2.60 (m, 4H, CH$_2$), 1.60-1.72 (m, 4H, CH$_2$), 1.12-1.22 (m, 4H, CH$_2$); ^{13}C NMR (125 MHz, CDCl$_3$): δ(ppm) 142.92, 142.44, 141.09, 140.34, 137.58, 133.35, 133.15, 129.21, 126.73, 126.63, 126.38, 126.04, 74.65, 74.47, 52.01, 51.92, 33.22, 29.44, 25.71; MALDI-TOF m/z calcd for C$_{52}$H$_{52}$O$_4$ (M)$^+$: 740.39, found: 740.83.

1,2,3,4,5,6,7(1,4)-heptabenzenacyclooctaphane **II.1**
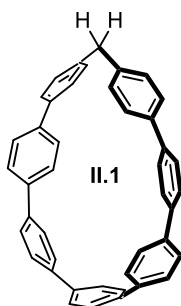
II.11 (79 mg, 0.118 mmol, 1 eq) was dissolved in 80 mL THF under nitrogen. The solution was cooled to −78 °C, at which point sodium naphthalenide (11 mL, 11 mmol, 93 eq) was added drop by drop. The reaction was stirred at −78 °C for two hours

and then quenched by adding I_2 (1 M solution in THF). The mixture was allowed to warm to room temperature and saturated $Na_2S_2O_3$ was added to remove excess I_2. After adding H_2O (30 mL), the mixture was extracted with DCM (3×100 mL). Combined organic layer was washed with brine and dried over anhydrous Na_2SO_4. After removing solvent, the crude yellow solid was purified by chromatography (silica, 0% to 30% DCM in hexanes) to give **II.1** as yellow powder (25 mg, 39%). IR (neat) 3020, 2920, 2851, 1718, 1485, 1261, 806, 734; ^{1}H NMR (500 MHz, $CDCl_3$): δ(ppm) 7.40-7.47 (overlap, 20H, Ar-H), 7.27 (d, $J = 8.3$ Hz, 4H, Ar-H), 7.08 (d, $J = 8.3$ Hz, 4H, Ar-H), 3.78 (s, 2H, CH_2); ^{13}C NMR (125 MHz, $CDCl_3$): δ(ppm) 143.77, 138.05, 137.97, 137.60, 137.15, 137.11, 136.73, 128.32, 127.78, 127.73, 127.35, 127.30, 126.89, 126.39, 42.12; MALDI-TOF m/z calcd for $C_{43}H_{30}$ (M)$^+$: 546.23, found: 546.89.

1,2,3,4,5,6,7(1,4)-heptabenzenacyclotridecaphane **II.2**
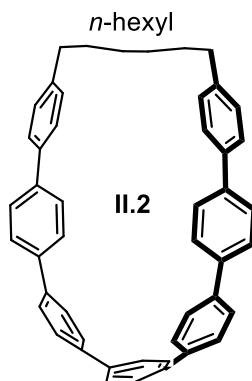
Procedure same as **II.1**. **II.12** (43 mg, 0.058 mmol, 1 eq), THF (50 mL), sodium naphthalenide (2.8 mL, 5.8 mmol, 100 eq), purified by column chromatography (silica, 0% to 30% DCM in hexanes), product as light yellow solid (17 mg, 47%). IR (neat) 3021, 2922, 2852, 1485, 1261, 822, 736; ^{1}H NMR (500 MHz, $CDCl_3$): δ(ppm) 7.60 (s, 4H, Ar-H), 7.56 (d, $J = 8.8$ Hz, 4H, Ar-H), 7.52 (d, $J = 8.8$ Hz, 4H, Ar-H), 7.44 (s, 8H, Ar-H), 7.35 (d, $J = 8.2$ Hz, 4H, Ar-H), 7.07 (d, $J = 8.2$ Hz, 4H, Ar-H), 2.55 (t, $J = 7.0$ Hz, 4H, CH_2) 1.35-1.45 (m, 4H, CH_2), 1.10-1.20 (m, 4H, CH_2); ^{13}C NMR (125 MHz, $CDCl_3$): δ(ppm) 142.19, 138.61, 138.33, 137.98, 137.69, 137.43, 137.33, 128.89, 127.67, 127.62, 127.50, 127.25, 126.91, 126.50, 35.76, 32.89, 29.73; MALDI-TOF m/z calcd for $C_{48}H_{40}$ (M)$^+$: 616.31, found: 616.80.

29

2.4.3. Photophysical Characterizations

Absorbance and fluorescence spectra were obtained in a 1cm Quartz cuvette with dichloromethane using a Varian 100 Bio UV-Vis spectrometer and a Horiba Jobin Yvon Fluoromax3 fluorimeter. Fluorescence was measured by excitation at 340 nm for [7]CPP and at 320 nm for **II.1** and **II.2**.The extinction coefficients were calculated by measuring the slope of Beer-Lambert plots (absorbance: [7]CPP, 340 nm; **II.1**, 323 nm; **II.2**, 318 nm) and averaging over three independent trials. The quantum yield was determine following the methods described by Williams[40] with anthracene (ethanol) and quinine sulphate (1 M H_2SO_4) as external standards. Anthracene, quinine sulphate and [7]CPP were excited at 340 nm and the fluorescence were integrated from 360-480 nm, from 380-630 nm and from 400-660 nm, respectively. **II.1** and **II.2** were excited at 320 nm and the fluorescence were integrated from 360-650 nm and from 400-600 nm, respectively.
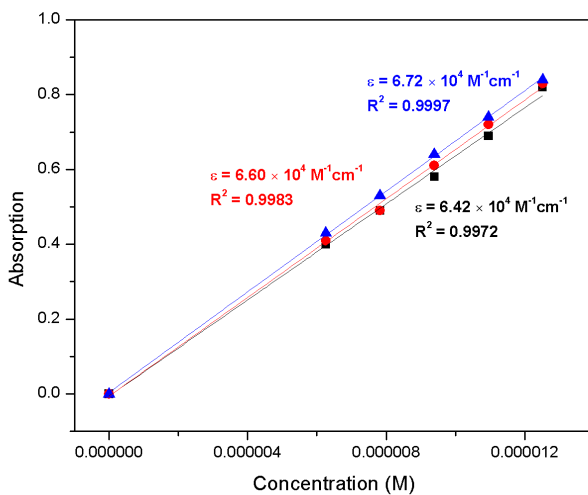
Figure 2.4. Beer-Lambert plots for the determination of extinction coefficient of [7]CPP ($\varepsilon = 6.58 \times 10^4$ $M^{-1}cm^{-1}$).
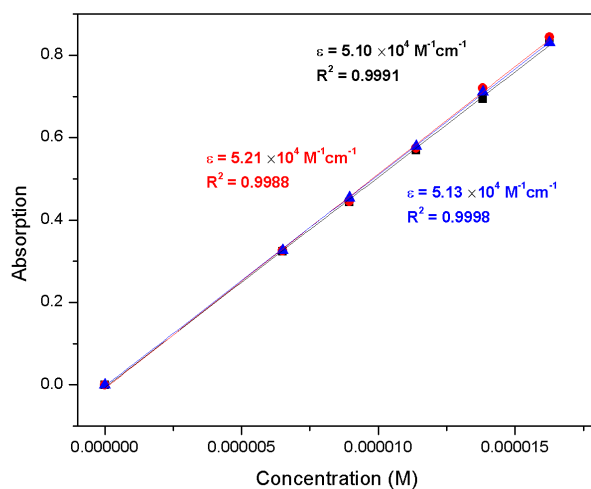
Figure 2.5. Beer-Lambert plots for the determination of extinction coefficient of **II.1** ($\varepsilon = 5.15 \times 10^4$ M^{-1}cm^{-1}).
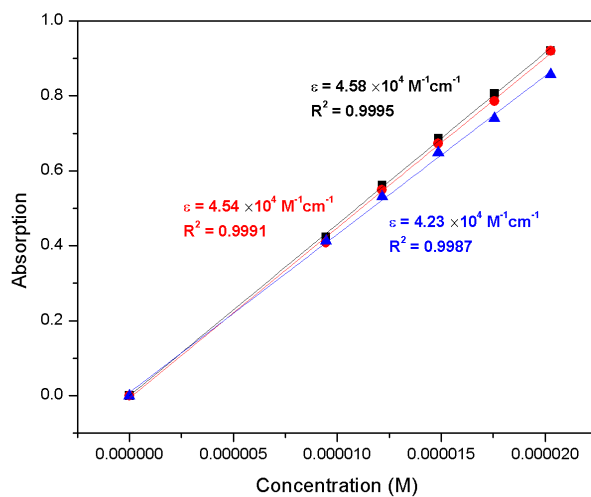
Figure 2.6. Beer-Lambert plots for the determination of extinction coefficient of **II.2** ($\varepsilon = 4.45 \times 10^4$ M^{-1}cm^{-1}).
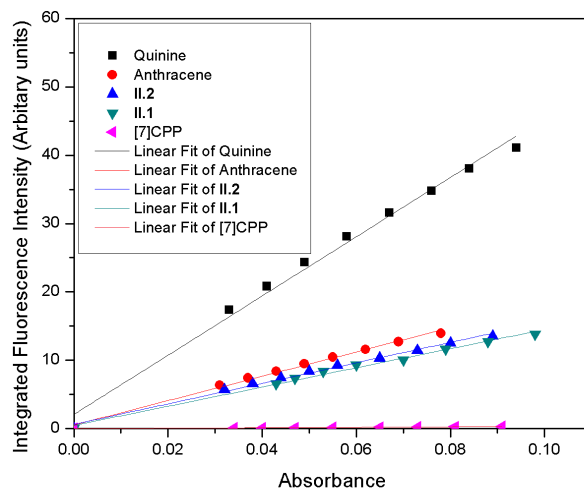
Figure 2.7. Quantum yield measurement of [7]CPP (0.06), **II.1** (0.23) and **II.2** (0.25).

2.4.4. Electrochemical Measurement

Circular voltammetry for all compounds is was performed on a Princeton Applied Research Potentiostat/Galvanastat Model 273 running M270/250 Electrochemical Software (Princeton Applied Research) with a silver reference electrode, a glassy carbon working electrode and a platinum counter electrode.. Ferrocene/ferrocenium couple was used as an internal or external reference. Supporting electrolyte tetra-*n*-butylammonium hexafluorophosphate (nBu$_4$PF$_6$) was purchased from Sigma-Aldrich and was recrystallized from methanol for 3 times before use. DCM, THF and acetonitrile were distilled according to literature procedure. Solvents were totally degassed by subjecting it to at least six successive freeze-pump-thaw cycles, after which they were transferred to a glove box under an N$_2$ atmosphere.

32
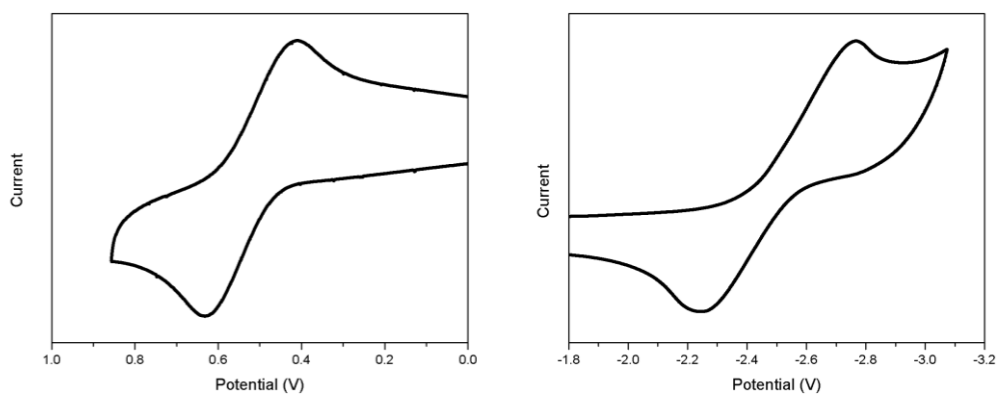
Figure 2.8. Cyclic Voltammetry of [7]CPP.
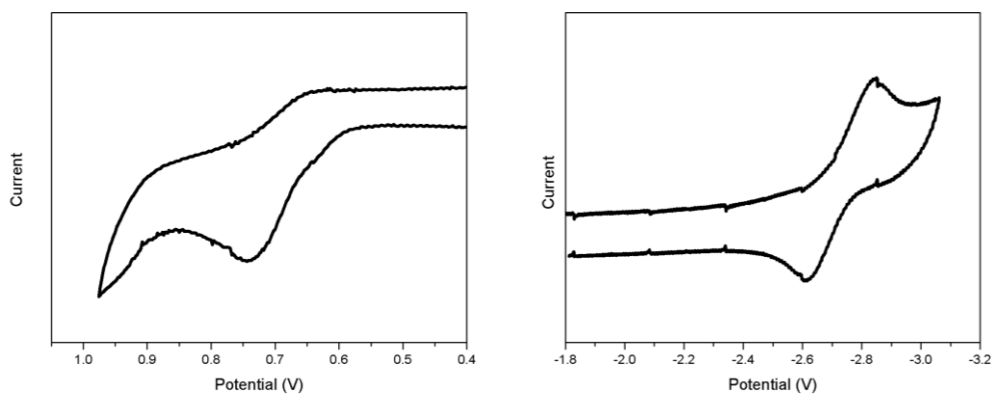
Figure 2.9. Cyclic Voltammetry of **II.1**.
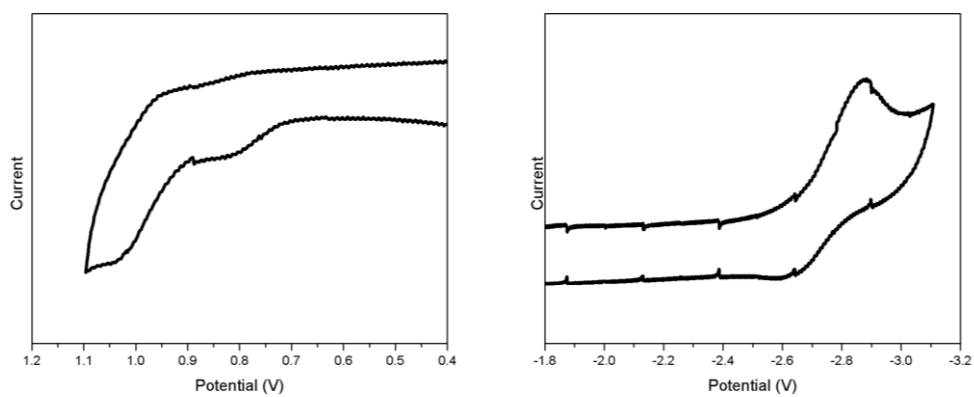
Figure 2.10. Cyclic Voltammetry of **II.2**.

2.4.5. Computational Details

All calculations were carried out with Gaussian 09 package at B3LYP/6-31g* level of theory.[41] All excited state calculations (TD-DFT) were performed on fully optimized structures. The fully optimized structures were confirmed to be true minima by vibrational analysis.
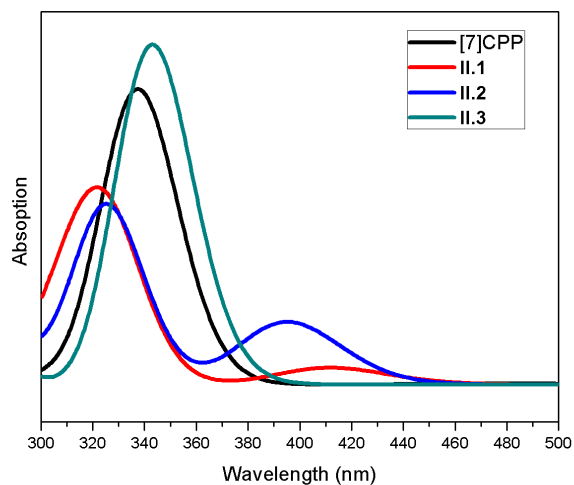
Figure 2.11. Calculated UV-Vis spectra using TD-DFT (at B3LYP/6-31g* level of theory).
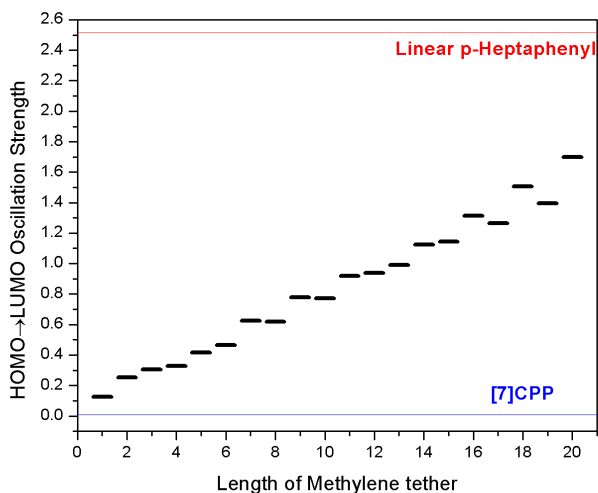
Figure 2.12. Oscillation strength of HOMO→LUMO transition with respect to methylene tether length.

34

Table 2.3. Major electronic transitions for [7]CPP determined by TD-DFT method using B3LYP/6-31G*.

Energy (cm⁻¹)	Wavelength (nm)	Osc. Strength (*f*)	Major contribs
21037	475	0.0087	HOMO->LUMO (98%)
27711	360	0	H-1->LUMO (51%), HOMO->L+1 (49%)
28296	353	0.0036	H-2->LUMO (56%), HOMO->L+2 (44%)
29397	340	1.1212	H-1->LUMO (48%), HOMO->L+1 (50%)
2993	334	1.1021	H-2->LUMO (43%), HOMO->L+2 (55%)
31519	317	0.0197	H-3->LUMO (13%), HOMO->L+3 (78%)
32789	305	0.0008	H-2->L+1 (41%), H-1->L+2 (37%)
32929	304	0.025	H-2->L+2 (21%), H-1->L+1 (77%)

Table 2.4. Major electronic transitions for **II.1** determined by TD-DFT method using B3LYP/6-31G*.

Energy (cm⁻¹)	Wavelength (nm)	Osc. Strength (*f*)	Major contribs
24308	411	0.1251	HOMO->LUMO (97%)
29319	341	0.0049	H-1->LUMO (55%), HOMO->L+1 (43%)
30712	325	1.13	H-1->LUMO (43%), HOMO->L+1 (53%)
31340	319	0.0002	H-2->LUMO (52%), HOMO->L+2 (47%)
32205	310	0.5081	H-2->LUMO (44%), HOMO->L+2 (48%)
33156	302	0.0722	H-5->LUMO (14%), HOMO->L+3 (74%)
33656	297	0.064	H-1->L+1 (84%)
34424	290	0.0333	HOMO->L+4 (65%)

Table 2.5. Major electronic transitions for **II.2** determined by TD-DFT method using B3LYP/6-31G*.

Energy (cm⁻¹)	Wavelength (nm)	Osc. Strength (*f*)	Major contribs
25324	395	0.4641	HOMO->LUMO (98%)
29536	339	0.0237	H-1->LUMO (63%), HOMO->L+1 (35%)
30760	325	1.3081	H-1->LUMO (35%), HOMO->L+1 (63%)
32900	304	0.0063	HOMO->L+2 (28%), HOMO->L+3 (38%)
33133	302	0.0411	H-2->LUMO (58%), HOMO->L+3 (27%)
33660	297	0.0368	H-1->L+1 (84%)

Table 2.6. Major electronic transitions for other tethered *p*-heptaphenyls determined by TD-DFT method using B3LYP/6-31G*. (N stands for the number of the carbon in the alkyl tether).

N=2

Energy (cm^{-1})	Wavelength (nm)	Osc. Strength (*f*)	Major contribs
23614	423	0.2543	HOMO->LUMO (97%)
28022	357	0.0078	H-1->LUMO (58%), HOMO->L+1 (41%)
29939	334	1.236	H-1->LUMO (41%), HOMO->L+1 (58%)
31502	317	0.0034	HOMO->L+2 (16%), HOMO->L+3 (64%)
32087	311	0.003	H-2->LUMO (66%), H-1->L+1 (23%)
32351	309	0.0122	H-1->L+1 (59%), HOMO->L+2 (26%)
33777	296	0.0007	H-6->LUMO (13%), HOMO->L+4 (61%)

N=3

Energy (cm^{-1})	Wavelength (nm)	Osc. Strength (*f*)	Major contribs
23710	422	0.3071	HOMO->LUMO (98%)
28586	350	0.0119	H-1->LUMO (59%), HOMO->L+1 (39%)
30210	331	1.361	H-1->LUMO (39%), HOMO->L+1 (59%)
31644	316	0.0496	H-2->LUMO (79%), HOMO->L+2 (19%)
31986	313	0.0028	H-4->LUMO (11%), HOMO->L+3 (77%)
32910	304	0.2081	H-1->L+1 (31%), HOMO->L+2 (56%)
33648	297	0.0559	H-1->L+1 (29%), HOMO->L+4 (38%)

N=4

Energy (cm^{-1})	Wavelength (nm)	Osc. Strength (*f*)	Major contribs
24056	416	0.3271	HOMO->LUMO (98%)
28465	351	0.0176	H-1->LUMO (61%), HOMO->L+1 (37%)
30152	332	1.3534	H-1->LUMO (38%), HOMO->L+1 (61%)
31898	313	0.004	HOMO->L+2 (19%), HOMO->L+3 (60%)
32287	310	0.0159	H-2->LUMO (71%), HOMO->L+2 (15%)
32834	305	0.0046	H-1->L+1 (73%), HOMO->L+2 (18%)
33988	294	0.0003	H-7->LUMO (10%), HOMO->L+4 (60%)

N=5

Energy (cm^{-1})	Wavelength (nm)	Osc. Strength (*f*)	Major contribs
26020	384	0.4162	HOMO->LUMO (97%)
29977	333	0.0569	H-1->LUMO (71%), HOMO->L+1 (27%)

308877	323	1.2237	H-1->LUMO (27%), HOMO->L+1 (71%)
329347	303	0.0375	H-2->LUMO (75%), HOMO->L+2 (19%)
335027	298	0.0063	H-1->L+1 (87%), HOMO->L+2 (10%)
341607	293	0.0225	HOMO->L+3 (70%)
34234	292	0.2353	H-2->LUMO (19%), HOMO->L+2 (54%)

N=7

Energy (cm^{-1})	Wavelength (nm)	Osc. Strength (f)	Major contribs
25295	395	0.6236	HOMO->LUMO (98%)
29407	340	0.0822	H-1->LUMO (74%), HOMO->L+1 (24%)
30587	327	1.2964	H-1->LUMO (24%), HOMO->L+1 (74%)
32983	303	0.0573	H-2->LUMO (79%), HOMO->L+2 (12%)
33263	301	0.001	H-5->LUMO (10%), HOMO->L+3 (73%)
33485	299	0.0048	H-1->L+1 (86%)
34408	291	0.0236	H-7->LUMO (11%), HOMO->L+4 (52%)

N=8

Energy (cm^{-1})	Wavelength (nm)	Osc. Strength (f)	Major contribs
25057	399	0.6202	HOMO->LUMO (98%)
29218	342	0.0555	H-1->LUMO (69%), HOMO->L+1 (29%)
30443	328	1.4186	H-1->LUMO (30%), HOMO->L+1 (69%)
32724	305	0.013	H-2->LUMO (62%), HOMO->L+2 (27%)
32924	304	0.0222	H-2->LUMO (13%), HOMO->L+3 (59%)
33390	300	0.0139	H-1->L+1 (79%), HOMO->L+2 (11%)
34530	290	0	H-7->LUMO (13%), HOMO->L+4 (55%)

N=9

Energy (cm^{-1})	Wavelength (nm)	Osc. Strength (f)	Major contribs
25765	388	0.7801	HOMO->LUMO (98%)
29769	336	0.1263	H-1->LUMO (79%), HOMO->L+1 (19%)
30885	324	1.2237	H-1->LUMO (19%), HOMO->L+1 (79%)
33394	299	0.065	H-2->LUMO (79%), HOMO->L+2 (11%)
33656	297	0.0006	H-6->LUMO (12%), HOMO->L+3 (72%)
33792	296	0.0094	H-1->L+1 (86%)

N=10

Energy (cm^{-1})	Wavelength (nm)	Osc. Strength (f)	Major contribs

25716	389	0.7719	HOMO->LUMO (98%)
29733	336	0.0917	H-1->LUMO (74%), HOMO->L+1 (24%)
30770	325	1.3446	H-1->LUMO (24%), HOMO->L+1 (75%)
33181	301	0.0259	H-2->LUMO (71%), HOMO->L+2 (22%)
33536	298	0.0314	H-1->L+1 (21%), HOMO->L+3 (47%)
33734	296	0.0132	H-1->L+1 (65%), HOMO->L+3 (19%)

N=11

Energy (cm^{-1})	Wavelength (nm)	Osc. Strength (f)	Major contribs
26124	383	0.9197	HOMO->LUMO (97%)
30081	332	0.1556	H-1->LUMO (82%), HOMO->L+1 (16%)
31165	321	1.1581	H-1->LUMO (16%), HOMO->L+1 (82%)
33725	297	0.0691	H-2->LUMO (80%), HOMO->L+2 (10%)
33948	295	0.0003	H-6->LUMO (15%), HOMO->L+3 (70%)
34086	293	0.0226	H-1->L+1 (87%)

N=12

Energy (cm^{-1})	Wavelength (nm)	Osc. Strength (f)	Major contribs
26215	381	0.9392	HOMO->LUMO (97%)
30096	332	0.1358	H-1->LUMO (80%), HOMO->L+1 (18%)
31003	323	1.2422	H-1->LUMO (19%), HOMO->L+1 (80%)
33517	298	0.0452	H-2->LUMO (70%), HOMO->L+2 (17%)
33842	295	0.0525	H-1->L+1 (76%), HOMO->L+2 (13%)
34127	293	0.0025	H-6->LUMO (12%), HOMO->L+3 (60%)

N=13

Energy (cm^{-1})	Wavelength (nm)	Osc. Strength (f)	Major contribs
27450	364	0.9916	HOMO->LUMO (97%)
30978	323	0.2931	H-1->LUMO (92%)
31843	314	0.9354	HOMO->L+1 (92%)
34215	292	0.0874	H-2->LUMO (69%), H-1->L+1 (17%)
34415	291	0.0225	H-2->LUMO (14%), H-1->L+1 (78%)
35306	283	0.0083	H-6->LUMO (17%), HOMO->L+3 (63%)
35485	282	0.0547	HOMO->L+2 (45%), HOMO->L+4 (18%)

N=14

Energy (cm⁻¹)	Wavelength (nm)	Osc. Strength (*f*)	Major contribs
26638	375	1.1238	HOMO->LUMO (97%)
30403	329	0.1838	H-1->LUMO (85%), HOMO->L+1 (13%)
31228	320	1.1033	H-1->LUMO (14%), HOMO->L+1 (85%)
33812	296	0.0909	H-2->LUMO (58%), H-1->L+1 (29%),
34036	294	0.0458	H-2->LUMO (17%), H-1->L+1 (64%),
34559	289	0.0032	H-6->LUMO (15%), HOMO->L+3 (61%)

N=15

Energy (cm⁻¹)	Wavelength (nm)	Osc. Strength (*f*)	Major contribs
26729	374	1.1428	HOMO->LUMO (97%)
30361	329	0.2077	H-1->LUMO (87%), HOMO->L+1 (11%)
31319	319	1.0486	H-1->LUMO (11%), HOMO->L+1 (87%)
33838	296	0.1678	H-2->LUMO (10%), H-1->L+1 (86%)
34151	293	0.0089	H-2->LUMO (71%), HOMO->L+2 (16%)
34414	291	0.003	H-6->LUMO (17%), HOMO->L+3 (62%)

N=16

Energy (cm⁻¹)	Wavelength (nm)	Osc. Strength (*f*)	Major contribs
27031	370	1.3121	HOMO->LUMO (97%)
30694	326	0.2258	H-1->LUMO (89%)
31457	318	0.9476	HOMO->L+1 (89%)
34050	294	0.1676	H-2->LUMO (31%), H-1->L+1 (62%)
34261	292	0.0179	H-2->LUMO (46%), H-1->L+1 (32%),
34948	286	0.0026	H-6->LUMO (15%), HOMO->L+3 (59%)

N=17

Energy (cm⁻¹)	Wavelength (nm)	Osc. Strength (f)	Major contribs
27842	359	1.2636	HOMO->LUMO (97%)
31286	320	0.3351	H-1->LUMO (95%)
32188	311	0.7704	HOMO->L+1 (95%)
34530	290	0.1064	H-2->LUMO (73%), H-1->L+1 (14%)
34717	288	0.0707	H-2->LUMO (12%), H-1->L+1 (81%)
35640	281	0.0048	H-6->LUMO (18%), HOMO->L+3 (61%)

N=18

Energy (cm⁻¹)	Wavelength (nm)	Osc. Strength (*f*)	Major contribs
27376	365	1.5065	HOMO->LUMO (97%)
30928	323	0.2587	H-1->LUMO (92%)
31641	316	0.784	HOMO->L+1 (93%)
34170	293	0.2403	H-2->LUMO (10%), H-1->L+1 (85%)
34484	290	0.0025	H-2->LUMO (67%), HOMO->L+2 (20%)
35291	283	0.0017	H-6->LUMO (15%), HOMO->L+3 (56%)

N=19

Energy (cm⁻¹)	Wavelength (nm)	Osc. Strength (*f*)	Major contribs
27987	357	1.3948	HOMO->LUMO (97%)
31406	318	0.3349	H-1->LUMO (96%)
32324	309	0.6999	HOMO->L+1 (95%)
34651	289	0.1091	H-2->LUMO (75%), H-1->L+1 (11%),
34839	287	0.1072	H-2->LUMO (10%), H-1->L+1 (83%)
35764	280	0.0036	H-6->LUMO (18%), HOMO->L+3 (60%)

N=20

Energy (cm⁻¹)	Wavelength (nm)	Osc. Strength (*f*)	Major contribs
27714	361	1.7003	HOMO->LUMO (96%)
31183	321	0.2748	H-1->LUMO (95%)
31880	314	0.619	HOMO->L+1 (95%)
34351	291	0.3023	H-1->L+1 (89%)
34738	288	0.0014	H-2->LUMO (73%), HOMO->L+2 (19%)
35594	281	0.0009	H-6->LUMO (16%), HOMO->L+3 (54%)

Table 2.7. Major electronic transitions for linear *p*-heptaphenyl determined by TD-DFT method using B3LYP/6-31G*.

Energy (cm⁻¹)	Wavelength (nm)	Osc. Strength (f)	Major contribs
29180	343	2.514	HOMO->LUMO (97%)
32883	304	0.0003	H-1->LUMO (91%)
33379	300	0.0006	HOMO->L+1 (91%)
36210	276	0.2181	H-2->LUMO (53%), H-1->L+1 (28%)
36294	276	0.4649	H-2->LUMO (21%), H-1->L+1 (67%)
36631	273	0.0001	H-6->LUMO (23%), HOMO->L+3 (54%)

Table 2.8. Frontier orbital energy summary.

n	E(H-2)	E(H-1)	E(HOMO)	E(LUMO)	E(L+1)	E(L+2)
0 ([7]CPP)	-5.72	-5.65	-4.97	-1.8	-1.12	-1.02
1	-5.88	-5.63	-5.11	-1.58	-1.03	-0.8
2	-6.04	-5.54	-5.03	-1.64	-1.09	-0.57
3	-5.95	-5.59	-5.05	-1.65	-1.07	-0.63
4	-6.02	-5.55	-5.05	-1.62	-1.07	-0.58
5	-5.69	-5.58	-5.2	-1.5	-1.07	-0.62
6	-6.03	-5.59	-5.14	-1.5	-1.05	-0.56
7	-6.03	-5.57	-5.15	-1.57	-1.08	-0.52
8	-6.02	-5.57	-5.13	-1.59	-1.09	-0.59
9	-6.05	-5.58	-5.18	-1.55	-1.07	-0.49
10	-6.03	-5.58	-5.18	-1.55	-1.08	-0.57
11	-6.07	-5.59	-5.2	-1.53	-1.05	-0.47
12	-6.05	-5.59	-5.21	-1.53	-1.08	-0.57
13	-6.04	-5.61	-5.29	-1.44	-1.03	-0.52
14	-6.06	-5.59	-5.25	-1.51	-1.08	-0.55
15	-6.08	-5.58	-5.25	-1.5	-1.07	-0.48
16	-6.08	-5.6	-5.27	-1.49	-1.08	-0.54
17	-6.05	-5.62	-5.32	-1.43	-1.02	-0.51
18	-6.09	-5.61	-5.3	-1.47	-1.08	-0.53
19	-6.06	-5.63	-5.34	-1.42	-1.01	-0.5
20	-6.1	-5.62	-5.32	-1.45	-1.08	-0.52
Linear **3**	-6.27	-5.81	-5.47	-1.43	-1.04	-0.51

2.5. Bridge to Chapter III

This chapter details our work in probing the structure-property relationship of strained oligophenylene macrocycles. It suggests that the nanohoop topology with structural bending offers a new venue to control the properties of conjugated materials. In Chapter II, we describe the reactivity studies of 1,4-anthracene-incorporated [12]CPP, a model substrate to examine the feasibility of using anthracene as the functional handle to crosslink CPPs towards novel solid materials.

CHAPTER III

INVESTIGATING THE REACTIVITY OF 1,4-ANTHRACENE-INCORPORATED
CYCLOPARAPHENYLENE

From Li, P.; Wong, B. M.; Zakharov, L. N.; Jasti, R., Investigating the Reactivity of 1,4-Anthracene-Incorporated Cycloparaphenylene. *Org. Lett.* **2016,** *18* (7), 1574-1577.

Cycloparaphenylenes (CPPs) and their derivatives are unique conjugated macrocycles with novel optoelectronic and host−guest properties. A better understanding of their reactivity is essential for creating new functional materials utilizing these strained aromatic molecules as building blocks. 1,4-Anthracene-incorporated CPP **III.1** was synthesized and exhibited Diels−Alder reactivity but was unable to photodimerize. Comparison studies with cyclophane **III.2** and unstrained **III.3** indicated that the distorted anthracene geometry is likely the major contributor to the anomalous reactivity of **III.1**.

3.1. Introduction

The development of novel synthetic porous materials has a direct impact on a variety of technologies such as catalysis, separation, gas storage, and electronics.[1] These porous materials are commonly prepared by linking organic building units through covalent bonds (covalent organic frameworks and porous polymers),[2-4] metal coordination (metal organic frameworks),[5-6] or noncovalent interactions (porous molecular solids).[7] In addition to the collective effects of the entire building components, porous materials also inherit the intrinsic properties of their organic building blocks.[1] Therefore, developing novel molecular building blocks with unique properties is beneficial in expanding the applications of porous materials.

Cycloparaphenylenes (CPPs) are conjugated molecules with hoop-shaped backbones comprised of 1,4-connected benzene rings.[8-28] These strained aromatics and their related macrocyclic structures have potential materials applications owing to their ring-size dependent optoelectronic properties,[29] selective host−guest properties,[13,31-34] as

well as scalable gram-scale syntheses.[13,17,19] We have been interested in utilizing CPPs as building blocks to construct new carbon materials, which would potentially preserve the useful properties of CPPs including discrete porosity and tunable electronic behavior.[18] Herein, we report the synthesis, characterization, and reactivity study of 1,4-anthracene-incorporated [12]CPP **III.1** (**Figure 3.1**), in order to evaluate the practicality of utilizing anthracene as the reactive functional handle for crosslinking CPP-related molecules. Additionally, compounds **III.2** and **III.3** were prepared and studied to further elucidate the structural influence on the reactivity of the 1,4-diphenylanthracene (DPA) core.
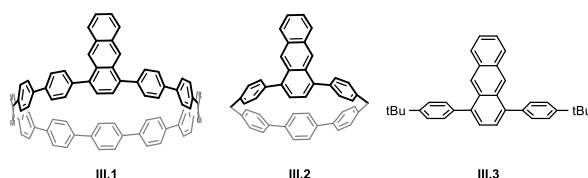
Figure 3.1. Structures of **III.1**-**3**.

The versatility and adaptability of anthracene chemistry have enabled chemists to create sophisticated architectures from complex molecules[35] to functional polymeric materials.[36] Recently, two-dimensional polymers (2DPs) were successfully prepared from the cycloaddition reactions of anthracene-containing monomers.[37-41] We envisioned that CPP structures with multiple 1,4-anthracene subunits could potentially be cross-linked to produce new types of network structures in a similar fashion as the case of 2DPs. However, previous seminal works on anthracenophanes suggest that the strained anthracene unit of **III.1** might have different reactivity compared to the planar counterparts.[42-44] Moreover, the substituent effect from the neighboring bent oligophenylene fragment might also impact the reactivity of the anthracene in **III.1**. Thus, we designed a strained cyclophane structure **III.2** that is free from the influence of this substituent effect, as well as a planar 1,4-DPA molecule **III.3**, in order to determine the key factors (bent geometry or substituent effect) that governs the reactivity of **III.1**. In this chapter, we surveyed the reactivity of **III.1**-**3** in photo-induced [4+4]-cycloaddition reactions and thermal Diels−Alder (DA) reactions, in combination with theoretical analyses to rationalize the structure−reactivity relationships.

3.2. Results and Discussion

3.2.1. Synthesis of III.1-3

In planning the synthesis of macrocyclic structures **III.1** and **III.2**, we adapted the generic strategy of CPP chemistry,[30] which takes advantage of the curved cyclohexadiene building units to assemble a less strained macrocyclic precursor which can be later aromatized to produce the target molecular skeleton. However, our initial synthetic attempt using anthryl intermediates failed to deliver isolable final products **III.1** and **III.2** (**Scheme 3.3**). We discovered that compounds **III.1** and **III.2** are unstable in the presence of light and oxygen, presumably due to the formation of labile endoperoxides.[42]

Inspired by Miller's works on hydrogen-protected acenes,[45] we developed a two-step aromatization strategy employing intermediates with a 9,10-dihydroanthryl moiety, which allowed for the purification and subsequent characterization of **III.1** and **III.2** in a glovebox with a chemically inert N_2 atmosphere. Depicted in Scheme **III.1**, the synthesis of macrocycles **III.8** and **III.9** was achieved by applying a Suzuki coupling condition using S-Phos Gen II precatalyst[46] from corresponding coupling partners in 30% and 27% yield, respectively. Treating **III.8** and **III.9** with single electron reductant sodium naphthalenide at −78 °C followed by quenching the reaction with I_2 gave the corresponding dihydroanthryl precursors **III.10** (71%) and **III.11** (50%). Finally, heating **III.10** or **III.11** with Pd/C in degassed toluene successfully yielded respective target molecule **III.1** (47%) or **III.2** (67%). Additionally, compound **III.3** and key intermediates **III.4**-**7** were easily prepared, and the synthetic details are provided in the Experimental Section (**Scheme 3.4**-**5**). The structures of **III.1**-**3** were confirmed by NMR (^{1}H, ^{13}C), IR, and mass spectrometry.

3.2.2. Electronic Properties of III.1-3

With these compounds in hand, we first investigated their electronic structures utilizing cyclic voltammetry and theoretical calculations. The first oxidation peaks for **III.1**-**3** are reversible with respective half wave potentials at 0.65, 0.60, and 0.72 V (vs Fc/ Fc$^+$). As Density Functional Theory (DFT, B3LYP/631G*) calculations predicted that the highest occupied molecular orbital (HOMO) and the lowest unoccupied molecular

orbital (LUMO) mainly delocalize on the DPA cores for compounds **III.1**-**3**, we confirmed that the measured first oxidation potentials truly represent the HOMO energy levels of the DPA segments. This observation of higher-lying HOMO energy levels in **III.1** and **III.2** compared to **III.3** is consistent with our previous finding that bending destabilizes the HOMO of the polycyclic aromatic hydrocarbons (PAHs).[47] We also observed an increasing calculated HOMO/LUMO energy gap from **III.1** (3.06 eV) to **III.2** (3.22 eV) to **III.3** (3.42 eV).
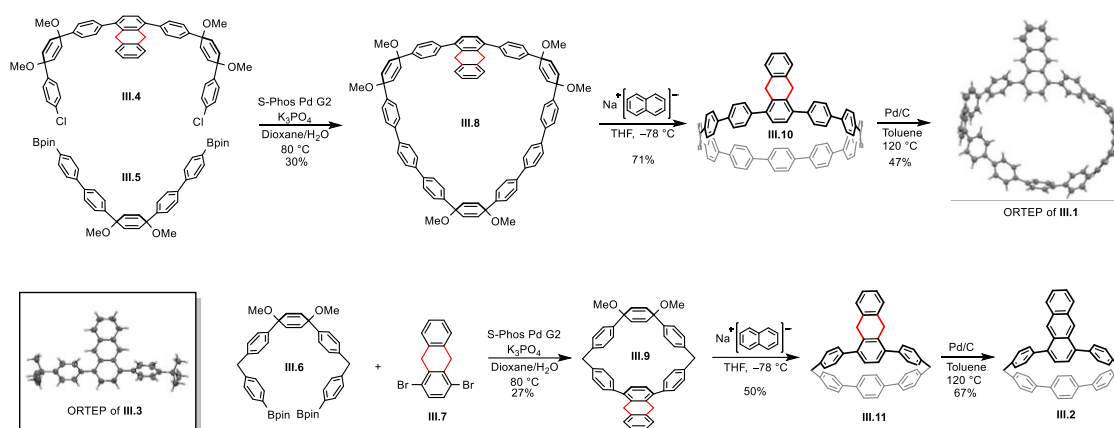
Scheme 3.1. Synthesis of **III.1** and **III.2** from 9,10-dihydroanthryl intermediates; X-ray single crystal structures of **III.1** and **III.3** (ORTEP).

3.2.3. Photophysical Properties of III.1-3

Next, we characterized the photophysical properties of **III.1**-**3** (**Figure 3.2**). The UV-Vis spectra of **III.1** exhibit an intense [12]CPP backbone absorption band (λ_{max} = 338 nm),[8] as well as anthracene absorption bands (λ_{max} = 268 nm and the broad band from 400 to 460 nm). Similarly, **III.2** displays both the *p*-terphenyl absorption (λ_{max} = 285 nm) and the anthracene absorption (λ_{max} = 268 nm and the broad band from 370 to 450 nm). For **III.3**, the UV−Vis spectra feature a characteristic anthracene absorption structure with well resolved vibrational bands (λ_{max} = 363 nm) and a high energy band at 263 nm.[48] From the onset absorption data, we calculated the optical band gaps to be 2.72 eV (**III.1**), 2.78 eV (**III.2**), and 2.98 eV (**III.3**), which is consistent with the trend of theoretical HOMO/LUMO energy gaps. Furthermore, TD-DFT calculations (B3LYP/6-

45

31G*) predicted that the lowest energy absorptions of **III.1**-**3** can be assigned to the HOMO/ LUMO transitions of the DPA cores. The fluorescence spectra were also recorded, where the emissions exhibit a hypsochromic shift from **III.1** (487 nm), to **III.2** (463 nm), to **III.3** (442 nm).
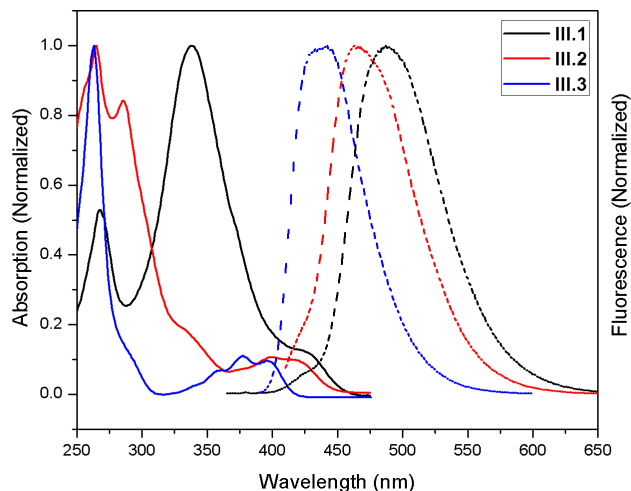
Figure 3.2. UV-Vis absorption and fluorescence spectra of **III.1**-**3** (measured in DCM solutions).

3.2.4. Molecular Structure Analysis of III.1-3

We were able to obtain single crystals of **III.1** and **III.3** suitable for X-ray crystallography (**Scheme 3.1** and **Figures 3.9**-**11**). For comparison, DFT calculations (B3LYP/6-31G*) were also performed to optimize the molecular geometries. Notably, the calculated molecular structures of **III.1** and **III.3** are in good agreement with the empirical X-ray crystal structures (**Table 3.2**). By analyzing the calculated structural data (**Table 3.1**), we found that the DPA cores of **III.1** and **III.2** have similar deformation angles α (7.4°, 9.5°), bent angles β (6.7°, 8.9°), and torsional angles θ (42.8°, 43.0°). By comparing **III.2** to **III.3**, it can be seen that the ring strain causes a decrease in torsional angles and an increase in the bent and deformation angles, which agrees with the observed trend when comparing CPPs to linear oligoparaphenylenes (LPPs).[29] Additionally, the calculated strain energies[49] on the DPA cores of **III.1**-**3** were 56.34, 62.04, and 4.78 kcal/mol, respectively. Interestingly, the strain energy trend correlates

well with the experimental trend of HOMO energy levels determined from the cyclic voltammetry. Overall, our electrochemical, photophysical, and theoretical studies demonstrated that the DPA cores in **III.1** and **III.2** share similar electronic and geometric characters that are distinct from those of **III.3**.

Table 3.1. Calculated structural properties of **III.1**-**3** (DFT, B3LYP6-31G*). Dihedral angles (θ) shown are average values.
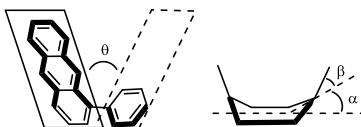
entry	θ, deg	α, deg	β, deg
III.1	42.8	7.4	6.7
III.2	43.0	9.5	8.9
III.3	54.5	4.5	0.7

3.2.5. Reaction Survey of III.1-3 in Cycloaddition Reactions

We examined the photodimerization and DA reactions of these anthracene-containing compounds. Upon UV irradiation, **III.3** undergoes [4+4]-cycloaddition to generate the head-to-tail photodimer **III.12** in quantitative yield (**Scheme 3.2**). In contrast, no reactions were observed for **III.1** and **III.2** when similar conditions were applied. Changing the light source to a different wavelength or altering solvent polarity still produced no photodimer products for **III.1** and **III.2**. We also attempted crossover experiments by mixing excess **III.3** with either **III.1** or **III.2** only to observe photodimer **III.12** and unreacted **III.1** or **III.2**. As for DA reactions, **III.1**-**3** readily reacted with dienophiles tetracyanoethylene (TCNE) and diethyl acetylenedicarboxylate to produce the corresponding DA-adducts **III.13**-**18**, of which the new bonds form at the 9,10-position of the anthracene core (**Scheme 3.2**). As **III.1** and **III.2** have higher-lying HOMO levels compared to **III.3**, it is expected that **III.1** and **III.2** should be more reactive with dienophiles than **III.3**.[50] Surprisingly, **III.1** and **III.3** show no DA reactivity with C_{60} while the DA-adduct of **III.3** with C_{60} was observed under similar and less energetic conditions. Additionally, we synthesized 1,4-anthracene incorporated [10]CPP, which is also unreactive with C_{60}, though the host−guest complex was observed as expected. These reaction studies clearly indicated that compound **III.2** exhibits identical

reactivity as **III.1**, from which we conclude that the distorted anthracene geometry is likely the main contributor to the anomalous photochemical and DA reactivity of **III.1** compared to unstrained **III.3**.
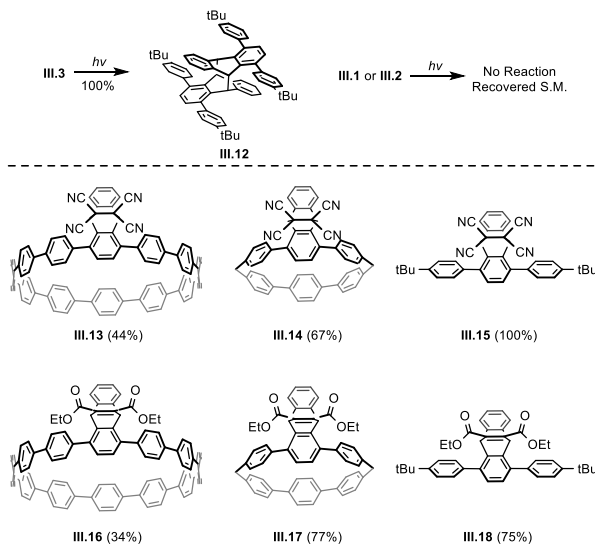
Scheme 3.2. Photodimerization of **III.1**-**3**; DA-adducts of **III.1**-**3** with tetracyanoethylene (**III.13**-**15**) and with diethyl acetylenedicarboxylate (**III.16**-**18**).

3.2.6. Computational Investigations

In order to rationalize the relationship between the distorted anthracene geometry and the observed anomalous reactivity, we conducted theoretical calculations at the ωB97XD/6-31G* level of theory[51] to analyze the reaction free energies and the transition state energy barriers. Since our calculations omitted the configurational entropic factors (ΔS), the actual free energy ($\Delta G = \Delta H - T\Delta S$) is higher than the calculated values ($T\Delta S > 0$).[52] We found that the reaction free energy for dimerization of **III.1** is endergonic (1.2 kcal/mol), which alone indicates that the dimerization is not favored in terms of thermodynamics. The free energies for the dimerization of **III.2** and **III.3** are exergonic with respective values of −1.6 and −6.7 kcal/mol. It is possible the change of the entropy for the dimerization of **III.2** is pronounced enough that the reversed dissociation reaction is favored.[53] We also calculated the reaction barriers for each of the cases but found that the transition state structures exhibited broken-symmetry and multireference effects which are beyond the scope of the single-reference DFT approach

48

used here.[54] Additionally, the reaction free energies for DA reactions of C_{60} with **III.1-3** are all calculated to be exergonic (**III.1**, −16.0 kcal/mol; **III.2**, −15.6 kcal/ mol; **III.3**, −20.9 kcal/mol) and the activation free energies for **III.1-3** are determined to be 17.9, 16.9, and 12.7 kcal/mol, respectively. Though no definitive conclusion could be made regarding the reaction outcomes from these data, the DA reaction of C_{60} with **III.3** is suggested to be both kinetically and thermodynamically favored. Likewise, the configurational entropy (i.e., the number of possible molecular configurations increases in the order of **III.3**, **III.2**, and **III.1**) could play an important role in differentiating the DA reaction outcome between **III.1** (**III.2**) and **III.3**. Thus, our theoretical analysis seemed to suggest that the bent geometry influences the reactivity by elevating the transition energy barriers and by destabilizing the products.

3.3. Conclusion and Outlook

We have synthesized and characterized 1,4-anthracene incorporated [12]CPP **III.1** and two reference compounds **III.2** and **III.3**. We discovered that **III.1**, though unable to photodimerize, can still react with certain dienophiles. Therefore, the DA reaction is a potential strategy to construct new carbon materials from anthracene-incorporated CPPs. Additionally, through the comparison studies with reference compounds **III.2** and **III.3**, we determined that the unusual reactivity of **III.1** is likely to originate from the bent and distorted geometry, rather than the substituent effect from the backbone. Importantly, our work suggests that the change in the reactivity of strained PAHs should be taken into consideration when planning cross-linking strategies.

3.4. Experimental
3.4.1. General Experimental Details

Tetrahydrofuran (THF) and dioxane were obtained from a solvent system with columns packed with activated alumina. Moisture and oxygen sensitive reactions were carried out under nitrogen atmosphere using standard Schlenk line techniques. Silica column chromatography was conducted with Zeochem Zeoprep n60 Eco 40-63 μm silica

gel. Thin layer chromatography (TLC) was performed using Sorbent Technologies Silica Gel XHT TLC plates. Developing plates were visualized using UV light at wavelength of 254 and 365 nm. UV-Vis spectra were measured on an Agilent Cary 100 UV-Vis spectrophotometer. NMR spectra were recorded on a Bruker Avance-III-HD 600 (or 500) spectrometer with a Prodigy multinuclear broadband cryoProbe. Chemical shifts were reported in parts per million (ppm) and were referenced to the residual protio-solvent (CDCl$_3$, ^{1}H: 7.26 and ^{13}C: 77.16). IR spectra were recorded on a Thermo Scientific Nicolet 6700 spectrometer equipped with a diamond crystal Smart ATR Attachment. Cyclic voltammetry was performed in a N$_2$ atmosphere glove box using a Solartron 1287 potentiostat. A 3-electrode set-up was employed comprising a glassy carbon working electrode, a platinum coil counter electrode and a silver wire pseudo reference electrode. Electrolyte solutions (0.1 M) were prepared from HPLC-grade DCM and anhydrous Bu$_4$NBF$_4$, and the solutions were thoroughly degassed prior to analysis.

3.4.2. Synthetic Details
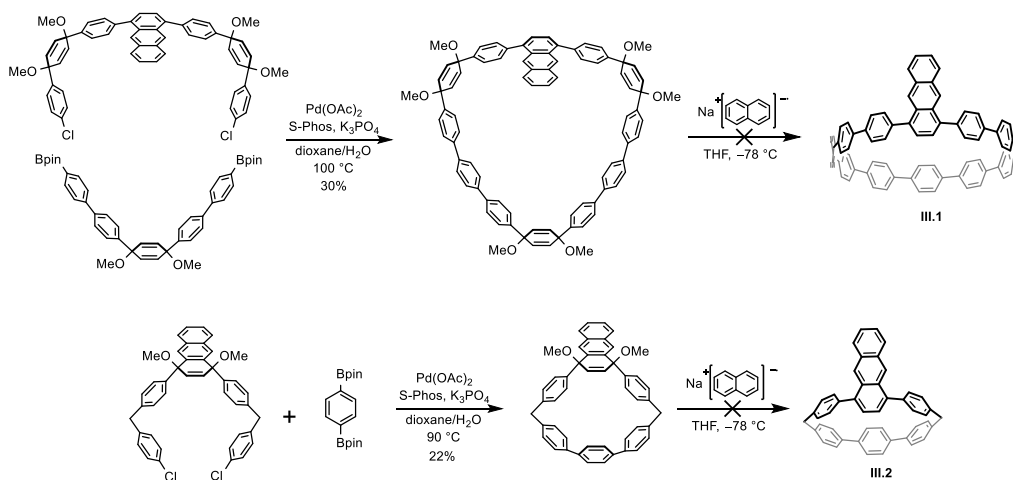
Scheme 3.3. Initial synthetic scheme using anthryl intermediates.

50
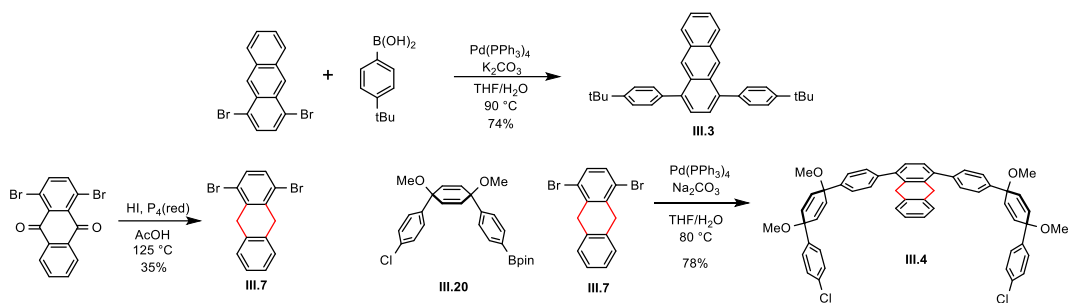
Scheme 3.4. Synthesis of compounds **III.3**, **III.4** and **III.7**.
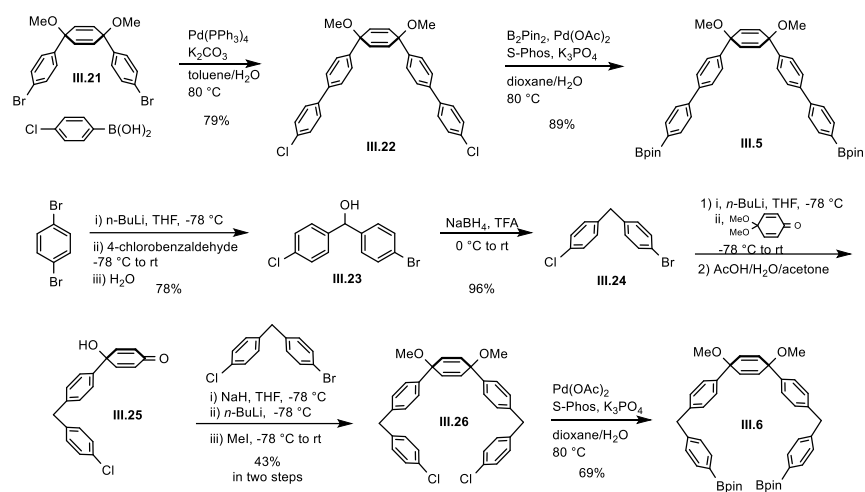
Scheme 3.5. Synthesis of key intermediates **III.5** and **III.6**.
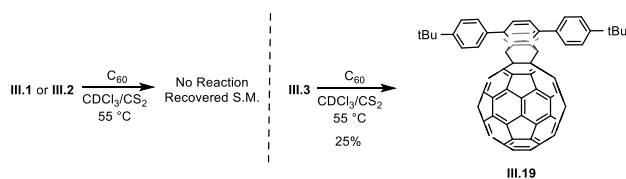
Scheme 3.6. DA reactions of **III.1-3** with C$_{60}$.
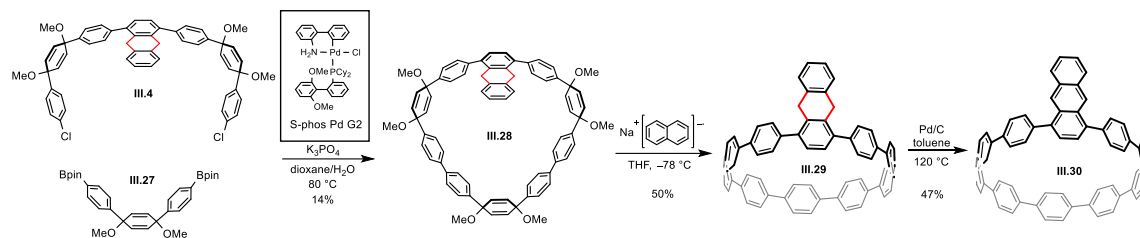
Scheme 3.7. Synthesis of 1,4-anthrancene-incorporated [10]CPP **III.30**.

1,4-dibromo-9,10-dihydroanthracene **III.7**
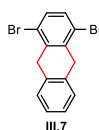
To a 1 L round bottom flask equipped with a stir bar was added 1,4-dibromoanthracene-9,10-dione (8.56 g, 23.4 mmol, 1 eq), red phosphorus (8.56 g. 276 mmol, 12 eq), hydriodic acid (47%, 50 mL) and glacial acetic acid (350 mL). The mixture was heated at 125 °C in dark for three days. When cooled to room temperature, the mixture was poured into water (1 L) and filtrated. The red solid collected was washed with DCM (200 mL) to dissolve the product. Then the solution was concentrated to about 20 mL, at which point methanol (5 mL) was added. After sitting overnight, the product crystalized as colorless needle and was collected via filtration (2.75g, 35%). IR (neat) 3096, 3066, 3027, 3010, 2891, 1665, 1479, 1455, 1435, 1194, 890 cm^{-1}; ^{1}H NMR (600 MHz, CDCl$_3$): δ(ppm) 7.38-7.34 (overlap, 4H, Ar-H), 7.30-7.26 (dd, J = 5.3, 3.3 Hz, 2H, Ar-H), 4.14 (s, 4H, CH$_2$); ^{13}C NMR (150 MHz, CDCl$_3$): δ(ppm) 137.73, 134.63, 131.41, 127.83, 126.80, 123.13, 36.52; HRMS (Q-TOF, EI+) m/z cald for C$_{14}$H$_{10}$Br$_2$ (M)$^+$ 335.9150, found 335.9135.

1-((1's,4's)-4''-chloro-1',4'-dimethoxy-1',4'-dihydro-[1,1':4',1''-terphenyl]-4-yl)-4-(4''-chloro-1',4'-dimethoxy-1',4'-dihydro-[1,1':4',1''-terphenyl]-4-yl)-9,10-dihydroanthracene **III.4**

52
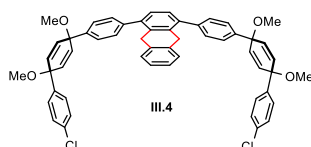
III.20 (3.38 g, 7.45 mmol, 2.4 eq), **III.7** (1.05 g, 3.11 mmol, 1 eq), Na_2CO_3 (1.65 g, 15.5 mmol, 5 eq) and $Pd(PPh_3)_4$ (0.36 g, 0.31 mmol, 0.1 eq) were placed in a 250 mL round bottom flask equipped with condenser and stir bar. The flask was evacuated and backfilled with N_2 for 10 times. Then THF (75 mL) and H_2O (15 mL) were transferred to the flask via syringe. The resulting yellow mixture was heated at 80 °C under N_2 overnight. After cooling down to room temperature, DCM (80 mL) was added to the reaction. The mixture was washed with H_2O (50 mL) and brine (100 mL) and then dried with Na_2SO_4. Solvent was removed under reduced pressure and the crude was purified by column chromatography (silica, 0% to 12% ethyl acetate in hexanes) to yield product as white powder (1.90 g, 78%). IR (neat) 3030, 2935, 2822, 1745, 1474, 1402, 1264, 1227, 1172, 1079, 1013, 949, 823 cm^{-1}; ^{1}H NMR (600 MHz, CDCl$_3$): δ(ppm) 7.51 (d, J = 8.2 Hz, 4H, Ar-H), 7.41-7.36 (overlap, 8H, Ar-H), 7.29 (d, J = 8.6 Hz, 4H, Ar-H), 7.21 (s, 2H, Ar-H), 7.15-7.11 (m, 4H, Ar-H), 6.25 (d, J = 10.3 Hz, 4H, CH=CH), 6.14 (d, J = 10.3 Hz, 4H, CH=CH), 3.93 (s, 4H, CH$_2$), 3.51 (s, 6H, OCH$_3$), 3.47 (s, 6H, OCH$_3$); ^{13}C NMR (150 MHz, CDCl$_3$): δ(ppm) 142.12, 142.10, 141.00, 139.53, 137.54, 135.33, 133.87, 133.58, 133.46, 129.80, 128.64, 127.65, 127.48, 127.13, 126.23, 125.99, 74.90, 74.70, 52.30, 52.22, 34.62; MALDI-TOF m/z cald for C$_{54}$H$_{44}$Cl$_2$O$_4$ (M)$^+$ 828.28, found 828.02.

(1″s,4″s)-4,4″″-dichloro-1″,4″-dimethoxy-1″,4″-dihydro-1,1′:4′,1″:4″,1‴:4‴,1″″-quinquephenyl **III.22**
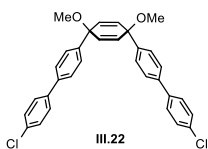
III.21 (3.00 g, 6.66 mmol, 1 eq), 4-chlorophenylboronic acid (6.13 g, 40.0 mmol, 6 eq), K_2CO_3 (4.60 g, 33.3 mmol, 5 eq) and $Pd(PPh_3)_4$ (0.38 g, 0.33 mmol, 0.05 eq) were placed in a 250 mL round bottom flask equipped with condenser and stir bar. The flask was evacuated and backfilled with N_2 for 10 times. Then THF (100 mL) and H_2O (20 mL) were transferred to the flask via syringe. The resulting yellow mixture was heated at 90 °C under N_2 overnight. After cooling down to room temperature, DCM (100 mL) was added to the reaction. The mixture was washed with H_2O (50 mL) and brine (100 mL)

and then dried with Na_2SO_4. Solvent was removed to yield black solid to which and acetone (100 mL) was added. Then the mixture was sonicated for 5 min and then filtered. The filtrate was concentrated and re-subjected to filtration. The combined crude solid was purified by chromatography (silica, 0% to 100% DCM in hexanes) to yield product as white solid (2.70 g, 79%). IR (neat) 3030, 2980, 2396, 2821, 1484, 1392, 1264, 1231, 1175, 1090, 1004, 948 cm^{-1}; ^{1}H NMR (600 MHz, CDCl$_3$): δ(ppm) 7.53–7.48 (overlap, 12H, Ar-H), 7.39 (d, J = 8.5 Hz, 4H, Ar-H), 6.17 (s, 4H, CH=CH), 3.48 (s, 6H, OCH$_3$); ^{13}C NMR (150 MHz, CDCl$_3$): δ(ppm) 142.98, 139.39, 139.29, 133.58, 133.57, 129.05, 128.46, 127.12, 126.71, 74.84, 52.20; HRMS (Q-TOF, EI+) m/z cald for $C_{32}H_{26}Cl_2O_2$ (M)$^+$ 512.1209, found 512.1315.

2,2'-((1"s,4"s)-1",4"-dimethoxy-1",4"-dihydro-[1,1':4',1":4",1"':4"',1""-quinquephenyl]-4,4""-diyl)bis(4,4,5,5-tetramethyl-1,3,2-dioxaborolane) **III.5**
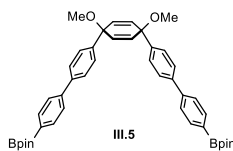
To a 100 mL round bottom flask was added **III.4** (2.70 g, 5.26 mmol, 1 eq), B$_2$Pin$_2$ (10.5 g, 42.1 mmol, 8 eq), K$_3$PO$_4$ (8.90 g, 42.1 mmol, 8 eq), Pd(OAc)$_2$ (0.140 g, 0.21 mmol, 0.01 eq) and S-Phos (0.217 g, 0.53 mmol, 0.1 eq). The flask was evacuated and backfilled with N$_2$ for 10 times. After switching the vacuum adapter with septum, the flask was purged with N$_2$ for another 30 min. At this point, degassed dioxane (40 mL) was added to the flask and the mixture was heated at 80 °C overnight. Upon cooling down to room temperature, solvent was removed under reduced pressure. Then the residue was mixed with hexanes (100 mL) and sonicated for 10 min. Light-grey colored product (3.24 g, 89%) was collected using vacuum filtration. Analytical pure sample can be achieved using column chromatography (silica, 0% to 10% ethyl acetate in hexanes). IR (neat) 3029, 2977, 2933, 2821, 1608, 1525, 1469, 1396, 1356, 1271, 1142, 1020, 950cm^{-1}; ^{1}H NMR (600 MHz, CDCl$_3$): δ(ppm) 7.89 (d, J = 8.0 Hz, 4H, Ar-H), 7.65-7.56 (m, 8H, Ar-H), 7.51 (d, J = 8.4 Hz, 4H, Ar-H), 6.18 (s, 4H, CH=CH), 3.48 (s, 6H, OCH$_3$), 1.37 (s, 24H, CH$_3$); ^{13}C NMR (150 MHz, CDCl$_3$): δ(ppm) 143.49, 142.92, 140.35, 135.38, 133.50, 127.36, 126.58, 126.51, 83.93, 74.84, 52.15, 25.01, C-B signal

not observed; HRMS (TOF, ES+) m/z cald for $C_{44}H_{50}B_2O_6Na$ (M+Na)$^+$ 719.3691, found 719.3706.

(4-bromophenyl)(4-chlorophenyl)methanol **III.23**
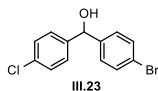
A solution of 1,4-dibromobenzene (40.3 g, 171 mmol, 1.2 eq) in THF (200 mL) was cooled to −78 °C, at which point nBuLi (2.1 M, 163 mmol, 1.15 eq) was added drop-wise over 30 min. The resulting white slurry was kept stirring at −78 °C for another 20 min and then 4-chlorobenzaldehyde (20.0 g, 142 mmol, 1 eq) was added as solid in one portion. The mixture was allowed to warm to room temperature overnight. To the solution was added H_2O (10 mL) to quench the remaining nBuLi. The reaction was extracted with ethyl acetate (200 mL), washed with brine (300 mL) and dried over Na_2SO_4. The solution was concentrated to 50 mL and hexanes (50 mL) was added. The mixture was placed in freezer (−20 °C) for 2 h. At this point, crude solid product precipitated on the bottom of the flask and was collected by vacuum filtration. The solid was washed with hexanes (50 mL) and dried under vacuum to give product as white powder (33.0 g, 78%). IR (neat) 3330, 2901, 1904, 1590, 1484, 1404, 1292, 1189, 1088, 1037, 1008, 863, 791 cm^{-1}; ^{1}H NMR (600 MHz, CDCl$_3$): δ(ppm) 7.46 (d, *J* = 8.4 Hz, 2H, Ar-H), 7.31 (d, *J* = 8.6 Hz, 2H, Ar-H), 7.27 (d, *J* = 8.6 Hz, 2H, Ar-H), 7.22 (d, *J* = 8.4 Hz, 2H, Ar-H), 5.76 (d, *J* = 3.3 Hz, 1H, CH), 2.31 (d, *J* = 3.3 Hz, 1H, OH); ^{13}C NMR (150 MHz, CDCl$_3$): δ(ppm) 142.45, 141.86, 133.74, 131.83, 128.90, 128.31, 127.98, 121.86, 75.12; HRMS (Q-TOF, EI+) m/z cald for $C_{13}H_{10}BrClO$ (M)$^+$ 295.9603, found 295.9605.

1-bromo-4-(4-chlorobenzyl)benzene **III.24**
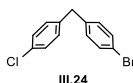
III.23 (24.46 g, 82.2 mmol, 1 eq) was dissolved in a mixture of DCM (150 mL) and trifluoroacetic acid (150 mL) in a 1 L round bottom flask. The solution was chilled with brine-ice bath for 30 min. Sodium borohydride (8.40 g, 222 mmol) was added

55

portion-wise over 20 min. The mixture was allowed to stir for extra 2h, at which point concentrated NaOH solution was slowly added until pH > 7. Then the mixture was extracted with diethyl ether (3 × 200 mL). Combined organic extract was washed with H$_2$O (200 mL), brine (300 mL) and dried over Na$_2$SO$_4$. The solvent was removed to give product as light yellow oil which, upon standing, solidified to white solid (22.3 g, 96%). IR (neat) 3079, 3060, 3023, 2939, 2922, 2852, 1907, 1485, 1438, 1402, 1132, 1112, 1069, 1010, 859 808, 778 cm^{-1}; ^{1}H NMR (600 MHz, CDCl$_3$): δ(ppm) 7.40 (d, J = 8.4 Hz, 2H, Ar-H), 7.24 (d, J = 8.4 Hz, 2H, Ar-H), 7.07 (d, J = 8.3 Hz, 2H, Ar-H), 7.02 (d, J = 8.3 Hz, 2H, Ar-H), 3.88 (s, 2H, CH$_2$); ^{13}C NMR (150 MHz, CDCl$_3$): δ(ppm) 139.64, 139.02, 132.28, 131.76, 130.71, 130.31, 128.81, 120.31, 40.73; MS (TOF, CI+) m/z cald for C$_{13}$H$_{10}$BrCl (M)$^+$ 279.9654, found 279.9655.

4,4''-bis(4-chlorobenzyl)-1',4'-dimethoxy-1',4'-dihydro-1,1':4',1''-terphenyl **III.26**
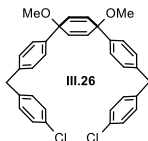
A solution of **III.24** (4.00 g, 24.0 mmol, 1.2 eq) in THF (80 mL) was cooled to −78 °C, at which point nBuLi (2.1 M, 6.8 mL, 14.2 mmol, 1.2 eq) was slowly added in 10 min. The resulting orange solution was allowed to stir at −78 °C for 10 min, then a solution of 4,4-dimethoxy-2,5-cyclohexadien-1-one (1.82 g, 11.8 mmol, 1 eq) in THF (6 mL) was added in stream. Then the cold bath was removed and the resulting mixture was allowed to warm to room temperature in 2 hours and quenched with water (2 mL). DCM (100 mL) was and the resulting mixture was washed with brine (200 mL) then dried over Na$_2$SO$_4$. After removing the solvent, acetone (30 mL) and acetic acid (10 wt% in water, 30 mL) was added to the residue. The resulting mixture was stir at room temperature for 30 min, at which point DCM (50 mL) was added. The organic layer was separated and washed saturated aqueous NaHCO$_3$ solution (4 × 100 mL), brine (100 mL) and dried over Na$_2$SO$_4$. Removing solvent produced crude yellow oil **III.25**, which was used without further purification.

Crude **III.25** and **III.24** (7.00 g, 24.9 mmol, 2.1 eq) was dissolved in THF (80 mL). The resulting solution was cooled to −78 °C, at which point NaH (60 wt%, 24.9

mmol, 1.00 g, 2.1 eq) was added as solid. The resulting mixture was allowed to stir at
−78 °C for 2 hours. Then nBuLi (2.1 M, 6.8 mL, 14.2 mmol, 1.2 eq) was slowly added
over the course of 20 min. The mixture was kept stirring at −78 °C for another 2 hours.
Afterwards, methyl iodide (15.2 mL, 249 mmol, 20 eq) and DMF (50 mL) were added.
The mixture was eventually allowed to warm to room temperature and stir overnight.
Water (10 mL) was slowly added to quench the reaction. Then DCM (100 mL) was
added and resulting mixture was washed with aqueous LiCl solution (5 wt%, 3×150 mL),
brine (150 mL) and dried over Na_2SO_4. After removing solvent, the crude orange oil was
purified by column chromatography (silica, 0% to 6% ethyl acetate in hexanes) to yield
product as colorless oil (4.32 g, 43% over two steps). IR (neat) 3022, 2935, 2820, 1505,
1489, 1405, 1264, 1230, 1171, 1080, 1015, 948, 812, 789 cm^{-1}; ^{1}H NMR (600 MHz,
CDCl$_3$): δ(ppm) 7.31 (d, J = 8.3 Hz, 4H, Ar-H), 7.21 (d, J = 8.4 Hz, 4H, Ar-H), 7.09-7.03
(overlap, 8H, Ar-H), 6.07 (s, 4H, CH=CH), 3.88 (s, 4H, CH$_2$), 3.40 (s, 6H, OCH$_3$); ^{13}C
NMR (150 MHz, CDCl$_3$): δ(ppm) 141.64, 139.89, 139.53, 133.44, 131.96, 130.35,
128.96, 128.60, 126.29, 74.68, 52.06, 40.91; MALDI-TOF m/z cald for $C_{34}H_{31}Cl_2O_2$
(M+H)$^+$ 541.17, found 541.14.

2,2'-(((1',4'-dimethoxy-1',4'-dihydro-[1,1':4',1''-terphenyl]-4,4''-
diyl)bis(methylene))bis(4,1-phenylene))bis(4,4,5,5-tetramethyl-1,3,2-dioxaborolane) **III.6**
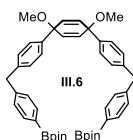
A similar procedure to synthesize **III.5** was adapted. **III.26** (1.3 g, 2.40 mmol, 1
eq), B$_2$Pin$_2$ (4.87 g, 19.2 mmol, 8 eq), K$_3$PO$_4$ (4.07 g, 19.2 mmol, 8 eq), Pd(OAc)$_2$ (0.130
g, 0.19 mmol, 0.08 eq) and S-Phos (0.197 g, 0.48 mmol, 0.2 eq), product was purified by
column chromatography (silica, 0% to 10% ethyl acetate in hexanes) as white powder
(1.2 g, 69%). IR (neat) 2977, 2936, 2816, 1613, 1555, 1510, 1360, 1270, 1143, 1018,
951, 858, 810 cm^{-1}; ^{1}H NMR (500 MHz, CDCl$_3$): δ(ppm) 7.73 (d, J = 7.6 Hz, 4H, Ar-H),
7.29 (d, J = 7.9 Hz, 4H, Ar-H), 7.18 (d, J = 7.9 Hz, 4H, Ar-H), 7.10 (d, J = 7.6 Hz, 4H,
Ar-H), 6.07 (s, 4H, CH=CH), 3.96 (s, 4H, CH$_2$), 3.40 (s, 6H, OCH$_3$), 1.33 (s, 24H, CH$_3$);
^{13}C NMR (150 MHz, CDCl$_3$): δ(ppm) 144.43, 141.42, 140.22, 135.10, 133.41, 129.06,

128.57, 126.21, 83.80, 74.74, 52.06, 41.87, 24.99, C-B signal not observed; HRMS (Q-TOF, ES+) m/z cald for $C_{46}H_{54}B_2O_6$ (M)$^+$ 725.4185, found 725.4222.

Macrocycle **III.8**

III.8
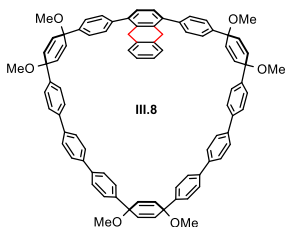
To a 250 mL round bottom flask was added **III.4** (542 mg, 0.653 mmol, 1 eq), **III.5** (500 mg, 0.718 mmol, 1.1 eq), S-Phos Gen II precatalyst (52 mg, 0.072 mmol, 0.1 eq) and dioxane (180 mL). The mixture was deoxygenated by bubbling N_2 for 2 h and was then heated to 80 °C. At this point, aqueous K_3PO_4 solution (2 M, 18 mL) was added. The solution gradually turned light orange within 5 min and was kept stirring at 80 °C overnight. Upon cooling to room temperature, the crude reaction was passed through a short plug of Celite. DCM (50 mL) was used to wash the Celite and combined with the filtrate. The solution was added extra DCM (200 mL) and washed with H_2O (100 mL), brine (200 mL) and dried over Na_2SO_4. After removing solvent, the crude reaction was purified with column chromatography (silica, 0% to 4% ethyl acetate in DCM) to give product as white powder (236 mg, 30%). IR (neat) 3030, 2933, 2819, 1487, 1449, 1389, 1264, 1174, 1076, 948, 814 cm^{-1}; ^{1}H NMR (600 MHz, CDCl$_3$): δ(ppm) 7.68-7.54 (overlap, 24H, Ar-H), 7.52 (d, J = 8.3 Hz, 4H, Ar-H), 7.41 (d, J = 8.0 Hz, 4H, Ar-H), 7.27 (s, 2H, Ar-H), 7.17-7.09 (overlap, 4H, Ar-H), 6.26 (d, J = 10.3 Hz, 4H, CH=CH), 6.23 (d, J = 10.3 Hz, 4H, CH=CH), 6.19 (s, 4H, CH=CH), 3.95 (s, 4H, CH$_2$), 3.56 (s, 6H, OCH$_3$), 3.53 (s, 6H, OCH$_3$), 3.50 (s, 6H, OCH$_3$); ^{13}C NMR (150 MHz, CDCl$_3$): δ(ppm) 142.75, 142.67, 142.36, 140.36, 139.97, 139.90, 139.73, 139.60, 137.57, 135.33, 133.85, 133.67, 133.64, 129.80, 127.52, 127.51, 127.45, 127.17, 127.10, 127.07, 126.65, 126.21, 126.03, 75.16, 75.12, 75.10, 52.32, 52.25, 52.22, 34.67; MALDI-TOF m/z cald for $C_{85}H_{69}O_5$ (M-OMe)$^+$ 1169.51, found 1169.20, cald for $C_{86}H_{72}O_6$ (M)$^+$ 1200.53, found 1200.22.

6¹,6⁴-dimethoxy-2⁹,2¹⁰-dihydro-2(1,4)-anthracena-1,3,5,7(1,4)-tetrabenzena-6(1,4)-cyclohexanacyclooctaphane-62,65-diene **III.9**
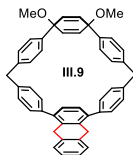
A similar procedure to synthesize **III.8** was adapted. **III.6** (500 mg, 0.690 mmol, 1.1 eq), **III.7** (212 mg, 0.627 mmol, 1 eq), S-Phos Gen II precatalyst (23 mg, 0.031 mmol, 0.05 eq), dioxane (200 mL), K_3PO_4 solution (2 M, 20 mL), product purified by column chromatography (silica, 0% to 15% ethyl acetate in hexanes) as white powder (110 mg, 27%). IR (neat) 3020, 2922, 2835, 1599, 1503, 1488, 1383, 1263, 1222, 1178, 1059, 1024, 946, 732 cm^{-1}; ^{1}H NMR (600 MHz, CDCl$_3$): δ(ppm) 7.39 (d, J = 8.0 Hz, 4H, Ar-H), 7.35 (dd, J = 5.3, 3.3 Hz, 2H, Ar-H), 7.21 (dd, J = 5.3, 3.3 Hz, 2H, Ar-H), 7.15 (d, J = 8.0 Hz, 4H, Ar-H), 7.07 (d, J = 8.3 Hz, 4H, Ar-H), 6.82 (s, 2H, Ar-H), 6.57 (d, J = 8.3 Hz, 4H, Ar-H), 5.97 (s, 4H, CH=CH), 4.32 (s, 4H, CH$_2$), 3.92 (s, 4H, CH$_2$), 3.26 (s, 6H, OCH$_3$); ^{13}C NMR (150 MHz, CDCl$_3$): δ(ppm) 142.56, 140.86, 140.77, 140.05, 138.48, 138.03, 135.31, 132.63, 131.58, 130.20, 129.17, 128.42, 126.82, 126.32, 126.03, 73.34, 51.60, 40.94, 35.55; MALDI-TOF m/z cald for $C_{48}H_{41}O_2$ (M+H)$^+$ 649.31, found 649.28.

1,4-(9,10-dihydroanthryl)-[12]CPP **III.10**
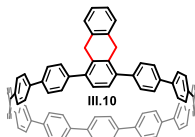
Under N$_2$, **III.8** (120 mg, 0.1 mmol, 1 eq) dissolved in dry THF (40 mL) was cooled to −78 °C. Freshly prepared sodium naphthalenide (0.25 M, 12 mL, 3.0 mmol, 30 eq) was added drop-wise to the solution, which was kept stirring at −78 °C for 30 min. Then I$_2$ (1 M solution in THF) was added until green color disappeared, followed by adding saturated Na$_2$S$_2$O$_3$ solution (2 mL). The mixture was allowed to warm to room temperature at which point DCM (50 mL) was added. The crude reaction was washed with H$_2$O (80 mL), brine (100 mL) and dried over Na$_2$SO$_4$. Removing solvent, the product was isolated using column chromatography (silica, 0% to 30% DCM in hexanes) as yellow solid (72 mg, 71%). IR (neat) 3075, 3023, 2925, 2808, 1593, 1482, 1384, 1263,

1001, 809 cm^{-1}; ^{1}H NMR (600 MHz, CDCl$_3$): δ(ppm) 7.75-7.58 (overlap, 40H, Ar-H), 7.49 (d, J = 8.4 Hz, 4H, Ar-H), 7.32 (dd, J = 5.5, 3.3 Hz, 2H, Ar-H), 7.22 (dd, J = 5.5, 3.3 Hz, 2H, Ar-H), 6.81 (s, 2H, Ar-H), 4.31 (s, 4H, CH$_2$); ^{13}C NMR (150 MHz, CDCl$_3$): δ(ppm) 140.45, 138.84, 138.80, 138.72, 138.70, 138.67, 138.65, 137.99, 135.06, 129.94, 129.69, 127.57, 127.52, 127.49, 127.43, 127.17, 127.14, 126.39, 35.39; MALDI-TOF m/z cald for C$_{80}$H$_{54}$ (M)$^+$ 1014.42, found 1014.42.

2^9,2^{10}-dihydro-2(1,4)-anthracena-1,3,5,6,7(1,4)-pentabenzenacyclooctaphane **III.11**

III.11
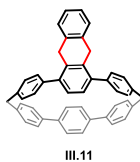
A similar procedure to synthesize **III.10** was adapted. **III.9** (93 mg, 0.14 mmol, 1 eq), sodium naphthalenide (5.7 mL, 1.43 mmol, 10 eq), product purified by column chromatography (silica, 0% to 30% ethyl acetate in DCM) as yellow powder (42 mg, 50%). IR (neat) 3040, 3018, 2969, 2927, 2856, 2808, 1898, 1591, 1502, 1440, 1382, 1264, 1065, 966, 862 cm^{-1}; ^{1}H NMR (600 MHz, CDCl$_3$): δ(ppm) 7.27 (s, 4H, Ar-H), 7.21 (d, J = 8.3 Hz, 4H, Ar-H), 7.16-7.09 (overlap, 8H, Ar-H), 7.07 (d, J = 8.2 Hz, 4H, Ar-H), 6.10 (s, 2H, Ar-H), 4.11 (s, 4H, CH$_2$), 3.91 (s, 4H, CH$_2$); ^{13}C NMR (150 MHz, CDCl$_3$): δ(ppm) 144.45, 143.87, 139.82, 138.77, 138.53, 138.41, 137.83, 134.10, 130.64, 129.26, 128.28, 128.11, 127.40, 127.29, 127.04, 126.22, 43.40, 34.99; MALDI-TOF m/z cald for C$_{46}$H$_{35}$ (M+H)$^+$ 587.27, found 587.03.

1,4-anthryl-[12]CPP **III.1**
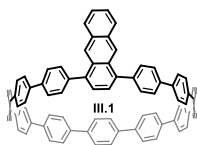
III.1

To a 50 mL Schlenk flask was added **III.10** (17 mg, 0.0017 mmol, 1 eq), Pd/C (10 wt%, 107 mg, 0.104 mmol, 5.9 eq) and dry toluene (25 mL). The mixture was degassed through free-pump-thaw for 5 times, after which it was covered with aluminum foil and heated at 120 °C for 3 days. After cooling to room temperature, the Schlenk flask with the crude reaction was transferred into a glove box. The crude reactions was passed

through a short plug of Celite. The solvent was then removed to produce product as yellow solid (8 mg, 47%).IR (neat) 3026, 1907, 1598, 1482, 1389, 1264, 1281, 1264, 1108, 1102, cm^{-1}; ^{1}H NMR (500 MHz, CDCl$_3$): δ(ppm) 8.96 (s, 2H, Ar-H), 8.02 (dd, J = 6.5, 3.3 Hz, 2H, Ar-H), 7.74-7.57 (overlap, 44H, Ar-H), 7.51 (dd, J = 6.5, 3.3 Hz, 2H, Ar-H), 7.07 (s, 2H, Ar-H); ^{13}C NMR (125 MHz, CDCl$_3$): δ(ppm) 140.43, 139.35, 138.85, 138.75, 138.70, 138.68, 138.32, 131.81, 130.67, 129.69, 128.65, 128.52, 127.55, 127.50, 127.45, 127.37, 125.94, 125.87; MALDI-TOF m/z cald for C$_{80}$H$_{52}$ (M)$^{+}$ 1012.41, found 1012.92.

2(1,4)-anthracena-1,3,5,6,7(1,4)-pentabenzenacyclooctaphane **III.2**

III.2
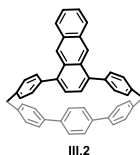
A similar procedure to synthesize **III.1** was adapted. **III.11** (42 mg, 0.072 mmol, 1 eq), Pd/C (Pd 10 wt%, 30 mg, 0.028 mmol, 0.38 eq), product was purified by filtering through a short pug of celite as greenish yellow powder (28 mg, 67%). IR (neat) 3053, 2929, 2855, 1636, 1594, 1500, 1485, 1411, 1265, 1195, 1120, 959, 903 cm^{-1}; ^{1}H NMR (600 MHz, CDCl$_3$): δ(ppm) 8.78 (s, 2H, Ar-H), 7.92 (dd, J = 6.6, 3.3 Hz, 2H, Ar-H), 7.43 (dd, J = 6.6, 3.3 Hz, 2H, Ar-H), 7.32-7.26 (overlap, 8H, Ar-H), 7.22 (d, J = 8.3 Hz, 4H, Ar-H), 7.16-7.10 (overlap, 8H, Ar-H), 6.43 (s, 2H, Ar-H), 3.91 (s, 4H, CH$_2$); ^{13}C NMR (150 MHz, CDCl$_3$): δ(ppm) 143.91, 142.89, 138.77, 137.79, 137.49, 137.13, 130.58, 129.04, 128.23, 128.22, 127.46, 127.31, 127.25, 126.44, 126.35, 124.62, 124.60, 42.35; MALDI-TOF m/z cald for C$_{46}$H$_{32}$ (M)$^{+}$ 584.25, found 584.89.

1,4-bis(4-(tert-butyl)phenyl)anthracene **III.3**

tBu — — — — tBu
III.3
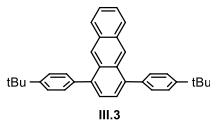
A similar procedure to synthesize **III.22** was adapted. 1,4-Dibromobenzene (642 mg, 1.91 mmol, 1 eq), 4-tbutylphenyl boronic acid (1360 mg, 7.64 mmol, 4 eq), K$_2$CO$_3$ (1320 mg, 9.55 mmol, 5 eq) and Pd(PPh$_3$)$_4$ (441 mg, 0.38 mmol, 0.2 eq), THF (50 mL),

H$_2$O (12 mL), column chromatography (silica, 100%,hexanes) product as off-white solid (622 mg, 74%). IR (neat) 3043, 2959, 2900, 2864, 1509, 1460, 1360, 1326, 1266, 1114, 1019, 889, 828 cm^{-1}; ^{1}H NMR (600 MHz, CDCl$_3$): δ(ppm) 8.60 (s, 2H, Ar-H), 7.92 (dd, J = 6.5, 3.2 Hz, 2H, Ar-H), 7.62-7.56 (overlap, 8H, Ar-H), 7.45 (s, 2H, Ar-H), 7.41 (dd, J = 6.5, 3.2 Hz, 2H, Ar-H), 1.47 (s, 18H, CH$_3$); ^{13}C NMR (150 MHz, CDCl$_3$): δ(ppm) 150.39, 139.72, 138.18, 131.47, 130.85, 129.99, 128.52, 126.01, 125.52, 125.50, 34.86, 31.66; HRMS (Q-TOF, EI+) m/z cald for C$_{34}$H$_{34}$ (M)$^+$ 442.2660, found 422.2648.

(5R,11S,12S)-1,4,7,10-tetrakis(4-(tert-butyl)phenyl)-5,6,11,12-tetrahydro-5,12:6,11-bis([1,2]benzeno)dibenzo[a,e][8]annulene **III.12**
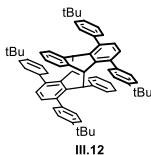
A small conical containing **III.3** (10 mg, 0.023 mmol) was evacuated and backfilled with N$_2$ for 10 times, at which point degassed DCM (0.5 mL) was added to fully dissolve the solid. The vial was sealed and irradiated with LED light (360 nm) for 3 h. The solvent was removed to produce product as off white powder (10 mg, 100%). IR (neat) 3022, 2961, 2901, 2865, 1518, 1474, 1456, 1392, 1360, 1269, 1195, 1112, 1016, 828 cm^{-1}; ^{1}H NMR (600 MHz, CDCl$_3$): δ(ppm) 7.47 (d, J = 8.2 Hz, 8H, Ar-H), 7.29 (d, J = 8.2 Hz, 8H, Ar-H), 7.04 (dd, J = 5.5, 3.2 Hz, 4H, Ar-H), 6.87 (dd, J = 5.5, 3.2 Hz, 4H, Ar-H), 6.82 (s, 4H, Ar-H), 4.81 (s, 4H, CH), 1.42 (s, 36H, CH$_3$); ^{13}C NMR (150 MHz, CDCl$_3$): δ(ppm) 149.72, 144.18, 141.35, 138.49, 138.46, 129.08, 127.07, 126.98, 125.68, 125.01, 50.01, 34.72, 31.60; MALDI-TOF m/z cald for C$_{68}$H$_{68}$Na (M+Na)$^+$ 907.52, found 907.91.

DA-adduct **III.13**
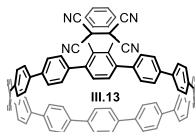
In a glove box with N$_2$ atmosphere, **III.1** (6 mg, 6 μmol, 1 eq) and TCNE (15 mg, 120 μmol, 20 eq) was mixed in DCM (2 mL) in a small conical vial. The vial was capped

and shaken for 10 seconds until deep blue color appeared. Then the vial was transferred out of the glove box and the crude mixture was purified by preparative thin layer chromatography (100% DCM) to give product as dull yellow solid (3 mg, 44%). IR (neat) 3077, 3026, 2921, 2850, 1907, 1596, 1481, 1392, 1276, 1001, 908, 810 768 cm^{-1}; ^{1}H NMR (600 MHz, CDCl$_3$): δ(ppm) 7.79 (dd, J = 5.4, 3.2 Hz, 2H, Ar-H), 7.70 (d, J = 8.1 Hz, 4H, Ar-H), 7.71 (d, J = 8.1 Hz, 4H, Ar-H), 7.63-7.58 (overlap, 40H, Ar-H), 7.33 (d, J = 8.1 Hz, 4H, Ar-H), 7.03 (s, 2H, Ar-H), 5.75 (s, 2H, CH); ^{13}C NMR (150 MHz, CDCl$_3$): δ(ppm) 140.53, 139.20, 138.94, 138.85, 138.71, 138.70, 138.68, 138.63, 138.43, 138.06, 136.86, 135.00, 132.54, 131.40, 130.37, 129.86, 128.04, 127.60-127.48 (overlap), 126.91, 110.81, 110.68, 51.01, 46.56; MALDI-TOF m/z cald for C$_{86}$H$_{52}$N$_4$ (M)$^+$ 1140.42, found 1139.65, cald for C$_{80}$H$_{52}$ (M-C$_6$N$_4$)$^+$ 1112.41, found 1112.47.

(29R,210S)-29,210-dihydro-2(1,4)-9,10-ethanoanthracena-1,3,5,6,7(1,4)-pentabenzenacyclooctaphane-211,211,212,212-tetracarbonitrile **III.14**

III.14
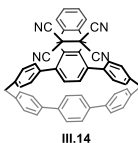
A similar procedure to synthesize **III.13** was adapted. **III.2** (5 mg, 8.5 µmol, 1 eq) and TCNE (22 mg, 170 µmol, 20 eq). Product was purified by preparative thin layer chromatography (100% DCM) as white solid (4 mg, 67%). IR (neat) 3016, 2927, 2861, 1595, 1501, 1486, 1479, 1388, 1188, 1115, 954, 835, 814, 790 cm^{-1}; ^{1}H NMR (600 MHz, CD$_2$Cl$_2$): δ(ppm) 7.69 (dd, J = 5.3, 3.2 Hz, 2H, Ar-H), 7.70 (broad s, 2H, Ar-H), 7.37-6.73 (overlap, 20H, Ar-H), 6.49 (s, 2H, Ar-H), 5.62 (s, 2H, CH), 3.92 (s, 4H, CH$_2$); ^{13}C NMR (150 MHz, CD$_2$Cl$_2$): δ(ppm) 146.39, 144.07, 139.06, 139.01, 138.72, 136.74, 135.40, 133.42, 131.15, 130.45, 129.49 (broad), 128.78 (broad), 127.63, 127.20, 111.44, 111.31, 51.23, 47.00, 43.61. MALDI-TOF m/z cald for C$_{51}$H$_{33}$N$_3$ (M-CN+H)$^+$ 687.27, found 687.68, cald for C$_{46}$H$_{33}$ (M-C$_6$N$_4$+H)$^+$ 585.25, found 585.60.

(9R,10S)-1,4-bis(4-(tert-butyl)phenyl)-9,10-dihydro-9,10-ethanoanthracene-11,11,12,12-tetracarbonitrile **III.15**

III.15
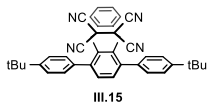
A mixture of **III.3** (50 mg, 0.11 mmol, 1 eq), TCNE (57 mg, 0.452 mmol, 4 eq) and in a 10 mL conical vial was sonicated at room temperature for 10 min. After removed the solvent, the crude solid was purified via column chromatography (silica, 0% to 5% ethyl acetate in hexanes) to give pure product as white powder (64 mg, 100%). IR (neat) 3019, 2962, 2866, 1466, 1360, 1264, 1120, 1016, 830 cm^{-1}; ^{1}H NMR (600 MHz, CDCl$_3$): δ(ppm) 7.67-7.59 (overlap, 6H, Ar-H), 7.52 (dd, J = 5.5, 3.1 Hz, 2H, Ar-H), 7.43 (s, 2H, Ar-H), 7.36 (d, J = 7.8 Hz, 4H, Ar-H), 5.42 (s, 2H, CH), 1.47 (s, 18H, CH$_3$); ^{13}C NMR (150 MHz, CDCl$_3$): δ(ppm) 151.57, 140.34, 135.03, 134.85, 132.20, 130.38, 130.04, 129.11, 126.79, 126.25, 111.00, 110.77, 49.81, 46.21, 34.95, 31.54; MALDI-TOF m/z cald for C$_{40}$H$_{34}$N$_4$Na (M+Na)$^+$ 593.2681, found 593.2681.

DA-adduct **III.16**

III.16
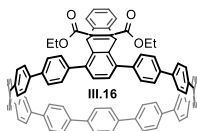
In a glove box with N$_2$ atmosphere, a solution of **III.1** (5 mg, 5 μmol, 1 eq) in DCM (2 mL) was added to a microwave reaction vial with a stir bar. The vial was sealed with a septum cap then transferred out the glove box. DCM was removed by N$_2$ stream with a vent needle, at which point a degassed solution of diethyl acetylenedicarboxylate (0.08 mL, 0.5 mmol, 100 eq) in toluene (2 mL) was added. The mixture was heated on a microwave reactor at 160 °C for 16 hours. Upon cooling to room temperature, the solvent was removed and the crude product was purified via preparative thin layer chromatography (10% hexanes in DCM) to yield product as colorless oil (2 mg, 34%). IR (neat) 3025, 2880, 2902, 1712, 1636, 1482, 1390, 1368, 1302, 1258, 1204, 1058, 1001, 908, 810, 733 cm^{-1}; ^{1}H NMR (600 MHz, CDCl$_3$): δ(ppm) 7.70-7.58 (overlap, 40H, Ar-H), 7.50-7.44 (overlap, 6H, Ar-H), 7.08 (dd, J = 5.4, 3.1 Hz, 2H, Ar-H), 6.63 (s, 2H, Ar-H), 6.10 (s, 2H, CH), 4.29 (q, J = 7.1 Hz, 4H, OCH$_2$), 1.32 (t, J = 7.1 Hz, 6H, CH$_3$); ^{13}C

NMR (150 MHz, CDCl₃): δ(ppm) 165.71, 147.44, 144.62, 141.02, 139.09, 138.96, 138.84, 138.75-138.65 (overlap), 138.55, 136.04, 129.95, 129.19, 127.65-127.40 (overlap), 127.28, 125.66, 124.17, 61.71, 50.41, 14.29, ; MALDI-TOF m/z cald for $C_{88}H_{63}O_4$ (M+H)$^+$ 1183.47, found 1183.80.

diethyl ($2^1R,2^4S$)-$2^1,2^4$-dihydro-2(5,8)-naphthalena-1,3,5,6,7(1,4)-pentabenzenacyclooctaphane-22,23-dicarboxylate **III.17**

III.17
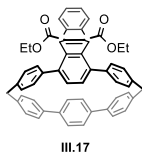
A similar procedure to synthesize **III.16** was adapted. **III.2** (4.0 mg, 6.8 µmol, 1 eq), diethyl acetylenedicarboxylate (0.11 mL, 0.69 mmol, 100 eq), toluene (3 mL). After heating at 160 °C on a microwave reactor for 14 hours, the solution was allowed to cool to room temperature and the solvent was removed under vacuum to yield the crude orange oil, at which point hexanes (2 mL) was added. After 10 min, product precipitated from the solution and was further washed with hexanes and n-pentane to give off-white solid (4 mg, 77%). IR (neat) 3018, 2982, 2922, 2855, 1711, 1635, 1594, 1485, 1368, 1262, 1202, 1094, 1058, 906, 794 cm^{-1}; ^{1}H NMR (600 MHz, CDCl₃): δ(ppm) 7.34 (dd, J = 5.4, 3.1 Hz, 2H, Ar-H), 7.21 (s, 4H, Ar-H), 7.16 (d, J = 8.3 Hz, 4H, Ar-H), 7.11 (d, J = 8.2 Hz, 4H, Ar-H), 7.08-7.03 (overlap, 8H, Ar-H), 7.01 (dd, J = 5.4, 3.1 Hz, 2H, Ar-H), 5.93 (s, 2H, Ar-H), 5.89 (s, 2H, CH), 4.23 (q, J = 7.1 Hz, 4H, OCH₂), 3.88 (s, 4H, CH₂), 1.27 (t, J = 7.1 Hz, 6H, CH₃); ^{13}C NMR (150 MHz, CDCl₃): δ(ppm) 165.59, 147.30, 144.53, 144.45, 143.71, 139.83, 138.73, 138.53, 138.53, 135.87, 129.91, 128.27, 128.22, 127.40, 127.32, 125.53, 124.04, 61.59, 50.08, 43.38, 14.25; MALDI-TOF m/z cald for $C_{54}H_{43}O_4$ (M+H)$^+$ 755.32, found 755.86.

diethyl (9R,10S)-1,4-bis(4-(tert-butyl)phenyl)-9,10-dihydro-9,10-ethenoanthracene-11,12-dicarboxylate **III.18**

III.18
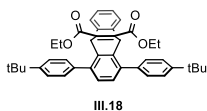
A similar procedure to synthesize **III.16** was adapted. **III.3** (20.0 mg, 0.045 mmol, 1 eq), diethyl acetylenedicarboxylate (0.15 mL, 0.904 mmol, 20 eq), product was purified by using chromatography (silica, 0% to 80% DCM in hexanes) to yield product as colorless oil (21 mg, 75%) IR (neat) 3053, 3027, 2962, 2903, 2867, 1711, 1636, 1478, 1365, 1264, 1203, 1105, 1057, 1016, 819, 785 cm^{-1}; ^{1}H NMR (600 MHz, CDCl$_3$): δ(ppm) 7.53 (d, J = 8.1 Hz, 4H, Ar-H), 7.41 (d, J = 8.1 Hz, 4H, Ar-H), 7.31 (dd, J = 5.3, 3.1 Hz, 2H, Ar-H), 7.05 (s, 2H, Ar-H), 7.00 (dd, J = 5.3, 3.1 Hz, 2H, Ar-H), 5.84 (s, 2H, CH), 4.23 (m, 4H, OCH$_2$), 1.26 (t, J = 7.1 Hz, 6H, CH$_3$); ^{13}C NMR (150 MHz, CDCl$_3$): δ(ppm) 165.70, 150.20, 147.40, 144.45, 141.67, 137.21, 137.06, 129.19, 126.50, 125.49, 125.43, 124.05, 61.49, 49.70, 34.79, 31.61, 14.14; MALDI-TOF m/z cald for C$_{42}$H$_{44}$O$_4$Na (M+Na)$^+$ 635.31, found 636.09, cald for C$_{39}$H$_{39}$O$_2$ (M-CO$_2$Et)$^+$, 539.30, found 540.11.

DA-adduct **III.19**

III.19
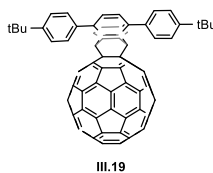
A mixture of **III.3** (6 mg, 14 µmol, 1 eq) and C$_{60}$ (14 mg, 19 µmol, 1.4 eq) in CS$_2$/C$_6$D$_6$ (7:1, 2 mL) was placed in a sealed vial and sonicated at 50 °C overnight. After removing solvent, the residue was purified by chromatography (0% to 30% chloroform in hexanes) to yield product as dark brown solid (4 mg, 25%). IR (neat) 3026, 2960, 2901, 2865, 1479, 1461, 1429, 1267, 1188, 1110, 1017, 905, 821, 747 cm^{-1}; ^{1}H NMR (600 MHz, CDCl$_3$): δ(ppm) 7.76 (dd, J = 5.4, 3.2 Hz, 2H, Ar-H), 7.52-7.46 (overlap, 6H, Ar-H), 7.45-7.40 (overlap, 6H, Ar-H), 6.11 (s, 2H, CH), 1,39 (s, 18H, CH$_3$); ^{13}C NMR (150 MHz, CDCl$_3$): δ(ppm) 156.05, 155.97, 150.33, 147.67, 146.59, 146.53, 146.31, 146.29, 145.80, 145.54, 145.52, 145.52, 145.47, 145.34, 144.78, 144.73, 143.14, 143.01, 142.68, 142.67, 142.47, 142.39, 142.21, 142.14, 142.12, 141.75, 141.71, 139.99, 139.77, 139.56, 139.05, 137.36, 137.09, 136.73, 129.30, 128.32, 127.43, 126.01, 125.62, 72.65, 55.04, 34.81, 31.60; MALDI-TOF m/z cald for C$_{98}$H$_{43}$ (M+NH$_4$)$^+$ 1219.33, found 1219.25, cald for C$_{34}$H$_{35}$ (M-C$_{60}$+H)$^+$ 442.27, found 443.26, cald for (C$_{60}$+H)$^+$ 721.01, found 721.84.

Macrocyle **III.28**
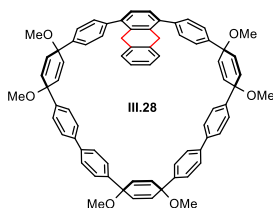
A similar procedure to synthesize **III.8** was adapted. **III.27** (505 mg, 0.928 mmol, 1.1 eq), **III.4** (700 mg, 0.844 mmol, 1 eq), S-phos Gen II precatalyst (31 mg, 0.031 mmol, 0.05 eq), dioxane (230 mL) K_3PO_4 solution (2 M, 23 mL) product purified by column chromatography (silica, 0% to 15% ethyl acetate in DCM) as white powder (120 mg, 14%). IR (neat) 3027, 2933, 2896, 2817, 1609, 1490, 1456, 1396, 1228, 1173, 1081, 1027, 949, 819, 744, 659 cm^{-1}; ^{1}H NMR (600 MHz, CDCl$_3$): δ(ppm) 7.56 (d, J = 8.4 Hz, 4H, Ar-H), 7.53 (d, J = 8.4 Hz, 4H, Ar-H), 7.52 (d, J = 8.4 Hz, 4H, Ar-H), 7.49 (d, J = 8.4 Hz, 4H, Ar-H), 7.42-7.36 (overlap, 8H, Ar-H), 7.24 (s, 2H, Ar-H), 7.09 (m, 4H, Ar-H), 6.28 (d, J = 10.3 Hz, 4H, CH=CH), 6.16 (d, J = 10.3 Hz, 4H, CH=CH), 6.12 (s, 4H, CH=CH), 3.96 (s, 4H, CH$_2$), 3.54 (s, 6H, OCH$_3$), 3.50 (s, 6H, OCH$_3$), 3.43 (s, 6H, OCH$_3$); ^{13}C NMR (150 MHz, CDCl$_3$): δ(ppm) 143.07, 142.29, 141.93, 140.99, 140.00, 139.87, 139.56, 137.55, 135.25, 133.85, 133.73, 133.11, 139.70, 127.89, 127.24, 127.17, 126.98, 126.70, 126.50, 126.25, 75.52, 75.34, 74.16, 52.45, 52.12, 52.07, 34.72; MALDI-TOF m/z cald for $C_{74}H_{62}O_6$ (M□H$_2$)$^+$ 1046.45, found 1046.93, cald for $C_{74}H_{62}O_6$ (M)$^+$ 1048.47, found 1048.92.

1,4-(9,10-dihydroanthryl)-[10]CPP **III.29**
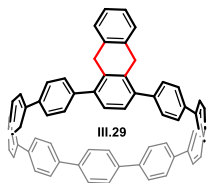
A similar procedure to synthesize **III.10** was adapted. **III.28** (57 mg, 0.056 mmol, 1 eq), sodium naphthalenide (12.1 mL, 2.81 mmol, 50 eq), product purified by column chromatography (silica, 0% to 30% DCM in hexanes) as light yellow solid (42 mg, 50%). IR (neat) 3033, 2922, 2850, 1903, 1590, 1482, 1384, 1262, 1000, 858, 809, 720 cm^{-1}; ^{1}H NMR (500 MHz, CDCl$_3$): δ(ppm) 7.85 (dd, J = 6.1, 3.4 Hz, 2H, Ar-H), 7.66-7.51

(overlap, 32H, Ar-H), 7.48 (dd, $J = 6.1$, 3.4 Hz, 2H, Ar-H), 7.41 (d, $J = 8.6$ Hz, 4H, Ar-H), 7.32 (dd, $J = 5.5$, 3.3 Hz, 2H, Ar-H), 7.21 (dd, $J = 5.5$, 3.3 Hz, 2H, Ar-H), 6.68 (s, 2H, Ar-H), 4.29 (s, 4H, CH$_2$); ^{13}C NMR (150 MHz, CDCl$_3$): δ(ppm) 140.42, 138.83, 138.55, 138.52, 138.51, 138.49, 138.45, 138.44, 138.43, 138.16, 135.19, 133.74, 130.45, 129.58, 128.06, 127.59, 127.57, 127.55, 127.49, 127.33, 127.11, 126.44, 125.97, 35.49; MALDI-TOF m/z cald for C$_{68}$H$_{46}$ (M)$^+$ 862.36, found 862.44, cald for C$_{68}$H$_{46}$ (M+H)$^+$ 863.37, found 863.47.

1,4-anthryl-[10]-CPP **III.30**
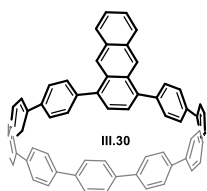
A similar procedure to synthesize **III.1** was adapted. **III.29** (15 mg, 0.072 mmol, 1 eq), Pd/C (Pd 10 wt%, 74 mg, 0.028 mmol, 4 eq), product was purified by filtering through a short pug of celite as greenish yellow powder (7 mg, 47%). IR (neat) 3023, 1904, 1590, 1482, 1391, 1264, 1085, 1001, 905, 812, 737 cm^{-1}; ^{1}H NMR (600 MHz, CDCl$_3$): δ(ppm) 8.96 (s, 2H, Ar-H), 8.02 (dd, $J = 6.5$, 3.3 Hz, 2H, Ar-H), 7.65 (d, $J = 8.3$ Hz, 4H, Ar-H), 7.63-7.53 (overlap, 32H, Ar-H), 7.52 (dd, $J = 6.5$, 3.3 Hz, 2H, Ar-H), 7.00 (s, 2H, Ar-H); ^{13}C NMR (125 MHz, CDCl$_3$): δ(ppm) 140.27, 139.28, 138.46, 138.45, 138.42, 138.36, 138.32, 138.30, 138.30, 137.93, 131.78, 130.70, 129.34, 129.19, 128.51, 128.38, 127.55, 127.54, 127.53, 127.50, 127.47, 125.96, 129.50; MALDI-TOF m/z cald for C$_{68}$H$_{46}$ (M+H)$^+$ 861.35, found 861.50.

68

3.4.3. Electrochemical and Photophysical Characterizations
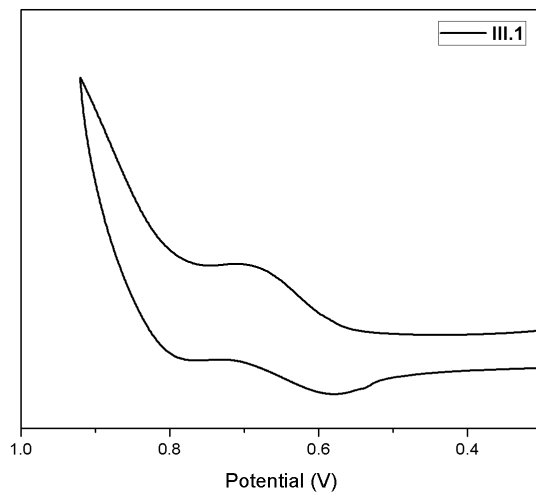
Figure 3.3. Cyclic Voltammetry of **III.1** (vs Fc/Fc$^+$).
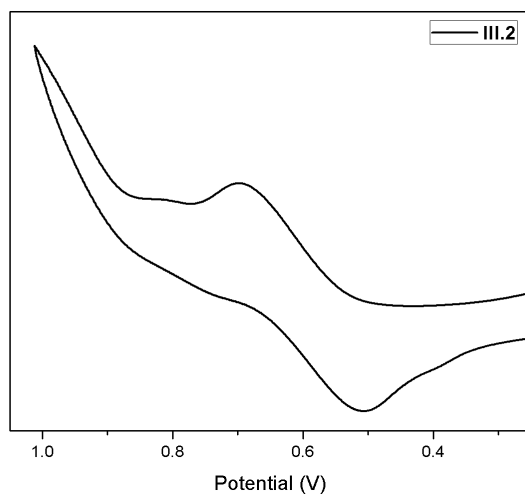
Figure 3.4. Cyclic Voltammetry of **III.2** (vs Fc/Fc$^+$).
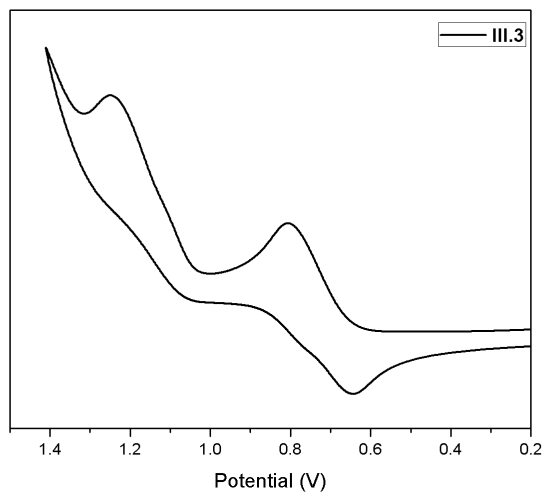
Figure 3.5. Cyclic Voltammetry of **III.3** (vs Fc/Fc$^+$).
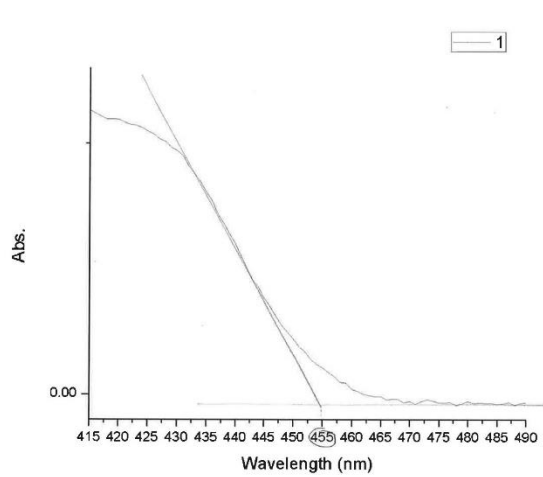
Figure 3.6. Tauc plot of **III.1** for calculating the optical band gap.
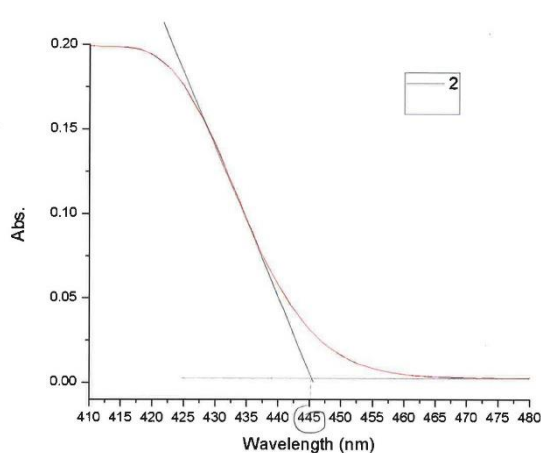
Figure 3.7. Tauc plot of **III.2** for calculating the optical band gap.
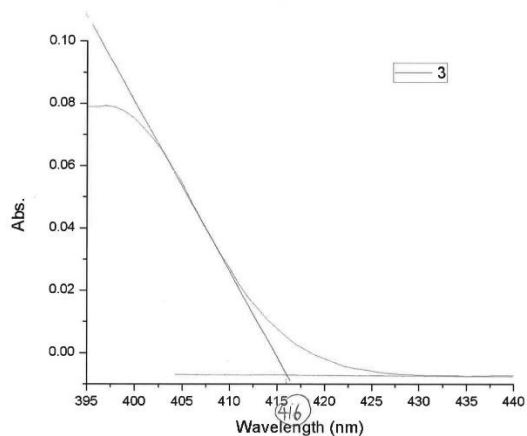
Figure 3.8. Tauc plot of **III.3** for calculating the optical band gap.

3.4.4. X-ray Crystallography Data

Diffraction intensities were collected at 173 (1) and 200(2) (5) on a Bruker Apex2 CCD diffractometer using an Incoatec IµS micro-focus source with CuKα radiation, λ= 1.54178 Å. Space groups were determined based on systematic absences. Absorption corrections were applied by SADABS.[56] Structures were solved by direct methods and Fourier techniques and refined on F^2 using full matrix least-squares procedures. All non-H atoms were refined with anisotropic thermal parameters. H atoms in both structures

were refined in calculated positions in a rigid group model. All calculations were performed by the SHELXL-2013 packages.[57]
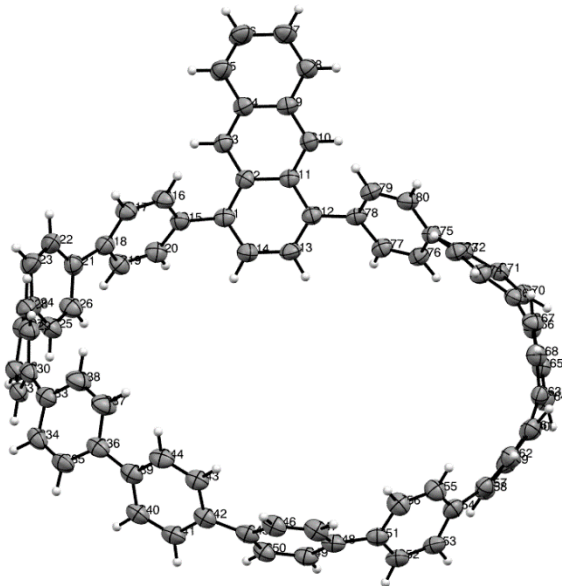
Figure 3.9. ORTEP representation of the X-ray crystallographic structure of **III.1** (CCDC Registry #1452467).

Crystallographic data for **III.1**: $C_{108}H_{42}$, M = 1381.75, 0.09 x 0.06 x 0.02 mm, T = 173(2) K, Triclinic, space group *P1*, a = 10.8797(11) Å, b = 19.060(2) Å, c = 19.762(2) Å, α = 10.8797(11)°, β = 84.259(8)°, γ = 79.119(7)°, V = 3941.9(7) Å^3, Z = 2, Dc = 1.164 Mg/m^3, μ(Mo) = 0.495 mm^{-1}, F(000) = 1464, θ = 2.28-59.80°, 38159 reflections, 7981 independent reflections [R_{int} = 0.0635], R1 = 0.0705, wR2 = 0.1844 and GOF = 1.028 for 13411 reflections (800 parameters) with I>2σ(I), R1 = 0.1085, wR2 = 0.2015 and GOF = 1.031 for all reflections, max/min residual electron density +0.676/-0.483 eÅ^3. Two highly distorted toluene molecules located in the unit cell of the crystal and were treated by SQUEEZE.[58]
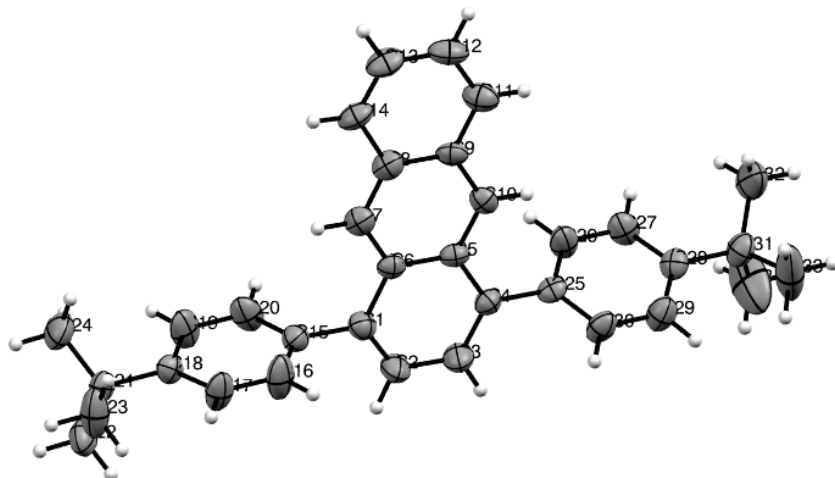
Figure 3.10. ORTEP representation of the X-ray crystallographic structure of **III.3** (CCDC Registry #1452466).

Crystallographic data for **III.3**: $C_{34}H_{34}$, M = 442.61, 0.23 x 0.21 x 0.14 mm, T = 173(2) K, Monoclinic, space group *Pn*, a = 11.8562(4) Å, b = 16.2582(5) Å, c = 26.9243(8) Å, α = 90°, β = 94.715(2)°, γ = 90°, V = 5172.4(3) $Å^3$, Z = 8, Dc = 1.137 Mg/m^3, μ(Mo) = 0.476 mm^{-1}, *F*(000) = 1904, θ = 3.29-66.58°, 31975 reflections, 7893 independent reflections [R_{int} = 0.0466], R1 = 0.0602, wR2 = 0.1641 and GOF = 1.035 for 14421 reflections (1225 parameters) with I>2σ(I), R1 = 0.784, wR2 = 0.1837 and GOF = 1.035 for all reflections, max/min residual electron density +0.436/-0.265 $eÅ^3$.
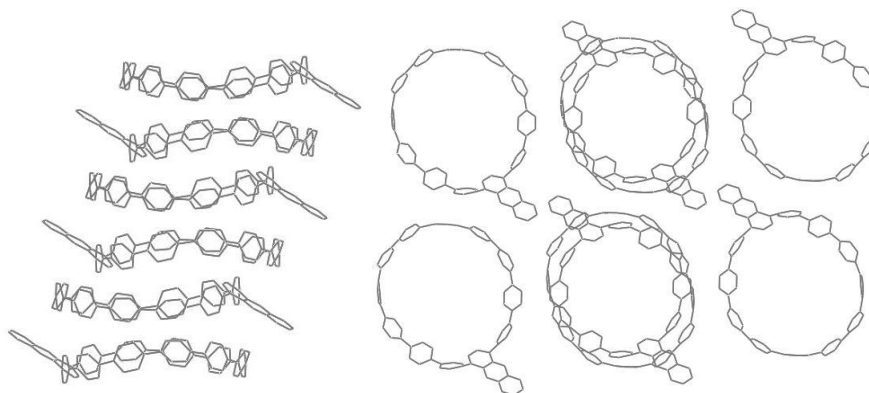
Figure 3.11. Crystal packing of **III.1** (hydrogen atoms are omitted for clarity).
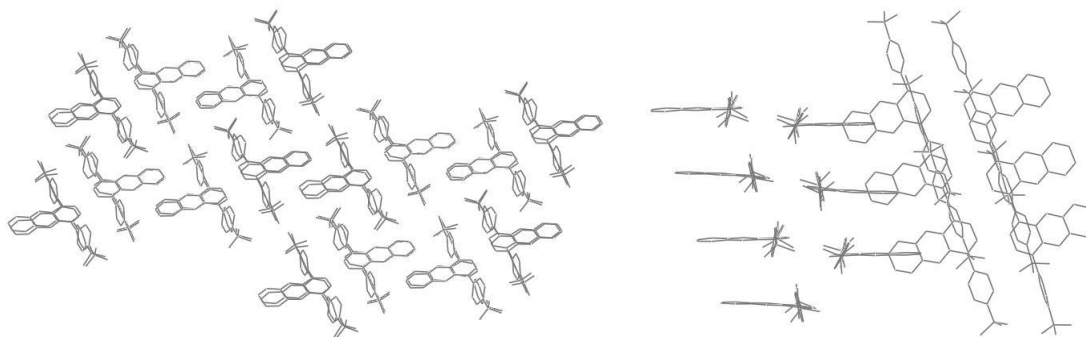
Figure 3.12. Crystal packing of **III.3** (hydrogen atoms are omitted for clarity).

Table 3.2. Structural properties from the empirical crystallographic data and from the calculated data (DFT, BL3YP/6-31G*).
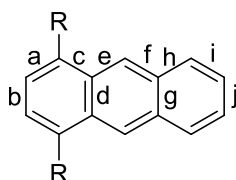
	Bond length (Å)				
	a	b	c	d	e
III.1[a]	1.365(4)	1.404(4)	1.436(4)	1.446(4)	1.396(4)
III.1[b]	1.380	1.411	1.447	1.457	1.400
III.3[a]	1.349(8)	1.425(9)	1.455(8)	1.427(8)	1.391(8)
III.3[b]	1.377	1.417	1.446	1.452	1.402
	Bond length (Å)				
	f	g	h	i	j
III.1[a]	1.397(4)	1.435(4)	1.421(4)	1.358(4)	1.424(4)
III.1[b]	1.402	1.440	1.429	1.371	1.425
III.3[a]	1.397(8)	1.432(9)	1.432(8)	1.359(9)	1.406(10)
III.3[b]	1.400	1.440	1.430	1.370	1.426
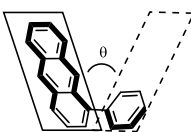
Dihedral Angle θ   Bending Angles α, β

	θ, deg	α, deg	β, deg
III.1[a]	49.9	7.6	6.3
III.1[b]	42.8	7.4	6.7
III.3[a]	57.5, 75.2	4.4	2.3
III.3[b]	54.5	4.5	0.7

[a]Crystallographic data.
[b]Calculated data.

3.4.5. Computational Details

3.4.5.1. Methods selection.

Calculations were carried out with Gaussian 09 package.[59] Molecular geometry optimization, FMO plots and energy levels, strain energy calculations and optical transition predictions were computed at B3LYP/6-31G* level of theory. The excited state calculations were performed on fully optimized structures. Reaction free energies and transition state energies and related structure optimizations were computed at ωB97XD/6-31G* level of theory.

Reasons for level of theory selections: 1) ωB97XD functional incorporates a large amount of exact exchange as well as a description of dispersion effects. The large amount of exact exchange is essential for accurately calculating thermodynamic properties including reaction energy barriers; 2) the hybrid B3LYP/6-31G* has the advantages of cost-effectiveness and accuracy in optimizing molecular structures, calculating orbital energies and predicting optical transitions. However, B3LYP/6-31G* basis set exhibits obvious limitation in calculating thermodynamic properties when non-covalent interactions are involved.

3.4.5.2. Molecular Geometry Optimizations, Electronic Structures and Optical transitions
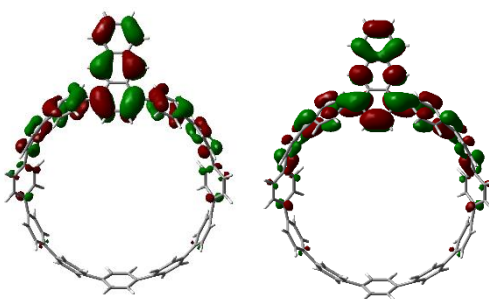
Figure 3.13. Representative HOMO (left) and LUMO (right) surfaces of **III.1**. (DFT, B3LYP-6-31G*).
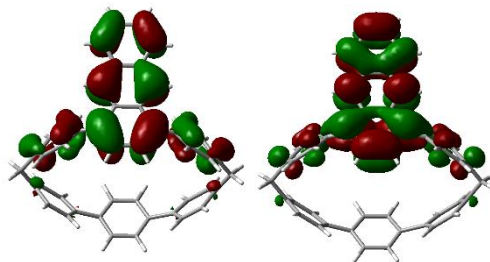
Figure 3.14. Representative HOMO (left) and LUMO (right) surfaces of **III.2**. (DFT, B3LYP-6-31G*).
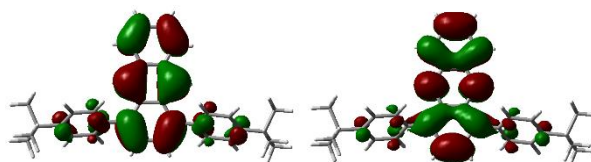
Figure 3.15. Representative HOMO (left) and LUMO (right) surfaces of **III.3**. (DFT, B3LYP-6-31G*).

Table 3.3. Calculated FMO properties of **III.1**-**3** (B3LYP-6-31G*).

	E_{HOMO} (eV)	E_{LUMO} (eV)	ΔE_{L-H} (eV)
III.1	-4.97	-1.91	3.06
III.2	-4.93	-1.71	3.22
III.3	-5.02	-1.60	3.42

Table 3.4. Major electronic transitions for **III.1** determined by TD-DFT method (B3LYP-6-31G*).

Energy (cm^{-1})	Wavelength (nm)	Osc. Strength	Major contribs
21518.21424	464.7225782	0.3476	HOMO->LUMO (95%)
24919.47776	401.2925189	0.1689	HOMO->L+1 (78%)
25354.2136	394.4117596	0.109	H-1->LUMO (79%), HOMO->L+1 (10%)
25709.90656	388.9551281	0.2027	H-2->LUMO (16%), HOMO->L+2 (80%)
25997.84848	384.6472145	1.3261	H-2->LUMO (80%), HOMO->L+2 (16%)
27137.51776	368.4935405	0.3727	H-2->L+2 (10%), H-1->L+1 (73%)
27473.04672	363.9931203	0.0775	H-3->LUMO (13%), HOMO->L+3 (73%)
28255.40992	353.9145257	0.3781	H-3->LUMO (76%), HOMO->L+3 (14%)
28703.05072	348.3950225	0.9675	H-2->L+1 (75%), H-1->L+2 (20%)
28800.64448	347.2144523	0.0792	H-2->L+1 (21%), H-1->L+2 (75%)
29743.51312	336.2077627	0.0234	H-2->L+2 (81%), H-1->L+1 (13%)

Energy (cm^{-1})	Wavelength (nm)	Osc. Strength	Major contribs
30191.96048	331.2140001	0.0009	H-6->LUMO (22%), H-4->LUMO (11%), HOMO->L+4 (29%), HOMO->L+6 (18%)

Table 3.5. Major electronic transitions for **III.2** determined by TD-DFT method (B3LYP-6-31G*).

Energy (cm^{-1})	Wavelength (nm)	Osc. Strength	Major contribs
22930.5	436.1004	0.1371	HOMO->LUMO (97%)
27113.32	368.8224	0.0294	H-1->LUMO (97%)
27162.52	368.1543	0.006	HOMO->L+1 (95%)
30382.31	329.1389	0.0145	H-4->LUMO (39%), HOMO->L+3 (27%), HOMO->L+4 (13%), HOMO->L+5 (18%)
30486.35	328.0156	0.0031	H-2->LUMO (31%), HOMO->L+2 (63%)
31106.6	321.4752	0.1203	H-2->LUMO (28%), H-1->L+1 (63%)
32018.82	312.3163	0.0205	H-3->LUMO (85%)
32535.02	307.3611	0.4793	H-2->LUMO (37%), H-1->L+1 (31%), HOMO->L+2 (28%)
33027.02	302.7824	0.2394	H-3->LUMO (10%), HOMO->L+3 (59%), HOMO->L+5 (19%)
33494.02	298.5608	0.0131	HOMO->L+4 (61%), HOMO->L+5 (24%)
34252.99	291.9453	0.0159	H-6->LUMO (10%), HOMO->L+6 (79%)
35470.9	281.9213	0.016	H-5->LUMO (74%)

Table 3.6. Major electronic transitions for **III.3** determined by TD-DFT method (B3LYP-6-31G*).

Energy (cm^{-1})	Wavelength (nm)	Osc. Strength	Major contribs
24714.61	404.6189	0.2246	HOMO->LUMO (98%)
30958.19	323.0163	0.0007	H-2->LUMO (43%), HOMO->L+2 (51%)
31714.75	315.3107	0.0001	H-1->LUMO (61%), HOMO->L+1 (38%)
33209.3	301.1205	0.2206	H-1->LUMO (37%), HOMO->L+1 (61%)
34251.38	291.9591	0.0208	H-3->LUMO (83%), H-2->LUMO (13%)
36004.03	277.7467	0.0044	H-5->LUMO (31%), HOMO->L+3 (66%)

36053.23	277.3676	0.0046	H-4->LUMO (41%), HOMO->L+4 (51%)
36333.91	275.225	0.1328	HOMO->L+5 (72%)
36686.38	272.5807	0.0002	H-5->LUMO (67%), HOMO->L+3 (32%)
36706.55	272.431	0.0046	H-4->LUMO (53%), HOMO->L+4 (30%), HOMO->L+5 (14%)
39069.77	255.9524	0.0004	H-6->LUMO (71%), HOMO->L+6 (27%)
40105.39	249.343	0.9139	H-2->LUMO (27%), H-1->L+2 (13%), HOMO->L+2 (31%)

3.4.5.3. Strain Energies

Strain Energies were calculated by subtracting the total energy of the optimized 1,4-diphenylanthracene from the total energies of the DPA cores from **III.1**-**3** (terminated with hydrogen atoms).[49]
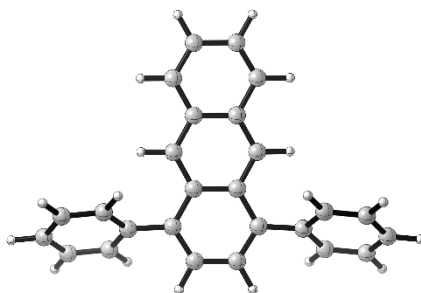
Total Energy: −1001.63775776 Hartrees (DFT, B3LYP-6-31G*)

Figure 3.16. Optimized geometry of DPA molecule (DFT, B3LYP-6-31G*).
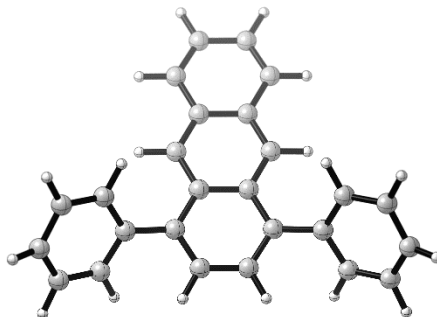
Total Energy: −1001.61630062 Hartrees (DFT, B3LYP-6-31G*)

Figure 3.17. The bent DPA core of **III.1** (terminated with hydrogen atoms).

78
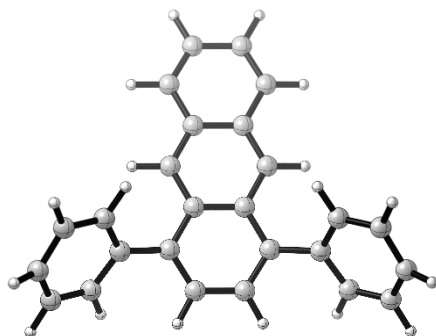
Total Energy: −1001.61412722 Hartrees (DFT, B3LYP-6-31G*)

Figure 3.18. The bent DPA core of **III.2** (terminated with hydrogen atoms).
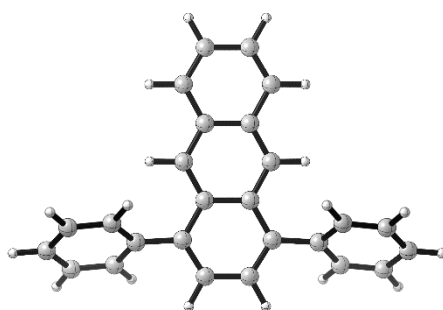
Total Energy: −1001.63593799 Hartrees (DFT, B3LYP-6-31G*)

Figure 3.19. The bent DPA core of **III.3** (terminated with hydrogen atoms).

3.4.5.4. Reaction Free Energies and Transition Barriers

Table 3.7. Reaction free energies and transition energy barriers for the dimerization of **III.1**-3 (DFT, ωB97XD/6-31G*).

	E^{a} (Hartrees)	$E_{TS}{}^{b}$ (Hartrees)	$E_{dimer}{}^{c}$ (Hartrees)	$\Delta E_{act}{}^{d}$ (kcal/mol)	$\Delta H_{r}{}^{e}$ (kcal/mol)
III.1	-3077.877496	NA	-6155.753083	NA	1.1979
III.2	-1771.022704	NA	-3542.048008	NA	-1.6315
III.3	-1315.202096	NA	-2630.414845	NA	-6.6848

[a]E refers to the total energies shown in Figure **III.20** (**III.1**), **III.24** (**III.2**) and **III.28** (**III.3**).
[b]Attempts to calculate E_{TS} were unsuccessful.
[c]E_{dimer} refers to the total energies shown in Figure **III.21** (**III.1**), **III.25** (**III.2**) and **III.29** (**III.3**).
[d]Attempts to calculate ΔE_{act} were unsuccessful.
[e]$\Delta H_{r} = E_{dimer} - 2E$.

79

Table 3.8. Reaction free energies and transition energy barriers for the DA reactions of C_{60} with **III.1**-**3** (DFT, ωB97XD/6-31G*).

	E^a (Hartrees)	E_{TS}^b (Hartrees)	$E_{DA-adduct}^c$ (Hartrees)	ΔE_{act}^d (kcal/mol)	ΔH_r^e (kcal/mol)
III.1	-3077.877496	-5362.964109	-6155.753083	17.8526	-16.0033
III.2	-1771.022704	-4056.110862	-3542.048008	16.8831	-15.6124
III.3	-1315.202096	-3600.296994	-2630.414845	12.6537	-20.8710

$^a E$ refers to the total energies shown in Figure **III.20** (**III.1**), **III.24** (**III.2**) and **III.28** (**III.3**). $E_{C60} = -2285.115063$ (Hartrees).
$^b E_{TS}$ refers to the transition state (TS) energies shown in Figure **III.23** (**III.1**), **III.27** (**III.2**) and **III.31** (**III.3**).
$^c E_{DA-adduct}$ refers to the total energies shown in Figure **III.22** (**III.1**), **III.26** (**III.2**) and **III.30** (**III.3**).
$^d \Delta E_{act} = E_{TS} - E - E_{C60}$.
$^e \Delta H_r = E_{DA-adduct} - E - E_{C60}$.
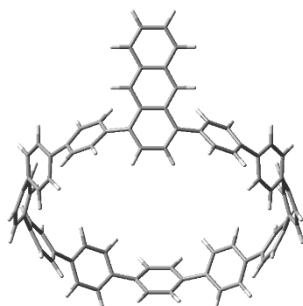
Total Energy: -3077.877496 Hartrees (DFT, ωB97XD/6-31G*)

Figure 3.20. Optimized molecular structure of **III.1** for reaction free energy calculation (DFT, ωB97XD/6-31G*).
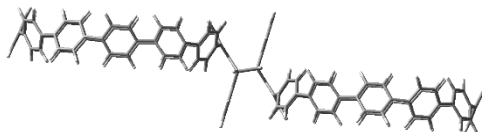
Total Energy: -6155.753083 Hartrees (DFT, ωB97XD/6-31G*)

Figure 3.21. Optimized dimer structure of **III.1** for reaction free energy calculation (DFT, ωB97XD/6-31G*).
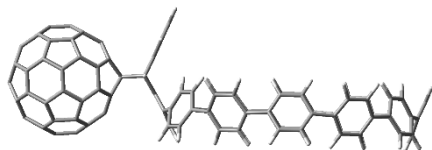
Total Energy: −5363.018062 Hartrees (DFT, ωB97XD/6-31G*)

Figure 3.22. Optimized DA-adduct of C_{60} with **III.1** for reaction free energy calculation (DFT, ωB97XD/6-31G*).
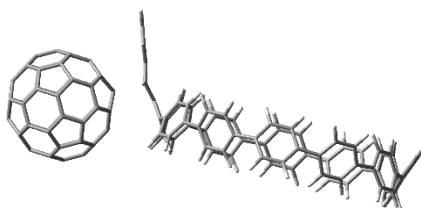
TS Energy: −5362.964109 Hartrees (DFT, ωB97XD/6-31G*)

Figure 3.23. DA transition state of C_{60} with **III.1** for reaction activation barrier calculation (DFT, ωB97XD/6-31G*).
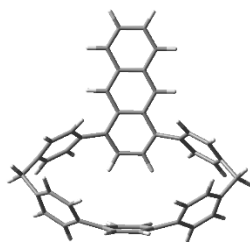
Total Energy: −1771.022704 Hartrees (DFT, ωB97XD/6-31G*)

Figure 3.24. Optimized molecular structure of **III.2** for reaction free energy calculation (DFT, ωB97XD/6-31G*).
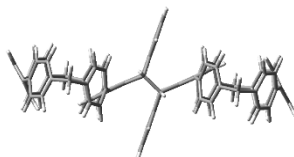
Total Energy: −3542.048008 Hartrees (DFT, ωB97XD/6-31G*)

Figure 3.25. Optimized dimer structure of **III.2** for reaction free energy calculation (DFT, ωB97XD/6-31G*).
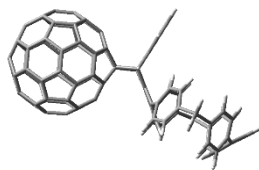
Total Energy: −4056.162647 Hartrees (DFT, ωB97XD/6-31G*)

Figure 3.26. Optimized DA-adduct of C_{60} with **III.2** for reaction free energy calculation (DFT, ωB97XD/6-31G*).
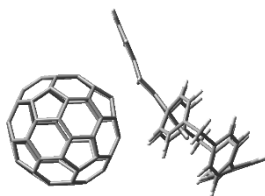
TS Energy: −4056.110862 Hartrees (DFT, ωB97XD/6-31G*)

Figure 3.27. DA transition state of C_{60} with **III.2** for reaction activation barrier calculation (DFT, ωB97XD/6-31G*).
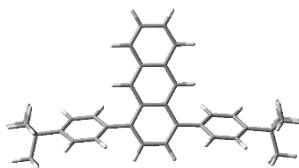
Total Energy: −1315.202096 Hartrees (DFT, ωB97XD/6-31G*)

Figure 3.28. Optimized molecular structure of **III.3** for reaction free energy calculation (DFT, ωB97XD/6-31G*).
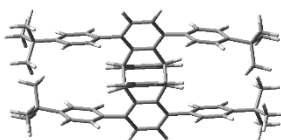
Total Energy: −2630.414845 Hartrees (DFT, ωB97XD/6-31G*)

Figure 3.29. Optimized dimer structure of **III.3** for reaction free energy calculation (DFT, ωB97XD/6-31G*).

82
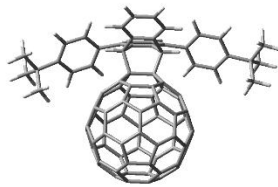
Total Energy: −3600.350419 Hartrees (DFT, ωB97XD/6-31G*)

Figure 3.30. Optimized DA-adduct of C_{60} with **III.3** for reaction free energy calculation (DFT, ωB97XD/6-31G*).
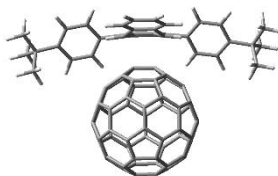
TS Energy: −3600.296994 Hartrees (DFT, ωB97XD/6-31G*)

Figure 3.31. DA transition state of C_{60} with **III.3** for reaction activation barrier calculation (DFT, ωB97XD/6-31G*).

3.5. Bridge to Chapter IV

In this chapter, with the aim to create CPP-based solid materials, we explored the possibility of using 1,4-anthracene as the functional handle to crosslink nanohoops. Chapter IV describes the synthesis of a nanohoop-related molecular propeller that exhibits ubiquitous hexagonal porous packing structure. It represents a new molecular design strategy to access functional soft materials.

CHAPTER IV

A MOLECULAR PROPELLER WITH THREE NANOHOOP BLADES: SYNTHESIS, CHARACTERIZATION, AND SOLID STATE PACKING

Nanoscale carbon-rich molecular architectures are not only aesthetically appealing but also of practical importance for energy and biomedical technologies. Herein we report the synthesis of cyclic-oligophenylene-based nanopropeller **IV.1** via an efficient synthon strategy involving sequential intramolecular bisboronate homocoupling and reductive aromatization by H_2SnCl_4. The nanopropeller molecules pack into a layered hexagonal lattice featuring long-ranged nano-sized channels and a total guest accessible volume of 48%, as revealed by X-ray diffraction studies. We suggest that such solid state arrangement is determined by an interplay between the propeller architecture and the intermolecular van der Waals interactions.

4.1. Introduction

Over the last three decades, sp^2-hybridized carbon allotropes including fullerene, carbon nanotubes (CNTs) and graphenes have been the subject of intense scientific research across disciplines owing to their exotic physics as well as potential applications in a broad range of technologies.[1-7] The properties of these materials are directly related to their shape, size and geometric arrangement of the carbon atoms.[8-10] This has prompted the synthesis of a variety of molecular fragments of these carbon structures by organic chemists as new forms of nanocarbon materials.[11-13] Among these, hoop-shaped cycloparaphenylenes (CPPs), as unit cross sections of CNTs, are gaining increasing attention since the initial synthesis in 2008.[14] In addition to the envisioned application in seeding the growth of uniform CNTs,[15-16] these strained nanohoops have proven to be of

a unique carbon-rich molecular entity, possessing attractive structural, optoelectronic and supramolecular properties that have direct implications in materials science.[17-29]

Most of the current nanohoop syntheses rely on a step-wise strategy wherein a less strained macrocyclic precursor is constructed from curved building units that contain masked arenes or *cis*-platinum complexes, followed by a late-stage reaction (aromatization or reductive elimination) to complete the buildup of the strained framework.[30-35] Not only has this synthetic approach permitted the diversification of nanohoop structures,[35-47] but also enabled the creation of unique 3D oligophenylene molecules (shown in **Figure 4.1**).[48-51] In this respect, the chemistry developed in the context of the nanohoops presents a facile platform for the synthesis of structurally-unique, nonplanar nanocarbon architectures that may give rise to novel functions.

| Cabon Nanocage | 3D Carbon Ball | Nanopropeller **IV.1** |
| 2013 & 2014 | 2013 | |
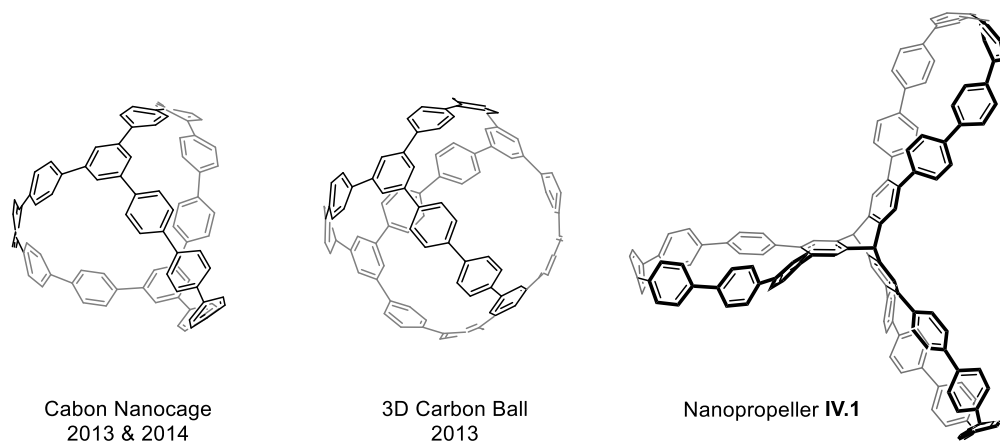
Figure 4.1. Unique nanocarbon architectures (from left to right): carbon nanocage,[48-49] 3D carbon ball,[50] and nanopropeller **IV.1** in this chapter.

Herein, we described the synthesis of a carbon nanopropeller **IV.1** with three cyclic-oligophenylene blades on a triptycene hub, employing an efficient synthon strategy that involves intramolecular bisboronate homocoupling and subsequent reductive aromatization by H_2SnCl_4. The crystal structure of the nanopropeller displays a ubiquitous hexagonal layered packing motif with uniform 1D nanochannel arrays and a total guest-accessible volume of 48%, suggesting potential applications as guest-inclusion materials and porous molecular solids.

4.2. Synthesis

The Pd-mediated intramolecular bisboronate homocoupling was serendipitously discovered in our synthesis of [5]CPP.[52] This operationally simple homocoupling method has demonstrated satisfying efficiency and adaptability that have allowed us to synthetically achieve a variety of intrinsically strained macrocycles.[53-54] When planning the synthesis of nanopropeller **IV.1** using the homocoupling chemistry, we realized that a bisboronate synthon with a high tendency to undergo intramolecular homocoupling is required in order to execute the multi-fold macrocyclization process. Depicted in **Scheme 4.1**, a model bisboronate substrate **IV.2**, which consists of two *ortho*-fused masked *p*-terphenyl moieties, was found to fulfill the criteria, giving intramolecularly cyclized product **IV.3** as the major product when subjected to the standard oxidative homocoupling conditions. Utilizing a modified tin(II)-mediated reduction protocol,[55] macrocycle **IV.3** was cleanly aromatized to afford teardrop shaped nanohoop **IV.4** in 67% yield. Adapting the synthon strategy based on this facile two-step transformation, the synthetic route towards the nanopropeller **IV.1** was designed (**Scheme 4.2**).
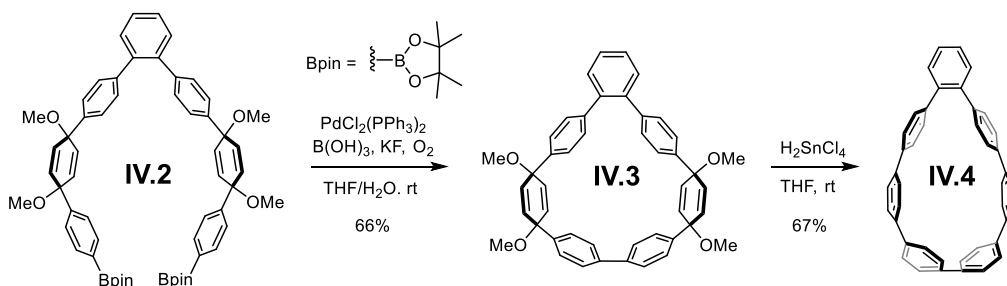
Scheme 4.1. An efficient two-step transformation from bisboronate **IV.2** to nanohoop **IV.4**.

First, a Suzuki coupling of hexabromotriptycene with six equivalents of **IV.5** produced hexachloride **IV.6**, which was then converted to the key intermediate hexaboronate **IV.7** using a Miyaura borylation condition in the presence of Pd(OAc)$_2$, S-Phos, B$_2$Pin$_2$ and anhydrous K$_3$PO$_4$ in dioxane. As expected, under the standard bisboronate homocoupling conditions at room temperature in oxygenated THF/water with PdCl$_2$(PPh$_3$)$_2$, B(OH)$_3$ and KF, **IV.7** proceeded through a three-fold intramolecular

cyclization, yielding compound **IV.8** in 46% yield. Finally, compound **IV.8** was successfully aromatized by H_2SnCl_4 to give the target product **IV.1** as yellow solid in 72% yield. Overall, the efficiency corresponds to a 77% yield for each macrocyclization and a 90% yield for each aromatization, which again underscores the power of this synthon strategy. It is worth mentioning that a similar strategy utilizing aryl halide homocoupling was recently reported by Cong in the synthesis of a dual-macrocyclic oligophenylene structure.[43]
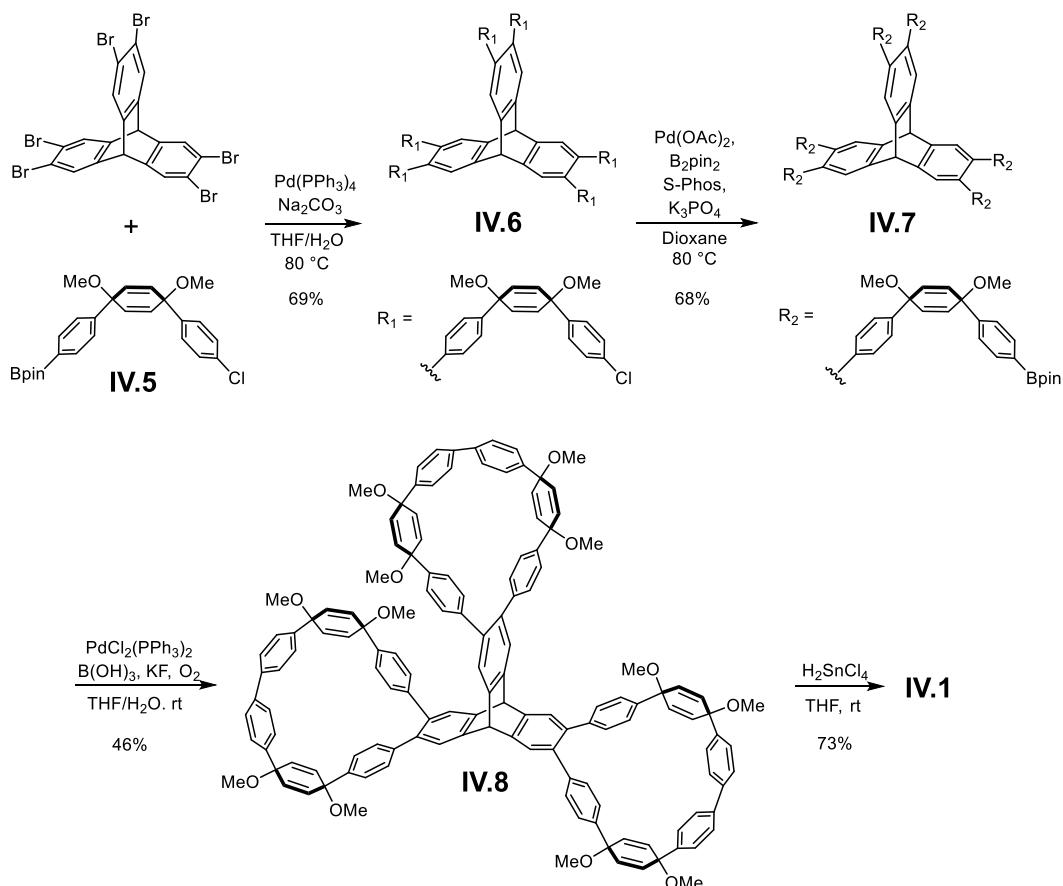
Scheme 4.2. Synthesis of nanopropeller **IV.1**.

The formation of nanopropeller **IV.1** was confirmed by NMR spectroscopy and mass spectrometry. The ^1H NMR spectra showed only seven peaks (6.90−7.60 ppm) in the aromatic region and one peak at 5.60 ppm that can be assigned to the triptycene bridgehead protons. Such simple features confirm that the three cyclic blades are

87

equivalent. No broadening of the peaks was observed, suggesting free rotation of the phenyl rings at room temperature. Additionally, a parent peak ion corresponding to [**IV.1**]$^{+}$ (m/z = 1616.6) was detected in MALDI-TOF spectrometry. These observations are consistent with the nanopropeller structure with three-fold symmetry. Notably, nanopropeller **IV.1**, though comprised of twenty-one phenyl rings without any solubilizing side chains, is soluble in common organic solvents. This phenomena can be attributed to its rigid 3D geometry with contorted nanohoop blades, which impedes intermolecular π-π stacking.[39,56]

4.3. Solid State Packing Ananlysis

By slow diffusion of *n*-pentane vapor into a solution of **IV.1** in chlorobenzene, single crystals suitable for X-ray crystallography were obtained. The nano-sized propeller architecture was thus unambiguously confirmed (**Figure 4.1a**). The crystal structure was solved in the hexagonal space group *P6$_3$/m* with two molecules in the unit cell. Molecules of **IV.1**, displaying a *C$_{3h}$* symmetry conformation, adopt a lamellar packing motif with 11 Å diameter channels that lie perpendicular to the layers (**Figure 4.2b**-**c**). Each layer is comprised of a 2D trigonal lattice wherein molecules are organized into repetitive patterns of triangular cavities and cyclic trimers via self-complementary CH$\cdots\pi$ interactions (**Figure 4.3a**-**b**). This nested supramolecular network prevents the in-plane translations and rotations therefore reinforcing the integrity of the 2D lattice. Furthermore, the layers are held in position by inter-layer CH$\cdots\pi$ interactions and are stacked in an alternating fashion with a rotation offset of 60° between adjacent layers (**Figure 4.3c**), thereby aligning the triangular cavities along the *c* axis to form the observed 1D nanochannels with a hexagonal honeycomb cross section. This alternating pattern also allows a dense inter-layer packing through shape matching in which the convex surfaces (where the cyclic trimers are located) of the 2D lattice are in close contact with the concave surfaces (where the triptycene units are located) of the neighboring layers. Additionally, twelve residual chlorobenzene molecules are trapped in the unit cell. Six are highly disordered and located in the free volumes near the triptycene unit. Their electron density was removed with the SQUEEZE function in the PLATON

88

software package. The other six solvent molecules are well refined, residing in the intrinsic cavities of the nanohoop blades via $\pi\cdots\pi$ stacking (**Figure 4.6**). Void analysis using CrystalExplorer software revealed that the solvent-free hexagonal crystal model has a total guest accessible volume of 48%, as well as a low density of 0.69 g/cm^2.[57] These features suggest potential applications as guest-inclusion materials[58] and porous molecular solids.[59-61] We also expect this hexagonal packing motif to open up possible applications in the bottom-up construction of new graphitic layer materials.[62-63]
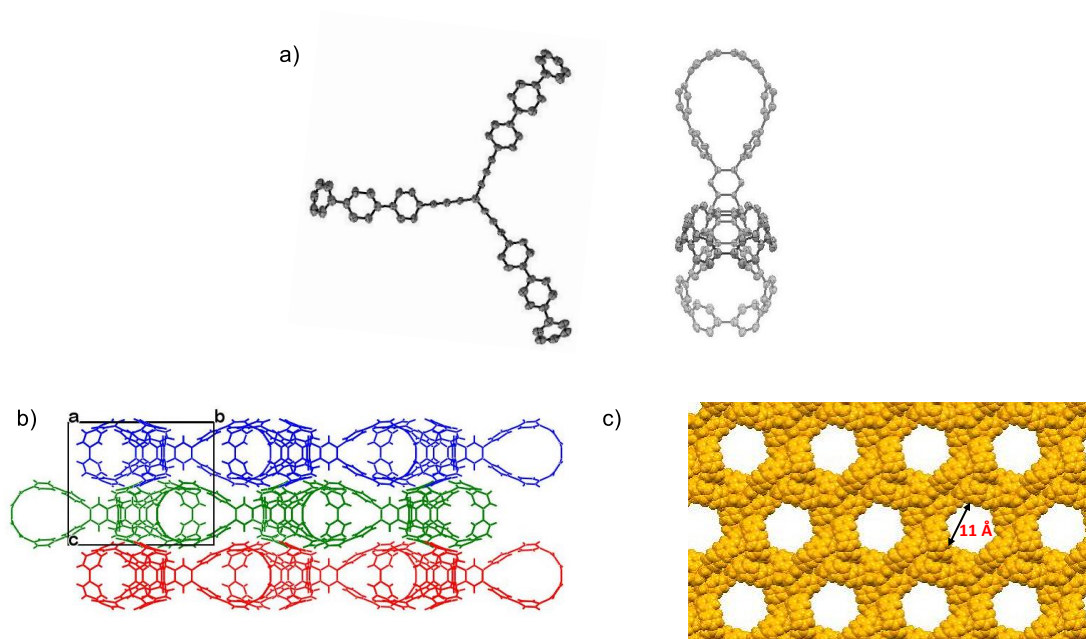
Figure 4.2. a) Solid state molecular structure of **IV.1** with a C_{3h} conformation (ellipsoids set at 50% possibility, hydrogen atoms removed for clarity). b) Layered packing arrangement, viewed along the *a* axis. c) 1D hexagonal channels with a minimum diameter of 11 Å (spacefilling model), viewed along the *c* axis (solvent molecules removed for clarity).
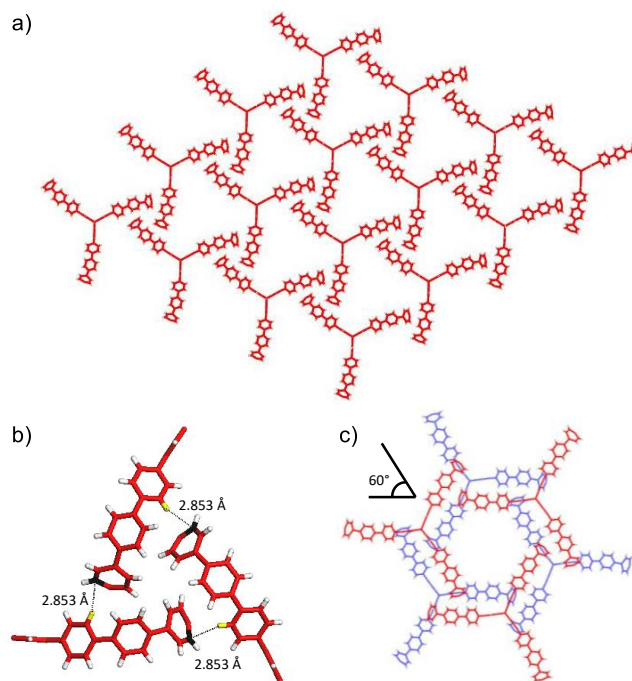
Figure 4.3. a) Representation of 2D trigonal lattice with triangular cavities and cyclic trimers. b) Self-complementary CH···π interactions in the cyclic trimer structure. Involved hydrogen atoms and carbon atoms highlighted in yellow and black, respectively. c) Rotation offset of 60° between adjacent layers.

A bulk powdered nanopropeller sample, simply prepared by solvent evaporation of a solution of **IV.1** in dichloromethane, exhibits high crystallinity, as exemplified in its powder X-ray diffraction (PXRD) pattern with strong and distinct diffraction peaks (**Figure 4.9**). The majority of the powder crystallites is likely to adopt a hexagonal packing motif that is different from the packing structure of the single crystal. However, it is not trivial to obtain crystal structure solely from PXRD data. Further studies are in progress in order to elucidate the crystalline phase of the bulk powders and the self-assembly process during rapid solvent evaporation.

It is noteworthy that the observed hexagonal packing structure closely resembles that found in tris(*o*-phenylenedioxy)cyclo-triphosphazene (TPP) and its inclusion adducts.[64-68] Both TPP and nanopropeller **IV.1** possess a three-fold symmetric molecular architecture that plays an important role in introducing free volumes and directing attractive intermolecular forces. In contrast, nanohoop **IV.4**, as a fragment of **IV.1**, adopts a densely packed crystal structure with no substantial extrinsic cavities (**Figure 4.8**). In

addition, the cyclic trimer supramolecular structure is not observed in case of **IV.4**. Therefore, it is plausible that the bulky propeller architecture and intermolecular CH⋯π interactions work cooperatively in dictating the self-assembly process, leading preferentially to the formation of the observed hexagonal packing motif that maximizes attractive intermolecular interactions, minimizes steric hindrance within the 2D lattice, and provides maximal inter-layer packing efficiency.

4.4. Photophysical and Electrochemical Studies

The photophysical and electrochemical properties of nanopropeller **IV.1** were investigated in comparison with nanohoop **IV.4** (data summarized in **Table 4.1**). Interestingly, we observed similar photophysical properties for **IV.1** and **IV.4** (**Figure 4.4**). Both compounds display an absorption maxima near 330 nm and a low energy absorption band around 410 nm that corresponds to the HOMO-LUMO transition according to time-dependent DFT calculations. Additionally, a similar greenish yellow fluorescence was observed with a major emission peak at around 520 nm. The fluorescence decays of both molecules obey single-exponential kinetics with a similar lifetime (1.64 ns for **IV.1** and 1.49 ns for **IV.4**). Taken together, it suggests a lack of significant intramolecular electronic interactions of the nanopropeller in either the ground state or excited state. However, a slightly less positive oxidation potential was recorded for **IV.1** (0.55 V vs Fc^+/Fc^0) compared to **IV.4** (0.63 V vs Fc^+/Fc^0) in cyclic voltammetry. Further electrochemical studies are underway in order to understand this phenomena.

Table 4.1. Major UV-Vis absorption peaks (λ_{abs}), fluorescence emission peaks (λ_{em}), optical band gap (E_{gap}), fluorescence lifetimes (τ), and oxidation potetial maximum (E_{ox}) at room temperature.

Compound	λ_{abs} [nm]	λ_{em} [nm]	E_{gap} [eV] [a]	τ [ns]	E_{ox} [V][b
IV.1	328, 406	519	3.05	1.64	0.55
IV.4	322, 416	515	2.95	1.49	0.63

[a] Calculated from the lowest energy absorption peaks. [b] V versus Fc^+/Fc^0
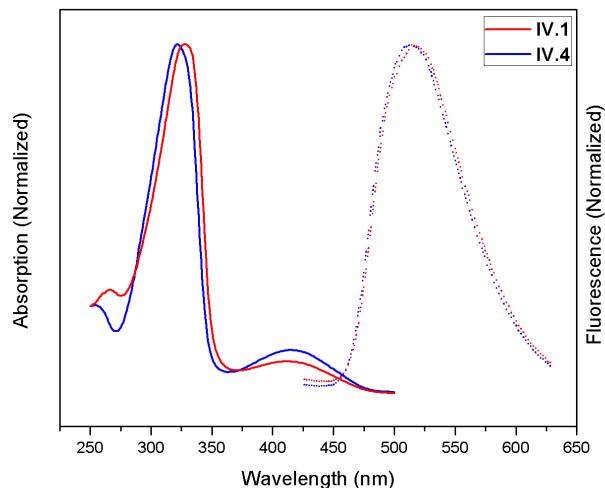
Figure 4.4. UV-Vis absorption and fluorescence spectra of **IV.1** and **IV.4**.

4.5. Conclusion and Outlook

In summary, we have demonstrated the synthesis of a carbon-rich nanopropeller employing an efficient synthon strategy via Pd-catalyzed bisboronate homocoupling and tin(II)-mediated reductive aromatization. The layered hexagonal crystal structure of **IV.1** features long-ranged 1D nanochannel arrays and large guest accessible volume (48%). With its ubiquitous molecular architecture and self-assembly properties, we envision nanopropeller **IV.1** and its functionalized derivatives to have potential uses as molecular porous materials, as building blocks for artificial molecular rotors, and as tectons for crystal engineering. Our efforts towards these applications are underway and will be reported in due course.

4.6. Experimental Sections
4.6.1. General Experimental Considerations

Tetrahydrofuran (THF) and dioxane were obtained from a solvent system with columns packed with activated alumina. Moisture and oxygen sensitive reactions were carried out under nitrogen atmosphere using standard Schlenk line techniques. Silica column chromatography was conducted with Zeochem Zeoprep n60 Eco 40-63 μm silica

gel. Thin layer chromatography (TLC) was performed using Sorbent Technologies Silica Gel XHT TLC plates. Developing plates were visualized using UV light at wavelength of 254 and 365 nm. NMR spectra were recorded on a Bruker Avance-III-HD 600 (or 500) spectrometer with a Prodigy multinuclear broadband cryoProbe. Chemical shifts were reported in parts per million (ppm) and were referenced to the residual protio-solvent (CDCl$_3$, ^{1}H: 7.26 and ^{13}C: 77.16). IR spectra were recorded on a Thermo Scientific Nicolet 6700 spectrometer equipped with a diamond crystal Smart ATR Attachment. Cyclic voltammetry was performed in a N$_2$ atmosphere glove box using a Solartron 1287 potentiostat. A 3-electrode set-up was employed comprising a glassy carbon working electrode, a platinum coil counter electrode and a silver wire pseudo reference electrode. Electrolyte solutions (0.1 M) were prepared from HPLC-grade DCM and anhydrous Bu$_4$NBF$_4$, and the solutions were thoroughly degassed prior to analysis.

UV-Vis absorption and fluorescence spectra were obtained in Quartz cuvette on an Agilent Cary 100 spectrophotometer and a Horiba Jobin Yvon Fluoromax-4 Fluorometer, respectively. The fluorescence decay curves were measured using a time-resolved fluorimeter (Horiba Tempro Fluorescence lifetime system) equipped with a NanoLED (Model: N-360, 360±10 nm). The scatter curves were measured using a diluted Ludox® solution (from Sigma-Aldrich).

4.6.2. Synthetic Details
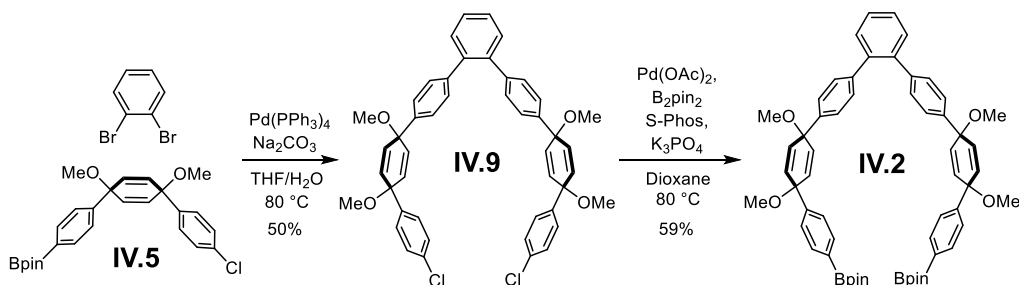
Scheme 4.3. Synthesis of bisboronate **IV.2**.

93

(1's,4's)-4,4'''''-dichloro-1',1''''',4',4''''-tetramethoxy-1',1''''',4',4'''''-tetrahydro-1,1':4',1'':4'',1''':2''',1''':4'''',1''''':4''''',1''''''-sepiphenyl **IV.9**
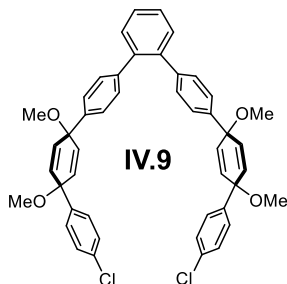
Compound **IV.5** was prepared according to reported procedure.[39] To a 250 mL round bottom flask was added *o*-dibromobenzene (1.00 g, 4.24 mol, 1 eq), **IV.5** (4.22 g, 9.33 mmol, 2.2 eq), K_2CO_3 (2.93 g, 21.2 mmol, 5 eq) and $Pd(PPh_3)_4$ (0.49 g, 0.42 mmol, 0.1 eq). Then a condenser was attached to the flask and the setup was evacuated and refilled with N_2 for 10 times. Then degassed THF (65 mL) and water (25 mL) were transferred to the flask via syringe. The resulting yellow mixture was heated at 90 °C under N_2 overnight. After cooling down to room temperature, DCM (80 mL) was added to the reaction. The mixture was washed with H_2O (50 mL) and brine (100 mL) and then dried with Na_2SO_4. Solvent was removed under reduced pressure and the crude was purified by column chromatography (silica, 0% to 20% ethyl acetate in hexanes) to yield product as yellow oil (1.53 g, 50%). ^{1}H NMR (500 MHz, $CDCl_3$): δ(ppm) 7.39 (s, 4H, Ar-H), 7.27 (d, *J* = 8.6 Hz, 4H, Ar-H), 7.20-7.25 (overlap, 8H, Ar-H), 7.10 (d, *J* = 8.6 Hz, 4H, Ar-H), 6.11 (d, *J* = 10.2 Hz, 4H, C=C-H), 6.02 (d, *J* = 10.2 Hz, 4H, C=C-H), 3.42 (s, 6H, CH_3), 3.41 (s, 6H, OCH_3); ^{13}C NMR (125 MHz, $CDCl_3$): δ(ppm) 142.12, 141.56, 140.99, 140.11, 133.90, 133.46, 133.14, 130.97, 130.06, 128.60, 127.67, 127.57, 125.66, 74.81, 74.66, 52.15; IR (neat) 3055, 3025, 2980, 2934, 2896, 2820, 1915, 1608, 1593, 1505, 0477, 1401, 1360, 1172, 1074, 1021, 949, 826, 783 cm^{-1}; HRMS (TOF, ES+) m/z cald for $C_{46}H_{40}Cl_2O_4Na$ (M)$^+$ 749.2201, found 749.2196.

2,2'-((1's,4's)-1',1'''',4',4''''-tetramethoxy-1',1'''',4',4''''-tetrahydro-[1,1':4',1'':4,1''':2''',1'''':4'''',1''''':4''''',1''''''-sepiphenyl]-4,4'''''-diyl)bis(4,4,5,5-tetramethyl-1,3,2-dioxaborolane) **IV.2**
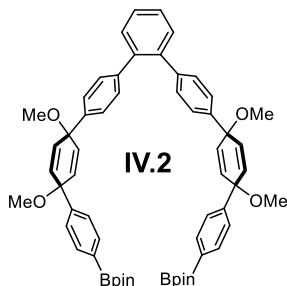
To a 50 mL round bottom flask was added **IV.9** (1.53 g, 2.10 mmol, 1 eq), B_2Pin_2 (4.27 g, 16.8 mmol, 8 eq), K_3PO_4 (3.57 g, 16.8 mmol, 8 eq), $Pd(OAc)_2$ (0.071 g, 0.11 mmol, 0.05 eq) and S-Phos (0.120 g, 0.27 mmol, 0.13 eq). The flask was evacuated and backfilled with N_2 for 10 times. After switching the vacuum adapter with septum, the flask was purged with N_2 for another 30 min. At this point, degassed dioxane (25 mL) was added to the flask and the mixture was heated at 80 °C overnight. Upon cooling to room temperature, the mixture was filtered through a short plug of Celite to remove the base. Then solvent was removed under reduced pressure and the resulting grey residue was purified via column chromatography (silica, 0% to 15% ethyl acetate in DCM) to yield product as white powder (1.12 g, 59%). ^{1}H NMR (600 MHz, $CDCl_3$): δ(ppm) 7.73 (d, J = 8.2 Hz, 4H, Ar-H), 7.39 (s, 4H, Ar-H), 7.38 (d, J = 8.2 Hz, 4H, Ar-H), 7.24 (d, J = 8.3 Hz, 4H, Ar-H), 7.09 (d, J = 8.3 Hz, 4H, Ar-H), 6.11 (d, J = 10.3 Hz, 4H, C=C-H), 6.06 (d, J = 10.3 Hz, 4H, C=C-H), 3.42 (s, 6H, OCH_3), 3.41 (s, 6H, OCH_3), 1.33 (s, 24H, CH_3); ^{13}C NMR (150 MHz, $CDCl_3$): δ(ppm) 146.55, 141.62, 140.86, 140.22, 135.04, 133.64, 133.21, 130.98, 129.98, 127.53, 125.72, 125.45, 83.87, 75.10, 74.87, 52.07, 25.02; IR (neat) 2978, 2933, 2895, 2819, 1609, 1507, 1475, 1398, 1355, 1319, 1272, 1086, 1076, 1053, 1031, 962, 833, 762 cm^{-1}; HRMS (TOF ES+) m/z cald for $C_{58}H_{64}B_2O_8K$ (M+K)$^+$ 949.4434, found 949.4436.

(41s,44s,71s,74s)-41,44,71,74-tetramethoxy-1,3,5,6(1,4),2(1,2)-pentabenzena-4,7(1,4)-dicyclohexanacycloheptaphane-42,45,72,75-tetraene **IV.3**
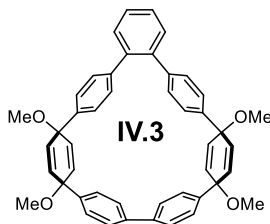
Bisboronate **IV.2** (400 mg, 0.439 mmol, 1 eq), $PdCl_2(PPh_3)_2$ (62 mg, 0.088 mmol, 0.2 eq) and $B(OH)_3$ (136 mg, 2.20 mmol, 5 eq) were dissolved in THF (100 mL) in a 250 mL round bottom flask equipped with a stir bar. The yellow solution was sparged with O_2 for 15 min. Then solid KF (25 mg, 0.439 mmol, 1 eq) and H_2O (10 mL) were subsequently added. The mixture was subjected to sonication until orange color appeared, after which it was kept stirring over night at room temperature. After THF was removed under vacuum, DCM (70 mL) was added. The solution was washed with H_2O (30 mL) and brine (30 mL) and dried over Na_2SO_4. The solution was then concentrated and the crude solid was purified via column chromatography (silica, 0% to 5% ethyl acetate in DCM) to yield product as white powder (198 mg, 66%). ^1H NMR (600 MHz, $CDCl_3$): δ(ppm) 7.40 (d, J = 8.7 Hz, 4H, Ar-H), 7.37 (d, J = 8.7 Hz, 4H, Ar-H), 7.31-7.25 (overlap, 10H, Ar-H), 7.13 (dd, J = 5.8, 3.4 Hz, 2H, Ar-H), 6.35 (d, J = 10.3 Hz, 4H, C=C-H), 6.21 (d, J = 10.3 Hz, 4H, C=C-H), 3.51 (s, 6H, OCH_3), 3.33 (s, 6H, OCH_3); ^{13}C NMR (150 MHz, $CDCl_3$): δ(ppm) 141.98, 141.85, 141.51, 139.50, 138.84, 134.92, 133.98, 132.35, 129.59, 127.25, 126.81, 126.55, 126.35, 75.48, 74.41, 52.70, 51.66; IR (neat) 3028, 2980, 2933, 2897, 2820, 1605, 1556, 1479, 1397, 1264, 1225, 1185, 1174, 1070, 1030, 947, 821, 760 cm^{-1}; HRMS (TOF ES+) m/z cald for $C_{46}H_{40}O_4Na$ (M+Na)$^+$ 679.2824, found 679.2831, cald $C_{45}H_{37}O_3$ (M-OMe) 625.2743, found 625.2751.

1(1,2),2,3,4,5,6,7(1,4)-heptabenzenacycloheptaphane **IV.4**
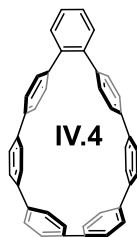
A modified procedure from Ref. 55 was adapted. First, H_2SnCl_4/THF (0.04 mol/L) was prepared by adding concentrated HCl/H_2O (0.52 mL, 12 mol/L) into a solution of $SnCl_2\cdot2H_2O$ (690 mg) in THF (63 mL) and was allowed to stir at room temperature for 30 min. In a 50 mL round bottom flask equipped with a stir bar, **IV.3** (56 mg, 0.085 mmol, 1 eq) was dissolved in dry THF (10 mL). Then freshly prepared H_2SnCl_4/THF solution (4.9 mL, 0.194 mmol, 2.3 eq) was added in stream. After stirring at room temperature for 30 min, the reaction was quenched with NaOH/H_2O solution. Then DCM (30 mL) was added to the mixture. The organic layer was separated and washed with H_2O (80 mL), brine (100 mL) and dried over Na_2SO_4. Removing solvent, the product was isolated using column chromatography (silica, 0% to 40% DCM in hexanes) as yellow solid (30 mg, 67%). ^{1}H NMR (600 MHz, CDCl$_3$): δ(ppm) 7.54 (d, $J = 9.2$ Hz, 4H, Ar-H), 7.52 (d, $J = 8.7$ Hz, 4H, Ar-H), 7.48 (d, $J = 9.2$ Hz, 4H, Ar-H), 7.45-7.37 (overlap, 8H, Ar-H), 7.22 (d, $J = 8.2$ Hz, 4H, Ar-H), 7.01 (d, $J = 8.2$ Hz, 4H, Ar-H); ^{13}C NMR (150 MHz, CDCl$_3$): δ(ppm) 140.78, 140.06, 138.50, 138.09, 137.52, 137.23, 135.46, 130.43, 130.12, 128.33, 127.68, 127.46, 127.33, 127.25, 126.97; IR (neat) 3051, 3022, 2923, 2850, 1899, 1667, 1593, 1574, 1489, 1469, 1441, 1387, 1261, 1186, 1105, 1004, 984, 810, 760 cm^{-1}; MALDI TOF, m/z cald for $C_{42}H_{29}$ (M+H)$^+$ 533.23, found 533.12.

Hexachloride **IV.6**

IV.6
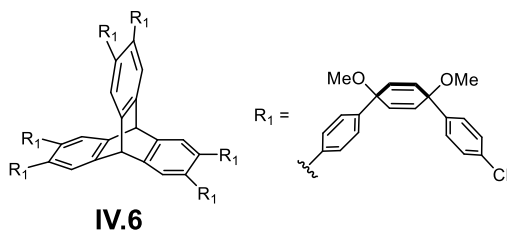
Hexabromotriptycene (0.42 g, 0.58 mol, 1 eq), **IV.5** (2.00 g, 4.42 mmol, 7.6 eq) and Pd(PPh₃)₄ (0.20 g, 0.17 mmol, 0.3 eq) were placed in a 25 mL microwave glass vial equipped with a stir bar. The vial was evacuated and refilled with N_2 for 10 times, at which point degassed THF (13 mL) and NaOH (1M in H_2O, 7 mL) were added. The reaction was stirred and heated with a microwave reactor at 90 °C for 4 hours. Upon cooling to room temperature, aqueous layer was removed with a glass pipette. Then DCM (50 mL) was mixed with the remaining yellow solution. The mixture was washed with brine (30 mL) and then dried over Na_2SO_4. Solvent was removed under reduced pressure and the crude was purified by column chromatography (silica, 0% to 10% ethyl acetate in DCM) to produce an orange oil residual, which was further washed with acetone to yield product as white power (0.88 g, 69%). ¹H NMR (600 MHz, CDCl₃): δ(ppm) 7.50 (s, 6H, Ar-H), 7.26 (d, J = 8.7 Hz, 12H, Ar-H), 7.23 (d, J = 8.7 Hz, 12H, Ar-H), 7.19 (d, J = 8.4 Hz, 12H, Ar-H), 7.05 (d, J = 8.4 Hz, 12H, Ar-H), 6.10 (d, J = 10.3 Hz, 12H, C=C-H), 6.01 (d, J = 10.3 Hz, 12H, C=C-H), 5.62 (s, 2H, Ph₃C-H), 3.43-3.39 (overlap, 36H, OCH₃); ¹³C NMR (150 MHz, CDCl₃): δ(ppm) 144.24, 142.07, 141.41, 140.90, 137.30, 133.88, 133.44, 133.09, 130.12, 128.58, 127.54, 126.43, 125.65, 74.79, 74.65, 53.20, 52.13; IR (neat) 3026, 2981, 2935, 2896, 2821, 1913, 1791, 1673, 1593, 1506, 1483, 1461, 1402, 1301, 1263, 1227, 1172, 1107, 1072, 1011, 985, 949, 805, 825, 764 cm⁻¹; HRMS (Q-TOF, ES+) m/z cald for C₁₄₀H₁₁₆Cl₆O₁₂Na (M+Na)⁺ 2221.6496, found 2221.6497.

Hexaboronate **IV.7**

IV.7
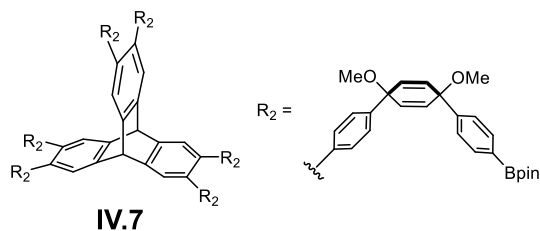
A similar procedure to synthesize **IV.2** was adapted. **IV.6** (0.800 g, 0.363 mmol, 1 eq), B$_2$Pin$_2$ (1.844 g, 7.26 mmol, 20 eq), K$_3$PO$_4$ (1.540 g, 7.26 mmol, 20 eq), Pd(OAc)$_2$ (0.037 g, 0.054 mmol, 0.15 eq) and S-Phos (0.058 g, 0.142 mmol, 0.39 eq), dioxane (10 mL). Product was purified by column chromatography (silica, 0% to 10% ethyl acetate in DCM) as white powder (0.683 g, 68%). ^{1}H NMR (600 MHz, CDCl$_3$): δ(ppm) 7.72 (d, $J =$ 7.8 Hz, 12H, Ar-H), 7.52 (s, 6H, Ar-H), 7.36 (d, $J =$ 7.8 Hz, 12H, Ar-H), 7.19 (d, $J =$ 8.0 Hz, 12H, Ar-H), 7.05 (d, $J =$ 8.0 Hz, 12H, Ar-H), 6.09 (d, $J =$ 10.3 Hz, 12H, C=C-H), 6.03 (d, $J =$ 10.3 Hz, 12H, C=C-H), 5.69 (s, 2H, Ph$_3$C-H), 3.41 (s, 18H, OCH$_3$), 3.39 (s, 18H, OCH$_3$), 1.29 (s, 72H, CH$_3$); ^{13}C NMR (150 MHz, CDCl$_3$): δ(ppm) 146.52, 144.30, 141.31, 140.98, 137.28, 135.04, 133.66, 133.09, 130.12, 126.49, 125.62, 125.41, 83.84, 75.11, 74.86, 53.18, 52.04, 52.04, 25.00; IR (neat) 3027, 2976, 2932, 2899, 2822, 1609, 1506 1462, 1397, 1358, 1318, 1271, 1215, 1143, 1075, 1017, 948, 857, 827, 761 cm^{-1}. MALDI TOF, EI+ Q-TOF and other methods were attempted, but unable to obtain HRMS data.

Nanopropeller precursor **IV.8**

IV.8
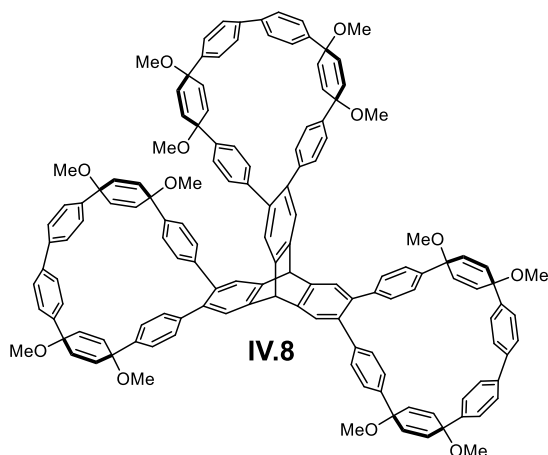
A similar procedure to synthesize **IV.3** was adapted. **IV.7** (683 mg, 0.248 mmol, 1 eq), PdCl$_2$(PPh$_3$)$_2$ (105 mg, 0.149 mmol, 0.6 eq) and B(OH)$_3$ (230 mg, 3.720 mmol, 15 eq), KF (44 mg, 0.744 mmol, 3 eq), THF (260 mL), H$_2$O (26 mL). Product was purified by column chromatography (silica, 0% to 20% ethyl acetate in DCM) as white powder (225 mg, 46%). ^{1}H NMR (500 MHz, CDCl$_3$): δ(ppm) 7.36 (d, J = 8.5 Hz, 12H, Ar-H), 7.32 (d, J = 8.5 Hz, 12H, Ar-H), 7.22 (d, J = 8.6 Hz, 12H, Ar-H), 7.17 (d, J = 8.6 Hz, 12H, Ar-H), 7.13 (s, 6H, Ar-H), 6.33 (d, J = 10.4 Hz, 12H, C=C-H), 6.19 (d, J = 10.4 Hz, 12H, C=C-H), 5.25 (s, 2H, Ph$_3$C-H), 3.49 (s, 18H, OCH$_3$), 3.33 (s, 18H, OCH$_3$); ^{13}C NMR (150 MHz, CDCl$_3$): δ(ppm) 143.49, 141.88, 141.78, 141.50, 139.55, 136.05, 134.86, 132.38, 129.66, 129.22, 126.83, 126.56, 126.39, 75.48, 74.44, 52.72, 51.66; IR (neat) 3028, 2976, 2933, 2899, 2821 1609, 1507, 1464, 1397, 1356, 1317, 1270, 1222, 1172, 1143, 1077, 1015, 982, 945, 905, 852, 823, 760, 739 cm^{-1}; HRMS (Q-TOF ES+), m/z cald for C$_{140}$H$_{116}$O$_{12}$Na (M)$^+$ 2011.8364, found 2011.8326.

Nanopropeller **IV.1**
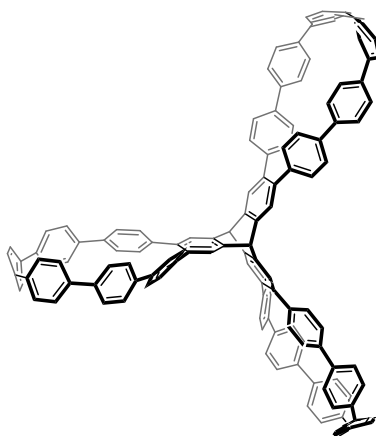
A similar procedure to synthesize **IV.4** was adapted. **IV.8** (20 mg, 0.010 mmol, 1 eq), H$_2$SnCl$_4$/THF solution (4.3 mL, 0.075 mmol, 7.5 eq). Product was purified by preparative gel permeation chromatography (chloroform as eluent) as yellow solid (12 mg, 73%). ^{1}H NMR (600 MHz, CDCl$_3$): δ(ppm) 7.56-7.49 (m, 30H, Ar-H), 7.47 (d, J = 8.9 Hz, 12H, Ar-H), 7.40 (d, J = 8.2 Hz, 12H, Ar-H), 7.19 (d, J = 7.9 Hz, 12H, Ar-H), 6.95 (d, J = 7.9 Hz, 12H, Ar-H), 5.60 (s, 2H, Ph$_3$C-H), ^{13}C NMR (150 MHz, CDCl$_3$): δ(ppm) 144.16, 139.96, 138.46, 138.06, 138.00, 137.51, 137.24, 135.44, 130.20, 128.32, 127.67, 127.32, 127.24, 126.99, 125.96, 53.30; IR (neat) 3020, 2955, 2920, 2852, 1303,

1592, 1576, 1563, 1385, 1310, 1248, 1179, 1108, 1067, 1020, 1001, 961, 942, 902, 810, 740, 714 cm^{-1}; MALDI TOF, m/z cald for $C_{128}H_{80}$ (M)$^+$ 1616.626 found 1616.657.

4.6.3. Single Crystal X-ray Diffraction Studies

Diffraction intensities for **IV.1** and **IV.4** were collected at 173 (2) on a Bruker Apex2 CCD diffractometer using an Incoatec IµS micro-focus source with CuKα radiation, λ= 1.54178 Å. Space groups were determined based on systematic absences and intensity statistics. Absorption corrections were applied by SADABS.[69] Structures were solved by direct methods and Fourier techniques and refined on F^2 using full matrix least-squares procedures. All non-H atoms were refined with anisotropic thermal parameters. H atoms in both structures were refined in calculated positions in a rigid group model. Both crystal structures have solvent molecules and some of them are disordered. In the crystal of **IV.1**, there are two types of chlorobenzene molecules. One of them is highly disordered and was treated by SQUEEZE.[70] Diffractions from the crystal of **IV.1** were weak and it was only possible to collect diffraction data up to 2θmax = 99.134° even using a strong *Incoatec* Cu *I*µ*S* source. Single crystals of **IV.4** were grown overnight from a mixed solution of DCM and *n*-pentane. A highly distorted *n*-pentane molecule fills the void of **IV.4** and was also treated by SQUEEZE. All calculations were performed by the SHELXL-2014/7 packages.[71]
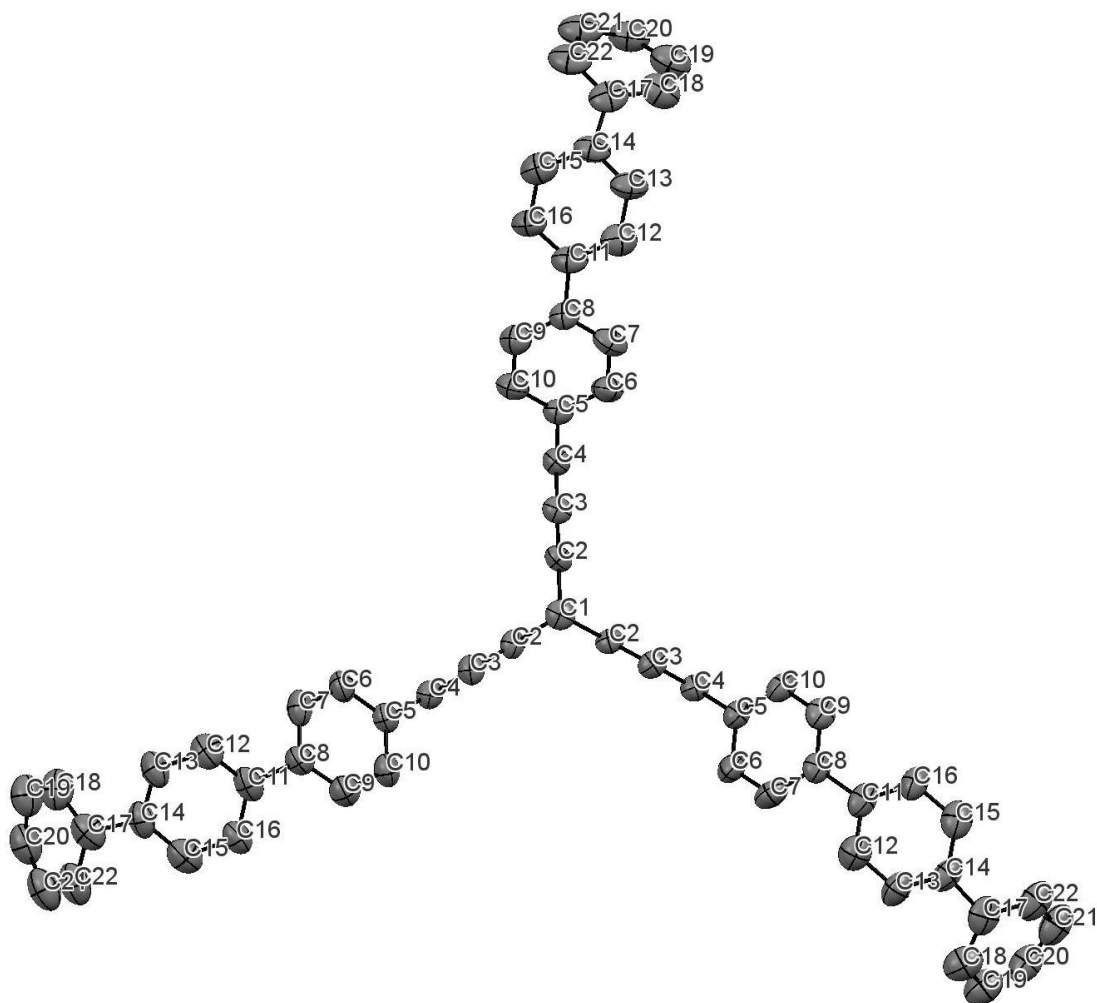
Figure 4.5. ORTEP representation of the X-ray crystallographic structure of **IV.1** (CCDC Registry # 1528934).

Crystallographic data for **IV.1**: $C_{164}H_{110}Cl_6$, M = 2293.21, Size = 0.19 x 0.14 x 0.10 mm, T = 173(2) K, Hexagonal, space group *P63/m*, a = 22.375(8) Å, b = 22.375(8) Å, c = 16.323(6) Å, α = 90°, β = 90°, γ = 120°, V = 7077(6) Å^3, Z = 2, Dc = 1.076 Mg/m^3, μ(Mo) = 1.477 mm^{-1}, *F*(000) = 2392, θ = 2.280-49.670°, 12474 reflections, 2498 independent reflections [R_{int} = 0.0512], R1 = 0.0885, wR2 = 0.2540 and GOF = 1.042 for 2498 reflections (235 parameters) with I>2σ(I), R1 = 0.1172, wR2 = 0.2756 and GOF = 1.042 for all reflections, max/min residual electron density +0.715/-0.470 eÅ^3.
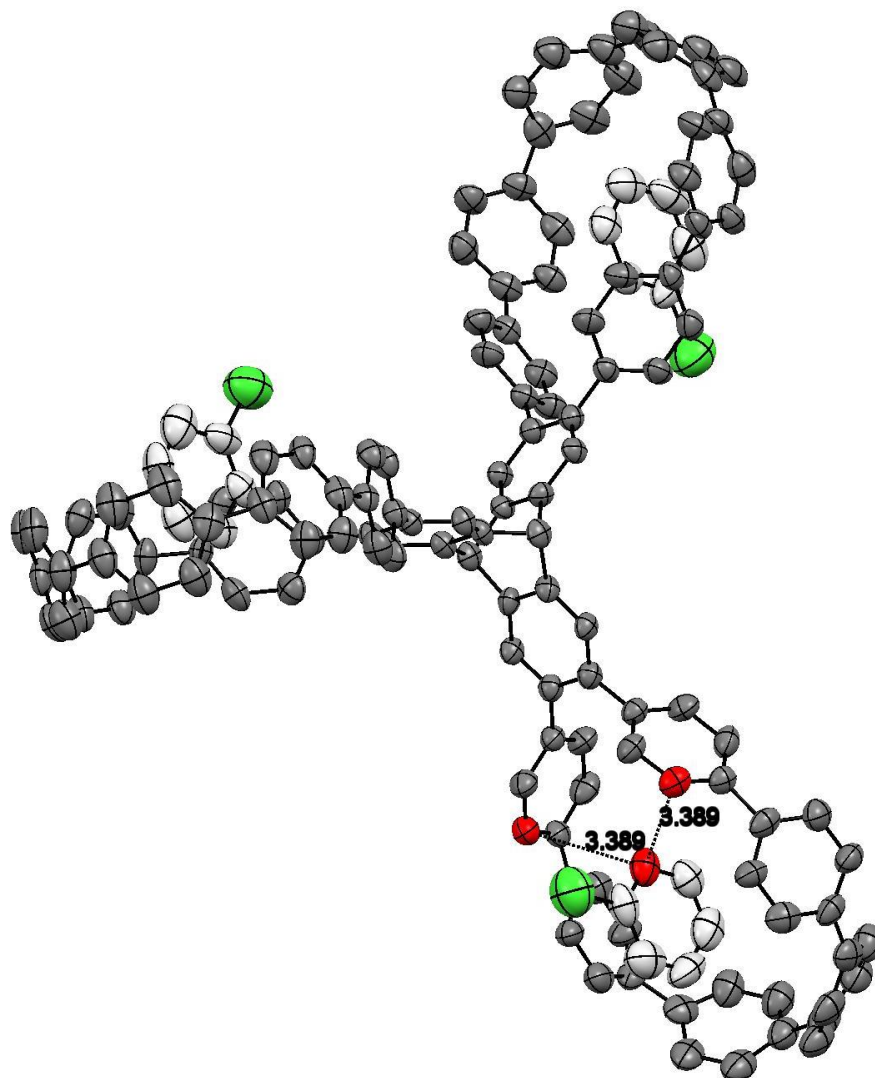
Figure 4.6. ORTEP representation of the X-ray crystallographic structure of **IV.1** and three trapped chlorobenzene molecules. Carbon atoms involved in π-π stacking are highlighted in red.
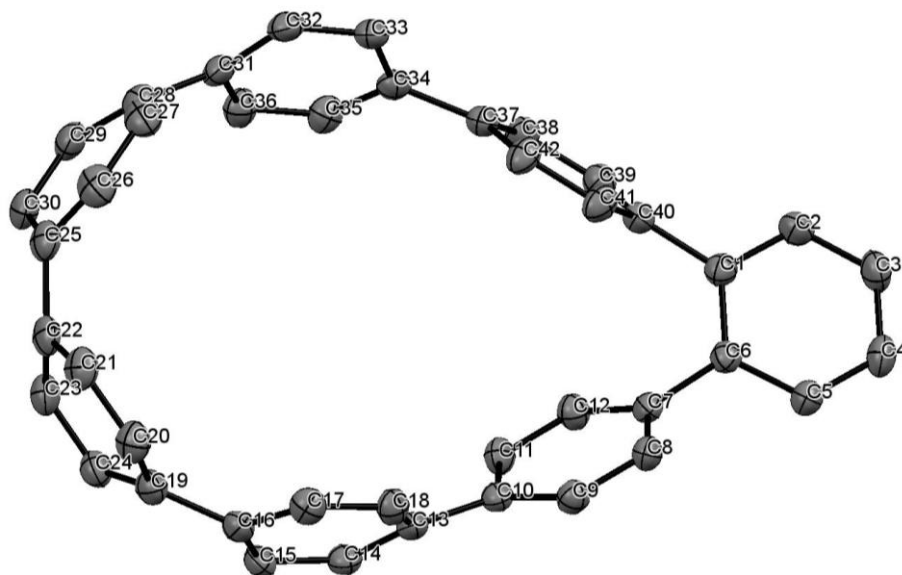
Figure 4.7. ORTEP representation of the X-ray crystallographic structure of **IV.4** (CCDC Registry # 1528930).

Crystallographic data for **IV.4**: $C_{47}H_{40}$, M = 604.79, Size = 0.19 x 0.14 x 0.10 mm, T = 173(2) K, Triclinic, space group *P-1*, a = 10.8942(4) Å, b = 10.8972(3) Å, c = 14.3818(5) Å, α = 103.020(2)°, β = 93.561(2)°, γ = 107.252(2)°, V = 1573.30(9) Å^3, Z = 2, Dc = 1.277 Mg/m^3, μ(Mo) = 0.540 mm^{-1}, *F*(000) = 644, θ = 3.185-67.524°, 27565 reflections, 5492 independent reflections [R_{int} = 0.0468], R1 = 0.0462, wR2 = 0.1299 and GOF = 1.073 for 5492 reflections (379 parameters) with I>2σ(I), R1 = 0.0531, wR2 = 0.1337 and GOF = 1.073 for all reflections, max/min residual electron density +0.256/-0.189 eÅ^3.
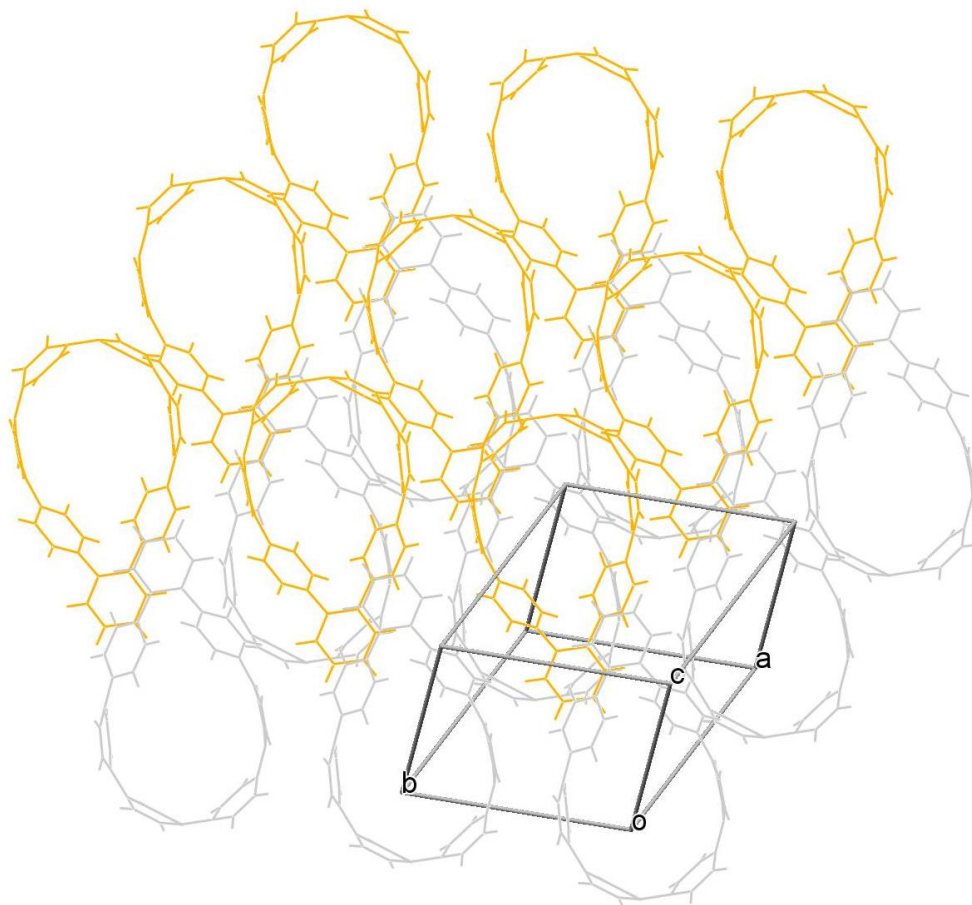
Figure 4.8. Representation of the triclinic packing structure of **IV.4**.

4.6.4. Powder X-ray Diffraction Studies

Powder X-ray diffraction (PXRD) patterns were acquired on a Rigaku Smartlab X-ray diffractometer with general Bragg-Brentano configuration using Cu Kα line focused radiation (40 kV, 30 mA) and with a 0.3 mm radiation entrance slit. Samples were prepared by first dispersing solid in DCM and dropping the mixture to zero ground sample holders, and allowed to dry overnight at ambient condition. ^{1}H NMR spectra were recorded prior to the PXRD studies to confirm that DCM was fully evaporated. The PXRD pattern of the solvent free single crystal model was simulated using the Reflex module of Materials Studio.[72]

PXRD discussion: We have attempted indexing of the experimental PXRD pattern using Materials Studio software package for unit cell parameter determination but

without success. For lower angle diffraction peaks (larger d-spacings), the ratio of d-spacings of peaks at 4.4° and 8.8° is 1: 2, which agrees with the values required for diffractions from (100) and (200) in cubic, tetragonal or hexagonal lattices. As nanopropeller **IV.1** has three-fold symmetry, we tentatively rule out the possibility of cubic and tetragonal lattices. The simulated PXRD pattern (Figure S6) exhibits distinct peaks at 4.5° and 9.1° (corresponding to (100) and (200) diffractions, respectively), suggesting that the powder crystallites might have a hexagonal packing structure. However, other diffraction peaks in the experimental PXRD pattern are obviously different from these in the simulated PXRD pattern. Therefore, we tentatively conclude that "the majority of the powder crystallites is likely to adopt a hexagonal packing motif that is different from the packing structure of the single crystal".
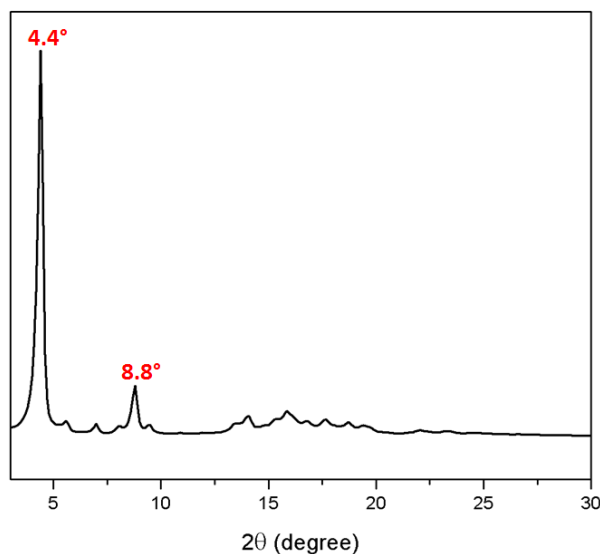
Figure 4.9. Experimental PXRD pattern of **IV.1**.
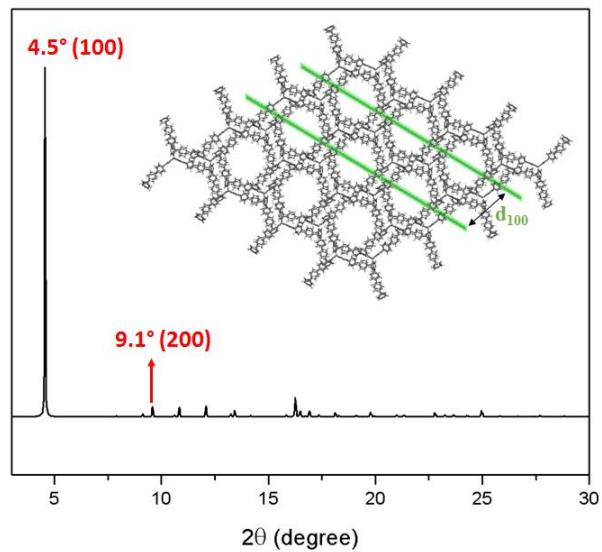
Figure 4.10. Simulated PXRD pattern of **IV.1** from the solvent free hexagonal crystal structure, (100) plane (green) shown in the hexagonal lattice.

4.6.5. Photophysical and Electrochemical Characterizations
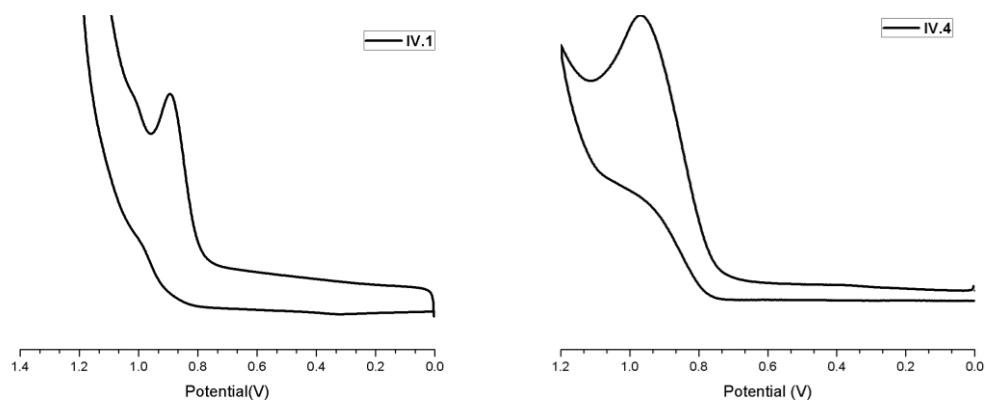
Figure 4.11. Cyclic voltammetry of **IV.1** and **IV.4** (vs Fc^+/Fc^0).
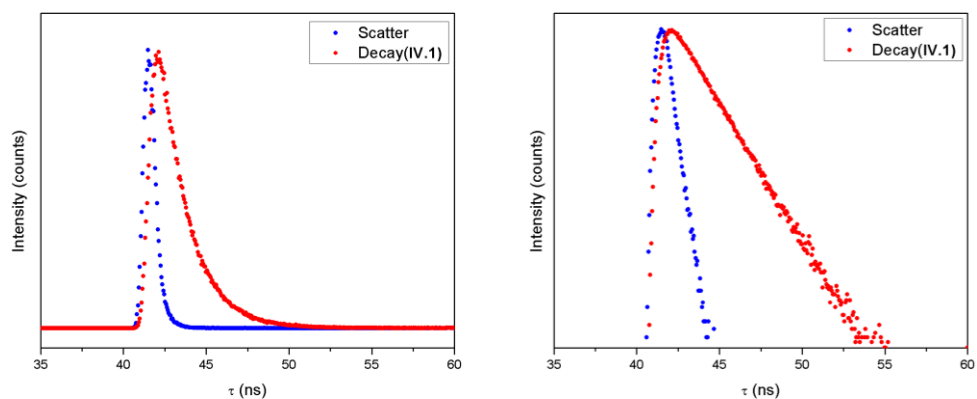
Figure 4.12. Fluorescence decay of **IV.1**. Left, exponential. Right, linearized.
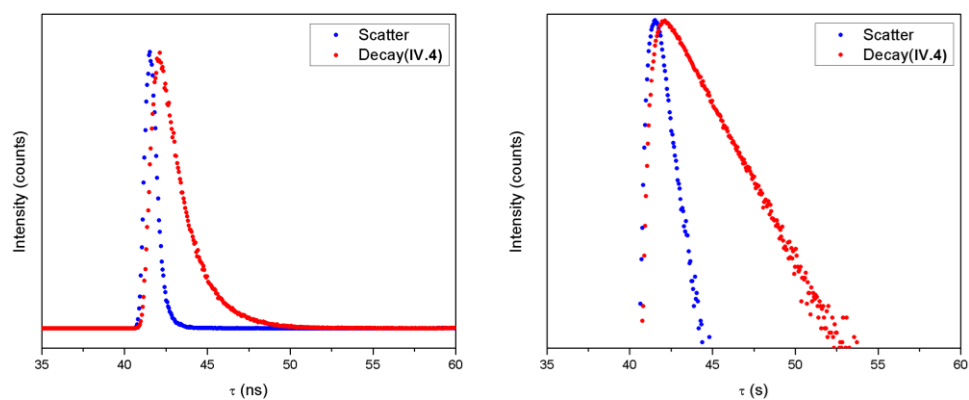
Figure 4.13. Fluorescence decay of **IV.4**. Left, exponential. Right, linearized.

4.6.6. Computational Details

All computations were carried out with Gaussian 09 package.[7] Molecular geometry optimizations and optical transition predictions were computed at the B3LYP/6-31G* level. The fully optimized structures were confirmed to be true minima by vibrational analysis.
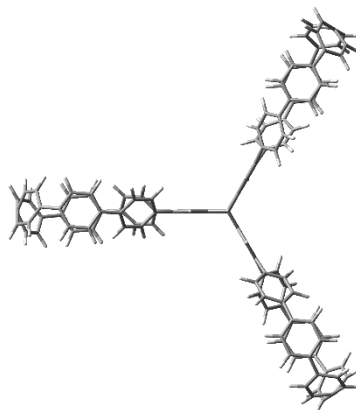
Figure 4.14. Optimized molecular structure of **IV.1** using DFT calculation (B3LYP/6-31G*), exhibiting a C_3 symmetric conformation.
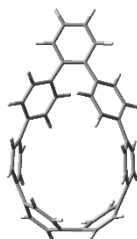
Figure 4.15. Optimized molecular structure of **IV.4** using DFT calculation (B3LYP/6-31G*), exhibiting a C_2 symmetric conformation.

Table 4.2. Major electronic transitions of **IV.1** determined by TD-DFT calculation (B3LYP/6-31G*).

Energy (cm^{-1})	Wavelength (nm)	Osc. Strength	Major contribs
22482.05	444.7992	0.0002	H-2->LUMO (15%), H-1->L+1 (16%), H-1->L+2 (24%), **HOMO->LUMO (41%)**
22489.31	444.6557	0.0025	H-2->L+1 (10%), H-2->L+2 (25%), H-1->LUMO (20%), HOMO->L+1 (40%)
22539.32	443.6691	0.1994	H-2->L+1 (33%), H-1->LUMO (24%), HOMO->L+2 (35%)
25379.22	394.0232	0.0026	H-2->LUMO (15%), H-1->L+1 (15%), HOMO->LUMO (53%)
25382.44	393.9731	0.0027	H-2->L+1 (13%), H-1->LUMO (15%), HOMO->L+1 (54%)
25491.33	392.2903	0.0017	H-2->L+1 (17%), H-1->LUMO (15%), HOMO->L+2 (64%)
25622.8	390.2774	0	H-2->LUMO (46%), H-1->L+1 (43%)
25752.65	388.3095	0.0017	H-2->L+1 (16%), H-2->L+2 (41%), H-1->LUMO (13%), H-1->L+2 (21%)

25755.07	388.273	0.0018	H-2->LUMO (13%), H-2->L+2 (21%), H-1->L+1 (14%), H-1->L+2 (43%)
28171.53	354.9683	0.1188	H-4->LUMO (10%), H-1->L+5 (15%), HOMO->L+3 (12%), HOMO->L+4 (21%)
28175.56	354.9175	0.1193	H-4->L+1 (11%), H-2->L+5 (14%), HOMO->L+3 (20%), HOMO->L+4 (11%)
28240.89	354.0965	0.0003	H-6->LUMO (12%), H-5->L+1 (13%), H-4->L+2 (12%), H-2->L+3 (17%), H-1->L+4 (15%), HOMO->L+5 (19%)

Table 4.3. Major electronic transitions of **IV.4** determined by TD-DFT calculation (B3LYP/6-31G*).

Energy (cm^{-1})	Wavelength (nm)	Osc. Strength	Major contribs
22682.89	440.861	0.0798	**HOMO->LUMO** (98%)
28307.03	353.2691	0.0158	H-1->LUMO (39%), HOMO->L+1 (60%)
30546.04	327.3747	1.229	H-1->LUMO (56%), HOMO->L+1 (34%)
30792.85	324.7507	0	H-2->LUMO (50%), HOMO->L+2 (48%)
31513.11	317.3283	0.4023	H-2->LUMO (46%), HOMO->L+2 (48%)
31567.15	316.7851	0.1632	HOMO->L+3 (75%)
33253.66	300.7188	0.0012	H-6->LUMO (10%), HOMO->L+4 (65%)
33873.1	295.2195	0.0793	H-1->L+1 (87%)
34617.56	288.8708	0	H-2->L+1 (39%), H-1->L+2 (29%), HOMO->L+5 (20%)
35166.02	284.3655	0.0017	H-7->LUMO (11%), H-2->L+1 (13%), HOMO->L+5 (31%), HOMO->L+7 (20%)
35191.02	284.1634	0.0006	H-6->LUMO (14%), H-4->LUMO (10%), HOMO->L+6 (52%)
35655.6	280.4609	0.0197	H-3->LUMO (26%), HOMO->L+5 (21%), HOMO->L+7 (16%)

4.7. Bridge to Chapter V

In Chapter IV, we have shown that structurally unique nanocarbon architectures are accessible with estalished nanohoop chemistry. Chapter V continues to explore the application of nanohoop chemistry and highlights our efforts to synthesize highly strained stilbene macrocycles that represents a new class of monomer for ring-openig metathesis polymerization.

CHAPTER V

STRAINED STILBENE MACROCYCLES AS A NEW CLASS OF MACROCYCLIC
MONOMERS FOR RING-OPENING METATHESIS POLYMERIZATION

This chapter is based on unpublished work. Dr. Yosuke Ashikari and Prof. Andrew J. Boydston from University of Washington provided assistance with the polymerization studies as well as the initial characterization of the polymers. Dr. Lev N. Zakharov conducted the X-ray crystallographic studies.

Ring-opening metathesis polymerization (ROMP) has proven to be a powerful methodology to create macromolecules with unique architectures and functionalities. The most widely used monomers for ROMP are strained bicyclic olefins including norbornenes and oxonorbornenes of which the polymerization is driven by enthalpy gain via release of the ring strain. Non-strained macrocyclic olefins have also been extensively investigated as the monomers for entropy-driven ROMP (ED-ROMP). Though capable of introducing main chain functionalities, ED-ROMP, as a non-living polymerization process, is not a feasible strategy to create complex polymeric architectures. Therefore, there is a need for the development of strained macrocyclic olefins to achieve enthalpy-driven living ROMP. In this chapter, we describe the synthesis of ROMPable strained stilbene macrocycles by employing an efficient intramolecular bisboronate homocoupling strategy. In addition to the advantage of scalable synthesis and easy functionalization, our monomers are shown to polymerize in a living fashion as indicated by our initial ROMP studies. We expect these novel ROMP monomers to open the doors to structurally unique polymeric materials with diverse functions.

5.1. Background

Ring opening metathesis polymerization (ROMP) has emerged as one of the most important methodologies in polymer chemistry since the discovery of well-defined olefin metathesis catalyst based on the alkylidene complexes of titanium (Ti), tantalum (Ta), tungsten (W), molybdenum (Mo) and ruthenium (Ru).[1] With the availability of stable and

functionality-tolerant Ruthenium-based catalysts (**V.1-6** in **Figure 5.1**) developed by Grubbs, Hoveyda and many others, ROMP has been widely employed among polymer chemists and material scientists to access polymeric materials with unique architectures and functionalities for the applications in biomedical technologies, (bio)electronics and renewable energies.[2-3]
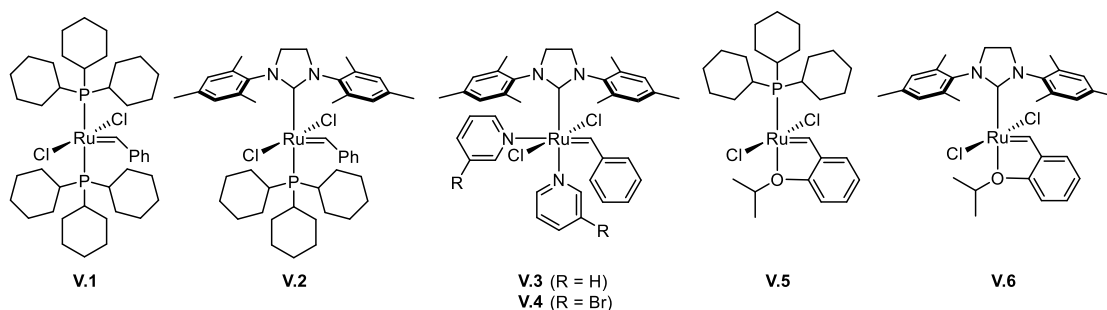
Figure 5.1. Common Ruthenium-based olefin metathesis catalysts: Grubbs 1st Gen (**V.1**), Grubbs 2nd Gen (**V.2**), Grubbs 3st Gen (**V.3-4**), Hoveyda-Grubbs 1st Gen (**V.5**) and Hoveyda-Grubbs 2nd Gen (**V.6**).[1]

The most common ROMP monomers are strained bicyclic olefins including norbornenes and oxonorbornenes.[2] The strain stored in the hydrocarbon skeletons provides the enthalpic driving force for chain growth and compensates for the loss of entropy during the ROMP process. A generalized ROMP mechanism is depicted in **Figure 5.2**.[1] First, the metal-alkylidene complex (the initiator) coordinates with the olefin, which subsequently undergoes a [2+2]-cycloaddition to generate a metallocyclobutane intermediate. Cycloreversion of this intermediate affords a terminal metal-alkylidene that is reactive towards olefin metathesis, thus allowing chain propagation. Finally, the polymerization is terminated when the monomers are consumed or a quenching reagent (such as ether vinyl ether) is added. With an optimized combination of initiator, solvent and temperature, living ROMP of strained olefins can be achieved, which permits the synthesis of nearly mono-dispersed polymers with controlled chemical sequence and topologies.
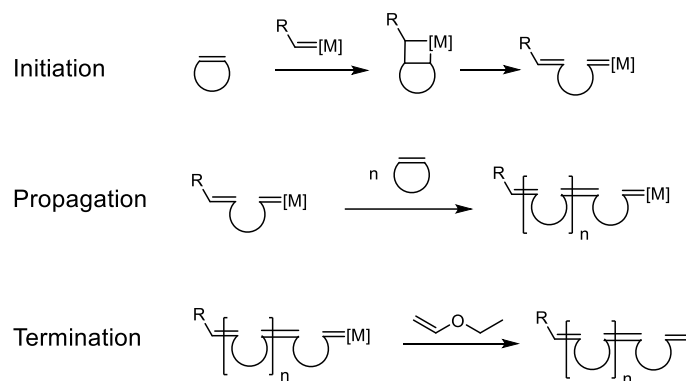
Figure 5.2. The mechanism of ROMP: initiation, propagation and termination.[1]

Strainless macrocyclic olefins have also been extensively used as monomers for entropy-driven ROMP (ED-ROMP) of which the main driving force is the gain of conformational entropy.[4] One of the most prominent features of ED-ROMP is the ease to install novel main chain functionalities via the chemical modification of the macrocyclic monomers. However, ED-ROMP, as a biased ring-chain equilibrium, is not a living polymerization. As a result, block-copolymers and other macromolecules with complex architectures are not achievable utilizing the ED-ROMP methodology.

Strained olefin macrocycles that exhibit living ROMP behaviors hold the potential to access structurally unique macromolecules with diverse functions.[5] However, examples of ROMPable strained macrocyclic olefins remain scarce. This is mainly limited by the lack of efficient and versatile synthetic strategies to access desirable macrocyclic monomers.[4]

In 1994, Bazan and coworkers pioneered the ROMP of strained paracyclophanes.[6] Schrock-type molybdenum carbene complex **V.8** was discovered to initiate the polymerization of paracyclophane **V.7** to produce polymer **V.9** with high regio-regularity (98% *cis*-double bond) and a narrow polydispersity index (PDI) of 1.1 (**Figure 5.3a**), indicating a living polymerization process. The ROMP of paracyclophanes was later applied to synthesize well-defined poly(*para*-phenylvinylene) (PPV) which was not achievable using the conventional Gilch polymerization method. To circumvent the synthetic challenge posed by the insolubility of unsubstituted PPV units, paracyclophane **V.10** with a solubilizing silyloxy group was designed as a masked precursor for

unsubstituted PPV polymers (**Figure 5.3b**).[7] Indeed, ROMP of **V.10** with **V.8** produced a soluble and monodisperse polymer **V.11**, which was then successfully converted to the target PPV polymer **V.12**.
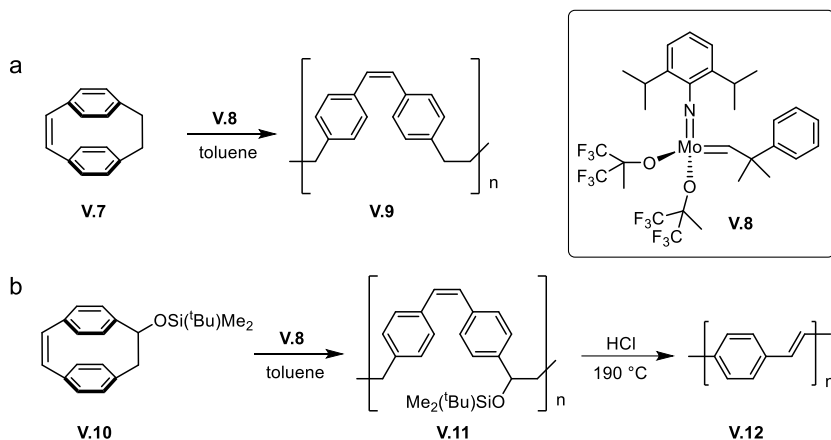
Figure 5.3. Bazan's pioneering ROMP studies of strained paracyclophanes.[6-7]

It was not until twenty-two years later that Turner and coworkers reported the first ROMP approach to synthesize soluble PPV polymers.[8] Highly substituted [2.2]paracyclophane-diene **V.13** was polymerized using initiator **V.2**, producing polymer **V.14** with PDI below 1.2 (**Figure 5.4a**). The number average molecular weight of **V.14** has a linear correlation (0.999) with the monomer/initiator ratio, confirming the living nature of the polymerization. As shown in **Figure 5.4b**, ROMP of cyclophane **V.15** with **V.2** was also found to be living, giving mono-dispersed polymer **V.16** with a unique cross-conjugated 1,3-phenylenevinylene sequence.[9] Additionally, block copolymers containing **V.14** and **V.16** segments were synthesized using the ROMP of these cyclophane monomers.[10]
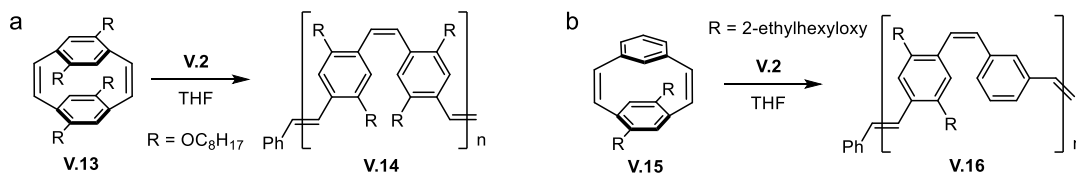
Figure 5.4. Turner's direct ROMP approach towards soluble PPV polymers.[8-9]

In 2014, the Bunz group reported the synthesis of [2.2.2]paracyclophane-triene **V.20** as a new type of ROMP monomer for PPV polymers (**Figure 5.5**).[11] The synthesis began with the Grignard reduction of linear bisalkyne **V.17** to form bis-(Z)-alkene **V.18**, which was then converted to **V.19** via the deprotection of the ketals with hydrochloride in THF. Finally, intramolecular McMurry coupling of **V.19** furnished the product **V.20** in decent efficiency. Macrocycle **V.20**, with a lowered ring strain than that of **V.13**, is less reactive with metathesis catalysts. Thus, elevated temperature was needed for the ROMP of **V.20** to occur. The resulted polymer **V.21** was well-soluble in common organic solvents and its photophysical properties can be modulated via modification of the substituents.
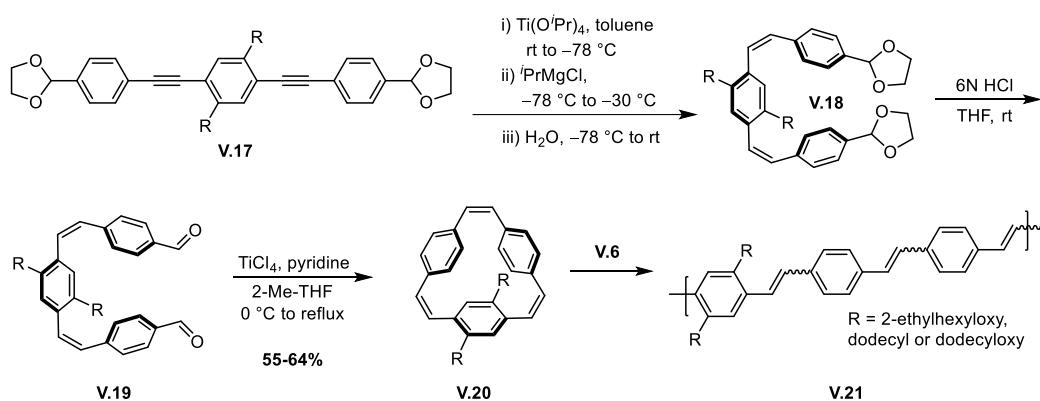
Figure 5.5. Bunz's synthesis of macrocycle **V.20** as the monomer for polymer **V.21**.[11]

In 2015, the McMurry coupling strategy was also utilized by the Horie group in the synthesis of conjugated macrocycle **V.23** with electron donating cyclopentadithiophene and **V.25a-b** with electron accepting dithienobenzothiadiazole (**Figure 5.6**).[12] Crystallographic analysis revealed that the molecular structures of **V.23** and **V.25a-b** possess significant amount of torsional strain. A fully conjugated donor-acceptor block copolymer **V.26** was prepared by sequential ROMP of **V.25a-b** and **V.23** using **V.2** as the initiator. The PDIs of polymer **V.26** and the homopolymers of **V.23** and **V.25a-b** are relatively broad (1.6-1.8) compared to that of **V.14**, which the authors attributed to the lower ring strain of **V.23** and **V.25a-b** compared to that of **V.13**.
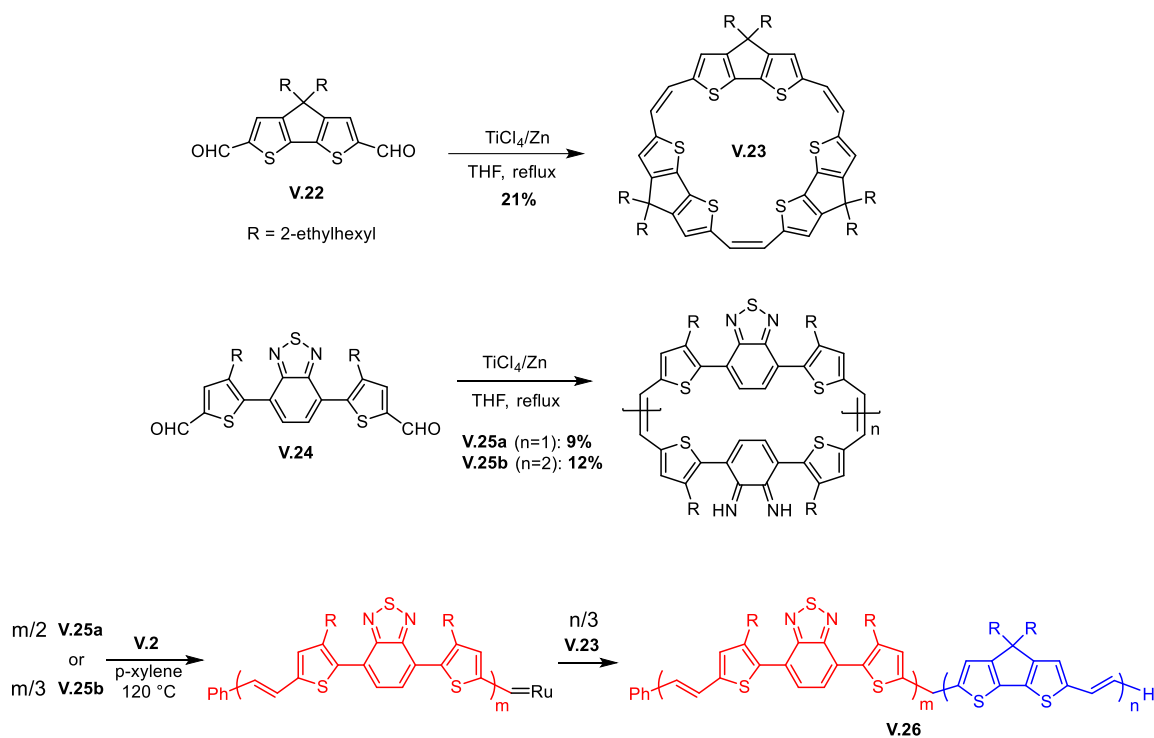
Figure 5.6. Horie's synthesis of a donor-acceptor conjugated polymer **V.26** via sequential ROMP of **V.25a-b** and **V.23**.[12]

Of particular importance of the work discussed above is to demonstrate that ROMP of strained macrocycles is a feasible strategy to access functional polymers with unique topologies. Nevertheless, the lack of efficient synthetic routes to macrocyclic monomers with sufficient ring strain is the major drawback that hinders the further development of this research area.

For further note, the group of Shimizu reported the synthesis of a bifunctional carbonate-stilbene macrocyle **V.28** from the reaction of *cis*-stilbene diol **V.27** with 1,1'-carbonyldiimidazole (**Figure 5.7**).[13] With a low strain energy of only 1.56 kcal/mol, macrocycle **V.28** experienced ED-ROMP of which the monomer conversion and the polymer molecular weight were dependent upon the monomer concentration. This example further confirms that the *cis*-stilbene is a useful component for the design of new macrocyclic ROMP monomers.

116
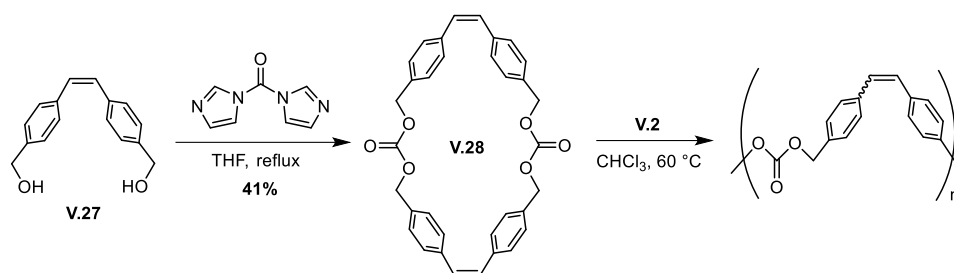
Figure 5.7. ROMP of a low strained carbonate stilbene macrocycle **V.26**.

5.2. Progress towards ROMPable Strained Macrocyclic Stilbenes

5.2.1. Synthesis of Strained Stilbene Macrocycles

In 2013, we serendipitously discovered Pd-mediated oxidative homocoupling of bisboronate which ultimately led to the successful synthesis of [5]CPP, the smallest nanohoop to date.[14] This operationally simple bisboronate homocoupling chemistry has proven to be a powerful method to synthesize strained biaryl macrocycles.[15] We surmised that strained macrocyclic stilbene **V.29** could be accessed from the homocoupling of the curved bisboronate precursor **V.30** (**Figure 5.8**). A representative stilbene macrocycle **V.29a** possesses a strain energy of 28.9 kcal/mol, which is comparable to those of known ROMPable paracyclophanes, demonstrating the potential use of **V.29** as monomers for enthalpy-driven ROMP.

E_{strain} = 28.9 kcal/mol E_{strain} = 53.4 kcal/mol E_{strain} = 39.6 kcal/mol E_{strain} = 14.7 kcal/mol
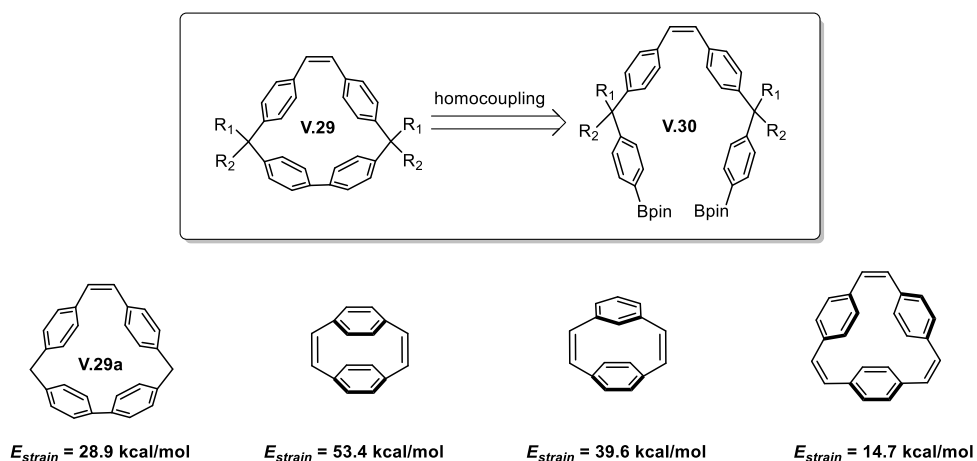
Figure 5.8. Strained stilbene macrocycle **V.29** accessible via the intramolecular homocoupling of bisboronate **V.30**, and the strain energies of the known ROMPable paracyclopanes.

117

A series of bisboronates (**V.30a-e**) with different R^1 and R^2 substituents were synthesized in order to examine the substrate scope of the macrocyclization. As shown in **Table 5.1**, under standard homocoupling conditions, all bisboronate substrates (**V.30a-e**) underwent efficacious intramolecular cyclization to give the corresponding macrocycles (**V.29a-e**) in 41-50%, indicating that the bulkiness of substituents on the sp^3-carbons has trivial effect on the overall cyclization efficiency. No higher cyclic products were observed in these reactions. It is noteworthy to point out that **V.29b-e** exist as a mixture of *trans-* and *cis*-isomers because the synthetic routes to **V.30b-e** are non-stereoselective (**Scheme 5.4** in **Experimental Sections**). Comparing entry 4 to entry 3, it can be seen that the installation of the bulky triethylsilane (TES) disfavors the formation of the *cis*-isomer due to steric hindrance. Additionally, deprotection of the silyl groups of **V.29d** afforded **V.29f** comprised of hydroxyl groups, which, along with **V.29e** that contains aryl-chloride, will allow further derivatization of this macrocyclic scaffold.

Table 5.1. Pd-mediated oxidative homocoulping of bisboronate **V.30** to produce macrocycle **V.29**.
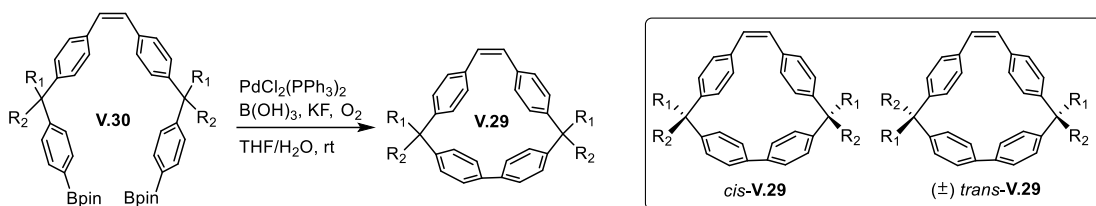
Entry	Bisboronate	R_1	R_2	Macrocycle	Yield (%)	*trans*/*cis* ratio
1	**V.30a**	H	H	**V.29a**	41	NA
2	**V.30b**	H	OCH$_3$	**V.29b**	46	1:1
3	**V.30c**	H	OC$_6$H$_{13}$	**V.29c**	50	1:1
4	**V.30d**	H	OSi(C$_2$H$_5$)$_3$	**V.29d**	48	4:1
5	**V.30e**	OCH$_3$	*p*-chlorophenyl	**V.29e**	45	1:1
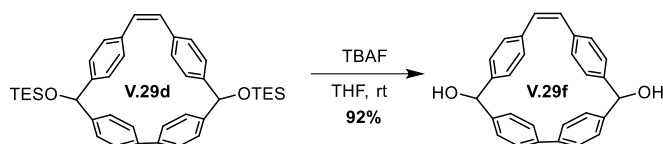
Scheme 5.1. Deprotection of **V.29d** to afford **V.29f**.

Single crystals of **V.29a** and *trans*-**V.29e** suitable for X-ray crystallography were obtained. The solid state molecular structures are shown in **Figure 5.9**. It can be seen that the strain is mainly distributed on the biphenylene unit that is severely bent out of collinearity. Additionally, the sp^3-carbon angles are compressed to 107° for **V.29a** and 104° for **V.29e**, which are deviated from the ideal angle of 114°. The stilbene fragments are not constrained with an average alkene angle of 130° for **V.29a** and 129° for **V.29e**, which are similar to the angle of 131° for non-strained stilbenes.
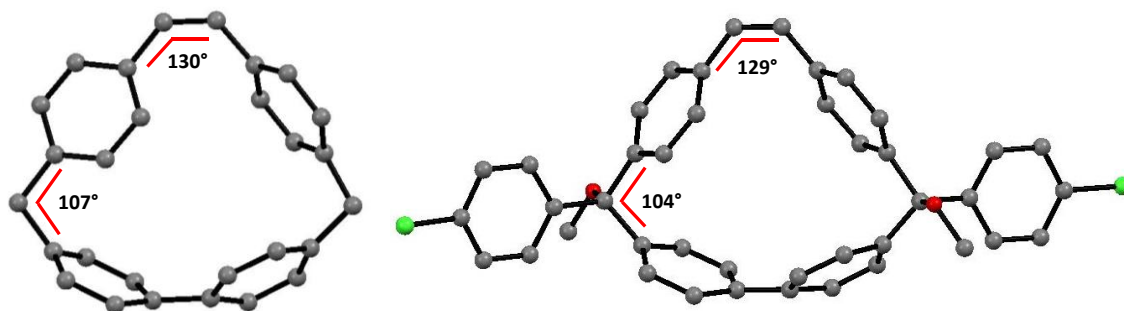
Figure 5.9. Molecular structure of **V.29a** (left), *trans*-**V.29e** (right) from crystallographic analysis. Hydrogen atoms and residual solvent molecules are omitted for clarity.

5.2.2. Preliminary ROMP Studies

We first surveyed the reactivity of **V.29a-c** with Grubbs metathesis catalysts. Reaction of **V.29a** with **V.2** at 100 °C gave highly insoluble polymers due to the lack of solubilizing chains. ROMP of **V.29b-c** was initiated by **V.2** at 60 °C to produce well soluble polymers **V.31b-c** (**Scheme 5.2**). The ^{1}H NMR spectra of **V.31b-c** are simple with only four aromatic doublet resonances and a singlet peak at 7.05 ppm that can be assigned to the *trans*-alkene protons, demonstrating a regio-regular microstructure of the polymers.

119
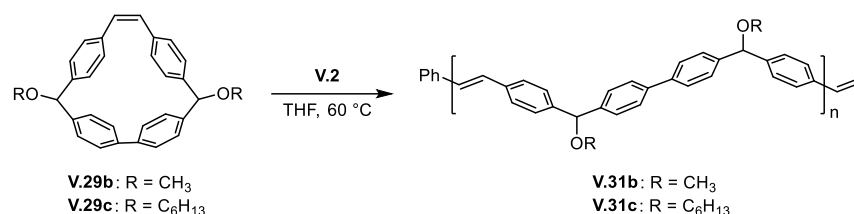
Scheme 5.2. ROMP of **V29b-c** initiated by **V.2**.

The ROMP of highly soluble macrocycle **V.29c** was further investigated using the fast initiating catalyst **V.3**.[16] As shown in **Table 5.2**, the polymerization proceeded slowly at 21°C. The reaction rate was accelerated at elevated temperatures. At 60 °C, full monomer conversion was achieved within six hours. The GPC traces of the polymers were symmetric and monomodal, indicating the lack of early chain termination. Additionally, the observed number average molecular weights ($\bar{M}_n$) matched nicely with the expected values, indicating a high initiation efficiency. These observations suggested a living polymerization character. The PDI values of the polymers are relatively high, which is likely attributed to the gel-effect wherein the increased viscosity of the reaction solution alters the rate of the chain propagation.[17]

Table 5.2. ROMP of **V.29c** with **V3** (monomer concentration at 1 mol/L and monomer/initiator ratio at 100/1 for all entries).
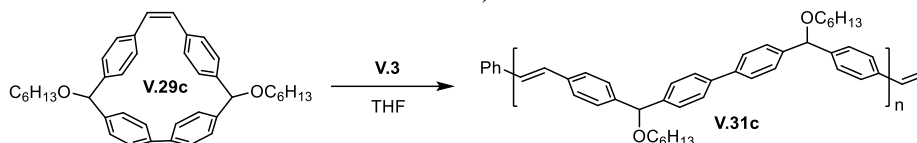
entry	temperature (°C)	time (h)	conversion (%)	Theo. $\bar{M}_n$ (kDa)	Obs. $\bar{M}_n$ (kDa)	Obs. $\bar{M}_w$ (kDa)	PDI ($\bar{M}_w/\bar{M}_n$)
1	21	1	0	--	--	--	--
2	21	40	47	--	--	--	--
3	21	132	93	52.0	52.4	81.3	1.55
4	45	2	36	--	--	--	--
5	45	6	81	45.3	48.7	77.1	1.58
6	60	2	34	--	--	--	--
7	60	4	93	52.0	50.2	94.0	1.87
8	60	6	>99	55.9	62.1	107	1.72

5.2.3. Stillbene Macrocycles Containing Triarylamines (TAAs)

Redox-active triarylamines (TAAs) have found applications as hole-transporting materials for photovoltaic[18-20] and as luminogens for organic light emitting diodes.[21-22] With a molecular design strategy similar to that of **V.29**, conjugated stilbene macrocycle **V.32** that contains TAA moieties was synthesized via the homocoupling of bisboronate **V.34** (**Scheme 5.3**). Bisboronate **V.34** was discovered to undergo rapid isomerization to the E-isomers during purification. Therefore, crude **V.34** from the borylation of **V.33** was directly used for the subsequent homocoupling without purification. Satisfyingly, decent yields were obtained for **V.32a** (27%) and **V.32c** (35%) over two steps. Macrocycle **V.32b** was isolated in a poor yield of 3% due to its instability at ambient conditions. Furthermore, the aryl-chloride groups of **V.32c** permit the installation of a variety of functionalities using the well-established transition-metal-mediated coupling chemistry.[23-24]
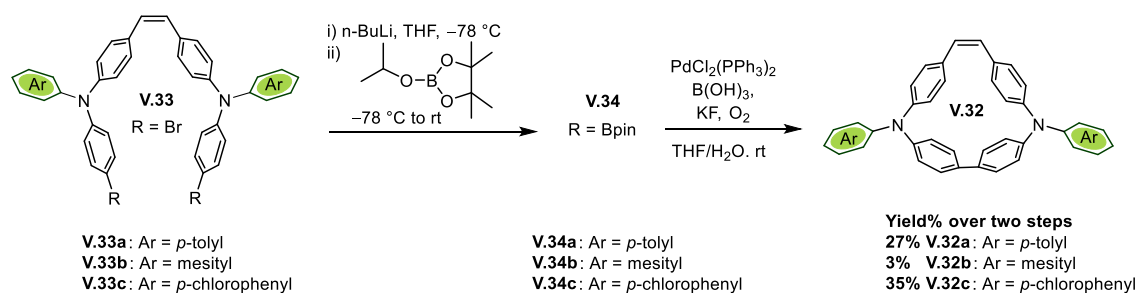
Scheme 5.3. Conjugated macrocyclic stilbene **V.32** accessible via the homocoupling of bisboronate **V.34**.

We were able to grow single crystals of **V.32a** via slow evaporation of a dichloromethane solution. The molecular structure was obtained from the crystallographic analysis (**Figure 5.10**). Similar to the case of **V.29a** and *trans*-**V.29e**, **V.32a** displays a severely bent biphenylene unit, a non-strained stilbene unit with an alkene angle of 129°, as well as a compressed sp^2-nitrogen angle (110°). Additionally, the strain energy of **V.32a** was estimated to be 36.5 kcal/mol, indicating a sufficient enthalpy driving force for ROMP.

121
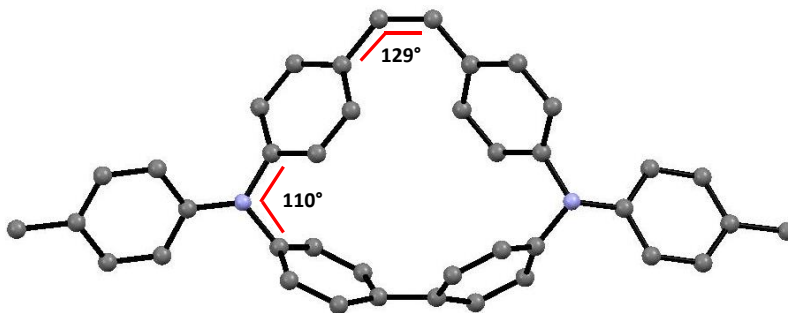
Figure 5.10. Molecular structure of **V.32a** from crystallographic analysis. Hydrogen atoms and residual solvent molecules are omitted for clarity.

With a highly strained conjugated backbone, **V.32** represents a potential ROMP monomeric scaffold for the synthesis of conjugated TAA polymers. However, **V.32a-c** have poor solubility in common organic solvent, which precludes the investigation of their ROMP behaviors. Nevertheless, reactions of **V.32a-c** with **V.2** or **V.6** at 100 °C produced insoluble yellow solids, suggesting that the ring opening metathesis might take place.

5.3. Summary

We have presented the synthesis of strained stilbene macrocycles based on an efficient intramolecular homocoupling strategy. The ROMP of a representative macrocycle **V.29e** were investigated, revealing a living polymerization process. Further optimization of the ROMP condition is needed to narrow the PDI of the resulted polymers. Additionally, it is necessary to prepare soluble versions of macrocycle **V.32** in order to examine the feasibility of using **V.32** as the precursor for conjugated TAA polymers as well as to probe its polymerization behavior. We expect these novel ROMP monomers to open the doors to structurally unique polymeric materials with diverse functionalities. This project is ongoing in collaboration with Prof. Andrew J. Boydston (University of Washington).

5.4. Experimental Sections

5.4.1. General Experimental Considerations

Tetrahydrofuran (THF) and dioxane were obtained from a solvent system with columns packed with activated alumina. Moisture and oxygen sensitive reactions were carried out under nitrogen atmosphere using standard Schlenk line techniques. Silica column chromatography was conducted with Zeochem Zeoprep n60 Eco 40-63 μm silica gel. Thin layer chromatography (TLC) was performed using Sorbent Technologies Silica Gel XHT TLC plates. Developing plates were visualized using UV light at wavelength of 254 and 365 nm. NMR spectra were recorded on a Bruker Avance-III-HD 600 (or 500) spectrometer with a Prodigy multinuclear broadband cryoProbe. Chemical shifts were reported in parts per million (ppm) and were referenced to the residual protio-solvent (CDCl$_3$: ^{1}H δ 7.26 ppm, ^{13}C δ 77.16 ppm; benzene-d_6 C$_6$D$_6$: ^{1}H δ 7.16 ppm, ^{13}C δ 128.06 ppm; acetone-d_6 (CD$_3$)$_2$CO: ^{1}H δ 2.05 ppm, ^{13}C δ 29.84 ppm). Automated flash chromatography was performed using a Biotage Isolera Flash System with pre-packed or re-packed cartridges (Biotage SNAP KP-Sil). Buchwald precatalysts (BINAP-Pd-G3 and XantPhos-Pd-G3) were prepared according to ref 25. Buchwald-hartwig amination reactions were performed using a Biotage Initiator Microwave Synthesizer.

Grubbs G1, G2 and Hoveyda-Grubbs G2 catalysts were purchased from Sigma-Aldrich. Grubbs G3 catalyst was prepared from Grubbs G2 according to ref 26. All polymerizations were carried out under an inert atmosphere of nitrogen in standard borosilicate glass vials purchased from Fisher Scientific with magnetic stirring unless otherwise noted. Gel permeation chromatography (GPC) was performed using a GPC setup consisting of: a Shimadzu pump, 3 in-line columns, and Wyatt light scattering and refractive index detectors with tetrahydrofuran (THF) as the mobile phase. Number-average molecular weights (M_n) and weight-average molecular weights (M_w) were calculated from light scattering. Thermogravimetric analysis was performed using a TA instrument Q50 TGA. Samples were analyzed using a heating rate of 10 °C/min under a N$_2$ stream.
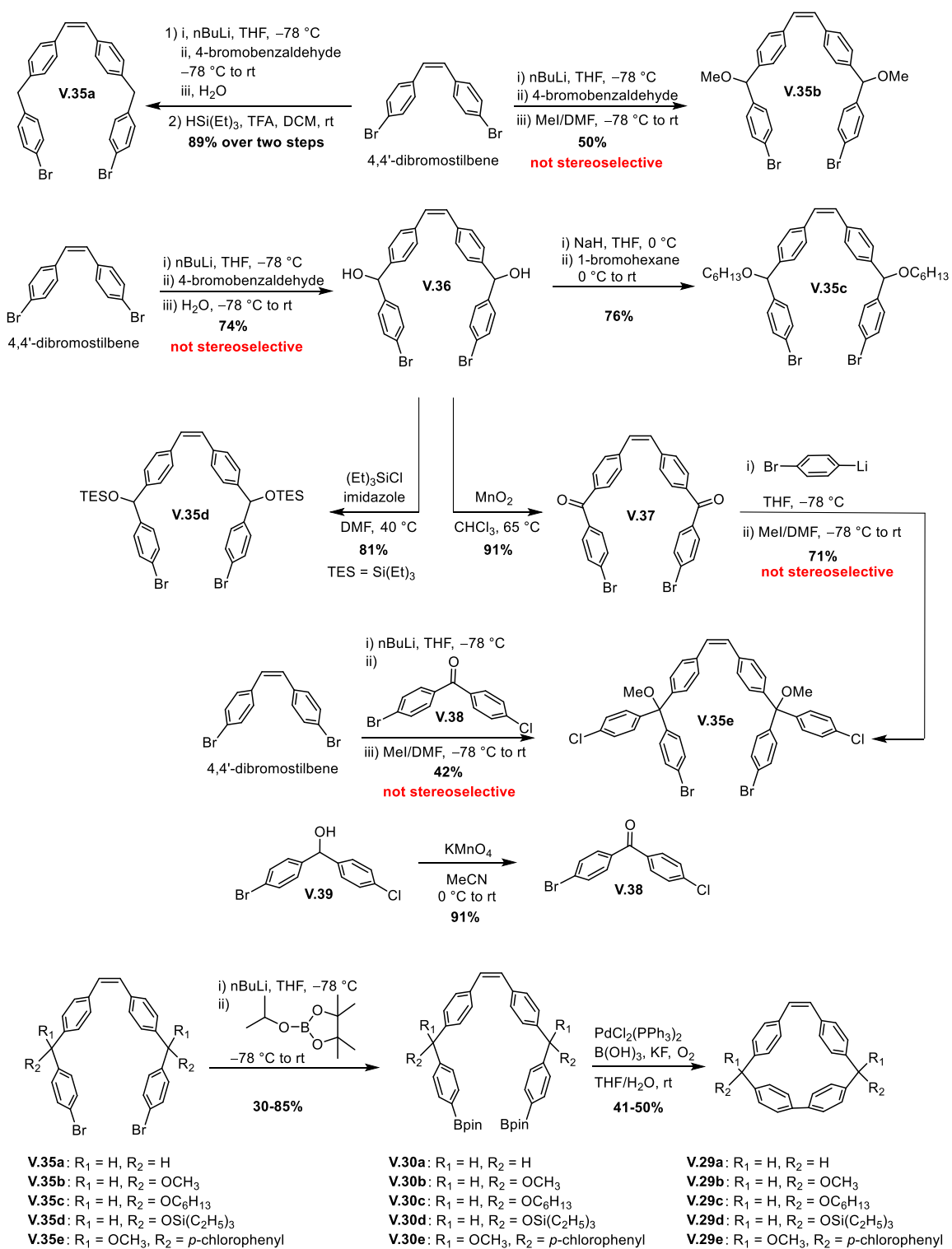
Scheme 5.4. Synthesis of the key intermediates for **V.29a-e**.
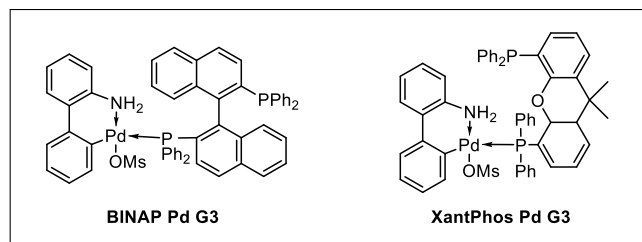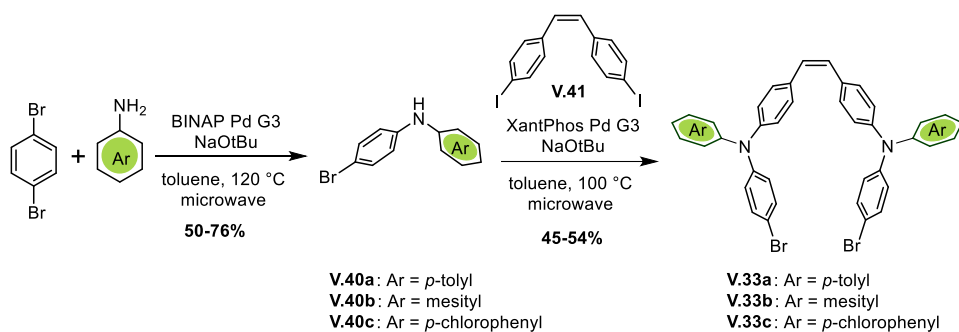
Scheme 5.5. Synthesis of the key intermediates for **V.32a-c**.

5.4.2. Synthetic Details

(Z)-1,2-bis(4-(4-bromobenzyl)phenyl)ethane **V.35a**
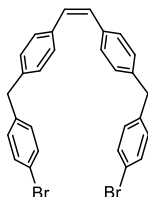
4,4'-Dibromostilbene was prepared according to reported procedure.[27] To a 250 mL round bottom flask with a magnetic stir bar was added **V.34** (3.45 g, 10.2 mmol, 1.0 eq) and THF (100 mL). The solution was cooled to −78 °C, at which point nBuLi in hexane (8.9 mL, 2.3 mol/L, 2.0 eq) was slowly added over the course of 5 min. After stirring at −78 °C for 3 min, 4-bromobenzaldehyde (4.15 g, 22.4 mmol, 2.2 eq) in THF (20 mL) was added in stream via syringe. Then the cold bath was removed and the reaction was kept stirring at room temperature for 2 hours. The reaction was quenched with water (5 mL). After solvent was removed under reduced pressure, DCM (100 mL) was added to the mixture, which was washed with H_2O (100 mL) and brine (100 mL) and then dried over Na_2SO_4. Solvent was removed under reduced pressure and the crude residue was dissolved in trifluoroacetic acid (15 mL), resulting a deep blue solution. Then

triethylsilane (24.4 mL, 153 mmol, 15 eq) was added and the reaction was kept stirring in dark overnight. The reaction was quenched with NaOH/H_2O and extracted with DCM (50 mL). The organic phase was washed with H_2O (100 mL) and brine (100 mL) and then dried over Na_2SO_4. Crude product was purified by column chromatography (silica, 0% to 5% ethyl acetate in hexanes) to yield product as colorless oil (2.34 g, 89%).^{1}H NMR (600 MHz, CDCl$_3$): δ(ppm) 7.43 (d, J = 8.3 Hz, 4H, Ar-H), 7.23 (d, J = 8.0 Hz, 4H, Ar-H), 7.08 (d, J = 8.3 Hz, 4H, Ar-H), 7.04 (d, J = 8.0 Hz, 4H, Ar-H), 6.56 (s, 2H, C=C-H), 3.91 (s, 4H, CH$_2$); ^{13}C NMR (150 MHz, CDCl$_3$): δ(ppm) 140.03, 139.45, 135.44, 131.62, 130.78, 129.79, 129.14, 128.81, 120.07, 41.14.

(Z)-1,2-bis(4-((4-bromophenyl)(methoxy)methyl)phenyl)ethene **V.35b**
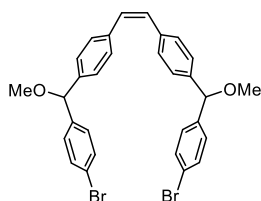
4,4'-Dibromostilbene (3.28 g, 9.70 mmol, 1 eq) was dissolved in THF (50 mL) in a 250 mL round bottom flask equipped with a magnetic stir bar. The solution was cooled to −78 °C, at which point nBuLi in hexane (8.8 mL, 2.2 mol/mL, 2.0 eq) was slowly added over the course of 5 min. After stirring at −78 °C for 3 min, 4-bromobenzaldehyde (3.95 g, 21.3 mmol, 2.2 eq) in THF (30 mL) in THF (40 mL) was added in stream via syringe. The reaction was allowed to stir at −78 °C for 2h. Then iodomethane (12.1 mL, 194 mmol, 20 eq) and DMF (20 mL) was added. Then the cold bath was removed and the mixture was kept stirring at room temperature overnight. The reaction was quenched with water (20 mL). After THF was removed under reduced pressure, DCM (100 mL) was added to the mixture, which was washed with H_2O (40 mL), 5 wt% aqueous LiCl solution (3 × 80 mL) and brine (40 mL) and then dried over Na_2SO_4. Solvent was the removed under reduced pressure. The product was isolated using column chromatography (silica, 0% to 10% ethyl acetate in hexanes) as colorless oil (2.81g, 50%). ^{1}H NMR (600 MHz, CDCl$_3$): δ(ppm) 7.45 (d, J = 8.4 Hz, 4H, Ar-H), 7.23-7.19 (overlap, 8H, Ar-H), 7.15 (d, J = 8.1 Hz, 4H, Ar-H), 6.52 (s, 2H, C=C-H), 5.15 (s, 2H,

CH), 3.36 (s, 6H, OCH$_3$); ^{13}C NMR (150 MHz, CDCl$_3$): δ(ppm) 141.14, 140.57, 136.76, 131.68, 130.04, 129.11, 128.76, 126.89, 121.54, 84.67, 57.17.

(Z)-(ethene-1,2-diylbis(4,1-phenylene))bis((4-bromophenyl)methanol) **V.36**
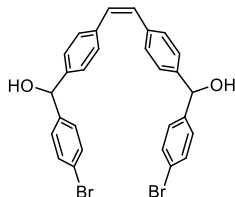
　　　To a 500 mL round bottom flask with a magnetic stir bar was added 4,4'-dibromostilbene (12.0 g, 35.5 mmol, 1 eq) and THF (200 mL). The solution was cooled to −78 °C, at which point nBuLi in hexane (31.6 mL, 2.3 mol/mL, 2.05 eq) was slowly added over the course of 20 min. After stirring at −78 °C for 3 min, 4-bromobenzaldehyde (13.1 g, 71.0 mmol, 2.0 eq) in THF (40 mL) was added in stream via cannula, during which the solution gradually became viscous with solid crashed out. Then the cold bath was removed and the mixture was kept stirring at room temperature for 2 hours. The reaction mixture was quenched with water (20 mL). After THF was removed under reduced pressure, DCM (200 mL) was added to the mixture, which was washed with H$_2$O (100 mL) and brine (100 mL) and then dried over Na$_2$SO$_4$. Solvent was removed under reduced pressure. The resulted yellow gel was dissolved in DCM (80 mL) and stored in freezer (−20 °C) overnight, resulting in powdered precipitate. The precipitate was collected by filtration and washed with DCM (10 mL) to give product as white powder (7.55 g). The filtrate was concentrated and the residual was purified by column chromatography (silica, 0% to 3% ethyl acetate in DCM) to yield more product (6.58 g). Overall, product was obtained in a yield of 74%. ^{1}H NMR (600 MHz, CDCl$_3$): δ(ppm) 7.46 (d, *J* = 8.4 Hz, 4H, Ar-H), 7.25 (d, *J* = 8.4 Hz, 4H, Ar-H), 7.22 (d, *J* = 8.4 Hz, 4H, Ar-H), 7.19 (d, *J* = 8.4 Hz, 4H, Ar-H), 6.55 (s, 2H, C=C-H), 5.76 (d, *J* = 3.4 Hz, 2H, CH), 2.18 (d, *J* = 3.4 Hz, 2H, OH); ^{13}C NMR (150 MHz, CDCl$_3$): δ(ppm) 142.74, 142.34, 136.90, 131.73, 130.11, 129.25, 128.34, 126.59, 121.63, 75.62.

(Z)-1,2-bis(4-((4-bromophenyl)(n-hexyloxy)methyl)phenyl)ethene **V.35c**
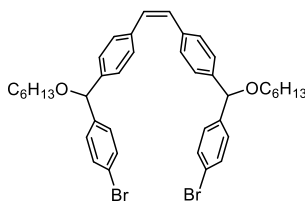
To a 500 mL round bottom flask was added NaH (4.10 g, 60 wt% in mineral oil, 102.5 mmol, 4 eq) and THF (150 mL). The slurry was cooled to 0 °C at which point **V.36** (14.1 g, 25.6 mmol, 1 eq) in THF (30 mL) was added in stream. The mixture was stirred at 0 °C for 1h. Then 1-bromohaxane (28.8 mL, 205 mmol, 8 eq) and DMF (30 mL) were added and the reaction was stirred at room temperature overnight. The reaction was carefully quenched with water. After THF was removed under vacuum, DCM (150 mL) was added. The solution was washed with H_2O (100 mL), 5 wt% aqueous LiCl solution (3×100 mL) and brine (100 mL), and dried over Na_2SO_4. The solution was then concentrated and the crude solid was purified via column chromatography (silica, 0% to 8% ethyl acetate in hexanes) to yield product as colorless oil (15.0 g, 83%). ^{1}H NMR (600 MHz, CDCl$_3$): δ(ppm) 7.44 (d, *J* = 8.4 Hz, 4H, Ar-H), 7.22 (d, *J* = 8.4 Hz, 4H, Ar-H), 7.20 (d, *J* = 8.1 Hz, 4H, Ar-H), 7.15 (d, *J* = 8.1 Hz, 4H, Ar-H), 6.52 (s, 2H, C=C-H), 5.24 (s, 2H, CH), 3.42 (td, *J* = 6.6, 3.1 Hz, 4H, OCH$_2$), 1.62 (dt, *J* = 15.0, 6.6 Hz, 4H, CH$_2$), 1.37 (p, *J* = 7.0 Hz, 4H, CH$_2$), 1.33-1.22 (overlap, 8H, CH$_2$), 0.88 (t, *J* = 7.0 Hz, 6H, CH$_3$); ^{13}C NMR (150 MHz, CDCl$_3$): δ(ppm), 141.75, 141.14, 136.61, 131.58, 130.01, 129.03, 128.82, 126.89, 121.36, 82.87, 69.46, 31.79, 29.94, 26.04, 22.75, 14.21.

(Z)-1,2-bis(4-((4-bromophenyl)((triethylsilyl)oxy)methyl)phenyl)ethene **V.35d**
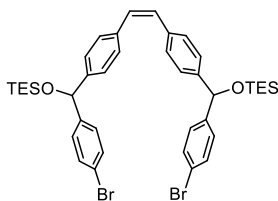
To a 250 mL round bottom flask was charged with **V.36** (3.00 g, 5.45 mmol, 1 eq), imidazole (1.48 g, 21.8 mmol, 4 eq) and dry DMF (40 mL). Then chlorotriethylsilane (2.8 mL, 16.4 mmol, 3 eq) was added drop-wise via syringe at room temperature. The

reaction was heated at 40 °C for 90 min. Saturated Na_2CO_3 solution was carefully added to quench the reaction until no gas bubbles evolved. The reaction mixture was extracted with ethyl acetate (3×50 mL). The combined organic fraction was further washed with H_2O (100 mL), 5 wt% LiCl solution (3 × 100 mL) and brine (100 mL), and dried over Na_2SO_4. The solution was then concentrated and the crude solid was purified via column chromatography (silica, 0% to 15 % DCM in hexanes) to yield product as colorless oil (3.46 g, 81%). ^{1}H NMR (600 MHz, $CDCl_3$): δ(ppm) 7.41 (d, J = 8.3 Hz, 4H, Ar-H), 7.23 (d, J = 8.3 Hz, 4H, Ar-H), 7.17-7.12 (m, 8H, Ar-H), 6.52 (s, 2H, C=C-H), 5.65 (s, 2H, CH), 0.88 (t, J = 8.0 Hz, 18H, CH_3), 0.56 (q, J = 8.0 Hz, 12H, CH_2); ^{13}C NMR (150 MHz, $CDCl_3$): δ(ppm) 144.33, 143.67, 136.41, 131.38, 130.09, 128.97, 128.08, 126.35, 120.92, 75.76, 6.90, 4.98.

(Z)-(ethene-1,2-diylbis(4,1-phenylene))bis((4-bromophenyl)methanone) **V.37**
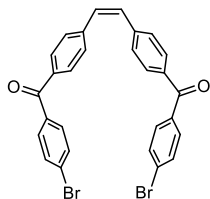
To a 250 mL round bottom flask equipped with a stir bar was charged with compound **V.36** (3.00 g, 5.45 mmol, 1.0 eq) and MnO_2 (14.2 g, 16.4 mmol, 30 eq) and chloroform (80 mL). Then a reflux condenser was attached and the mixture was heated at 65 °C overnight. When cooled to room temperature, the reaction mixture was filtered through a plug of celite and the plug was further washed with DCM (120 mL). Removing solvent under reduced pressure yielded product as white solid (2.70 g, 91%). ^{1}H NMR (600 MHz, $CDCl_3$): δ(ppm) 7.68 (d, J = 8.3 Hz, 4H, Ar-H), 7.65 (d, J = 8.5 Hz, 4H, Ar-H), 7.62 (d, J = 8.5 Hz, 4H, Ar-H), 7.36 (d, J = 8.3 Hz, 4H, Ar-H), 6.77 (s, 2H, C=C-H); ^{13}C NMR (150 MHz, $CDCl_3$): δ(ppm) 195.11, 141.43, 136.40, 136.12, 131.79, 131.57, 131.35, 130.35, 129.04, 127.64.

(Z)-1,2-bis(4-((4-bromophenyl)(4-chlorophenyl)(methoxy)methyl)phenyl)ethene **V.35e**
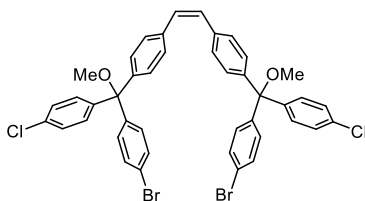
Method 1: a similar procedure to synthesize **V.35a** was adapted. 4,4'-dibromostilbene (3.18 g, 9.41 mmol, 1 eq), nBuLi in n-hexane (8.6 mL, 2.2 mol/L, 2 eq), **V.38** (6.12 g, 20.7 mmol, 2.2 eq), iodomethane (11.8 mL, 188 mmol, 20 eq). Product was purified by column chromatography (silica, 0% - 20% DCM in hexanes) as faint yellow oil (3.15 g, 42 %).

Method 2: A solution of 4-bromochlorobenzene (2.64 g, 13.8 mmol, 3 eq) in dry THF (80 mL) was cooled to −78 °C, at which point nBuLi in n-hexane (6.0 mL, 2.3 mol/mL, 3.0 eq) was slowly added over the course of 5 min. After stirring at −78 °C for 10 min, **V.37** (2.51 g, 4.59 mmol, 1.0 eq) in THF (10 mL) was added in stream via syringe. The reaction was allowed to stir at −78 °C for 1h. Then iodomethane (4.3 mL, 68.9 mmol, 15 eq) and DMF (20 mL) was added. The cold bath was removed and the mixture was kept stirring at room temperature overnight. The reaction mixture was quench with water (20 mL). The product was isolated using column chromatography (silica, 0% to 20% DCM in hexanes) as colorless oil (2.60 g, 71%). ^{1}H NMR (600 MHz, CDCl$_3$): δ(ppm) 7.43 (d, J = 8.6 Hz, 4H, Ar-H), 7.33 (d, J = 8.7 Hz, 4H, Ar-H), 7.29-7.26 (overlap, 8H, Ar-H), 7.21 (br s, 8H, Ar-H), 6.56 (s, 2H, C=C-H), 3.03 (s, 6H, CH$_3$); ^{13}C NMR (150 MHz, CDCl$_3$): δ(ppm) 142.86, 142.16, 141.77, 136.46, 133.28, 131.22, 130.33, 130.15, 130.03, 128.69, 128.62, 128.26, 121.48, 86.37, 52.23.

(4-bromophenyl)(4-chlorophenyl)methanone **V.38**
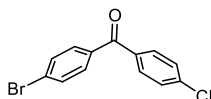
V.39 (8.60 g, 28.9 mmol, 1 eq) was dissolved in acetonitrile (550 mL) in a 1L round bottom flask equipped with a stir bar and the solution was cooled to 0 °C. KMnO$_4$ was added portion-wise over the course of 30 min. The reaction was kept stirring at 0 °C

for one hour and then warmed to room temperature. Acetonitrile was removed under reduced pressure and DCM (200 mL) was added to the solid residue. The mixture was subjected to sonication until homogenous and filtered through a short plug of celite. Removing the solvent gave product as white solid (7.80 g, 91%). Characterization was consistent with what was previously reported.[28]

(Z)-1,2-bis(4-(4-(4,4,5,5-tetramethyl-1,3,2-dioxaborolan-2-yl)benzyl)phenyl)ethene **V.30a**

Bpin   Bpin
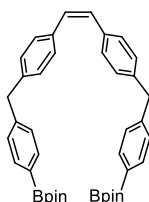
V.35a (1.35 g, 2.60 mmol, 1 eq) was dissolved in 30 mL THF and cooled to −78 °C. Then nBuLi in n-hexane (2.50 mL, 2.3 mol/L, 2.2 eq) was syringed into the solution over the course of 3 min. Neat isopropyl pinacol borate (2.20 mL, 10.4 mmol, 4 eq) was quickly added in stream. The mixture was stirred at −78 °C for 5 min and allowed to warm to room temperature slowly. After two hours, the reaction was carefully quenched with water (1 mL). The mixture was extracted with dichloromethane (3×20 mL) and combined the organic layers were washed with brine and dried over Na_2SO_4. After concentrating under reduced pressure, the crude product was put on high vacuum to remove the volatile which yielded the desired product as white powder (1.00 g, 63%). ^{1}H NMR (600 MHz, CDCl$_3$): δ(ppm) 7.74 (d, $J = 7.9$ Hz, 4H, Ar-H), 7.20 (d, $J = 7.9$ Hz, 4H, Ar-H), 7.16 (d, $J = 8.2$ Hz, 4H, Ar-H), 7.02 (d, $J = 8.2$ Hz, 4H, Ar-H), 6.50 (s, 2H, C=C-H), 3.95 (s, 4H, CH$_2$), 1.33 (s, 24H, CH$_3$); ^{13}C NMR (150 MHz, CDCl$_3$): δ(ppm) 144.41, 139.86, 135.30, 135.15, 129.77, 129.05, 128.88, 128.58, 83.80, 42.01, 25.00, ^{13}C-B signal not observed.

(Z)-1,2-bis(4-(methoxy(4-(4,4,5,5-tetramethyl-1,3,2-dioxaborolan-2-yl)phenyl)methyl)-phenyl)ethene **V.30b**
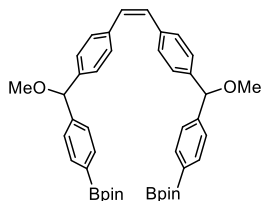
A similar procedure to synthesize **V.30a** was adapted. **V.35b** (7.22 g, 12.5 mmol, 1.0 eq), nBuLi in n-hexane (12.5 mL, 2.2 mol/L, 2.2 eq), isopropyl pinacol borate (10.2 mL, 50.0 mmol, 4 eq). After workup, hexanes was added to the crude and the mixture was subjected to sonication. Product precipitated as white solid and was collected via filtration (5.22 g). The filtrate was concentrated and stored in freezer overnight to yield more product (1.00g). Overall, 6.22 g of product was collected with a yield of 74%. ^{1}H NMR (600 MHz, CDCl$_3$): δ(ppm) 7.79 (d, J = 7.6 Hz, 4H, Ar-H), 7.36 (d, J = 7.6 Hz, 4H, Ar-H), 7.22-7.13 (m, 8H, Ar-H), 6.50 (s, 2H, C=C-H), 5.21 (s, 2H, CH), 3.73 (s, 6H, OCH$_3$), 1.34 (s, 24H, CH$_3$); ^{13}C NMR (150 MHz, CDCl$_3$): δ(ppm) 145.10, 140.96, 136.53, 135.07, 129.96, 128.99, 126.93, 126.36, 85.35, 83.88, 57.13, 25.00, ^{13}C-B signal not observed.

(Z)-1,2-bis(4-((n-hexyloxy)(4-(4,4,5,5-tetramethyl-1,3,2-dioxaborolan-2-yl)phenyl)-methyl)phenyl)ethene **V.30c**
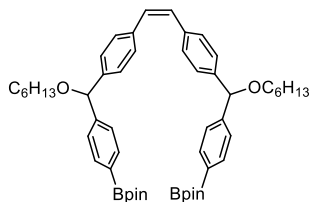
A similar procedure to synthesize **V.30a** was adapted. **V.35c** (14.7 g, 20.5 mmol, 1.0 eq), nBuLi in n-hexane (21.5 mL, 2.3 mol/L, 2.4 eq), isopropyl pinacol borate (16.7 mL, 81.8 mmol, 4 eq). Product was purified by column chromatography (silica, 0% to 8% ethyl acetate in hexanes) as colorless oil (12.4 g, 76%). ^{1}H NMR (600 MHz, CDCl$_3$): δ(ppm) 7.77 (d, J = 8.0 Hz, 4H, Ar-H), 7.36 (d, J = 8.0 Hz, 4H, Ar-H), 7.22-7.13 (m, 8H, Ar-H), 6.48 (s, 2H, C=C-H), 5.29 (s, 2H, CH), 3.42 (t, J = 6.7 Hz, 4H, OCH$_2$), 1.63 (dt, J

= 15.0, 6.7 Hz, 4H, CH$_2$), 1.42-1.20 (overlap, 36H, CH$_2$ and CH$_3$), 0.88 (t, J = 6.9 Hz,

6H, CH$_3$); ^{13}C NMR (150 MHz, CDCl$_3$): δ(ppm) 145.76, 141.52, 136.38, 135.01, 129.91,

128.92, 126.94, 126.48, 83.86, 83.53, 69.43, 31.82, 29.97, 26.05, 25.01, 22.76, 14.22,

^{13}C-B signal not observed.

(Z)-1,2-bis(4-((4-(4,4,5,5-tetramethyl-1,3,2-dioxaborolan-2-yl)phenyl)((triethylsilyl)-

oxy)methyl)phenyl)ethene **V.30d**
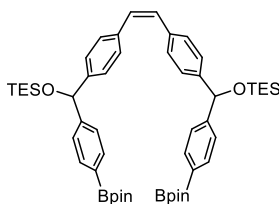
A similar procedure to synthesize **V.30a** was adapted. **V.35d** (3.34 g, 4.29 mmol,

1.0 eq), nBuLi in n-hexane (4.1 mL, 2.3 mol/L, 2.2 eq), isopropyl pinacol borate (3.1 mL,

15.0 mmol, 3.5 eq). After workup, hexanes was added to the crude and the mixture was

subjected to sonication. Product precipitated as white solid and was collected via

filtration (2.98 g). The filtrate was concentrated and subjected to sonication to yield more

product (0.18 g). Overall, 3.16 g of product was collected with a yield of 85%. ^{1}H NMR

(600 MHz, CDCl$_3$): δ(ppm) 7.74 (d, J = 7.9 Hz, 4H, Ar-H), 7.36 (d, J = 7.9 Hz, 4H, Ar-

H), 7.16 (d, J = 8.2 Hz, 4H, Ar-H), 7.13 (d, J = 8.2 Hz, 4H, Ar-H), 6.49 (s, 2H, C=C-H),

5.70 (s, 2H, CH), 1.33 (s, 24H, CH$_3$), 0.87 (t, J = 8.0 Hz, 18H, CH$_3$), 0.55 (q, J = 8.0 Hz,

12H, CH$_2$); ^{13}C NMR (150 MHz, CDCl$_3$): δ(ppm) 148.34, 143.99, 136.17, 134.84,

129.99, 128.85, 126.41, 125.74, 83.81, 76.39, 25.02, 6.92, 5.00, ^{13}C-B signal not

observed.

(Z)-1,2-bis(4-((4-chlorophenyl)(methoxy)(4-(4,4,5,5-tetramethyl-1,3,2-dioxaborolan-2-yl)phenyl)methyl)phenyl)ethene **V.30e**
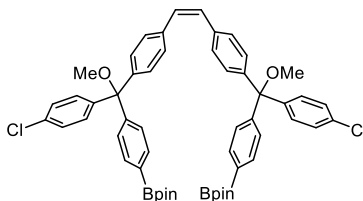
A similar procedure to synthesize **V.30a** was adapted. **V.35e** (3.20 g, 4.00 mmol, 1.0 eq), nBuLi in n-hexane (4.4 mL, 2.2 mol/L, 2.4 eq), isopropyl pinacol borate (3.4 mL, 16.0 mmol, 4.0 eq). Product was purified by column chromatography (silica, 0% to 80% DCM in hexanes) as faint yellow oil (1.09 g, 30 %).^{1}H NMR (600 MHz, CDCl$_3$): δ(ppm) 7.76 (d, *J* = 8.2 Hz, 4H, Ar-H), 7.42 (d, *J* = 8.2 Hz, 4H, Ar-H), 7.36 (d, *J* = 8.6 Hz, 4H, Ar-H), 7.25 (d, *J* = 8.6 Hz, 4H, Ar-H), 7.23 (d, *J* = 8.5 Hz, 4H, Ar-H), 7.21 (d, *J* = 8.5 Hz, 4H, Ar-H), 6.53 (s, 2H, C=C-H), 3.03 (s, 6H, CH$_3$), 1.32 (s, 24H, CH$_3$); ^{13}C NMR (150 MHz, CDCl$_3$): δ(ppm) 146.56, 142.66, 142.12, 136.27, 134.54, 133.01, 130.10, 130.06, 128.81, 128.48, 128.11, 127.93, 86.74, 83.93, 52.23, 25.00, ^{13}C-B signal not observed.

(Z)-1,2,4,7(1,4)-tetrabenzenacyclooctaphan-5-ene **V.29a**
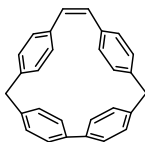
Bisboronate **V.30a** (200 mg, 0.372 mmol, 1 eq), PdCl$_2$(PPh$_3$)$_2$ (46 mg, 0.065 mmol, 0.2 eq) and B(OH)$_3$ (101 mg, 1.64 mmol, 5 eq) were dissolved in THF (250 mL) in a 500 mL round bottom flask equipped with a stir bar. The mixture was allowed to stir open to air at room temperature for 10 min until a clear yellow solution was achieved. Then KF (19 mg, 0.327 mmol, 1 eq) dissolved in H$_2$O (25 mL) was added. The mixture was subjected to sonication until orange color appeared, after which it was kept stirring overnight at room temperature. After THF was removed under vacuum, DCM (70 mL) was added. The solution was washed with H$_2$O (30 mL) and brine (30 mL) and dried over Na$_2$SO$_4$. The solution was then concentrated and the crude solid was purified via column

chromatography (silica, 0% to 30% DCM in hexanes) to yield product as white crystalline powder (48 mg, 41%). ^{1}H NMR (500 MHz, CDCl$_3$): δ(ppm) 7.37 (d, J = 8.4 Hz, 4H, Ar-H), 7.10 (d, J = 8.4 Hz, 4H, Ar-H), 6.63 (d, J = 8.3 Hz, 4H, Ar-H), 6.44 (s, 2H, C=C-H), 6.39 (d, J = 8.3 Hz, 4H, Ar-H), 3.73 (s, 4H, CH$_2$); ^{13}C NMR (125 MHz, CDCl$_3$): δ(ppm) 143.75, 141.62, 140.18, 134.86, 130.36, 130.15, 128.44, 127.97, 127.70, 41.51.

(Z)-3,8-dimethoxy-1,2,4,7(1,4)-tetrabenzenacyclooctaphan-5-ene **V.29b**
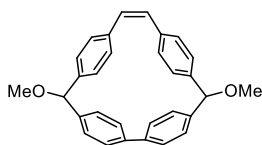
A similar procedure to synthesize **V.29a** was adapted. Bisboronate **V.30b** (400 mg, 0.596 mmol, 1 eq), PdCl$_2$(PPh$_3$)$_2$ (84 mg, 0.108 mmol, 0.2 eq), B(OH)$_3$ (184 mg, 1.64 mmol, 5 eq), KF (36 mg, 0.596 mmol, 1 eq), THF (240 mL), H$_2$O (24 mL). Product was purified by column chromatography (silica, 0% to 80% DCM in hexanes) as white powder (225 mg, 46%). ^{1}H NMR (600 MHz, CDCl$_3$): δ(ppm) trans 7.49 (dd, J = 8.5, 2.0 Hz, 2H, Ar-H), 7.40 (dd, J = 8.5, 2.0 Hz, 2H, Ar-H), 7.34 (dd, J = 8.3, 2.0 Hz, 2H, Ar-H), 7.02 (dd, J = 8.3, 2.0 Hz, 2H, Ar-H), 6.67 (d, J = 8.3 Hz, 4H, Ar-H), 6.53 (d, J = 8.3 Hz, 4H, Ar-H), 6.47 (s, 2H, C=C-H), 5.21 (s, 2H, CH), 3.59 (s, 6H, OCH$_3$); cis 7.47 (dd, J = 8.5, 2.0 Hz, 2H, Ar-H), 7.37 (dd, J = 8.5, 2.0 Hz, 2H, Ar-H), 7.35 (dd, J = 8.3, 2.0 Hz, 2H, Ar-H), 7.04 (dd, J = 8.3, 2.0 Hz, 2H, Ar-H), 6.67 (d, J = 8.3 Hz, 4H, Ar-H), 6.53 (d, J = 8.3 Hz, 4H, Ar-H), 6.47 (s, 2H, C=C-H), 5.20 (s, 2H, CH), 3.61 (s, 6H, OCH$_3$); ^{13}C NMR (150 MHz, CDCl$_3$): δ(ppm) trans 143.95, 141.83, 140.96, 136.04, 130.72, 128.33, 128.05, 127.72, 127.20, 126.40, 125.89, 84.43, 57.29; cis 143.99, 141.90, 141.02, 135.97, 130.70, 128.35, 128.01, 127.73, 126.08, 125.68, 84.34, 57.28.

(Z)-3,8-bis(n-hexyloxy)-1,2,4,7(1,4)-tetrabenzenacyclooctaphan-5-ene **V.29c**
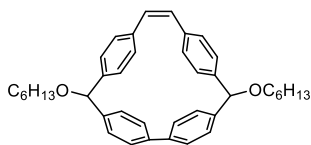
A similar procedure to synthesize **V.29a** was adapted. Bisboronate **V.30c** (3.00 g, 3.76 mmol, 1 eq), PdCl$_2$(PPh$_3$)$_2$ (0.26 g, 0.38 mmol, 0.1 eq), B(OH)$_3$ (1.16 g, 18.8 mmol, 5 eq), KF (0.44 g, 7.52 mmol, 2 eq), THF (450 mL), H$_2$O (45 mL). Product was purified by column chromatography (silica, 0% to 50% DCM in hexanes) as colorless oil (1.05 g, 50 %), which solidified upon standing. ^{1}H NMR (600 MHz, CDCl$_3$): δ(ppm) trans 7.45 (dd, J = 8.5, 2.0 Hz, 2H, Ar-H), 7.39 (dd, J = 8.5, 2.0 Hz, 2H, Ar-H), 7.35 (dd, J = 8.3, 2.0 Hz, 2H, Ar-H), 7.03 (dd, J = 8.3, 2.0 Hz, 2H, Ar-H), 6.65 (d, J = 8.3 Hz, 4H, Ar-H), 6.53 (d, J = 8.3 Hz, 4H, Ar-H), 6.46 (s, 2H, C=C-H), 5.28 (s, 2H, CH), 3.77 (dt, J = 9.0, 6.7 Hz, 2H, OCH$_2$), 3.61(dt, J = 9.0, 6.7 Hz, 2H, OCH$_2$), 1.78-1.69 (m, 4H, CH$_2$), 1.50-1.41 (m, 4H, CH$_2$), 1.37-1.26 (overlap, 8H, CH$_2$), 0.90 (t, J = 6.9 Hz, 6H, CH$_3$); cis 7.46 (dd, J = 8.5, 2.0 Hz, 2H, Ar-H), 7.39 (dd, J = 8.5, 2.0 Hz, 2H, Ar-H), 7.34 (dd, J = 8.3, 2.0 Hz, 2H, Ar-H), 7.03 (dd, J = 8.3, 2.0 Hz, 2H, Ar-H), 6.65 (d, J = 8.3 Hz, 4H, Ar-H), 6.53 (d, J = 8.3 Hz, 4H, Ar-H), 6.46 (s, 2H, C=C-H), 5.27 (s, 2H, CH), 3.77 (dt, J = 9.0, 6.7 Hz, 2H, OCH$_2$), 3.61(dt, J = 9.0, 6.7 Hz, 2H, OCH$_2$), 1.78-1.69 (m, 4H, CH$_2$), 1.50-1.41 (m, 4H, CH$_2$), 1.37-1.26 (overlap, 8H, CH$_2$), 0.90 (t, J = 6.9 Hz, 6H, CH$_3$); ^{13}C NMR (150 MHz, CDCl$_3$): δ(ppm) trans 144.47, 142.46, 140.92, 135.90, 130.71, 128.29, 128.02, 127.93, 127.36, 126.43, 125.86, 82.65, 69.59, 31.89, 30.07, 26.15, 22.81, 14.24; cis 144.49, 142.50, 140.95, 135.87, 130.69, 128.28, 127.90, 127.14, 126.58, 125.77, 82.59, 69.56, 31.89, 30.07, 25.16, 22.81, 14.24.

(Z)-3,8-bis((triethylsilyl)oxy)-1,2,4,7(1,4)-tetrabenzenacyclooctaphan-5-ene **V.29d**
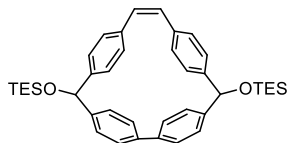
A similar procedure to synthesize **V.29a** was adapted. Bisboronate **V.30d** (500 mg, 0.573 mmol, 1 eq), PdCl$_2$(PPh$_3$)$_2$ (40 mg, 0.057 mmol, 0.1 eq), B(OH)$_3$ (177 mg,

2.87 mmol, 5 eq), KF (66 mg, 1.15 mmol, 2 eq), THF (100 mL), H$_2$O (10 mL). Product was purified by column chromatography (silica, 0% to 30% DCM in hexanes) as colorless oil (171 mg, 48 %). ^{1}H NMR (600 MHz, CDCl$_3$): δ(ppm) trans 7.40 (dd, J = 8.2, 1.8 Hz, 2H, Ar-H), 7.37 (dd, J = 8.5, 1.8 Hz, 2H, Ar-H), 7.33 (dd, J = 8.5, 1.8 Hz, 2H, Ar-H), 7.06 (dd, J = 8.2, 1.8 Hz, 2H, Ar-H), 6.65 (d, J = 8.2 Hz, 4H, Ar-H), 6.55 (d, J = 8.2 Hz, 4H, Ar-H), 6.46 (s, 2H, C=C-H), 5.64 (s, 2H, CH), 1.01 (t, J = 8.0 Hz, 18H, CH$_3$), 0.72 (q, J = 7.9 Hz, 12H, CH$_2$); cis 7.46 (dd, J = 8.5, 1.8 Hz, 2H, Ar-H), 7.42 (dd, J = 8.5, 1.8 Hz, 2H, Ar-H), 7.31 (dd, J = 8.3, 1.8 Hz, 2H, Ar-H), 6.99 (dd, J = 8.3, 1.8 Hz, 2H, Ar-H), 6.65 (d, J = 8.2 Hz, 4H, Ar-H), 6.54 (d, J = 8.2 Hz, 4H, Ar-H), 6.46 (s, 2H, C=C-H), 5.65 (s, 2H, CH), 1.00 (t, J = 8.0 Hz, 18H, CH$_3$), 0.70 (q, J = 7.9 Hz, 12H, CH$_2$); ^{13}C NMR (150 MHz, CDCl$_3$): δ(ppm) trans 146.82, 144.66, 140.97, 135.49, 130.66, 129.34, 128.15, 127.01, 126.55, 125.90, 124.92, 75.45, 7.06, 5.14; cis 146.86, 144.56, 140.93, 135.61, 130.67, 128.21, 128.20, 126.99, 126.66, 126.52, 125.24, 75.59, 7.06, 5.14.

(Z)-3,8-bis(4-chlorophenyl)-3,8-dimethoxy-1,2,4,7(1,4)-tetrabenzenacyclooctaphan-5-ene **V.29e**
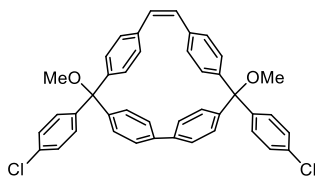
A similar procedure to synthesize **V.29a** was adapted. Bisboronate **V.30e** (1.09 g, 1.22 mmol, 1 eq), PdCl$_2$(PPh$_3$)$_2$ (171 mg, 0.024 mmol, 0.2 eq), B(OH)$_3$ (377 mg, 6.10 mmol, 5 eq), KF (71 mg, 1.22 mmol, 1 eq), THF (200 mL), H$_2$O (20 mL). Product was purified by column chromatography (silica, 0% to 30% DCM in hexanes) as white powder (340 mg, 45%). ^{1}H NMR (600 MHz, CDCl$_3$): δ(ppm) trans 7.55 (dd, J = 8.5, 2.1 Hz, 2H, Ar-H), 7.47-7.43 (overlap, 6H, Ar-H), 7.38 (d, J = 8.6 Hz, 4H, Ar-H), 7.30 (dd, J = 8.6, 2.1 Hz, 2H, Ar-H), 7.10 (dd, J = 8.6, 2.1 Hz, 2H, Ar-H), 6.72 (d, J = 8.6 Hz, 4H, Ar-H), 6.69 (d, J = 8.6 Hz, 4H, Ar-H), 6.51 (s, 2H, C=C-H), 3.31 (s, 6H, CH$_3$); cis 7.56-7.52 (overlap, 6H, Ar-H), 7.47 (dd, J = 8.6, 2.1 Hz, 2H, Ar-H), 7.41 (d, J = 8.6 Hz, 4H, Ar-H), 7.32 (dd, J = 8.6, 2.1 Hz, 2H, Ar-H), 6.98 (dd, J = 8.6, 2.1 Hz, 2H, Ar-H), 6.72 (d,

J = 8.6 Hz, 4H, Ar-H), 6.68 (d, J = 8.6 Hz, 4H, Ar-H), 6.53 (s, 2H, C=C-H), 3.26 (s, 6H, CH$_3$); ^{13}C NMR (150 MHz, CDCl$_3$): δ(ppm) trans 146.31, 142.94, 139.46, 137.05, 135.37, 134.28, 132.51, 130.79, 129.73, 129.17, 129.14. 128.27, 127.96, 126.27, 124.30, 88.06, 52.56; cis 145.82, 142.70, 139.33, 137.08, 135.46, 134.28, 132.57, 130.96, 129.72, 128.32, 127.99, 127.87, 127.61, 126.66, 126.51, 88.17, 52.60.

(Z)-1,2,4,7(1,4)-tetrabenzenacyclooctaphan-5-ene-3,8-diol **V.29f**
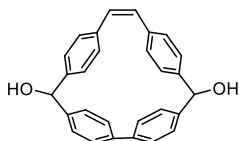
V.29d (146 mg, 0.236 mmol, 1 eq) was dissolved in dry THF (10 mL) in a 25 round bottom flask equipped with a stir bar. Tetrabutylammonium fluoride (0.71 mL, 1.0 mol/L, 3 eq) was added to the solution. The reaction went to completion after stirring at room temperature for 1h, as monitored by TLC. Solvent was then removed under reduced pressure. Water (5 mL) was added to the resulting crude oil and white solid precipitated. The solid was collected via filtration, washed with water (5 mL), DCM (5 mL) and methanol (5 mL), and dried over high vacuum to yield product as white powder (85 mg, 92%). ^{1}H NMR (500 MHz, acetone-d_6): δ(ppm) trans 7.51 (dd, J = 8.5, 1.8 Hz, 2H, Ar-H), 7.48 (dd, J = 8.5, 1.8 Hz, 2H, Ar-H), 7.42 (dd, J = 8.2, 1.8 Hz, 2H, Ar-H), 7.09 (dd, J = 8.2, 1.8 Hz, 2H, Ar-H), 6.64 (d, J = 8.4 Hz, 4H, Ar-H), 6.60 (d, J = 8.4 Hz, 4H, Ar-H), 6.48 (s, 2H, C=C-H), 5.73 (d, J = 3.1 Hz, 2H, CH), 4.98 (d, J = 3.1 Hz, 2H, OH); cis 7.52 (dd, J = 8.5, 1.8 Hz, 2H, Ar-H), 7.49 (dd, J = 8.5, 1.8 Hz, 2H, Ar-H), 7.41 (dd, J = 8.2, 1.8 Hz, 2H, Ar-H), 7.08 (dd, J = 8.2, 1.8 Hz, 2H, Ar-H), 6.64 (d, J = 8.4 Hz, 4H, Ar-H), 6.60 (d, J = 8.4 Hz, 4H, Ar-H), 6.48 (s, 2H, C=C-H), 5.73 (d, J = 3.1 Hz, 2H, CH), 4.98 (d, J = 3.1 Hz, 2H, OH); ^{13}C NMR (150 MHz, acetone-d_6): δ(ppm) 147.96, 147.92, 145.43, 145.41, 141.39, 141.38, 136.27, 131.34, 128.71, 128.61, 128.60, 127.85, 127.84, 127.73, 127.72, 126.86, 126.83, 126.16, 75.43, 75.32.

Polymer **V.31b**
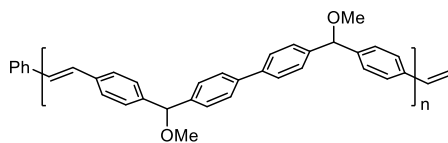
^{1}H NMR (500 MHz, CDCl$_3$): δ(ppm) 7.51 (d, J = 8.4 Hz, 4H, Ar-H), 7.46 (d, J = 8.4 Hz, 4H, Ar-H), 7.38 (d, J = 8.4 Hz, 4H, Ar-H), 7.35 (d, J = 8.4 Hz, 4H, Ar-H), 7.05 (s, 2H, C=C-H), 5.26 (s, 2H, CH), 3.40 (s, 6H, OCH$_3$).

Polymer **V.31c**
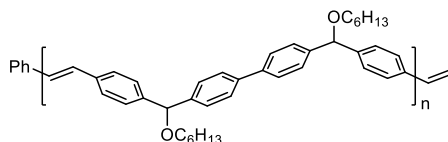
^{1}H NMR (500 MHz, CDCl$_3$): δ(ppm) 7.51 (d, J = 8.4 Hz, 4H, Ar-H), 7.46 (d, J = 8.4 Hz, 4H, Ar-H), 7.38 (d, J = 8.4 Hz, 4H, Ar-H), 7.35 (d, J = 8.4 Hz, 4H, Ar-H), 7.05 (s, 2H, C=C-H), 5.26 (s, 2H, CH), 3.40 (s, 6H, OCH$_3$).
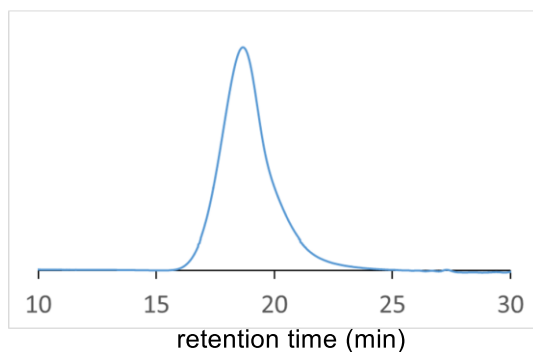
Figure 5.11. GPC trace (refractive index) of polymer **V.31c**.

(Z)-4,4'-(ethene-1,2-diyl)bis(N-(4-bromophenyl)-N-(p-tolyl)aniline) **V.33a**

139
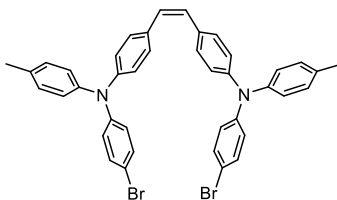
To a 20mL microwave reaction vial was charged with a stir bar, **V.40a** (2.08 g, 7.94 mmol, 2.2 eq), **V.41** (1.56 g, 3.61 mmol, 1 eq), Xantphos Pd G3 (0.17 g, 0.18 mmol, 0.05 eq), NaO^{t}Bu (1.39 g, 14.4 mmol, 4 eq). This set-up was transferred to a glove box with N$_2$ atmosphere and sealed with a septum cap. The sealed vial was then taken out of the glove box and degassed anhydrous toluene (15 mL) was added. The mixture was heated at 100 °C for 6h using a Biotage microwave reactor. When cooled to room temperature, the mixture was diluted with DCM (50 mL) and filtered through a plug of celite. Solvent was removed under reduced pressure and the residual solid was purified by column chromatography (silica, 0% to 20% DCM in hexanes) as yellow film (1.14 g, 45%). ^{1}H NMR (600 MHz, C$_6$D$_6$): δ(ppm) 7.26 (d, J = 8.8 Hz, 4H, Ar-H), 7.10 (d, J = 8.8 Hz, 4H, Ar-H), 6.91 (d, J = 8.3 Hz, 4H, Ar-H), 6.89 (d, J = 8.5 Hz, 4H, Ar-H), 6.84 (d, J = 8.3 Hz, 4H, Ar-H), 6.74 (d, J = 8.8 Hz, 4H, Ar-H), 6.41 (s, 2H, C=C-H), 2.07 (s, 6H, CH$_3$); ^{13}C NMR (125 MHz, C$_6$D$_6$): δ(ppm) 147.21, 146.95, 145.00, 133.65, 132.54, 132.06, 130.48, 130.28, 129.08, 125.72, 125.59, 123.06, 115.26, 20.82.

(Z)-N,N'-(ethene-1,2-diylbis(4,1-phenylene))bis(N-(4-bromophenyl)-2,4,6-trimethylaniline) **V.33b**
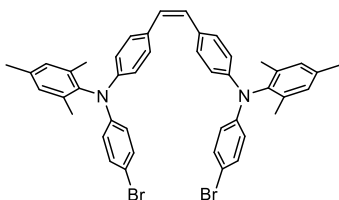
A similar procedure to synthesize **V.33a** was adapted. **V.41** (0.77 g, 1.78 mmol, 1 eq), **V.40b** (1.24 g, 4.27 mmol, 2.4 eq), Xantphos Pd G3 (84 mg, 0.09 mmol, 0.05 eq), NaO^{t}Bu (0.68 g, 7.12 mmol, 4 eq). Product was purified by column chromatography (silica, 0% - 15% DCM in hexanes) as yellow film (629 mg, 46 %). ^{1}H NMR (500 MHz, CDCl$_3$): δ(ppm) 7.34 (d, J = 8.7 Hz, 4H, Ar-H), 7.18 (d, J = 8.9 Hz, 4H, Ar-H), 6.89 (d, J = 8.7 Hz, 4H, Ar-H), 6.81 (s, 4H, Ar-H), 6.77 (d, J = 8.9 Hz, 4H, Ar-H), 6.51 (s, 2H, C=C-H), 2.24 (s, 6H, CH$_3$), 1.98 (s, 12H, CH$_3$).

(Z)-4,4'-(ethene-1,2-diyl)bis(N-(4-bromophenyl)-N-(4-chlorophenyl)aniline) **V.33c**
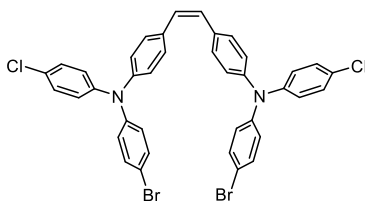
A similar procedure to synthesize **V.33a** was adapted. **V.41** (449 mg, 1.04 mmol, 1 eq), **V.44c** (705 mg, 2.49 mmol, 2.4 eq), Xantphos Pd G3 (50 mg, 0.05 mmol, 0.05 eq), NaO^{t}Bu (400 mg, 4.16 mmol, 4 eq). Product was purified by column chromatography (silica, 0% to 20% DCM in hexanes) as yellow film (417 mg, 54 %).^{1}H NMR (600 MHz, C$_6$D$_6$): δ(ppm) 7.24 (d, J = 8.6 Hz, 4H, Ar-H), 7.09 (d, J = 8.8 Hz, 4H, Ar-H), 6.94 (d, J = 8.8 Hz, 4H, Ar-H), 6.76 (d, J = 8.6 Hz, 4H, Ar-H), 6.64 (d, J = 8.8 Hz, 4H, Ar-H), 6.59 (d, J = 8.8 Hz, 4H, Ar-H), 6.42 (s, 2H, C=C-H), 2.07 (s, 6H, CH$_3$); ^{13}C NMR (125 MHz, C$_6$D$_6$): δ(ppm) 146.49, 146.38, 145.92, 132.76, 132.59, 130.37, 129.83, 129.20, 128.78, 126.11, 125.94, 123.45, 116.27.

(Z)-4-methyl-N-(4-(4,4,5,5-tetramethyl-1,3,2-dioxaborolan-2-yl)phenyl)-N-(4-(4-((4-(4,4,5,5-tetramethyl-1,3,2-dioxaborolan-2-yl)phenyl)(p-tolyl)amino)styryl)phenyl)aniline **V.34a**
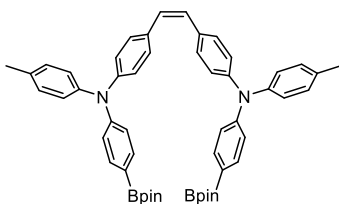
A similar procedure to synthesize **V.30a** was adapted. **V.33a** (1.13 g, 1.61 mmol, 1.0 eq), nBuLi in n-hexane (1.56 mL, 2.3 mol/L, 2.2 eq), isopropyl pinacol borate (1.18 mL, 5.80 mmol, 3.6 eq). After workup and removing solvent, the crude residue was used directly for homocoupling without purification. ^{1}H NMR (500 MHz, C$_6$D$_6$): δ(ppm) 8.05 (d, J = 8.6 Hz, 4H, Ar-H), 7.25 (d, J = 8.6 Hz, 4H, Ar-H), 7.17 (d, J = 8.2 Hz, 4H, Ar-H), 7.00 (d, J = 8.2 Hz, 4H, Ar-H), 6.98 (d, J = 8.2 Hz, 4H, Ar-H), 6.82 (d, J = 8.2 Hz, 4H, Ar-H), 6.38 (s, 2H, C=C-H), 2.06 (s, 6H, CH$_3$), 1.14 (s, 24H, CH$_3$).

(Z)-N-(4-(4-(mesityl(4-(4,4,5,5-tetramethyl-1,3,2-dioxaborolan-2-yl)phenyl)amino)-styryl)phenyl)-2,4,6-trimethyl-N-(4-(4,4,5,5-tetramethyl-1,3,2-dioxaborolan-2-yl)phenyl)aniline **V.34b**
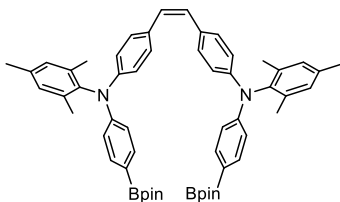
A similar procedure to synthesize **V.30a** was adapted. **V.33b** (629 mg, 0.831 mmol, 1.0 eq), nBuLi in n-hexane (1.10 mL, 2.3 mol/L, 3.0 eq), isopropyl pinacol borate (0.68 mL, 3.32 mmol, 4.0 eq). After workup and removing solvent, the crude residue was used directly for homocoupling without purification. ^{1}H NMR (500 MHz, C_6D_6): δ(ppm) 8.03 (d, *J* = 8.7 Hz, 4H, Ar-H), 7.20 (d, *J* = 8.7 Hz, 4H, Ar-H), 7.06 (d, *J* = 8.7 Hz, 4H, Ar-H), 6.90 (d, *J* = 8.7 Hz, 4H, Ar-H), 6.72 (s, 4H, Ar-H), 6.40 (s, 2H, C=C-H), 2.24 (s, 6H, CH_3), 1.93 (s, 12H, CH_3), 1.14 (s, 24H, CH_3).

(Z)-4-chloro-N-(4-(4-((4-chlorophenyl)(4-(4,4,5,5-tetramethyl-1,3,2-dioxaborolan-2-yl)phenyl)amino)styryl)phenyl)-N-(4-(4,4,5,5-tetramethyl-1,3,2-dioxaborolan-2-yl)phenyl)aniline **V.34c**
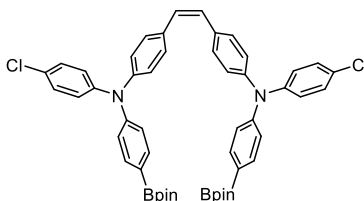
A similar procedure to synthesize **V.30a** was adapted. **V.33c** (387 mg, 0.522 mmol, 1.0 eq), nBuLi in n-hexane (0.52 mL, 2.3 mol/L, 2.3 eq), isopropyl pinacol borate (0.32 mL, 1.57 mmol, 3.0 eq). After workup and removing solvent, the crude residue was used directly for homocoupling without purification. ^{1}H NMR (600 MHz, C_6D_6): δ(ppm) 8.04 (d, *J* = 8.6 Hz, 4H, Ar-H), 7.21 (d, *J* = 8.6 Hz, 4H, Ar-H), 7.03 (d, *J* = 8.6 Hz, 4H, Ar-H), 6.92 (d, *J* = 8.8 Hz, 4H, Ar-H), 6.85 (d, *J* = 8.6 Hz, 4H, Ar-H), 6.74 (d, *J* = 8.8 Hz, 4H, Ar-H), 6.39 (s, 2H, C=C-H), 1.14 (s, 24H, CH_3).

(Z)-3,8-di-p-tolyl-3,8-diaza-1,2,4,7(1,4)-tetrabenzenacyclooctaphan-5-ene **V.32a**
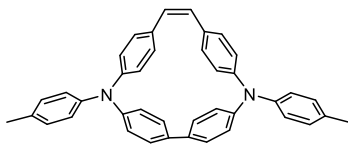
A similar procedure to synthesize **V.29a** was adapted. Crude bisboronate **V.34a**, PdCl$_2$(PPh$_3$)$_2$ (226 mg, 0.322 mmol, 0.2 eq), B(OH)$_3$ (538 mg, 8.05 mmol, 5 eq), KF (280 mg, 4.83 mmol, 3 eq), THF (300 mL), H$_2$O (30 mL). Product was purified by column chromatography (silica, 0% to 40% DCM in hexanes) as yellow powder (200 mg, 27% over two steps). ^{1}H NMR (500 MHz, CDCl$_3$): δ(ppm) 7.36 (d, J = 8.8 Hz, 4H, Ar-H), 7.25 (d, J = 8.8 Hz, 4H, Ar-H), 7.05 (d, J = 7.9 Hz, 4H, Ar-H), 6.95 (d, J = 8.5 Hz, 4H, Ar-H), 6.80 (d, J = 8.6 Hz, 4H, Ar-H), 6.47 (d, J = 8.6 Hz, 4H, Ar-H), 6.39 (s, 2H, C=C-H), 2.30 (s, 6H, CH$_3$); ^{13}C NMR (125 MHz, CDCl$_3$): δ(ppm) 150.03, 148.55, 144.30, 141.53, 132.84, 130.97, 130.19, 129.78, 129.74, 129.64, 128.76, 125.85, 116.61, 20.63;

(Z)-3,8-dimesityl-3,8-diaza-1,2,4,7(1,4)-tetrabenzenacyclooctaphan-5-ene **V.32b**
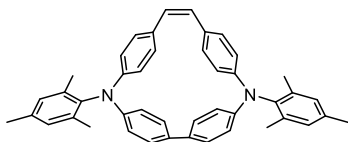
A similar procedure to synthesize **V.29a** was adapted. Crude bisboronate **V.34b**, PdCl$_2$(PPh$_3$)$_2$ (117 mg, 0.166 mmol, 0.2 eq), B(OH)$_3$ (278 mg, 4.16 mmol, 5 eq), KF (145 mg, 2.49 mmol, 3 eq), THF (250 mL), H$_2$O (25 mL). Product was purified by column chromatography (silica, 0% to 50% DCM in hexanes) as yellow powder (17 mg, 3% over two steps). ^{1}H NMR (500 MHz, CDCl$_3$): δ(ppm) 7.48 (d, J = 8.7 Hz, 4H, Ar-H), 7.29 (d, J = 8.7 Hz, 4H, Ar-H), 7.06 (d, J = 8.7 Hz, 4H, Ar-H), 6.94 (s, 4H, Ar-H), 6.90 (d, J = 8.7 Hz, 4H, Ar-H), 6.32 (s, 2H, C=C-H), 2.33 (s, 6H, CH$_3$), 2.01 (s, 12H, CH$_3$).

(Z)-3,8-bis(4-chlorophenyl)-3,8-diaza-1,2,4,7(1,4)-tetrabenzenacyclooctaphan-5-ene
V.32c
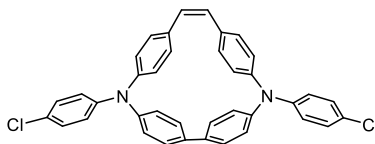
A similar procedure to synthesize **V.29a** was adapted. Crude bisboronate **V.34c**, PdCl$_2$(PPh$_3$)$_2$ (74 mg, 0.104 mmol, 0.2 eq), B(OH)$_3$ (161 mg, 2.61 mmol, 5 eq), KF (60 mg, 1.04 mmol, 2 eq), THF (450 mL), H$_2$O (45 mL). Product was purified by column chromatography (silica, 0% to 30% DCM in hexanes) as yellow powder (106 mg, 35% over two steps). ^{1}H NMR (600 MHz, CDCl$_3$): δ(ppm) 7.37 (d, *J* = 8.8 Hz, 4H, Ar-H), 7.24 (d, *J* = 8.8 Hz, 4H, Ar-H), 7.18 (d, *J* = 8.9 Hz, 4H, Ar-H), 6.95 (d, *J* = 8.9 Hz, 4H, Ar-H), 6.80 (d, *J* = 8.6 Hz, 4H, Ar-H), 6.47 (d, *J* = 8.6 Hz, 4H, Ar-H), 6.41 (s, 2H, C=C-H); ^{13}C NMR (150 MHz, CDCl$_3$): δ(ppm) 149.24, 147.80, 145.19, 141.75, 133.37, 130.84, 130.32, 129.90, 129.80, 129.15, 125.94, 124.14, 117.45.

5.4.3. X-Ray Crystallography Analysis

Diffraction intensities for **V.29a**, *trans*-**V.29e** and **V.32a** were collected at 173 (2) on a Bruker Apex2 CCD diffractometer using an Incoatec IµS micro-focus source with CuKα radiation, λ= 1.54178 Å. Space groups were determined based on systematic absences and intensity statistics. Absorption corrections were applied by SADABS.[29] Structures were solved by direct methods and Fourier techniques and refined on F^2 using full matrix least-squares procedures. All non-H atoms were refined with anisotropic thermal parameters. H atoms in both structures were refined in calculated positions in a rigid group model. All calculations were performed by the SHELXL-2014/7 packages.[30] All single crystals were grown from slow evaporation of a DCM solution.
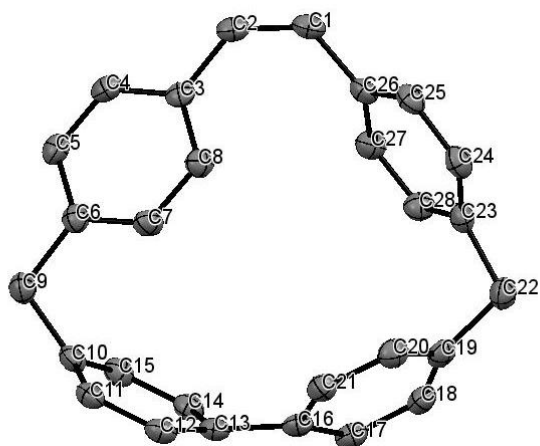
Figure 5.12. ORTEP representation of the X-ray crystallographic structure of **V29a**.

Crystallographic data for **V.29a**: $C_{28}H_{22}$, M = 358.45, Size = 0.17 x 0.16 x 0.12 mm, T = 173(2) K, Monoclinic, space group *P21/n*, a = 10.2051(3) Å, b = 10.2600(3) Å, c = 18.2832(5) Å, α = 90°, β = 91.5460(10)°, γ = 90°, V = 1913.63(10) Å^3, Z = 4, Dc = 1.244 Mg/m^3, μ(Mo) = 0.529 mm^{-1}, F(000) = 760, CuK/α (λ = 1.54178), θ = 4.84-66.62°, 13132 reflections, 3375 independent reflections [R_{int} = 0.0432], R1 = 0.0347, wR2 = 0.0867 and GOF = 1.026 for 3375 reflections (342 parameters) with I>2σ(I), R1 = 0.0396, wR2 = 0.0904 and GOF = 1.026 for all reflections, max/min residual electron density +0.184/-0.166 eÅ^3.
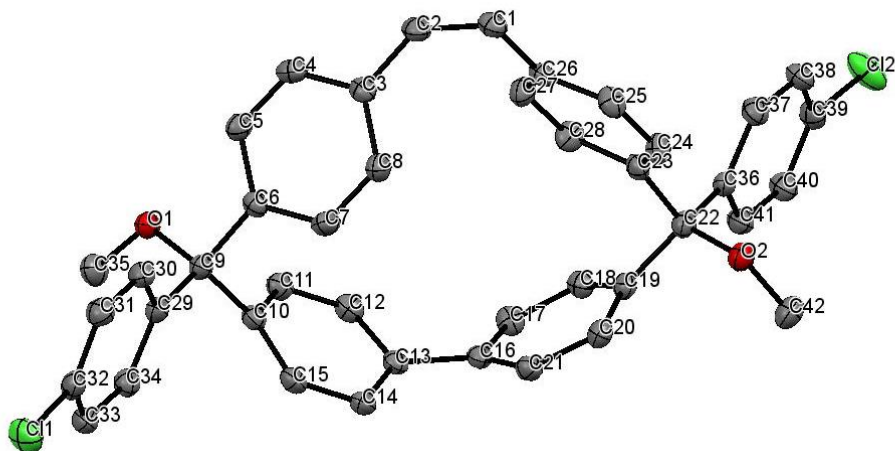
Figure 5.13. ORTEP representation of the X-ray crystallographic structure of *trans-***V.29e**.

145

In the unit cell, there is also a dichloromethane molecule which is disordered over two positions in a ratio of 50/50 and fills out the empty space in the crystal packing. Crystallographic data for *trans*-**V.29e**: $C_{43}H_{34}Cl_4O_2$, M = 724.50, Size = 0.25 x 0.24 x 0.05 mm, T = 173(2) K, Triclinic, space group *P/–1*, a = 10.7391(15) Å, b = 12.3787(17) Å, c = 14.292(2) Å, α = 84.562(3)°, β = 76.015(3)°, γ = 80.032(3)°, V = 1805.0(4) Å³, Z = 2, Dc = 1.333 Mg/m³, μ(Mo) = 0.365 mm⁻¹, *F*(000) = 752, MoK/α (λ=0.71073), θ = 1.477-25.000°, 29666 reflections, 6364 independent reflections [R_{int} = 0.0630], R1 = 0.0441, wR2 = 0.0947 and GOF = 1.015 for 6364 reflections (469 parameters) with I>2σ(I), R1 = 0.0774, wR2 = 0.1109 and GOF = 1.021 for all reflections, max/min residual electron density +0.255/-0.440 eÅ³.
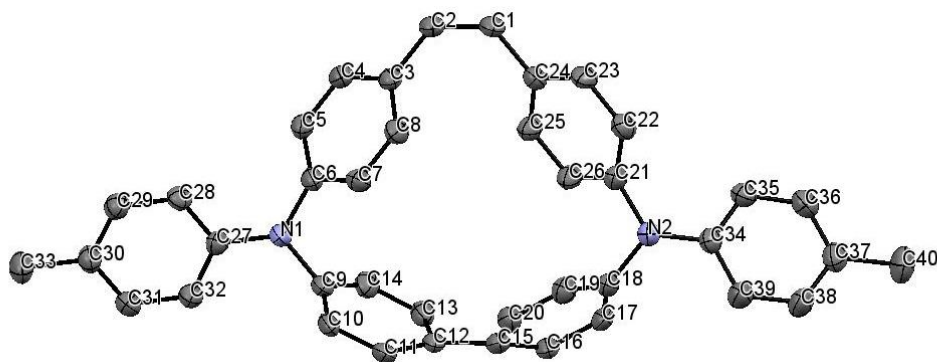
Figure 5.14. ORTEP representation of the X-ray crystallographic structure of **V.32a**.

In the crystal, there is an additional dichloromethane molecule per molecule **V.32a**. This dichloromethane molecule is disordered over two positions in a ratio of 50/50. Crystallographic data for **V.32a**: $C_{41}H_{34}Cl_2N_2$, M = 625.60, Size = 0.13 x 0.09 x 0.06 mm, T = 173(2) K, Trigonal, space group *P32*, a = 10.3752(3) Å, b = 10.3752(3) Å, c = 52.9434(15) Å, α = 90°, β = 90°, γ = 120°, V = 4935.5(3) Å³, Z = 6, Dc = 1.263 Mg/m³, μ(Mo) = 2.010 mm⁻¹, *F*(000) = 1968, CuK/α (λ=1.54178), θ = 2.504-66.689°, 37986 reflections, 11368 independent reflections [R_{int} = 0.0408], R1 = 0.0463, wR2 = 0.1183 and GOF = 1.046 for 11368 reflections (838 parameters) with I>2σ(I), R1 = 0.0514, wR2 = 0.1229 and GOF = 1.046 for all reflections, max/min residual electron density +0.298/-0.408 eÅ³.

5.4.4. Thermogravimetric Analysis (TGA)

The polymer from entry 8 in **Table V.2** was analyzed using a heating rate of 10 °C/min under a N_2 stream. No substantial weight loss was observed up to 290 °C. The onset temperature of weight loss was determined to be 352 °C. When temperature reached 600 °C, about 25% of the original weight remained.
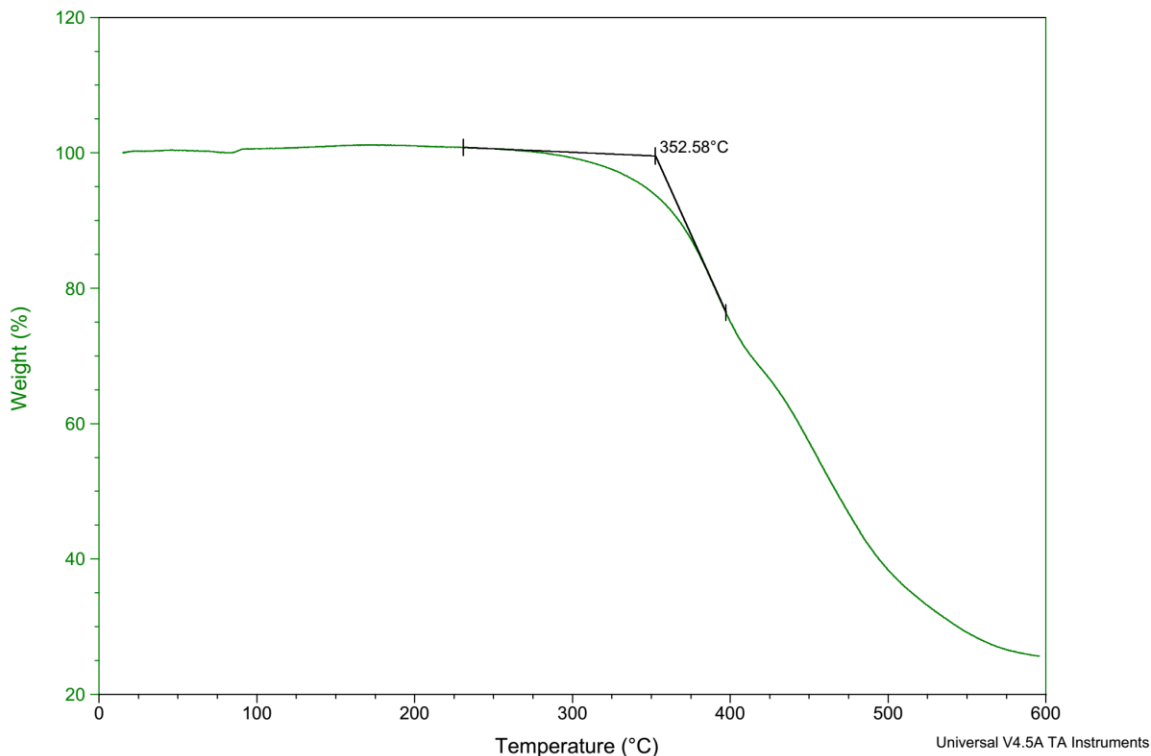
Figure 5.15. TGA analysis of the polymeric sample from entry 8 in **Table. V.2**.

5.4.5. Computational Studies

All computations were carried out with Gaussian 09 package.[31] Molecular geometry optimizations and optical transition predictions were computed utilizing DFT method at the B3LYP/6-31G* level of theory. The fully optimized structures were confirmed to be true minima by vibrational analysis. Strain energies were calculated using the homodesmotic reactions.
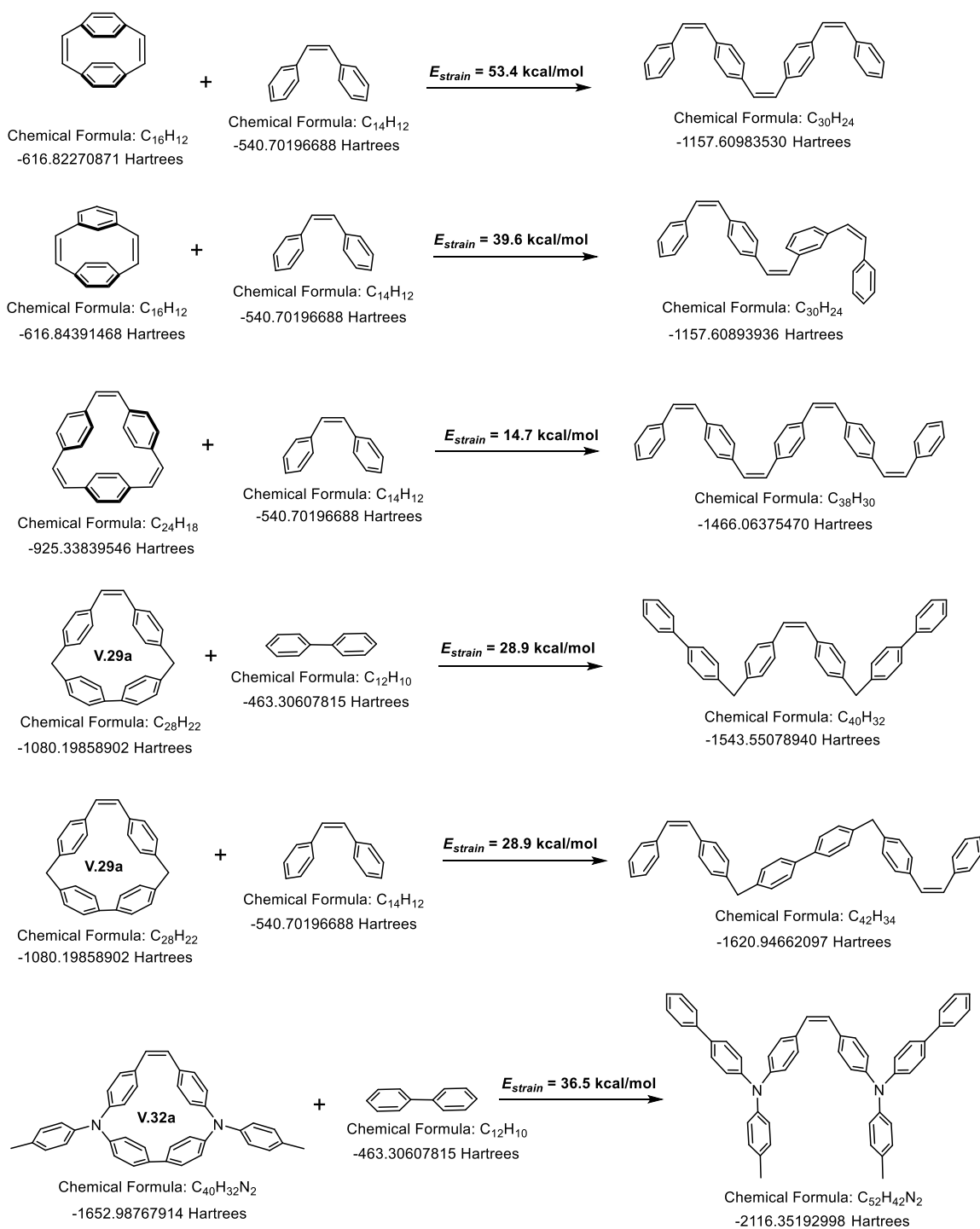
Figure 5.16. Homodesmotic reactions to estimate the strain energies (DFT at the B3LYP/6-31G* level of theory).

Table 5.3. Structural parameters from crystallographic analysis (exp.) and from DFT calculations (cal.).
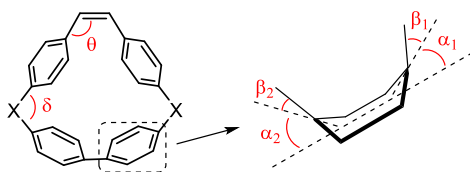
	V.29a	**V.29e**	**V.32a**
exp. θ (°)	130.2, 128.7	129.4, 127.8	128.5, 129.4
cal. θ (°)	128.7	129.0	128.8
exp. δ (°)	107.4, 106.5	103.8, 103.3	110.8, 109.7
cal. δ (°)	107.4	103.8	112.0
exp. α_1 (°)	11.8, 8.4	9.2, 8.0	11.0, 11.7
cal. α_1 (°)	10.5	9.2	11.8
exp. α_2 (°)	12.6, 8.2	9.9, 10.0	11.3, 10.8
cal. α_2 (°)	10.9	10.3	11.5
exp. β_1 (°)	17.1, 11.0	16.2, 14.5	14.8, 13.1
cal. β_1 (°)	13.2	14.7	12.1
exp. β_2 (°)	16.8, 16.6	15.6, 14.8	17.5, 16.0
cal. β_2 (°)	16.8	15.0	18.8

REFERENCES CITED

Chapter I

1.   Musgrave, R. A.; Russell, A. D.; Manners, I., Strained Ferrocenophanes. *Organometallics* **2013,** *32* (20), 5654-5667.

2.   Dommerholt, J.; Rutjes, F. P. J. T.; van Delft, F. L., Strain-Promoted 1,3-Dipolar Cycloaddition of Cycloalkynes and Organic Azides. *Top. Curr. Chem.* **2016,** *374* (2), 16.

3.   Jewett, J. C.; Bertozzi, C. R., Cu-free click cycloaddition reactions in chemical biology. *Chem. Soc. Rev.* **2010,** *39* (4), 1272-1279.

4.   Sletten, E. M.; Bertozzi, C. R., From Mechanism to Mouse: A Tale of Two Bioorthogonal Reactions. *Acc. Chem. Res.* **2011,** *44* (9), 666-676.

5.   Bogdan, A. R.; Jerome, S. V.; Houk, K. N.; James, K., Strained Cyclophane Macrocycles: Impact of Progressive Ring Size Reduction on Synthesis and Structure. *J. Am. Chem. Soc.* **2012,** *134* (4), 2127-2138.

6.   König, B., Carbon Rich Cyclophanes with Unusual Properties — an Update. In *Carbon Rich Compounds I*, Springer Berlin Heidelberg: Berlin, Heidelberg, 1998; pp 91-136.

7.   Bickelhaupt, F.; de Wolf, W. H., Unusual reactivity of highly strained cyclophanes. *J. Phys. Org. Chem.* **1998,** *11* (5), 362-376.

8.   Almeida, G. d.; Townsend, L. C.; Bertozzi, C. R., Synthesis and Reactivity of Dibenzoselenacycloheptynes. *Org. Lett.* **2013,** *15* (12), 3038-3041.

9.   Slugovc, C., The Ring Opening Metathesis Polymerisation Toolbox. *Macromol. Rapid Commun.* **2004,** *25* (14), 1283-1297.

10.   Leitgeb, A.; Wappel, J.; Slugovc, C., The ROMP toolbox upgraded. *Polymer* **2010,** *51* (14), 2927-2946.

11.   Darzi, E. R.; Jasti, R., The dynamic, size-dependent properties of [5]-[12]cycloparaphenylenes. *Chem. Soc. Rev.* **2015,** *44* (18), 6401-10.

12.   Segawa, Y.; Yagi, A.; Matsui, K.; Itami, K., Design and Synthesis of Carbon Nanotube Segments. *Angew. Chem. Int. Ed.* **2016,** *55* (17), 5136-5158.

13.   Li, P.; Wong, B. M.; Zakharov, L. N.; Jasti, R., Investigating the Reactivity of 1,4-Anthracene-Incorporated Cycloparaphenylene. *Org. Lett.* **2016,** *18* (7), 1574-1577.

14.   Kammula, S. L.; Iroff, L. D.; Jones, M.; Van Straten, J. W.; De Wolf, W. H.; Bickelhaupt, F., Interconversion of [6]paracyclophane and 1,4-hexamethylene(Dewar benzene). *J. Am. Chem. Soc.* **1977,** *99* (17), 5815-5815.

15.   Tobe, Y.; Takahashi, T.; Kobiro, K.; Kakiuchi, K., Thermal Valence Isomerization of Hemi-Dewar Type Isomers of [6](1,4)Naphthaleno- and [6](1,4)Anthracenophanes. *Chem. Lett.* **1990,** *19* (9), 1587-1590.

16.   Becker, H. D., Unimolecular photochemistry of anthracenes. *Chem. Rev.* **1993,** *93* (1), 145-172.

17.   Tobe, Y.; Takahashi, T.; Kobiro, K.; Kakiuchi, K., Photochemical [2+2] dimerization of [6](1,4)-anthracenophane. *J. Am. Chem. Soc.* **1991,** *113* (15), 5804-5808.

18.   Tobe, Y.; Takemura, A.; Jimbo, M.; Takahashi, T.; Kobiro, K.; Kakiuchi, K., Unusual reactivity of bent acenes: reactions of [6](1,4)naphthalenophane and [6](1,4)anthracenophane with electrophiles. *J. Am. Chem. Soc.* **1992,** *114* (9), 3479-3491.

19.   Sisto, T. J.; Zakharov, L. N.; White, B. M.; Jasti, R., Towards pi-extended cycloparaphenylenes as seeds for CNT growth: investigating strain relieving ring-openings and rearrangements. *Chem. Sci.* **2016,** *7* (6), 3681-3688.

20.   Dale, E. J.; Ferris, D. P.; Vermeulen, N. A.; Henkelis, J. J.; Popovs, I.; Juríček, M.; Barnes, J. C.; Schneebeli, S. T.; Stoddart, J. F., Cooperative Reactivity in an Extended-Viologen-Based Cyclophane. *J. Am. Chem. Soc.* **2016,** *138* (11), 3667-3670.

21.   Lee, S.; Chénard, E.; Gray, D. L.; Moore, J. S., Synthesis of Cycloparaphenyleneacetylene via Alkyne Metathesis: C70 Complexation and Copper-Free Triple Click Reaction. *J. Am. Chem. Soc.* **2016,** *138* (42), 13814-13817.

22.   Lecomte, P.; Jérôme, R., Ring Opening Polymerization. In *Encyclopedia of Polymer Science and Technology*, John Wiley & Sons, Inc.: 2002.

23.   Odian, G., Ring-Opening Polymerization. In *Principles of Polymerization*, John Wiley & Sons, Inc.: 2004; pp 544-618.

24.   Bielawski, C. W.; Grubbs, R. H., Living ring-opening metathesis polymerization. *Prog. Polym. Sci.* **2007,** *32* (1), 1-29.

25.   Miao, Y. J.; Bazan, G. C., Stereoselective Polymerization of [2.2]Paracyclophan-1-ene. *Macromolecules* **1994,** *27* (4), 1063-1064.

26.   Miao, Y.-J.; Bazan, G. C., Paracyclophene Route to Poly(p-phenylenevinylene). *J. Am. Chem. Soc.* **1994,** *116* (20), 9379-9380.

27.   Yu, C.-Y.; Turner, M. L., Soluble Poly(p-phenylenevinylene)s through Ring-Opening Metathesis Polymerization. *Angew. Chem. Int. Ed.* **2006,** *45* (46), 7797-7800.

28.   Yu, C.-Y.; Horie, M.; Spring, A. M.; Tremel, K.; Turner, M. L., Homopolymers and Block Copolymers of p-Phenylenevinylene-2,5-diethylhexyloxy-p-phenylenevinylene and m-Phenylenevinylene-2,5-diethylhexyloxy-p-phenylenevinylene by Ring-Opening Metathesis Polymerization. *Macromolecules* **2010,** *43* (1), 222-232.

29.   Mäker, D.; Maier, C.; Brödner, K.; Bunz, U. H. F., [2.2.2]Paracyclophane-Trienes—Attractive Monomers for ROMP. *ACS Macro Letters* **2014,** *3* (5), 415-418.
30.   Carnes, M.; Buccella, D.; Decatur, J.; Steigerwald, M. L.; Nuckolls, C., Helical (5Z, 11E)-Dibenzo[a,e]cyclooctatetrene: A Spring-Loaded Monomer. *Angew. Chem. Int. Ed.* **2008,** *47* (16), 2982-2985.

31.   Wong, H. N. C.; Garratt, P. J.; Sondheimer, F., Unsaturated eight-membered ring compounds. XI. Synthesis of sym-dibenzo-1,5-cyclooctadiene-3,7-diyne and sym-dibenzo-1,3,5-cyclooctatrien-7-yne, presumably planar conjugated eight-membered ring compounds. *J. Am. Chem. Soc.* **1974,** *96* (17), 5604-5605.

32.   Carnes, M.; Buccella, D.; Siegrist, T.; Steigerwald, M. L.; Nuckolls, C., Reactions of Strained Hydrocarbons with Alkene and Alkyne Metathesis Catalysts. *J. Am. Chem. Soc.* **2008,** *130* (43), 14078-14079.

33.   Fischer, F. R.; Nuckolls, C., Design of Living Ring-Opening Alkyne Metathesis. *Angew. Chem. Int. Ed.* **2010,** *49* (40), 7257-7260.

34.   Colquhoun, H. M.; Zhu, Z.; Williams, D. J., Synthesis and Ring-Expanding Oligomerization of an Extremely Strained Macrocyclic Aromatic Ether−Sulfone. *Org. Lett.* **2001,** *3* (25), 4031-4034.

35.   Colquhoun, H. M.; Zhu, Z.; Dudman, C. C.; O'Mahoney, C. A.; Williams, D. J.; Drew, M. G. B., Synthesis of Strained Macrocyclic Biaryls for Enthalpy-Driven Ring-Opening Polymerization. *Macromolecules* **2005,** *38* (25), 10413-10420.

Chapter II

1.   Jasti, R.; Bhattacharjee, J.; Neaton, J. B.; Bertozzi, C. R., Synthesis, Characterization, and Theory of [9]-, [12]-, and [18]Cycloparaphenylene: Carbon Nanohoop Structures. *J. Am. Chem. Soc.* **2008,** *130* (52), 17646-17647.

2.   Sisto, T. J.; Golder, M. R.; Hirst, E. S.; Jasti, R., Selective Synthesis of Strained [7]Cycloparaphenylene: An Orange-Emitting Fluorophore. *J. Am. Chem. Soc.* **2011,** *133* (40), 15800-15802.

3.   Darzi, E. R.; Sisto, T. J.; Jasti, R., Selective Syntheses of [7]-[12]Cycloparaphenylenes Using Orthogonal Suzuki-Miyaura Cross-Coupling Reactions. *J. Org. Chem.* **2012,** *77* (15), 6624-6628.

4.   Xia, J.; Bacon, J. W.; Jasti, R., Gram-scale synthesis and crystal structures of [8]- and [10]CPP, and the solid-state structure of C60@[10]CPP. *Chem. Sci.* **2012,** *3* (10), 3018-3021.

5.   Xia, J.; Jasti, R., Synthesis, Characterization, and Crystal Structure of [6]Cycloparaphenylene. *Angew. Chem., Int. Ed.* **2012,** *51* (10), 2474-2476.

6.   Hirst, E. S.; Jasti, R., Bending Benzene: Syntheses of [n]Cycloparaphenylenes. *J. Org. Chem.* **2012,** *77* (23), 10473-10478.

7.   Takaba, H.; Omachi, H.; Yamamoto, Y.; Bouffard, J.; Itami, K., Selective synthesis of [12]cycloparaphenylene. *Angew. Chem. Int. Ed.* **2009,** *48* (33), 6112-6116.

8.   Segawa, Y.; Miyamoto, S.; Omachi, H.; Matsuura, S.; Senel, P.; Sasamori, T.; Tokitoh, N.; Itami, K., Concise synthesis and crystal structure of [12]cycloparaphenylene. *Angew. Chem. Int. Ed.* **2011,** *50* (14), 3244-3248.

9.   Yasutomo, S.; Petr, Š.; Sanae, M.; Haruka, O.; Kenichiro, I., [9]Cycloparaphenylene: Nickel-mediated Synthesis and Crystal Structure. *Chem. Lett.* **2011,** *40* (4), 423-425.

10.   Ishii, Y.; Nakanishi, Y.; Omachi, H.; Matsuura, S.; Matsui, K.; Shinohara, H.; Segawa, Y.; Itami, K., Size-selective synthesis of [9]-[11] and [13]cycloparaphenylenes. *Chem. Sci.* **2012,** *3* (7), 2340-2345.

11.   Yamago, S.; Watanabe, Y.; Iwamoto, T., Synthesis of [8]cycloparaphenylene from a square-shaped tetranuclear platinum complex. *Angew. Chem. Int. Ed.* **2010,** *49* (4), 757-759.

12.   Iwamoto, T.; Watanabe, Y.; Sakamoto, Y.-I.; Suzuki, T.; Yamago, S., Selective and Random Syntheses of [n]Cycloparaphenylenes (n = 8-13) and Size Dependence of Their Electronic Properties. *J. Am. Chem. Soc.* **2011,** *133* (21), 8354-8361.

13.   Kayahara, E.; Sakamoto, Y.; Suzuki, T.; Yamago, S., Selective Synthesis and Crystal Structure of [10]Cycloparaphenylene. *Org. Lett.* **2012,** *14* (13), 3284-3287.

14.   Eiichi, K.; Takahiro, I.; Toshiyasu, S.; Shigeru, Y., Selective Synthesis of [6]-, [8]-, and [10]Cycloparaphenylenes. *Chem. Lett.* **2013,** *42* (6), 621-623.

15.   Bunz, U. H.; Menning, S.; Martin, N., para-Connected cyclophenylenes and hemispherical polyarenes: building blocks for single-walled carbon nanotubes? *Angew. Chem. Int. Ed.* **2012,** *51* (29), 7094-7101.

16.   Fort, E. H.; Scott, L. T., Carbon nanotubes from short hydrocarbon templates. Energy analysis of the Diels-Alder cycloaddition/rearomatization growth strategy. *J. Mater. Chem.* **2011,** *21* (5), 1373-1381.

17.   Schrettl, S.; Frauenrath, H., Elements for a rational polymer approach towards carbon nanostructures. *Angew. Chem. Int. Ed.* **2012,** *51* (27), 6569-71.

18.   Jasti, R.; Bertozzi, C. R., Progress and challenges for the bottom-up synthesis of carbon nanotubes with discrete chirality. *Chem. Phys. Lett.* **2010,** *494* (1–3), 1-7.

19.   Iwamoto, T.; Watanabe, Y.; Sadahiro, T.; Haino, T.; Yamago, S., Size-selective encapsulation of C60 by [10]cycloparaphenylene: formation of the shortest fullerene-peapod. *Angew. Chem. Int. Ed.* **2011,** *50* (36), 8342-8344.

20.   Iwamoto, T.; Watanabe, Y.; Takaya, H.; Haino, T.; Yasuda, N.; Yamago, S., Size- and Orientation-Selective Encapsulation of C70 by Cycloparaphenylenes. *Chem. Eur. J* **2013,** *19* (42), 14061-14068.

21.   Nijegorodov, N. I.; Downey, W. S.; Danailov, M. B., Systematic investigation of absorption, fluorescence and laser properties of some p- and m-oligophenylenes. *Spectrochim. Acta A* **2000,** *56* (4), 783-795.

22.   Banerjee, M.; Shukla, R.; Rathore, R., Synthesis, Optical, and Electronic Properties of Soluble Poly-p-phenylene Oligomers as Models for Molecular Wires. *J. Am. Chem. Soc.* **2009,** *131* (5), 1780-1786.

23.   Meerholz, K.; Heinze, J., Electrochemical solution and solid-state investigations on conjugated oligomers and polymers of the α-thiophene and the p-phenylene series. *Electrochim. Acta* **1996,** *41* (11), 1839-1854.

24.   Segawa, Y.; Fukazawa, A.; Matsuura, S.; Omachi, H.; Yamaguchi, S.; Irle, S.; Itami, K., Combined experimental and theoretical studies on the photophysical properties of cycloparaphenylenes. *Org. Biomol. Chem.* **2012,** *10* (30), 5979-5984.

25.   Fujitsuka, M.; Cho, D. W.; Iwamoto, T.; Yamago, S.; Majima, T., Size-dependent fluorescence properties of [n]cycloparaphenylenes (n = 8-13), hoop-shaped [small pi]-conjugated molecules. *Phys. Chem. Chem. Phys* **2012,** *14* (42), 14585-14588.

26.   Fujitsuka, M.; Iwamoto, T.; Kayahara, E.; Yamago, S.; Majima, T., Enhancement of the Quinoidal Character for Smaller [n]Cycloparaphenylenes Probed by Raman Spectroscopy. *ChemPhysChem* **2013**, *14* (8), 1570-1572.

27.   Chen, H.; Golder, M. R.; Wang, F.; Jasti, R.; Swan, A. K., Raman spectroscopy of carbon nanohoops. *Carbon* **2014,** *67*, 203-213.

28.   Nishihara, T.; Segawa, Y.; Itami, K.; Kanemitsu, Y., Excited States in Cycloparaphenylenes: Dependence of Optical Properties on Ring Length. *J. Phys. Chem. Lett.* **2012,** *3* (21), 3125-3128.

29.   Bodwell, G. J.; Bridson, J. N.; Chen, S.-L.; Poirier, R. A., Nonplanar Aromatic Compounds. 5.1 A Strategy for the Synthesis of cis-10b,10c-Dimethyl-10b,10c-dihydropyrenes. First Crystal Structure of a cis-10b,10c-Dimethyl-10b,10c-dihydropyrene. *J. Am. Chem. Soc.* **2001,** *123* (20), 4704-4708.

30.   Bodwell, G. J.; Miller, D. O.; Vermeij, R. J., Nonplanar Aromatic Compounds. 6. [2]Paracyclo[2](2,7)pyrenophane. A Novel Strained Cyclophane and a First Step on the Road to a "Vögtle" Belt. *Org. Lett.* **2001,** *3* (13), 2093-2096.

31.   Bodwell, G. J.; Bridson, J. N.; Cyrañski, M. K.; Kennedy, J. W. J.; Krygowski, T. M.; Mannion, M. R.; Miller, D. O., Nonplanar Aromatic Compounds. 8.1 Synthesis, Crystal Structures, and Aromaticity Investigations of the 1,n-Dioxa[n](2,7)pyrenophanes. How Does Bending Affect the Cyclic π-Electron Delocalization of the Pyrene System? *J Org. Chem.* **2003,** *68* (6), 2089-2098.

32.   Merner, B. L.; Dawe, L. N.; Bodwell, G. J., 1,1,8,8-Tetramethyl[8](2,11)teropyrenophane: half of an aromatic belt and a segment of an (8,8) single-walled carbon nanotube. *Angew. Chem. Int. Ed.* **2009,** *48* (30), 5487-5491.

33.   Tour, J. M.; Rawlett, A. M.; Kozaki, M.; Yao, Y.; Jagessar, R. C.; Dirk, S. M.; Price, D. W.; Reed, M. A.; Zhou, C.-W.; Chen, J.; Wang, W.; Campbell, I., Synthesis and Preliminary Testing of Molecular Wires and Devices. *Chem. Eur. J* **2001,** *7* (23), 5118-5134.
34.   Cammidge, A. N.; King, A. S. H., Model studies towards liquid crystalline dendrimers with mesogenic repeat units throughout the structure. *Tetrahedron Lett.* **2006,** *47* (31), 5569-5572.

35.   Barder, T. E.; Walker, S. D.; Martinelli, J. R.; Buchwald, S. L., Catalysts for Suzuki−Miyaura Coupling Processes: Scope and Studies of the Effect of Ligand Structure. *J. Am. Chem. Soc.* **2005,** *127* (13), 4685-4696.

36.   Wong, B. M., Optoelectronic Properties of Carbon Nanorings: Excitonic Effects from Time-Dependent Density Functional Theory. *J. Phys. Chem. C* **2009,** *113* (52), 21921-21927.

37.   Camacho, C.; Niehaus, T. A.; Itami, K.; Irle, S., Origin of the size-dependent fluorescence blueshift in [n]cycloparaphenylenes. *Chem. Sci.* **2013,** *4* (1), 187-195.

38.   Pangborn, A. B.; Giardello, M. A.; Grubbs, R. H.; Rosen, R. K.; Timmers, F. J., Safe and Convenient Procedure for Solvent Purification. *Organometallics* **1996,** *15* (5), 1518-1520.

39.   Wells, G.; Berry, J. M.; Bradshaw, T. D.; Burger, A. M.; Seaton, A.; Wang, B.; Westwell, A. D.; Stevens, M. F. G., 4-Substituted 4-Hydroxycyclohexa-2,5-dien-1-ones with Selective Activities against Colon and Renal Cancer Cell Lines. *J. Med. Chem.* **2003,** *46* (4), 532-541.

40.   Williams, A. T. R.; Winfield, S. A.; Miller, J. N., Relative fluorescence quantum yields using a computer-controlled luminescence spectrometer. *Analyst* **1983,** *108* (1290), 1067-1071.

41.   Gaussian 09, Revision B.01, Frisch, M. J.; Trucks, G. W.; Schlegel, H. B.; Scuseria, G. E.; Robb, M. A.; Cheeseman, J. R.; Scalmani, G.; Barone, V.; Mennucci, B.; Petersson, G. A.; Nakatsuji, H.; Caricato, M.; Li, X.; Hratchian, H. P.; Izmaylov, A. F.; Bloino, J.; Zheng, G.; Sonnenberg, J. L.; Hada, M.; Ehara, M.; Toyota, K.; Fukuda, R.; Hasegawa, J.; Ishida, M.; Nakajima, T.; Honda, Y.; Kitao, O.; Nakai, H.; Vreven, T.; Montgomery, Jr., J. A.; Peralta, J. E.; Ogliaro, F.; Bearpark, M.; Heyd, J. J.; Brothers, E.; Kudin, K. N.; Staroverov, V. N.; Kobayashi, R.; Normand, J.; Raghavachari, K.; Rendell, A.; Burant, J. C.; Iyengar, S. S.; Tomasi, J.; Cossi, M.; Rega, N.; Millam, J. M.; Klene, M.; Knox, J. E.; Cross, J. B.; Bakken, V.; Adamo, C.; Jaramillo, J.; Gomperts, R.; Stratmann, R. E.; Yazyev, O.; Austin, A. J.; Cammi, R.; Pomelli, C.; Ochterski, J. W.; Martin, R. L.; Morokuma, K.; Zakrzewski, V. G.; Voth, G. A.; Salvador, P.; Dannenberg, J. J.; Dapprich, S.; Daniels, A. D.; Farkas, Ö.; Foresman, J. B.; Ortiz, J. V.; Cioslowski, J.; Fox, D. J. Gaussian, Inc., Wallingford CT, 2009

Chapter III

1.   Slater, A. G.; Cooper, A. I., Function-led design of new porous materials. *Science* **2015,** *348* (6238).

2.   Feng, X.; Ding, X.; Jiang, D., Covalent organic frameworks. *Chem. Soc. Rev.* **2012,** *41* (18), 6010-6022.

3.   Xu, Y.; Jin, S.; Xu, H.; Nagai, A.; Jiang, D., Conjugated microporous polymers: design, synthesis and application. *Chem. Soc. Rev.* **2013,** *42* (20), 8012-8031.

4.   Ding, S.-Y.; Wang, W., Covalent organic frameworks (COFs): from design to applications. *Chem. Soc. Rev.* **2013,** *42* (2), 548-568.

5.   Kreno, L. E.; Leong, K.; Farha, O. K.; Allendorf, M.; Van Duyne, R. P.; Hupp, J. T., Metal–Organic Framework Materials as Chemical Sensors. *Chem. Rev.* **2012,** *112* (2), 1105-1125.

6.   Lee, J.; Farha, O. K.; Roberts, J.; Scheidt, K. A.; Nguyen, S. T.; Hupp, J. T., Metal-organic framework materials as catalysts. *Chem. Soc. Rev.* **2009,** *38* (5), 1450-1459.

7.   Zhang, G.; Mastalerz, M., Organic cage compounds - from shape-persistency to function. *Chem. Soc. Rev.* **2014,** *43* (6), 1934-1947.

8.   Jasti, R.; Bhattacharjee, J.; Neaton, J. B.; Bertozzi, C. R., Synthesis, Characterization, and Theory of [9]-, [12]-, and [18]Cycloparaphenylene: Carbon Nanohoop Structures. *J. Am. Chem. Soc.* **2008,** *130* (52), 17646-17647.

9.   Sisto, T. J.; Golder, M. R.; Hirst, E. S.; Jasti, R., Selective Synthesis of Strained [7]Cycloparaphenylene: An Orange-Emitting Fluorophore. *J. Am. Chem. Soc.* **2011,** *133* (40), 15800-15802.

10.   Xia, J.; Golder, M. R.; Foster, M. E.; Wong, B. M.; Jasti, R., Synthesis, Characterization, and Computational Studies of Cycloparaphenylene Dimers. *J. Am. Chem. Soc.* **2012,** *134* (48), 19709-19715.
11.   Darzi, E. R.; Sisto, T. J.; Jasti, R., Selective Syntheses of [7]-[12]Cycloparaphenylenes Using Orthogonal Suzuki-Miyaura Cross-Coupling Reactions. *J. Org. Chem.* **2012,** *77* (15), 6624-6628.

12.   Hirst, E. S.; Jasti, R., Bending Benzene: Syntheses of [n]Cycloparaphenylenes. *J. Org. Chem.* **2012,** *77* (23), 10473-10478.

13.   Xia, J.; Bacon, J. W.; Jasti, R., Gram-scale synthesis and crystal structures of [8]- and [10]CPP, and the solid-state structure of C60@[10]CPP. *Chem. Sci.* **2012,** *3* (10), 3018.

14.   Xia, J.; Jasti, R., Synthesis, Characterization, and Crystal Structure of [6]Cycloparaphenylene. *Angew. Chem., Int. Ed.* **2012,** *51* (10), 2474-2476.

15.   Hines, D. A.; Darzi, E. R.; Jasti, R.; Kamat, P. V., Carbon Nanohoops: Excited Singlet and Triplet Behavior of [9]- and [12]-Cycloparaphenylene. *J. Phys. Chem. A* **2014,** *118* (9), 1595-1600.

16.   Adamska, L.; Nayyar, I.; Chen, H.; Swan, A. K.; Oldani, N.; Fernandez-Alberti, S.; Golder, M. R.; Jasti, R.; Doorn, S. K.; Tretiak, S., Self-Trapping of Excitons, Violation of Condon Approximation, and Efficient Fluorescence in Conjugated Cycloparaphenylenes. *Nano Lett.* **2014,** *14* (11), 6539-6546.

17.   Evans, P. J.; Darzi, E. R.; Jasti, R., Efficient room-temperature synthesis of a highly strained carbon nanohoop fragment of buckminsterfullerene. *Nat. Chem.* **2014,** *6* (5), 404-408.

18.   Darzi, E. R.; Hirst, E. S.; Weber, C. D.; Zakharov, L. N.; Lonergan, M. C.; Jasti, R., Synthesis, Properties, and Design Principles of Donor–Acceptor Nanohoops. *ACS Cent. Sci.* **2015,** *1* (6), 335-342.

19.   Kayahara, E.; Patel, V. K.; Xia, J.; Jasti, R.; Yamago, S., Selective and Gram-Scale Synthesis of [6]Cycloparaphenylene. *Synlett* **2015,** *26* (11), 1615-1619.

20.   Patel, V. K.; Kayahara, E.; Yamago, S., Practical Synthesis of [n]Cycloparaphenylenes (n=5, 7-12) by H2SnCl4-Mediated Aromatization of 1,4-Dihydroxycyclo-2,5-diene Precursors. *Chem. - Eur. J.* **2015,** *21* (15), 5742-5749.

21.   Takaba, H.; Omachi, H.; Yamamoto, Y.; Bouffard, J.; Itami, K., Selective synthesis of [12]cycloparaphenylene. *Angew. Chem. Int. Ed..* **2009,** *48* (33), 6112-6116.

22.   Omachi, H.; Matsuura, S.; Segawa, Y.; Itami, K., A Modular and Size-Selective Synthesis of [n]Cycloparaphenylenes: A Step toward the Selective Synthesis of [n,n] Single-Walled Carbon Nanotubes. *Angew. Chem., Int. Ed.* **2010,** *49* (52), 10202-10205.
23.   Segawa, Y.; Miyamoto, S.; Omachi, H.; Matsuura, S.; Senel, P.; Sasamori, T.; Tokitoh, N.; Itami, K., Concise synthesis and crystal structure of [12]cycloparaphenylene. *Angew. Chem. Int. Ed.* **2011,** *50* (14), 3244-8.

24.   Ishii, Y.; Nakanishi, Y.; Omachi, H.; Matsuura, S.; Matsui, K.; Shinohara, H.; Segawa, Y.; Itami, K., Size-selective synthesis of [9]-[11] and [13]cycloparaphenylenes. *Chem. Sci.* **2012,** *3* (7), 2340-2345.

25.   Yamago, S.; Watanabe, Y.; Iwamoto, T., Synthesis of [8]cycloparaphenylene from a square-shaped tetranuclear platinum complex. *Angew. Chem. Int. Ed.* **2010,** *49* (4), 757-759.

26.   Iwamoto, T.; Watanabe, Y.; Sakamoto, Y.-I.; Suzuki, T.; Yamago, S., Selective and Random Syntheses of [n]Cycloparaphenylenes (n = 8-13) and Size Dependence of Their Electronic Properties. *J. Am. Chem. Soc.* **2011,** *133* (21), 8354-8361.

27.   Kayahara, E.; Sakamoto, Y.; Suzuki, T.; Yamago, S., Selective Synthesis and Crystal Structure of [10]Cycloparaphenylene. *Org. Lett.* **2012,** *14* (13), 3284-3287.

28.   Kayahara, E.; Patel, V. K.; Yamago, S., Synthesis and Characterization of [5]Cycloparaphenylene. *J. Am. Chem. Soc.* **2014,** *136* (6), 2284-2287.

29.   Darzi, E. R.; Jasti, R., The dynamic, size-dependent properties of [5]-[12]cycloparaphenylenes. *Chem. Soc. Rev.* **2015,** *44* (18), 6401-10.

30.   Golder, M. R.; Jasti, R., Syntheses of the Smallest Carbon Nanohoops and the Emergence of Unique Physical Phenomena. *Acc. Chem. Res.* **2015,** *48* (3), 557-566.

31.   Iwamoto, T.; Watanabe, Y.; Sadahiro, T.; Haino, T.; Yamago, S., Size-selective encapsulation of C60 by [10]cycloparaphenylene: formation of the shortest fullerene-peapod. *Angew. Chem. Int. Ed.* **2011,** *50* (36), 8342-8344.

32.   Iwamoto, T.; Watanabe, Y.; Takaya, H.; Haino, T.; Yasuda, N.; Yamago, S., Size-and Orientation-Selective Encapsulation of C70 by Cycloparaphenylenes. *Chem. Eur. J* **2013,** *19* (42), 14061-14068.

33.   Iwamoto, T.; Slanina, Z.; Mizorogi, N.; Guo, J.; Akasaka, T.; Nagase, S.; Takaya, H.; Yasuda, N.; Kato, T.; Yamago, S., Partial Charge Transfer in the Shortest Possible Metallofullerene Peapod, La@C82⊂[11]Cycloparaphenylene. *Chem. - Eur. J.* **2014,** *20* (44), 14403-14409.

34.   Ueno, H.; Nishihara, T.; Segawa, Y.; Itami, K., Cycloparaphenylene-Based Ionic Donor-Acceptor Supramolecule: Isolation and Characterization of Li+@C60⊂[10]CPP. *Angew. Chem., Int. Ed.* **2015,** *54* (12), 3707-3711.

35.   Yoshizawa, M.; Klosterman, J. K., Molecular architectures of multi-anthracene assemblies. *Chem. Soc. Rev.* **2014,** *43* (6), 1885-1898.

36.   Tasdelen, M. A., Diels-Alder "click" reactions: recent applications in polymer and material science. *Polymer Chemistry* **2011,** *2* (10), 2133-2145.

37.   Li, M.; Schlüter, A. D.; Sakamoto, J., Solid-State Photopolymerization of a Shape-Persistent Macrocycle with Two 1,8-Diazaanthracene Units in a Single Crystal. *J. Am. Chem. Soc.* **2012,** *134* (28), 11721-11725.

38.   Kissel, P.; Erni, R.; Schweizer, W. B.; Rossell, M. D.; King, B. T.; Bauer, T.; Götzinger, S.; Schlüter, A. D.; Sakamoto, J., A two-dimensional polymer prepared by organic synthesis. *Nat. Chem.* **2012,** *4* (4), 287-291.

39.   Bhola, R.; Payamyar, P.; Murray, D. J.; Kumar, B.; Teator, A. J.; Schmidt, M. U.; Hammer, S. M.; Saha, A.; Sakamoto, J.; Schlüter, A. D.; King, B. T., A Two-Dimensional Polymer from the Anthracene Dimer and Triptycene Motifs. *J. Am. Chem. Soc.* **2013,** *135* (38), 14134-14141.

40.   Kory, M. J.; Worle, M.; Weber, T.; Payamyar, P.; van de Poll, S. W.; Dshemuchadse, J.; Trapp, N.; Schluter, A. D., Gram-scale synthesis of two-dimensional polymer crystals and their structure analysis by X-ray diffraction. *Nat. Chem.* **2014,** *6* (9), 779-784.
41.   Murray, D. J.; Patterson, D. D.; Payamyar, P.; Bhola, R.; Song, W.; Lackinger, M.; Schluter, A. D.; King, B. T., Large area synthesis of a nanoporous two-dimensional polymer at the air/water interface. *J. Am. Chem. Soc.* **2015,** *137* (10), 3450-3453.

42.   Tobe, Y.; Takahashi, T.; Ishikawa, T.; Yoshimura, M.; Suwa, M.; Kobiro, K.; Kakiuchi, K.; Gleiter, R., Bent acenes. Synthesis and molecular structure of [6](1,4)naphthalenophane and [6](1,4)anthracenophane. *J. Am. Chem. Soc.* **1990,** *112* (24), 8889-8894.

43.   Tobe, Y.; Takahashi, T.; Kobiro, K.; Kakiuchi, K., Photochemical [2+2] dimerization of [6](1,4)-anthracenophane. *J. Am. Chem. Soc.* **1991,** *113* (15), 5804-5808.

44.   Tobe, Y.; Takemura, A.; Jimbo, M.; Takahashi, T.; Kobiro, K.; Kakiuchi, K., Unusual reactivity of bent acenes: reactions of [6](1,4)naphthalenophane and [6](1,4)anthracenophane with electrophiles. *J. Am. Chem. Soc.* **1992,** *114* (9), 3479-3491.

45.   Athans, A. J.; Briggs, J. B.; Jia, W.; Miller, G. P., Hydrogen-protected acenes. *J. Mater. Chem.* **2007,** *17* (25), 2636-2641.

46.   Kinzel, T.; Zhang, Y.; Buchwald, S. L., A New Palladium Precatalyst Allows for the Fast Suzuki−Miyaura Coupling Reactions of Unstable Polyfluorophenyl and 2-Heteroaryl Boronic Acids. *J. Am. Chem. Soc.* **2010,** *132* (40), 14073-14075.

47.   Li, P.; Sisto, T. J.; Darzi, E. R.; Jasti, R., The effects of cyclic conjugation and bending on the optoelectronic properties of paraphenylenes. *Org. Lett.* **2014,** *16* (1), 182-185.

48.   Becker, H. D., Unimolecular photochemistry of anthracenes. *Chem. Rev.* **1993,** *93* (1), 145-172.

49.   Dobrowolski, M. A.; Cyrański, M. K.; Merner, B. L.; Bodwell, G. J.; Wu, J. I.; Schleyer, P. v. R., Interplay of π-Electron Delocalization and Strain in [n](2,7)Pyrenophanes. *The Journal of Organic Chemistry* **2008,** *73* (20), 8001-8009.

50.   Atherton, J. C. C.; Jones, S., Diels–Alder reactions of anthracene, 9-substituted anthracenes and 9,10-disubstituted anthracenes. *Tetrahedron* **2003,** *59* (46), 9039-9057.

51.   Chai, J.-D.; Head-Gordon, M., Long-range corrected hybrid density functionals with damped atom-atom dispersion corrections. *PCCP* **2008,** *10* (44), 6615-6620.

52.   Cao, Y.; Liang, Y.; Zhang, L.; Osuna, S.; Hoyt, A.-L. M.; Briseno, A. L.; Houk, K. N., Why Bistetracenes Are Much Less Reactive Than Pentacenes in Diels–Alder Reactions with Fullerenes. *J. Am. Chem. Soc.* **2014,** *136* (30), 10743-10751.

53.   Jezowski, S. R.; Zhu, L.; Wang, Y.; Rice, A. P.; Scott, G. W.; Bardeen, C. J.; Chronister, E. L., Pressure Catalyzed Bond Dissociation in an Anthracene Cyclophane Photodimer. *J. Am. Chem. Soc.* **2012,** *134* (17), 7459-7466.

54.   Paldus, J.; Čížek, J., Hartree–Fock stability and symmetry breaking: oxygen doubly negative ion. *Can. J. Chem.* **1985,** *63* (7), 1803-1811.

55.   Sherrill, C. D.; Lee, M. S.; Head-Gordon, M., On the performance of density functional theory for symmetry-breaking problems. *Chem. Phys. Lett.* **1999,** *302* (5–6), 425-430.

56.   Sheldrick, G. M., Bruker/Siemens Area Detector Absorption Correction Program, Bruker AXS, Madison, WI, 1998.

57.   Sluis, P. V. d.; Spek, A. L., BYPASS: an effective method for the refinement of crystal structures containing disordered solvent regions. Acta Cryst. **1990**, *A46*, 194-201.

58.   Sheldrick, G. M., A short history of SHELX. Acta Cryst. **2008**, *A64*, 112-122.

59.   Gaussian 09, Revision B.01, Frisch, M. J.; Trucks, G. W.; Schlegel, H. B.; Scuseria, G. E.; Robb, M. A.; Cheeseman, J. R.; Scalmani, G.; Barone, V.; Mennucci, B.; Petersson, G. A.; Nakatsuji, H.; Caricato, M.; Li, X.; Hratchian, H. P.; Izmaylov, A. F.; Bloino, J.; Zheng, G.; Sonnenberg, J. L.; Hada, M.; Ehara, M.; Toyota, K.; Fukuda, R.; Hasegawa, J.; Ishida, M.; Nakajima, T.; Honda, Y.; Kitao, O.; Nakai, H.; Vreven, T.; Montgomery, Jr., J. A.; Peralta, J. E.; Ogliaro, F.; Bearpark, M.; Heyd, J. J.; Brothers, E.; Kudin, K. N.; Staroverov, V. N.; Kobayashi, R.; Normand, J.; Raghavachari, K.; Rendell, A.; Burant, J. C.; Iyengar, S. S.; Tomasi, J.; Cossi, M.; Rega, N.; Millam, J. M.; Klene, M.; Knox, J. E.; Cross, J. B.; Bakken, V.; Adamo, C.; Jaramillo, J.; Gomperts, R.; Stratmann, R. E.; Yazyev, O.; Austin, A. J.; Cammi, R.; Pomelli, C.; Ochterski, J. W.; Martin, R. L.; Morokuma, K.; Zakrzewski, V. G.; Voth, G. A.; Salvador, P.; Dannenberg, J. J.; Dapprich, S.; Daniels, A. D.; Farkas, Ö.; Foresman, J. B.; Ortiz, J. V.; Cioslowski, J.; Fox, D. J. Gaussian, Inc., Wallingford CT, **2009**.

Chapter IV

1.   De Volder, M. F. L.; Tawfick, S. H.; Baughman, R. H.; Hart, A. J., Carbon Nanotubes: Present and Future Commercial Applications. *Science* **2013,** *339* (6119), 535-539.

2.   Katsnelson, M. I., Graphene: carbon in two dimensions. *Mater. Today* **2007,** *10* (1–2), 20-27.

3.   Geim, A. K., Graphene: Status and Prospects. *Science* **2009,** *324* (5934), 1530-1534.

4.   Novoselov, K. S.; Jiang, Z.; Zhang, Y.; Morozov, S. V.; Stormer, H. L.; Zeitler, U.; Maan, J. C.; Boebinger, G. S.; Kim, P.; Geim, A. K., Room-Temperature Quantum Hall Effect in Graphene. *Science* **2007,** *315* (5817), 1379-1379.

5.   E. Osawa, Perspectives of Fullerene Nanotechnology, Springer, Berlin, 2002.

6.   H. Aoki, M. S. Dresselhaus, Physics of Graphene, Springer, Berlin, 2014.

7.   W. Andreoni, The Physics of Fullerene-Based and Fullerene-Related Materials, Springer, Berlin, 2000; e) L. Dai, Carbon Nanotechnology, Wiley-VCH, Weinheim, 2006.

8.   Kroto, H. W.; Heath, J. R.; O'Brien, S. C.; Curl, R. F.; Smalley, R. E., C60: Buckminsterfullerene. *Nature* **1985,** *318* (6042), 162-163.

9.   Novoselov, K. S.; Geim, A. K.; Morozov, S. V.; Jiang, D.; Zhang, Y.; Dubonos, S. V.; Grigorieva, I. V.; Firsov, A. A., Electric Field Effect in Atomically Thin Carbon Films. *Science* **2004,** *306* (5696), 666-669.

10.   Iijima, S., Helical microtubules of graphitic carbon. *Nature* **1991,** *354* (6348), 56-58.

11.   Narita, A.; Wang, X.-Y.; Feng, X.; Mullen, K., New advances in nanographene chemistry. *Chem. Soc. Rev.* **2015,** *44* (18), 6616-6643.
12.   Segawa, Y.; Ito, H.; Itami, K., Structurally uniform and atomically precise carbon nanostructures. *Nature Reviews Materials* **2016,** *1*, 15002.

13.   M. A. Petrukhina, L. T. Scott, H. W. Kroto, Fragments of Fullerenes and Carbon Nanotubes: Design Synthesis, Unusual Reactions, and Coordination Chemistry, Wiley-VCH, Weinheim, 2011.

14.   Jasti, R.; Bhattacharjee, J.; Neaton, J. B.; Bertozzi, C. R., Synthesis, Characterization, and Theory of [9]-, [12]-, and [18]Cycloparaphenylene: Carbon Nanohoop Structures. *J. Am. Chem. Soc.* **2008,** *130* (52), 17646-17647.

15.   Omachi, H.; Nakayama, T.; Takahashi, E.; Segawa, Y.; Itami, K., Initiation of carbon nanotube growth by well-defined carbon nanorings. *Nat. Chem.* **2013,** *5* (7), 572-576.

16.   Jasti, R.; Bertozzi, C. R., Progress and challenges for the bottom-up synthesis of carbon nanotubes with discrete chirality. *Chem. Phys. Lett.* **2010,** *494* (1–3), 1-7.

17.   Darzi, E. R.; Jasti, R., The dynamic, size-dependent properties of [5]-[12]cycloparaphenylenes. *Chem. Soc. Rev.* **2015,** *44* (18), 6401-10.

18.   Golder, M. R.; Jasti, R., Syntheses of the Smallest Carbon Nanohoops and the Emergence of Unique Physical Phenomena. *Acc. Chem. Res.* **2015,** *48* (3), 557-566.

19.   Sakamoto, H.; Fujimori, T.; Li, X.; Kaneko, K.; Kan, K.; Ozaki, N.; Hijikata, Y.; Irle, S.; Itami, K., Cycloparaphenylene as a molecular porous carbon solid with uniform pores exhibiting adsorption-induced softness. *Chem. Sci.* **2016,** *7* (7), 4204-4210.

20.   Kayahara, E.; Kouyama, T.; Kato, T.; Yamago, S., Synthesis and Characterization of [n]CPP (n = 5, 6, 8, 10, and 12) Radical Cation and Dications: Size-Dependent Absorption, Spin, and Charge Delocalization. *J. Am. Chem. Soc.* **2016,** *138* (1), 338-344.

21.   Alvarez, M. P.; Burrezo, P. M.; Kertesz, M.; Iwamoto, T.; Yamago, S.; Xia, J.; Jasti, R.; Navarrete, J. T. L.; Taravillo, M.; Baonza, V. G.; Casado, J., Properties of Sizeable [n]Cycloparaphenylenes as Molecular Models of Single-Wall Carbon Nanotubes Elucidated by Raman Spectroscopy: Structural and Electron-Transfer Responses under Mechanical Stress. *Angew. Chem. Int. Ed.* **2014,** *53* (27), 7033-7037.

22.   Golder, M. R.; Wong, B. M.; Jasti, R., Photophysical and theoretical investigations of the [8]cycloparaphenylene radical cation and its charge-resonance dimer. *Chem. Sci.* **2013,** *4* (11), 4285-4291.

23.   Kayahara, E.; Kouyama, T.; Kato, T.; Takaya, H.; Yasuda, N.; Yamago, S., Isolation and Characterization of the Cycloparaphenylene Radical Cation and Dication. *Angew. Chem. Int. Ed.* **2013,** *52* (51), 13722-13726.
24.   Xia, J.; Bacon, J. W.; Jasti, R., Gram-scale synthesis and crystal structures of [8]- and [10]CPP, and the solid-state structure of C60@[10]CPP. *Chem. Sci.* **2012,** *3* (10), 3018.

25.   Iwamoto, T.; Watanabe, Y.; Sadahiro, T.; Haino, T.; Yamago, S., Size-selective encapsulation of C60 by [10]cycloparaphenylene: formation of the shortest fullerene-peapod. *Angew. Chem. Int. Ed. Engl.* **2011,** *50* (36), 8342-4.

26.   Xia, J.; Jasti, R., Synthesis, Characterization, and Crystal Structure of [6]Cycloparaphenylene. *Angew. Chem., Int. Ed.* **2012,** *51* (10), 2474-2476, S2474/1-S2474/23.

27.   Hitosugi, S.; Yamasaki, T.; Isobe, H., Bottom-up Synthesis and Thread-in-Bead Structures of Finite (n,0)-Zigzag Single-Wall Carbon Nanotubes. *J. Am. Chem. Soc.* **2012,** *134* (30), 12442-12445.

28.   Liu, Y.-Y.; Lin, J.-Y.; Bo, Y.-F.; Xie, L.-H.; Yi, M.-D.; Zhang, X.-W.; Zhang, H.-M.; Loh, T.-P.; Huang, W., Synthesis and Crystal Structure of Highly Strained [4]Cyclofluorene: Green-Emitting Fluorophore. *Org. Lett.* **2016,** *18* (2), 172-175.

29.   Matsuno, T.; Sato, S.; Yokoyama, A.; Kamata, S.; Isobe, H., Self-Sorting of Two Hydrocarbon Receptors with One Carbonaceous Ligand. *Angew. Chem. Int. Ed.* **2016,** *55* (49), 15339-15343.

30.   Lewis, S. E., Cycloparaphenylenes and related nanohoops. *Chem. Soc. Rev.* **2015,** *44* (8), 2221-2304.

31.   Hirst, E. S.; Jasti, R., Bending Benzene: Syntheses of [n]Cycloparaphenylenes. *J. Org. Chem.* **2012,** *77* (23), 10473-10478.

32.   Yamago, S.; Kayahara, E.; Iwamoto, T., Organoplatinum-Mediated Synthesis of Cyclic π-Conjugated Molecules: Towards a New Era of Three-Dimensional Aromatic Compounds. *Chem. Rec.* **2014,** *14* (1), 84-100.

33.   Sun, Z.; Miyamoto, N.; Sato, S.; Tokuyama, H.; Isobe, H., An Obtuse-angled Corner Unit for Fluctuating Carbon Nanohoops. *Chem Asian J* **2017,** *12* (2), 271-275.

34.   S. Yamago, E. Kayahara, S. Hashimoto, in Polycyclic Arenes and Heteroarenes, Wiley-VCH, Weiheim, 2015, pp. 143-162;

35.   P. J. Evans, R. Jasti, in Polyarenes I (Eds.: J. S. Siegel, Y.-T. Wu), Springer, Berlin, Heidelberg, 2014, pp. 249-290.

36.   Segawa, Y.; Yagi, A.; Matsui, K.; Itami, K., Design and Synthesis of Carbon Nanotube Segments. *Angew. Chem. Int. Ed.* **2016,** *55* (17), 5136-5158.

37.   Darzi, E. R.; Hirst, E. S.; Weber, C. D.; Zakharov, L. N.; Lonergan, M. C.; Jasti, R., Synthesis, Properties, and Design Principles of Donor–Acceptor Nanohoops. *ACS Cent. Sci.* **2015,** *1* (6), 335-342.

38.   Golder, M. R.; Colwell, C. E.; Wong, B. M.; Zakharov, L. N.; Zhen, J.; Jasti, R., Iterative Reductive Aromatization/Ring-Closing Metathesis Strategy toward the Synthesis of Strained Aromatic Belts. *J. Am. Chem. Soc.* **2016,** *138* (20), 6577-6582.

39.   Li, P.; Sisto, T. J.; Darzi, E. R.; Jasti, R., The effects of cyclic conjugation and bending on the optoelectronic properties of paraphenylenes. *Org. Lett.* **2014,** *16* (1), 182-5.

40.   Li, P.; Wong, B. M.; Zakharov, L. N.; Jasti, R., Investigating the Reactivity of 1,4-Anthracene-Incorporated Cycloparaphenylene. *Org. Lett.* **2016,** *18* (7), 1574-1577.

41.   Sun, Z.; Suenaga, T.; Sarkar, P.; Sato, S.; Kotani, M.; Isobe, H., Stereoisomerism, crystal structures, and dynamics of belt-shaped cyclonaphthylenes. *Proc. Natl. Acad. Sci.* **2016,** *113* (29), 8109-8114.

42.   Lu, D.; Zhuang, G.; Wu, H.; Wang, S.; Yang, S.; Du, P., A Large pi-Extended Carbon Nanoring Based on Nanographene Units: Bottom-Up Synthesis, Photophysical Properties, and Selective Complexation with Fullerene C70. *Angew. Chem. Int. Ed. Engl.* **2017,** *56* (1), 158-162.

43.   Huang, Z.-A.; Chen, C.; Yang, X.-D.; Fan, X.-B.; Zhou, W.; Tung, C.-H.; Wu, L.-Z.; Cong, H., Synthesis of Oligoparaphenylene-Derived Nanohoops Employing an Anthracene Photodimerization–Cycloreversion Strategy. *J. Am. Chem. Soc.* **2016,** *138* (35), 11144-11147.

44.   Huang, C.; Huang, Y.; Akhmedov, N. G.; Popp, B. V.; Petersen, J. L.; Wang, K. K., Functionalized Carbon Nanohoops: Synthesis and Structure of a [9]Cycloparaphenylene Bearing Three 5,8-Dimethoxynaphth-1,4-diyl Units. *Org. Lett.* **2014,** *16* (10), 2672-2675.

45.   Van Raden, J. M.; Darzi, E. R.; Zakharov, L. N.; Jasti, R., Synthesis and characterization of a highly strained donor-acceptor nanohoop. *Org. Biomol. Chem.* **2016,** *14* (24), 5721-5727.

46.   Li, S.; Huang, C.; Thakellapalli, H.; Farajidizaji, B.; Popp, B. V.; Petersen, J. L.; Wang, K. K., Syntheses and Structures of Functionalized [9]Cycloparaphenylenes as Carbon Nanohoops Bearing Carbomethoxy and N-Phenylphthalimido Groups. *Org. Lett.* **2016,** *18* (9), 2268-2271.

47.   Hitosugi, S.; Nakanishi, W.; Yamasaki, T.; Isobe, H., Bottom-up synthesis of finite models of helical (n,m)-single-wall carbon nanotubes. *Nat. Commun.* **2011,** *2*, 492.
48.   Matsui, K.; Segawa, Y.; Namikawa, T.; Kamada, K.; Itami, K., Synthesis and properties of all-benzene carbon nanocages: a junction unit of branched carbon nanotubes. *Chem. Sci.* **2013,** *4* (1), 84-88.

49.   Matsui, K.; Segawa, Y.; Itami, K., All-Benzene Carbon Nanocages: Size-Selective Synthesis, Photophysical Properties, and Crystal Structure. *J. Am. Chem. Soc.* **2014,** *136* (46), 16452-16458.

50.   Kayahara, E.; Iwamoto, T.; Takaya, H.; Suzuki, T.; Fujitsuka, M.; Majima, T.; Yasuda, N.; Matsuyama, N.; Seki, S.; Yamago, S., Synthesis and physical properties of a ball-like three-dimensional π-conjugated molecule. *Nat. Commun.* **2013,** *4*.

51.   Xia, J.; Golder, M. R.; Foster, M. E.; Wong, B. M.; Jasti, R., Synthesis, Characterization, and Computational Studies of Cycloparaphenylene Dimers. *J. Am. Chem. Soc.* **2012,** *134* (48), 19709-19715.

52.   Evans, P. J.; Darzi, E. R.; Jasti, R., Efficient room-temperature synthesis of a highly strained carbon nanohoop fragment of buckminsterfullerene. *Nat. Chem.* **2014,** *6* (5), 404-408.

53.   Darzi, E. R.; White, B. M.; Loventhal, L. K.; Zakharov, L. N.; Jasti, R., An Operationally Simple and Mild Oxidative Homocoupling of Aryl Boronic Esters To Access Conformationally Constrained Macrocycles. *J. Am. Chem. Soc.* **2017,** *139* (8), 3106-3114.

54.   E. R. Darzi, PhD thesis, University of Oregon (USA), 2016.

55.   Patel, V. K.; Kayahara, E.; Yamago, S., Practical Synthesis of [n]Cycloparaphenylenes (n=5, 7-12) by H2SnCl4-Mediated Aromatization of 1,4-Dihydroxycyclo-2,5-diene Precursors. *Chem. - Eur. J.* **2015,** *21* (15), 5742-5749.

56.   Chen, Z.; Swager, T. M., Synthesis and Characterization of Poly(2,6-triptycene). *Macromolecules* **2008,** *41* (19), 6880-6885.

57.   Turner, M. J.; McKinnon, J. J.; Jayatilaka, D.; Spackman, M. A., Visualisation and characterisation of voids in crystalline materials. *CrystEngComm* **2011,** *13* (6), 1804-1813.

58.   Sozzani, P.; Comotti, A.; Simonutti, R.; Meersmann, T.; Logan, J. W.; Pines, A., A Porous Crystalline Molecular Solid Explored by Hyperpolarized Xenon. *Angew. Chem. Int. Ed.* **2000,** *39* (15), 2695-2699.

59.   Msayib, K. J.; Book, D.; Budd, P. M.; Chaukura, N.; Harris, K. D. M.; Helliwell, M.; Tedds, S.; Walton, A.; Warren, J. E.; Xu, M.; McKeown, N. B., Nitrogen and Hydrogen Adsorption by an Organic Microporous Crystal. *Angew. Chem. Int. Ed.* **2009,** *48* (18), 3273-3277.

60.   Mastalerz, M.; Oppel, I. M., Rational Construction of an Extrinsic Porous Molecular Crystal with an Extraordinary High Specific Surface Area. *Angew. Chem. Int. Ed.* **2012,** *51* (21), 5252-5255.

61.   Holst, J. R.; Trewin, A.; Cooper, A. I., Porous organic molecules. *Nat. Chem.* **2010,** *2* (11), 915-920.

62.   Seiki, N.; Shoji, Y.; Kajitani, T.; Ishiwari, F.; Kosaka, A.; Hikima, T.; Takata, M.; Someya, T.; Fukushima, T., Rational synthesis of organic thin films with exceptional long-range structural integrity. *Science* **2015,** *348* (6239), 1122-1126.

63.   Leung, F. K.; Ishiwari, F.; Kajitani, T.; Shoji, Y.; Hikima, T.; Takata, M.; Saeki, A.; Seki, S.; Yamada, Y. M.; Fukushima, T., Supramolecular Scaffold for Tailoring the Two-Dimensional Assembly of Functional Molecular Units into Organic Thin Films. *J. Am. Chem. Soc.* **2016,** *138* (36), 11727-33.

64.   Allcock, H. R.; Levin, M. L.; Whittle, R. R., Tris(o-phenylenedioxy)cyclo-triphosphazene: the clathration-induced monoclinic to hexagonal solid-state transition. *Inorg. Chem.* **1986,** *25* (1), 41-47.

65.   Allcock, H. R.; Primrose, A. P.; Sunderland, N. J.; Rheingold, A. L.; Guzei, I. A.; Parvez, M., Inclusion of Polymers within the Crystal Structure of Tris(o-phenylenedioxy)cyclotriphosphazene. *Chem. Mater.* **1999,** *11* (5), 1243-1252.

66.   Sozzani, P.; Comotti, A.; Bracco, S.; Simonutti, R., A Family of Supramolecular Frameworks of Polyconjugated Molecules Hosted in Aromatic Nanochannels. *Angew. Chem. Int. Ed.* **2004,** *43* (21), 2792-2797.

67.   Sozzani, P.; Bracco, S.; Comotti, A.; Ferretti, L.; Simonutti, R., Methane and Carbon Dioxide Storage in a Porous van der Waals Crystal. *Angew. Chem. Int. Ed.* **2005,** *44* (12), 1816-1820.

68.   Smith, G. W.; Wood, D., Crystal Structure of the Benzene tris(o-Phenylenedioxy) Phosphonitrile Trimer Complex. *Nature* **1966,** *210* (5035), 520-521.

69.   Sheldrick, G. M., Bruker/Siemens Area Detector Absorption Correction Program, Bruker AXS, Madison, WI, 1998.

70.   Sluis, P. V. d.; Spek, A. L., BYPASS: an effective method for the refinement of crystal structures containing disordered solvent regions. Acta Cryst. **1990**, *A46*, 194-201.

71.   Sheldrick, G. M., A short history of SHELX. Acta Cryst. **2008**, *A64*, 112-122.

72.   Materials Studio (Accelrys Software Inc.: San Diego, CA 92121, USA, 2001-2011).

73.   Gaussian 09, Revision B.01, Frisch, M. J.; Trucks, G. W.; Schlegel, H. B.; Scuseria, G. E.; Robb, M. A.; Cheeseman, J. R.; Scalmani, G.; Barone, V.; Mennucci, B.; Petersson, G. A.; Nakatsuji, H.; Caricato, M.; Li, X.; Hratchian, H. P.; Izmaylov, A. F.; Bloino, J.; Zheng, G.; Sonnenberg, J. L.; Hada, M.; Ehara, M.; Toyota, K.; Fukuda, R.; Hasegawa, J.; Ishida, M.; Nakajima, T.; Honda, Y.; Kitao, O.; Nakai, H.; Vreven, T.; Montgomery, Jr., J. A.; Peralta, J. E.; Ogliaro, F.; Bearpark, M.; Heyd, J. J.; Brothers, E.; Kudin, K. N.; Staroverov, V. N.; Kobayashi, R.; Normand, J.; Raghavachari, K.; Rendell, A.; Burant, J. C.; Iyengar, S. S.; Tomasi, J.; Cossi, M.; Rega, N.; Millam, J. M.; Klene, M.; Knox, J. E.; Cross, J. B.; Bakken, V.; Adamo, C.; Jaramillo, J.; Gomperts, R.; Stratmann, R. E.; Yazyev, O.; Austin, A. J.; Cammi, R.; Pomelli, C.; Ochterski, J. W.; Martin, R. L.; Morokuma, K.; Zakrzewski, V. G.; Voth, G. A.; Salvador, P.; Dannenberg, J. J.; Dapprich, S.; Daniels, A. D.; Farkas, Ö.; Foresman, J. B.; Ortiz, J. V.; Cioslowski, J.; Fox, D. J. Gaussian, Inc., Wallingford CT, **2009**.

Chapter V

1.   Bielawski, C. W.; Grubbs, R. H., Living ring-opening metathesis polymerization. *Prog. Polym. Sci.* **2007,** *32* (1), 1-29.

2.   Slugovc, C., The Ring Opening Metathesis Polymerisation Toolbox. *Macromol. Rapid Commun.* **2004,** *25* (14), 1283-1297.

3.   Leitgeb, A.; Wappel, J.; Slugovc, C., The ROMP toolbox upgraded. *Polymer* **2010,** *51* (14), 2927-2946.

4.   Xue, Z.; Mayer, M. F., Entropy-driven ring-opening olefin metathesis polymerizations of macrocycles. *Soft Matter* **2009,** *5* (23), 4600-4611.

5.   Herbert, D. E.; Mayer, U. F. J.; Manners, I., Strained Metallocenophanes and Related Organometallic Rings Containing π-Hydrocarbon Ligands and Transition-Metal Centers. *Angew. Chem. Int. Ed.* **2007,** *46* (27), 5060-5081.

6.   Miao, Y. J.; Bazan, G. C., Stereoselective Polymerization of [2.2]Paracyclophan-1-ene. *Macromolecules* **1994,** *27* (4), 1063-1064.

7.   Miao, Y.-J.; Bazan, G. C., Paracyclophene Route to Poly(p-phenylenevinylene). *J. Am. Chem. Soc.* **1994,** *116* (20), 9379-9380.

8.   Yu, C.-Y.; Turner, M. L., Soluble Poly(p-phenylenevinylene)s through Ring-Opening Metathesis Polymerization. *Angew. Chem. Int. Ed.* **2006,** *45* (46), 7797-7800.

9.   Yu, C.-Y.; Horie, M.; Spring, A. M.; Tremel, K.; Turner, M. L., Homopolymers and Block Copolymers of p-Phenylenevinylene-2,5-diethylhexyloxy-p-phenylenevinylene and m-Phenylenevinylene-2,5-diethylhexyloxy-p-phenylenevinylene by Ring-Opening Metathesis Polymerization. *Macromolecules* **2010,** *43* (1), 222-232.

10.   Yu, C.-Y.; Kingsley, J. W.; Lidzey, D. G.; Turner, M. L., Phenylenevinylene Block Copolymers via Ring-Opening Metathesis Polymerization. *Macromol. Rapid Commun.* **2009,** *30* (22), 1889-1892.

11.   Mäker, D.; Maier, C.; Brödner, K.; Bunz, U. H. F., [2.2.2]Paracyclophane-Trienes—Attractive Monomers for ROMP. *ACS Macro Letters* **2014,** *3* (5), 415-418.

12.   Chang, S.-W.; Horie, M., A donor-acceptor conjugated block copolymer of poly(arylenevinylene)s by ring-opening metathesis polymerization. *Chem. Commun.* **2015,** *51* (44), 9113-9116.

13.   Xu, Y.; Xu, W. L.; Smith, M. D.; Shimizu, L. S., Self-assembly and ring-opening metathesis polymerization of a bifunctional carbonate-stilbene macrocycle. *RSC Advances* **2014,** *4* (4), 1675-1682.

14.   Evans, P. J.; Darzi, E. R.; Jasti, R., Efficient room-temperature synthesis of a highly strained carbon nanohoop fragment of buckminsterfullerene. *Nat. Chem.* **2014,** *6* (5), 404-408.

15.   Darzi, E. R.; White, B. M.; Loventhal, L. K.; Zakharov, L. N.; Jasti, R., An Operationally Simple and Mild Oxidative Homocoupling of Aryl Boronic Esters To Access Conformationally Constrained Macrocycles. *J. Am. Chem. Soc.* **2017,** *139* (8), 3106-3114.

16.   Choi, T.-L.; Grubbs, R. H., Controlled Living Ring-Opening-Metathesis Polymerization by a Fast-Initiating Ruthenium Catalyst. *Angew. Chem. Int. Ed.* **2003,** *42* (15), 1743-1746.

17.   Allcock, H. R.; Lampe, F. W.; Mark, J. E., *Contemporary polymer chemistry*. Pearson Education: Upper Saddle River, 2003.

18.   Seo, J.; Noh, J. H.; Seok, S. I., Rational Strategies for Efficient Perovskite Solar Cells. *Acc. Chem. Res.* **2016**.

19.   Calió, L.; Kazim, S.; Grätzel, M.; Ahmad, S., Hole-Transport Materials for Perovskite Solar Cells. *Angew. Chem. Int. Ed.* **2016**, *55* (47), 14522-14545.

20.   Ning, Z.; Tian, H., Triarylamine: a promising core unit for efficient photovoltaic materials. *Chem. Commun.* **2009,** (37), 5483-5495.

21.   Wei, Y.; Chen, C.-T., Doubly Ortho-Linked cis-4,4'-Bis(diarylamino)stilbene/Fluorene Hybrids as Efficient Nondoped, Sky-Blue Fluorescent Materials for Optoelectronic Applications. *J. Am. Chem. Soc.* **2007,** *129* (24), 7478-7479.

22.   Shirota, Y., Photo- and electroactive amorphous molecular materials-molecular design, syntheses, reactions, properties, and applications. *J. Mater. Chem.* **2005,** *15* (1), 75-93.

23.   Ruiz-Castillo, P.; Buchwald, S. L., Applications of Palladium-Catalyzed C–N Cross-Coupling Reactions. *Chem. Rev.* **2016,** *116* (19), 12564-12649.

24.   Martin, R.; Buchwald, S. L., Palladium-Catalyzed Suzuki−Miyaura Cross-Coupling Reactions Employing Dialkylbiaryl Phosphine Ligands. *Acc. Chem. Res.* **2008,** *41* (11), 1461-1473.

25.   Bruno, N. C.; Tudge, M. T.; Buchwald, S. L., Design and preparation of new palladium precatalysts for C-C and C-N cross-coupling reactions. *Chemical Science* **2013,** *4* (3), 916-920.

26.   Sanford, M. S.; Love, J. A.; Grubbs, R. H., A Versatile Precursor for the Synthesis of New Ruthenium Olefin Metathesis Catalysts. *Organometallics* **2001,** *20* (25), 5314-5318.

27.   Linseis, M.; Záliš, S.; Zabel, M.; Winter, R. F., Ruthenium Stilbenyl and Diruthenium Distyrylethene Complexes: Aspects of Electron Delocalization and Electrocatalyzed Isomerization of the Z-Isomer. *J. Am. Chem. Soc.* **2012,** *134* (40), 16671-16692.

28.   Hao, W.; Liu, H.; Yin, L.; Cai, M., Phosphine-Free, Heterogeneous Palladium-Catalyzed Atom-Efficient Carbonylative Cross-Coupling of Triarylbismuths with Aryl Iodides: Synthesis of Biaryl Ketones. *J. Org. Chem.* **2016,** *81* (10), 4244-4251.

29.   Sheldrick, G. M., Bruker/Siemens Area Detector Absorption Correction Program, Bruker AXS, Madison, WI, 1998.

30.   Sheldrick, G. M., A short history of SHELX. Acta Cryst. 2008, A64, 112-122.

31.	Gaussian 09, Revision B.01, Frisch, M. J.; Trucks, G. W.; Schlegel, H. B.; Scuseria, G. E.; Robb, M. A.; Cheeseman, J. R.; Scalmani, G.; Barone, V.; Mennucci, B.; Petersson, G. A.; Nakatsuji, H.; Caricato, M.; Li, X.; Hratchian, H. P.; Izmaylov, A. F.; Bloino, J.; Zheng, G.; Sonnenberg, J. L.; Hada, M.; Ehara, M.; Toyota, K.; Fukuda, R.; Hasegawa, J.; Ishida, M.; Nakajima, T.; Honda, Y.; Kitao, O.; Nakai, H.; Vreven, T.; Montgomery, Jr., J. A.; Peralta, J. E.; Ogliaro, F.; Bearpark, M.; Heyd, J. J.; Brothers, E.; Kudin, K. N.; Staroverov, V. N.; Kobayashi, R.; Normand, J.; Raghavachari, K.; Rendell, A.; Burant, J. C.; Iyengar, S. S.; Tomasi, J.; Cossi, M.; Rega, N.; Millam, J. M.; Klene, M.; Knox, J. E.; Cross, J. B.; Bakken, V.; Adamo, C.; Jaramillo, J.; Gomperts, R.; Stratmann, R. E.; Yazyev, O.; Austin, A. J.; Cammi, R.; Pomelli, C.; Ochterski, J. W.; Martin, R. L.; Morokuma, K.; Zakrzewski, V. G.; Voth, G. A.; Salvador, P.; Dannenberg, J. J.; Dapprich, S.; Daniels, A. D.; Farkas, Ö.; Foresman, J. B.; Ortiz, J. V.; Cioslowski, J.; Fox, D. J. Gaussian, Inc., Wallingford CT, 2009.